Coordination Chemistry of *cis*-Dioxomolybdenum(VI) with Some Tri- and Tetradentate Ligands

A Thesis
Submitted for the Degree of
Doctor of Philosophy

By

SATHISH KUMAR KURAPATI

School of Chemistry
University of Hyderabad
Hyderabad 500 046
India

June 2015

Dedicated to

My Parents, My Wife and Family members

CONTENTS

STATEMENT

I hereby declare that the matter embodied in this thesis entitled "***Coordination Chemistry of cis-Dioxomolybdenum(VI) with Some Tri- and Tetradentate Ligands***"is the result ofthe investigation carried out by me in the School of Chemistry, University of Hyderabad, under the supervision of **Prof. Samudranil Pal**.

In keeping the general practice of reporting scientific observation, due acknowledgement has been made wherever the work described is based on findings of other investigations. Any omission which might have occurred by oversight or error is regretted.

30th June, 2015 **Sathish Kumar Kurapati**

DECLARATION

I **Sathish Kumar Kurapati** hereby declare that this thesis entitled "***Coordination Chemistry of cis-Dioxomolybdenum(VI) with Some Tri- and Tetradentate Ligands***" submitted by me under the guidance and supervision of **Prof. Samudranil Pal**, School of Chemistry, University of Hyderabad is a bonafide research work which is also free from plagiarism. I also declare that it has not been submitted previously in part or full to this University or any other University or Institution for the award of any degree or diploma. I hereby agree that my thesis can be deposited in shodhganga/INFLIBNET.

Date: 30th June 2015

Sathish Kumar Kurapati
Reg.No.: 10CHPH07

Signature of the supervisor:
Prof. Samudranil Pal

Prof. Samudranil Pal
School of Chemistry
University of Hyderabad
Hyderabad–500 046, India

Phone:+91-40-23134829
Fax: +91-40-2301 2460
Email: spsc@uohyd.ernet.in
spal@uohyd.ac.in

30th June, 2015

CERTIFICATE

Certified that the work embodied in the thesis entitled ***"Coordination Chemistry of cis-Dioxomolybdenum(VI) with Some Tri- and Tetradentate Ligands"*** has been carried out by **Mr. Sathish Kumar Kurapati** under my supervision and that the same has not been submitted elsewhere for any degree.

Prof. Samudranil Pal
(Thesis Supervisor)

Dean
School of Chemistry
University of Hyderabad

ACKNOWLEDGEMENTS

I would like to express my foremost and deep heartfelt gratitude and profound respect to my research supervisor ***Prof. Samudranil Pal*** *who shaped me as a successful research scholar with his guidance, encouragement, valuable discussions and suggestions throughout my research work. It is a great privilege and pleasure to associate with him. I was blessed to have my time with him as a student and I have experienced my growth in my personal and professional life with his generosity.*

I would like to extend my gratitude to the former and present Deans, School of Chemistry for providing all essential facilities to carry out my research work without any delay and interruption. In addition, I am extremely thankful to all the faculty members of the school including my doctoral committee members Prof. Samar Kumar Das and Dr. ViswanathanBaskarfor their help, cooperation and encouragement at various stages of my stay in the school.

I thank all non-teaching staff of the school for their help and cooperation to execute my research work. I am thankful to IGM library for providing an excellent collection of books and journals.

I sincerely acknowledge Council for Scientific and Industrial Research (CSIR), New Delhi for a research fellowship.Department of Science and Technology (DST), New Delhi and the University Grants Commission (UGC), New Delhi are also gratefully acknowledged for the facilities provided under theFIST and the CAS programs, respectively.

I regard teachersare the representatives of the God. I am thankful to all of my teachers from KG to PG for enlightening me at every stage of my life. It gives me an immense pleaser to thank Prof. K.C. Rajanna, Prof. M. Sayaji Rao and Dr. T. Sathyanarayanafor their valuable lectures, discussions and suggestions.

I am thankful to my labmates Dr. Tulika Ghosh, Dr. SwamyMaloth, Dr.NagarajuKoppanathi, Dr. A.R. Balavardhana Rao, Mr.Narendra babu, Dr.RupeshN.Prabhu, Dr. Srinivas Keesaraand Ms. Sabari Ghosh for creating a wonderful working atmosphere in the lab. My seniors Dr. Swamy, Dr. Balavardhana Rao and Dr. Nagarajuare very helpful and always willing to share their experience andknowledge with me.

I am very thankful to my best friends Mr. Mahender Ambati, Mr. Ramesh Rampalli, Dr. DevenderDamma, Mr. YadaiahSalwadi, Dr. SwamyMaloth, Dr. RajenderNasani, Dr. Naveen Naganaboina, Mr. Gangarampallikonda, and Mr. Kranthi Kumar Jaldi for being my side in all sorts of difficulties.

I am grateful to have friends like Swamy, Naveen, Shivaprasad, Madhava Chary, Bharani, Ashok, Sudheer, Babu, Chandrashekar (Chandu), Ilanna, Ashok (babai),Naidu (sunny), Sathish (Bijji) and Ugandharwho made my stay at University of Hyderabad peaceful, joyful and cheerful.

I am very glad to have seniors in my M.Sclike Dr. Ansari, Dr. SathishMukka, Dr. Anand, Venkanna and Anwar ali who gave me the inspiration and encouragement to reach here.

I am very happy to mention my childhood friends Kiran Jaldi, SathyamJogu, MadhuAppidi, Narsimha, SrikanthGuduru and Sridhar Guduru, who joins with me in all kinds of occasions.

I am also thankful to all the teaching, non-teaching staff and 2009-2015 period students of OUPGC Mirzapur (B) for their kind support and concern.

I extend my heartfelt thanks to my entire School, B.Sc,M.Scfriends, well-wishersand colleagues in school of chemistry for their help. Dr. Mallesh, Dr. Yasin, Dr. Kishore, Dr. Bharath, Dr. GDP, Dr. Kishore (ravada), Dr. Rambabu, Dr. Kishore (P.V.V.N), Dr. Thirupathi Reddy, Dr. Hariprasad, Dr. Karunakar, Nanda Kishore, Obaiah, Dr. Bhargavi, Dr. Dinesh, Dr. Bhanu, Dr. Ramu Yadav, Dr.Ramasuresh, Dr. Nagarjuna Reddy, Nagarjuna, Krishna

Chari, Madhusudan Reddy, Ramakrishna, Sridhar Reddy, Shivarama Krishna, Dr. Srinu (Dharavath), Rajender, Vikranth, Prakash, Dr. Tilak, Saianna, Lingam, Venkanna, Malkappa, Srinivas (billakanti), Harish, Ramakrishna (Gali), Murali, Shruthi, Sakthivel, A……Z are to mention.

As a follower of Indian tradition I believe even God is also after parents. It is not even considerable if I owe everything to my parents Andalu and Bikshapathifor their relentless support, care, love and blessings. They made my path with their hard work. They made me a good human being with their values. They made me a strong person with their spiritual knowledge. I would not be standing where I am today without their contribution.

To me, my wife Varshini is not a separate person. She is in me in every second of my life, at every place I went and every step I took. Without her unconditional love, support, care and concern I cannot be here.

My special thanks to my beloved sistersand brothers-in lawMamatha-Madhu, Uma-Srinivas, Vijaya-Ganesh and Uma-Devender for their love, concern and support. My brother Srinivas and my wife's parentsramachandru and Meena and brother Naresh are special to mention. Last but certainly not least, I am thankful to my nephews and nieces Chinnu, Sunny, Appu, Bablu, Honey and Cherri for their adorable affection.

Sathish Kumar Kurapati

SYNOPSIS

Chapter 1

In this chapter, the scope and objectives of the present work have been presented in the background of the importance of molybdenum and the coordination chemistry of *cis*-dioxomolybdenum(VI) with bi-, tri- and tetradentate ligands.

Chapter 2

Dioxomolybdenum(VI) complexes having the general formula *cis*-$[MoO_2(OMe)(L^n)]$ (**1**−**6)** with the tridentate 2-((2-(pyridin-2-yl)hydrazono)-methyl)phenol and its substituted derivatives (HL^n, n = 1−6) have been synthesized. Elemental analysis and various spectroscopic (IR, UV-Vis, ^1H NMR and fluorescence) measurements have been used for the characterization of the complexes. X-ray crystal structures of all the complexes except for one have been determined. In each of these analogous complexes, the metal centre is in distorted octahedral N_2O_4 coordination sphere assembled by the meridionally spanning pyridine-N, azomethine-N and phenolate-O donor

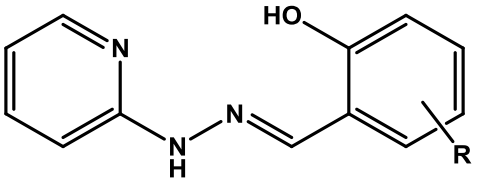

HL^n
(n = 1-5 for R = H, Cl, Br, Me and OMe *para* to OH and n = 6 for R = OMe *para* to azomethine)

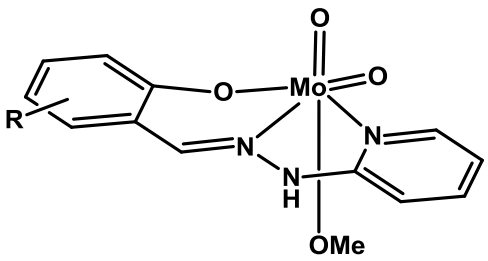

cis-$[MoO_2(OMe)(L^n)]$
1–6 (for n = 1-6)

Chart 1. Chemical structure diagrams of the Schiff bases and their complexes.

$(L^n)^-$, the methoxo-O and the two mutually *cis* oriented oxo groups. In the crystal, the complex molecules are involved in intermolecular N−H···O hydrogen bonding interaction involving the hydrazine NH and the metal coordinated methoxo-O. In four structures, discrete dimeric units are formed through a pair of reciprocal N−H···O hydrogen bonds, while N−H···O bridged linear one-dimesional polymeric structure is formed in the fifth structure.

Chapter 3

Reactions of $[MoO_2(acac)_2]$ ($acac^-$ = acetylacetonate) with the potentially N_2O-donor 5,5-membered fused chelate rings forming Schiff bases 2-(2-pyridylaldimine)ethanol (HL^1) and 4/5-*R*-2-(2-pyridylaldimine)phenols (HL^n; n = 2–5 for *R* = H, 4-Cl, 4-Me and 5-Me, respectively) lead to facile formation of the racemic complexes of general formula *cis*-$[MoO_2(acacL^{1-5})]$ (**1**–**5**) in 80–85% yields. Here, $(acacL^n)^{2-}$ represents a chiral N_2O_2-donor ligand system formed by a novel Mannich-type reaction that involves acetylacetonate and the azomethine fragment of HL^n both coordinated to the *cis*-$\{MoO_2\}^{2+}$ unit. Characterization of **1**–**5** has been performed with the help of microanalytical (CHN), spectroscopic (ESI-MS, IR, UV-Vis and ^{1}H- and ^{13}C-NMR) and electrochemical measurements. The molecular structures of all the complexes except for **5** are authenticated by single crystal X-ray crystallography. The Mo(VI) center in each of these analogous complexes is in a distorted octahedral N_2O_4 coordination sphere assembled by the chiral N_2O_2-donor transformed ligand $(acacL^n)^{2-}$ and the two mutually *cis*-oriented oxo ligands. In the crystal lattice, each of **1**–**4** exists as centrosymmetric discrete dimer *via* a pair of reciprocal N–H···O hydrogen bonds between its enantiomeric pairs.

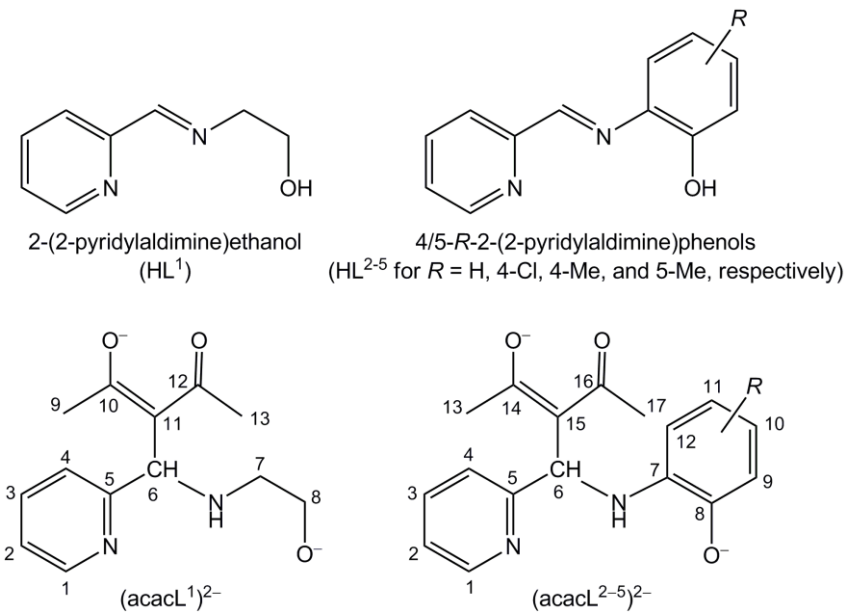

Chart 2. Chemical structure diagrams of the Schiff bases $HL^{1–5}$ and the transformed ligands $(acacL^{1–5})^{2–}$.

Chapter 4

A series of *cis*-dioxomolybdenum(VI) complexes of general formula *cis*-$[MoO_2(HL^n)]$ (**1**−**4**) have been synthesized in 80−85% yields by reacting equimolar amounts of $[MoO_2(acac)_2]$ ($acac^–$ = acetylacetonate) with 2,2'-(2-hydroxy-3,5-R_1,R_2-benzylazanediyl)diethanols (H_3L^n, n = 1–4) in methanol. Characterization of the complexes has been performed by elemental analysis, spectroscopic (IR, UV-Vis, ^{1}H- and ^{13}C-NMR) and electrochemical measurements. The molecular structures of all four complexes have been determined by single-crystal X-ray diffraction studies. In each of these analogous complexes, the metal centre is in a distorted octahedral NO_5 coordination sphere assembled by the single edge shared 5,5,6-membered chelate rings forming NO_3-donor $(HL^n)^{2–}$ and two *cis* oriented oxo groups. Crystal structures of the complexes reveal formation of discrete

centrosymmetric dimeric species via a pair of reciprocal intermolecular O−H···O hydrogen bonding interactions. Spectroscopic data of all the complexes are consistent with their molecular structures. In the cyclic voltammograms, the redox-active complexes display a quasi-reversible to irreversible metal centred reduction with the cathodic peak potential in the range −0.92 to −1.12 V (vs. Ag/AgCl). All the complexes have been evaluated for their catalytic activities in oxidative bromination reactions of styrene and salicylaldehyde and in benzoin oxidation reaction.

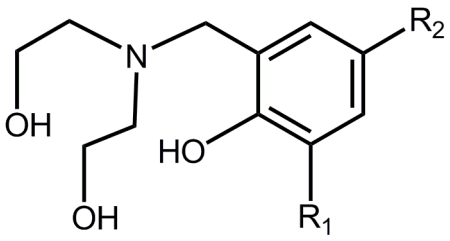

H_3L^n (n = 1–4)
n = 1 for R_1 = H and R_2 = Me
n = 2 for R_1 = H, R_2 = Et
n = 3 for R_1 = H and R_2 = ^{t}Bu
n = 4 for R_1 = ^{t}Bu and R_2 = ^{t}Bu

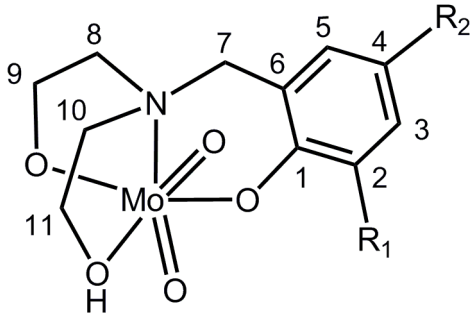

cis-[$MoO_2(HL^n)$]
1 (n = 1), **2** (n = 2),
3 (n = 3) and **4** (n = 4)

Chart 3. Chemical structure diagrams of N-caped tripodal $H_3L^{1–4}$ and their complexes *cis*-[$MoO_2(HL^{1–4})$] (**1**–**4**).

Chapter 5

Reactions of [$MoO_2(acac)_2$] ($acac^-$ = acetylacetonate), 2-((2-(2-hydroxyethylamino)-ethylamino)methyl)-4-*R*-phenols (H_2L^n, n = 1–5 for *R* = H, Me, OMe, Cl and Br, respectively) and KOH in 1:1:2 mole ration in methanol afford a series of complexes having the general formula *cis*-[$MoO_2(L^n)$] (**1**−**5**) in 81−86% yields. The complexes have been characterized by elemental analysis, spectroscopic (IR, UV-Vis, ^{1}H-, ^{13}C- and ^{13}C-DEPT NMR) and electrochemical measurements. The molecular structures of **1**−**4**

have been determined by single crystal X-ray crystallography. In each of **1**−**4**, the ONNO-donor 6,5,5-membered fused chelate rings forming $(L^n)^{2-}$ and the two mutually *cis* oxo groups assemble a distorted octahedral N_2O_4 coordination sphere around the metal centre. In the crystal lattice, each of **1**−**4** forms one dimensional infinite chain structure via intermolecular N−H···O hydrogen bonding interactions. In cyclic voltammograms, the diamagnetic redox active complexes display an irreversible metal centred reduction in the potential range –0.73 to –0.88 V (vs. Ag/AgCl). The physicochemical data are consistent with a very similar gross molecular structure for all of **1**−**5**. All the complexes exhibit decent bromoperoxidase activities and are also able to effectively catalyze benzoin and methyl(phenyl)sulfide oxidation reactions.

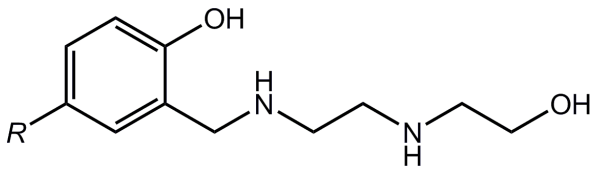

H_2L^n

(n = 1–5 for *R* = H, Me, OMe, Cl and Br, respectively)

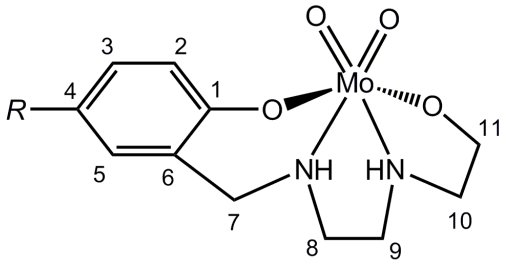

cis-$[MoO_2(L^n)]$

(**1**–**5** for n = 1–5, respectively)

Chart 4. Chemical structure diagrams of tetradentate linear $H_2L^{1–5}$ and their complexes *cis*-$[MoO_2(L^{1–5})]$ (**1**–**5**).

Chapter 1

Introduction

In this chapter, the scope and objectives of the present work have been presented in the background of the importance of molybdenum and the coordination chemistry of *cis*-dioxomolybdenum(VI) with bi-, tri- and tetradentate ligands.

1.1. Molybdenum

Molybdenum in its oxide form *molybdenite* was discovered in 1778 by Carl Wilhelm Scheele. The name molybdenum has originated from the Greek word '*molybdos'* which means lead-like. Molybdenum is one of the nonprecious elements and its ab undance on earth crust is about 1.2–1.5 ppm. The oxidation state of molybdenum varies from -2 to +6 [1]. Till date thirty three isotopes of molybdenum have been detected. Out of these isotopes only seven with mass numbers 92, 94, 95, 96, 97, 98, and 100 occur naturally. Among the seven naturally occurring isotopes of molybdenum, only ^{100}Mo undergoes radioactive decay. Due to these stable isotopes, the presence of molybdenum can be easily detected by its isotopic patterns in mass-spectrometry. Molybdenum is relatively less toxic in its most stable +6 oxidation state and hence it has attracted considerable attention of the chemistry world [2].

Molybdenum is present in various metalloenzymes which are essential for many physiological reactions occurring in the plant and animal kingdoms. Molybdenum containing CO oxidoreductase, arsenite oxidase, sulfite oxidase, xanthine oxidase, aldehyde oxidoreductase, DMSO reductase, nitrite reductase and nitrogenase play important roles in the metabolism of carbon, nitrogen, sulfur, and arsenic (Chart 1.1) [3]. Consequently molybdenum has been recognized as one of the essential elements for animals as well as plants. Its

deficiency or excess supply may cause several physiological abnormalities in humans including cancer [4]. Complexes of molybdenum also show anticancer [5–7], antibacterial [8], antifungal [7,9,10] and antifertility [10] activities.

Carbon monoxide oxidoreductase: $CO + H_2O \longrightarrow CO_2 + 2H^+ + 2e^-$.

Dimethyl sulfoxide reductase: $Me_2SO + 2H^+ + 2e^- \longrightarrow Me_2S + H_2O$.

Nitrate reductase: $NO_3^- + 2H^+ + 2e^- \longrightarrow NO_2^- + H_2O$.

Arsenite oxidase: $H_2AsO_3 + H_2O \longrightarrow HAsO_4^{2-} + 3H^+ + 2e^-$.

Sulfite oxidase: $SO_3^{2-} + H_2O \longrightarrow SO_4^{2-} + 2H^+ + 2e^-$.

Xanthine oxidase: Xanthine + $H_2O \longrightarrow$ Uric acid + $2H^+ + 2e^-$.

Aldehyde oxidoreductase: $RCHO + H_2O \longrightarrow RCO_2H + 2H^+ + 2e^-$.

Chart 1.1. Reactions involving molybdenum containing metalloenzymes.

1.2. Coordination chemistry of *cis*-$\{MoO_2\}^{2+}$

1.2.1. Bidentate Schiff bases

Most complexes of molybdenum in its +6 oxidation state contain *cis*-$\{MoO_2\}^{2+}$ core [11,12]. The *cis*-$\{MoO_2\}^{2+}$ complexes with bidentate Schiff bases have been well studied. Zelentsov and coworkers [13] first synthesized the $[MoO_2L_2]$ type of complex by reacting $[MoO_2Cl_2]$ with a bidentate Schiff base derived from salicylaldehyde and aniline. Yamanouchi and Yamada [14] prepared several *cis*-$\{MoO_2\}^{2+}$ complexes of monoanionic bidentate Schiff base ligands via template reactions between $[MoO_2(sal)_2]$ or $[MoO_2(3\text{-methoxysal})_2]$ and alkyl/aryl amines (Chart 1.2). Later similar type of complexes synthesized by following the same template reaction procedure were reported by Oh and koo [15]. K. Tsukuma and coworkers [16] determined the molecular structure of bis-(N-methylsalicylideneiminato)-dioxomolybdenum(VI) using single crystal X-ray crystallography (Fig. 1.1) from the crystals provided by Yamanouchi and Yamada [14].

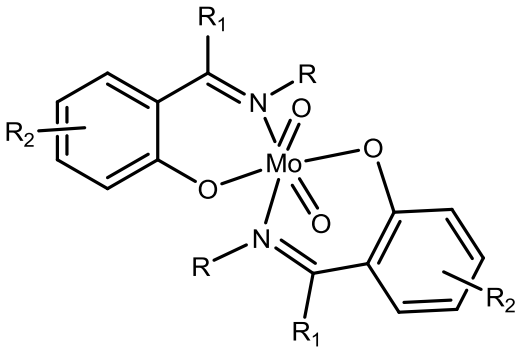

R, R_1 = H, Me, Et, Ph etc. R_2 = H, Me, OMe, Cl, Br etc.

Chart 1.2. Chemical diagram of *cis*-[MoO_2L_2].

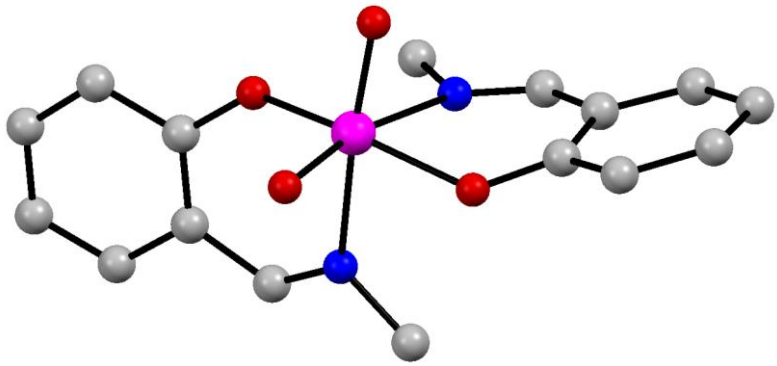

Fig. 1.1. An example of *cis*-[MoO_2L_2] type of complexes.

Several complexes possessing similar structural features were also reported with bidentate Schiff bases derived from 2-hydroxynaphaldehyde and various primary amines and bridged diamines [17–22]. Few bidentate hydroxylamine condensates of salicylaldehyde, 2-hydroxyacetophenone and 2-hydroxybenzophenone have been also employed as ligands to synthesize *cis*-[MoO_2L_2] type of complexes [23–26].

1.2.2. Tridentate Schiff bases

The *cis*-dioxomolybdenum(VI) complexes with tridentate Schiff bases have been extensively studied due to the potential availability of an open coordination site that can be occupied by an easily dissociable monodentate

ligand [11,12]. The tridentate Schiff bases used are mainly of two types. The 2-carbonylphenol condensates with 2-aminophenols or 2-aminoalcohols form the first type and the acid hydrazide condensates with 2-carbonylphenols or 1,3-diketones belong to the second type. These kinds of Schiff bases easily bind the *cis*-$\{MoO_2\}^{2+}$ core and the planar ligands coordinate the molybdenum(VI) center in a meridional fashion. The tridentate ligand and two *cis* oriented oxo groups occupy five coordination sites of the octahedral metal centre and the sixth coordination site is satisfied by an ancillary monodentate ligand (Chart 1.3).

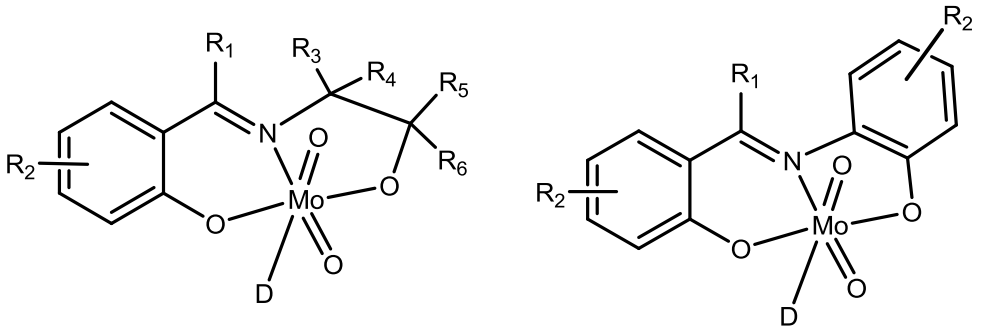

R_1 = H, Me, Ph etc. R_1 = H, Me, Ph etc.

R_2 = H, Me, OMe, Cl, Br etc. R_2 = H, Me, OMe, Cl, Br etc.

D = Neutral solvent molecule or other ancillary ligands.

Chart 1.3. Chemical diagrams of *cis*-{MoO2}$^{2+}$ complexes bearing tridentate ligands.

A. Chakravorty and coworkers [27] proposed the meridional spanning of tridentate Schiff base ligands based on the studies performed on *cis*-$\{MoO_2\}^{2+}$ complexes with salicylaldehyde condensates of 2-aminophenol, 2-aminothiophenol and 2-ethanolamine. Various monodentate ancillary ligands like water, alcohol, aldehyde, amide, N-oxide, phosphine oxide, amine, and phosphine ligands were screened and it was shown that these ligands occupy the labile coordination position *trans* to one of the two oxo ligands of the *cis*-$\{MoO_2\}^{2+}$ core.

R.H. Holm and coworkers [28] first reported the crystal structures of the *cis*-$\{MoO_2\}^{2+}$ complexes with two tridentate Schiff bases derived from 5-*t*-bu-/4-HSO_3 salicylaldehyde and 2-aminophenol / 2-aminothiophenol. The sixth labile coordination place is occupied by methanol or sulphate ion. Later, several similar type of complexes were reported with their crystal structures [19,29–38]. Some of these complexes are illustrated below in Fig. 1.2.

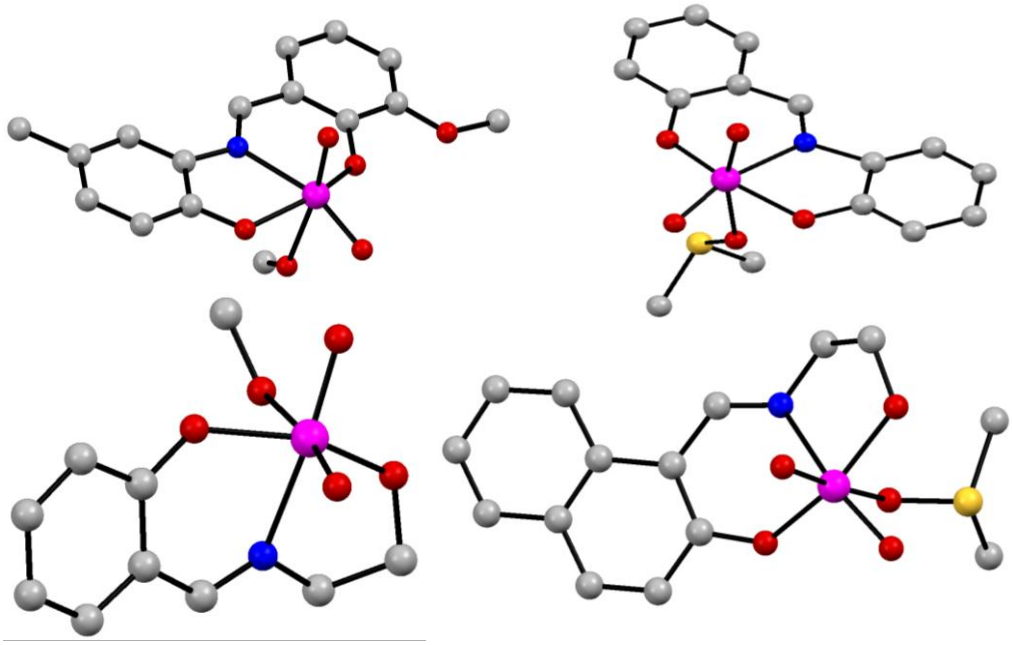

Fig. 1.2. Molecular structures of *cis*-$\{MoO_2\}^{2+}$ complexes of some tridentate Schiff bases derived from 2-carbonylphenol and 2-aminophenols or 2-aminoalcohols.

The acid hydrazones derived from acid hydrazides and various aromatic or aliphatic carbonyl compounds are another important class of Schiff bases. The acid hydrazones (aromatic/aliphatic) of 2-carbonylphenols and 1,3-diketones in the deprotonated state are known to act as tridentate phenolate-O, azomethine-N and amidate-O donor ligands [38,39]. These ligands also coordinate the metal center in a meridional fashion. As discussed in the previous section, a monodentate neutral ligand such as water [40,41], alcohol [42-44], N-oxide [45], phosphine oxide [46,47], N-donor ligand

[48,49] and amide [50] occupies the labile vacant coordination site *trans* to one of the oxo ligands (Fig. 1.3).

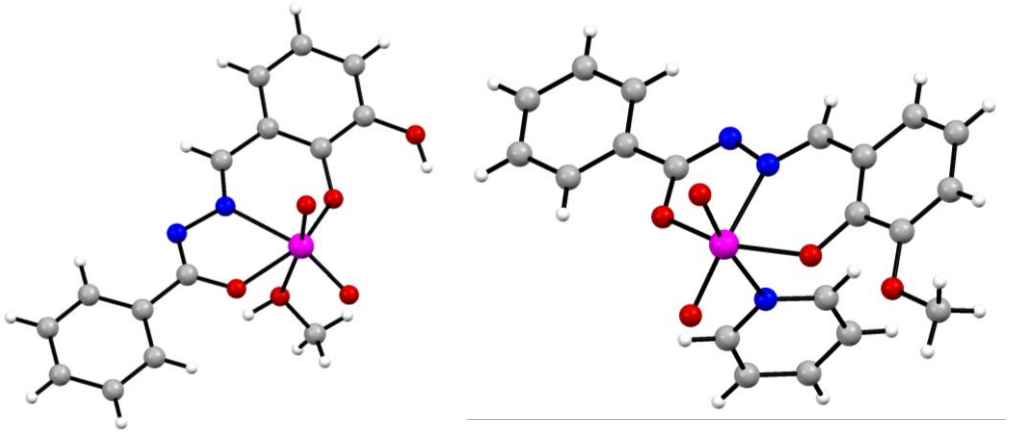

Fig. 1.3. Examples of *cis*-$\{MoO_2\}^{2+}$ complexes with acid hydrazides and 2-carbonylphenol condensates.

Apart from the biological activities of thiosemicarbazide based Schiff bases [51, 52], they also serve as dianionic tridentate ligands [53]. Several *cis*-$\{MoO_2\}^{2+}$ complexes with thiosemicarbazones of 2-carbonylphenols were reported with their structural characteristics. The thiosemicarbazones behave meridionally spanning phenolate-O, azomethine-N and amide-N or thioamidate-S (ONN or ONS) coordinating ligands in these complexes [54–59]. A couple of examples are depicted in Fig. 1.4.

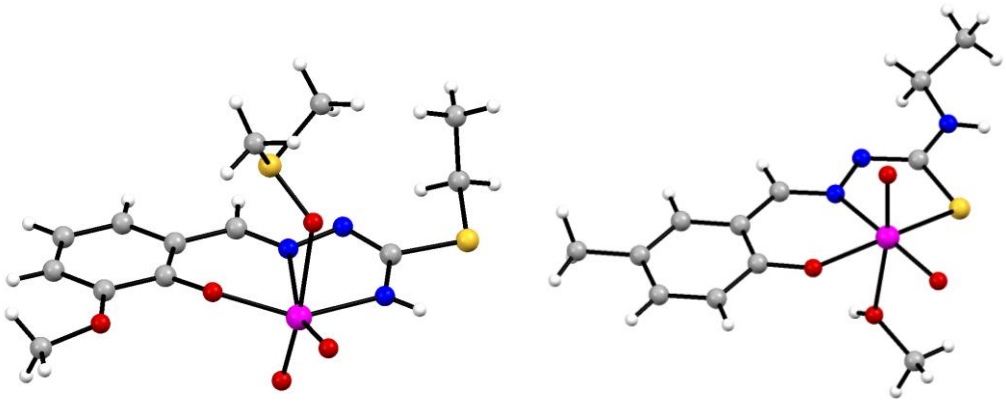

Fig 1.4. Examples for thiosemicarbazide based Schiff base complexes of *cis*-$\{MoO_2\}^{2+}$.

1.2.3. Tetradentate ligands

1.2.3.1. Tripodal ligands

Tripodal ligands are a versatile class of compounds and their metal complexes have found applications in a wide variety of research areas such as activation of small molecules [60], stabilization and scrutiny of reactive intermediates [61], biomodeling and biomimicking [60,62], catalysis in organic synthesis [63] and sensors [64]. The *cis*-$\{MoO_2\}^{2+}$ complexes with tripodal tetradentate ligands are relatively less compared to the *cis*-$\{MoO_2\}^{2+}$ complexes with bi- and tridentate Schiff bases. The ONNO [65–68] or ONOO [69–73] donor tripodal ligands are known to form very stable complexes with *cis*-$\{MoO_2\}^{2+}$ core (Fig. 1.5).

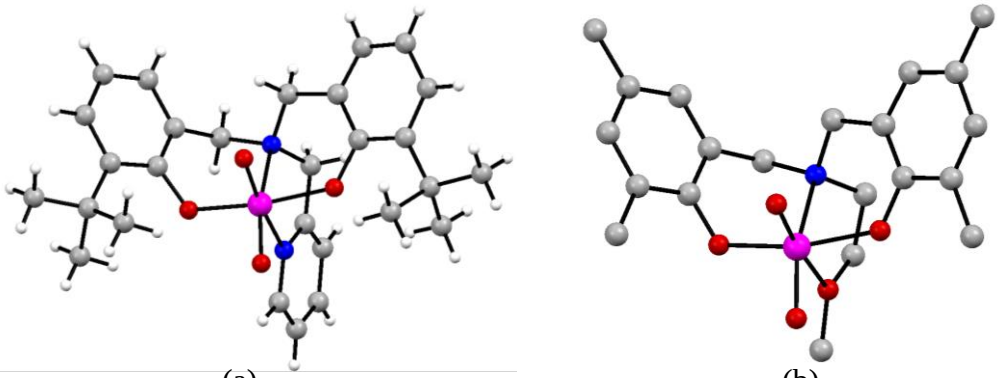

(a) (b)

Fig 1.5. Examples for *cis*-$\{MoO_2\}^{2+}$ complexes with tetradentate tripodal ligands.

1.2.3.2. Linear ligands

Tetradentate linear ligands based on diamines are also very important in coordination chemistry because of their greater order of flexibility and tunability. Complexes of this type of ligands are of considerable interest due to their potential applications in medicinal chemistry [74], stereoselective catalysis [75,76], metallo enzyme models [77] etc,. Like the *cis*-$\{MoO_2\}^{2+}$complexes of tripodal ligands, the linear tetradendate ligand containing complexes of this core are also limited [65,68,78–83]. The

complexes reported [65,68,78–83] so far are mostly with symmetrical linear tetradentate ligands as shown in Fig. 1.6.

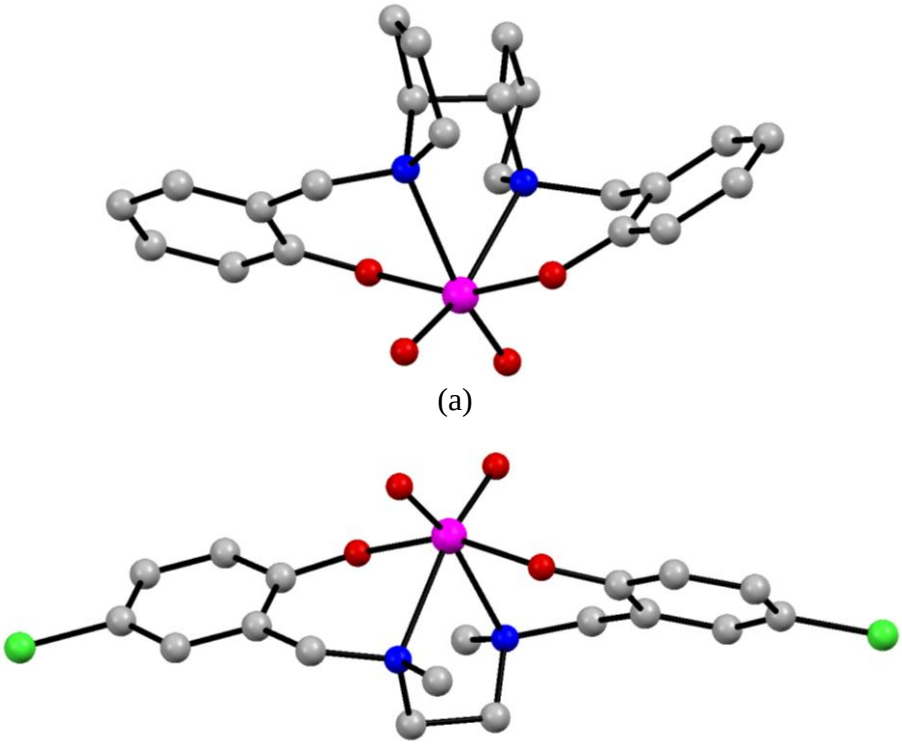

(a)

(b)

Fig 1.6. Examples for *cis*-$\{MoO_2\}^{2+}$ complexes with symmetrical linear flexible tetradentate ligands.

1.3. Catalytic applications of *cis*-$\{MoO_2\}^{2+}$ complexes

cis–dioxomolybdenum(VI) complexes are known to catalyze various organic reactions such as oxidation of alchohols [84], alkenes [84–86], alkanes [84,85], sulfides [85–88], phosphine[88], and xanthine [87]. The oxo–peroxo molybdenum(VI) species produced from *cis*–dioxomolybdenum(VI) complexes are considered to be the active species in these catalytic oxidation reactions [89]. The *cis*–dioxomolybdenum(VI) complexes are also employed as catalysts in various other than oxidation reactions such as hydrosilylation of carbonyl compounds [82,90,91], reduction of dinitrogen to ammonia [92], reductive pinacol coupling [80] and benzaldehyde and indole coupling [49].

The chiral complexes of *cis*-$\{MoO_2\}^{2+}$ core were also isolated and tested as catalysts in asymmetric epoxidation reactions [93,94]. Apart from the catalytic applications discussed above, complexes of *cis*-$\{MoO_2\}^{2+}$ also show haloperoxidase activities (Chart 1.4) which are commonly associated with various oxovanadium(IV/V) complexes [95–98]. A variety of substrates such as olefins, carbonyl compounds, phenols, aromatic amines etc. were used to explore the haloperoxidase activities of molybdenum complexes. Among all molybdenum based haloperoxidase models, majority of the examples were studied as bromoperoxidases. However, the amount of reported literature on *cis*–dioxomolybdenum(VI) complexes as haloperoxidases is very little [99–102]

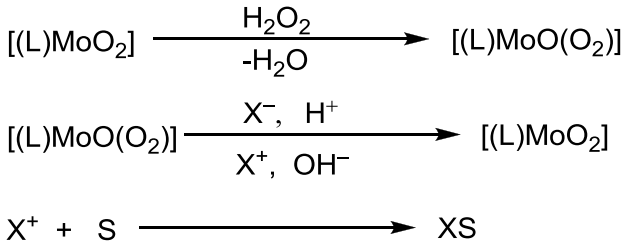

Chart 1.4. Haloperoxidase activity of *cis*-$\{MoO_2\}^{2+}$ complexes.

1.4. About the present investigation

In the present investigation, we have explored the coordination chemistry of *cis*-$\{MoO_2\}^{2+}$ with two tridentate Schiff base systems, a series of tetradentate tripodal aminotriols and a series of unsymmetrical tetradentate linear diaminodiols (Chart 1.5). The first series of tridentate Schiff bases were derived from 2-hydrazinopirydine and salicylaldehyde derivatives, while the second series of tridentate Schiff bases were obtained from the reactions of 2-pyridinealdehyde and 2-aminophenol derivatives. A novel metal assisted ligand transformation has been encountered during our study with the second tridentate Schiff base system. The tetradentate tripodal aminotriols are Mannich condensates of diethanolamine and 4-alkylphenols. The tetradentate linear diaminodiols are reduced imines derived from *N*-(2-hydroxyethyl)ethylenediamine and salicylaldehyde derivatives. The

bromoperoxidase activities of the complexes isolated with tetradentate tripodal ligands and tetradentate linear ligands were assessed. Their catalytic abilities in benzoin oxidation and sulfide oxidation reactions were also scrutinized.

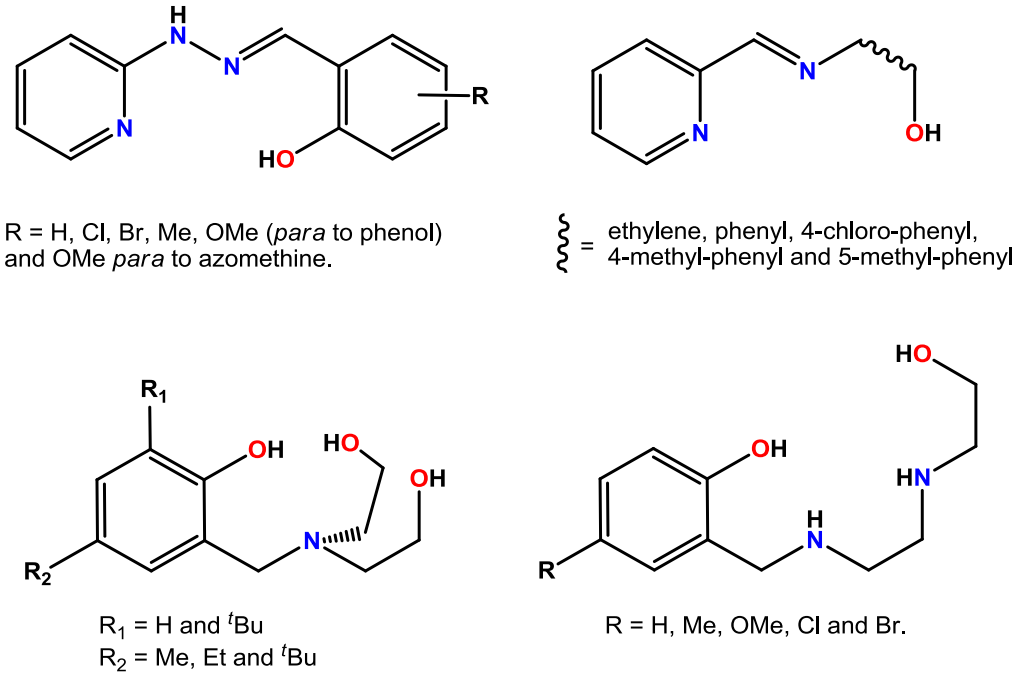

Chart 1.5. Tridentate Schiff bases, tetradentate tripodal aminotriols and tetradentate linear diaminodiols.

1.5. References

[1] C.L. Rollinson, *Inorg. Chem*., 21, **1973**, 691.

[2] S.D. Reid, *Compa. Biochem. Physio. Part C.*, 133, **2002,** 355–367.

[3] C. Kisker, H. Schindelin, D.C. Rees, *Annu. Rev. Biochem*., 66, **1997,** 233–67.

[4] V.M. Sardesai, *Nutr. Clin. Prac*., 8, **1983**, 277–281.

[5] H. Pfeiffer, M. Dragoun, A. Prokop, U. Schatzschneider, *Z. Anorg. Allg. Chem.*, 639, **2013**, 1568–1576.

[6] J. Feng, X.-M. Lu, G. Wang, S.-Z. Du, Y.-F. Cheng, *Dalton. Trans*., 41, **2014**, 8697–8702.

[7] M.L.H Nair, D. Thankamani, *Indian. J. Chem*., 48A, **2009**, 1212–1218.

[8] S.K. Sridhar, M. Saravanan, A. Ramesh, *Eur. J. Med. Chem*., 36, **2001**, 615–625.

[9] K. Saraswat, R. Kant, *De. Phar. Chim*., 5, **2013**, 347–356.

[10] N. Kanoongo, R.V. Singh, J.P Tandun, R.B. Goyal, *J. Inorg. Bio–Chem.*, 38, **1990**, 57–67.

[11] A. Syamal, M.R. Maurya, *Coord. Chem. Rev*., 95, **1989**, 183−238.

[12] R.D. Chakravarthy, D.K. Chand, *J. Chem. Sci*., 123, **2011**, 187−199.

[13] V.V. Zelentsov, I.A. Savich, V.I. Spitsyn, *Naukchn. DokI. Vyssh. Shk. Khim. Khim. Tekhnol.*, **1958**, 54–61.

[14] K. Yamanouchi, S. Yamada, *Inorg. Chim. Acta*., 9, **1974**, 83–87.

[15] S.O. Oh, B.K. Koo, *Taehan Hwa Hakhoe Chi.*, 30, **1986**, 441–447.

[16] K. Tsukuma, T. Kawaguchi, T. Watanabi, *Acta. Cryst: Sect. B*., 31, **1975**, 2165–2167.

[17] A.D. Garnovskii, V.L. Abramenko, *Zh. Obshch. Khim.*, 55, **1985,** 1836–1843.

[18] A. Syamal, S. Ahmed, D. Kumar, *Indian J. Chem.*, 28A, **1989**, 783–786.

[19] M. Cindric, N. Strukan, V. Vrdoljak, B. Kamenar, *Z. Anorg. Allg. Chem.*, 630, **2004**, 585–590.

[20] M.M. Ardakani, Z. Taleat, H. Beitollahi, M.S. Niasari, B.B.F. Mirjalili, N. Taghavinia, *J. Electroanal. Chem*., 624, **2008**, 73–78.

[21] S. Karahan, P. Kose, E. Subasi, H. Temel, Synth. React. *Inorg., Met.-Org., Nano-Met. Chem*., 38, **2008**, 422–427.

[22] M.S. Niasari, M. Bazarganipour, *Transition Met. Chem*., 33, **2008**, 751–757.

[23] K. Lal, J. Singh, S.P. Gupta, *J. Inorg. Nucl. Chem*., 40, **1978**, 359–361.

[24] H. Singh, U.K. Rathi, N. Singh, *J. Indian Chem. Soc*., 57, **1980**, 475–477.

[25] S.D. Sid, O.B. Baitich, Synth. React. *Inorg. Met.-Org. Chem*., 23, **1993**, 1693–1708.

[26] B.H. Mehta, F.F. Syed, *Asian J. Chem*., 14, **2002**, 732–738.

[27] O.A. Rajan, A. Chakravorty, *Inorg. Chem*., 20, **1981**, 660–664.

[28] J.A. Craig, E.W. Harlan, B.S. Snyder, M.A. Whitener, R.H. Holm, *Inorg. Chem*., 29, **1989**, 2082–2091.

[29] W. Bansse, J. Fliegner, S. Sawusch, U. Schilde, E. Uhlemann, *Z. Naturforsch. B: Chem. Sci*., 53, **1998**, 689–693.

[30] L.B. Jerzykiewicz, J.M. Sobczak, J.J. Ziolkowski, *J. Chem. Res., Synop.*, **2000**, 423–425.

[31] D. Agustin, C. Bibal, B. Neveux, J.-C. Daran, R. Poli, *Z. Anorg. Allg. Chem*., 635, **2009**, 2120–2125.

[32] S. Alghool, C. Slebodnick, *Polyhedron*, 67, **2014**, 11–18.

[33] S.L. Pandhare, R.R. Jadhao, V.G. Puranik, P.V. Joshi, F. Capet, M.K. Dongare, S.B. Umbarkar, C. Michon, F.A. Niedercorn, *J. Organomet. Chem*., 772–773, **2014**, 271–279.

[34] M. Cindric, N. Strukan, V. Vrdoljak, T. Kajfez, B. Kamenar, *Z. Anorg. Allg. Chem.*, 628, **2002**, 2113–2117.

[35] T. Glowiak, L. Jerzykiewicz, J.M. Sobczak, J.J. Ziolkowski, *Inorg. Chim. Acta.*, 356, **2003,** 387–392.

[36] S.-B. Ding, *Synth. React. Inorg., Met.-Org., Nano-Met. Chem.*, 43, **2013**, 877–881.

[37] V.S. Sergienko, V.L. Abramenko, Y.N. Mikhailov, M.D. Surazhskaya, *Russ. J. Inorg. Chem.*, 59, **2014**, 1259–1262.

[38] S.Pal, *Rev. Inorg. Chem*., 29, **2009**, 111–130.

[39] W. Plass, *Coord. Chem. Rev*., 237, **2003**, 205–212.

[40] H. Sur, R. Ghosh, S. Roychowdhari, S. Seth, *Acta. Cryst., Sect. C*., C47, **1991**, 306–308.

[41] N.-Y. Jin, *J. Coord. Chem*., 65, **2012**, 4013–4022.

[42] I. Sheikhshoaie, V. Langerb, S.A. Ali, *Acta. Cryst., Sect E*., E67, **2011**, m839–m840.

[43] A.-M. Li, *J. Coord. Chem*., 67, **2014**, 1022–1031.

[44] M. Nandy, S. Shit, C. Rizzoli, G. Pilet, S. Mitra, *Polyhedron*, 88, **2015,** 63–72.

[45] Prabhakaran, P. Chathakudam, B.G Nair, *Transition. Met. Chem*., 8, **1983**, 368–371.

[46] W. Banße, E. Ludwig, U. Schilde, E. Uhlemann, F. Weller, A. Lehmann, *Z. anorg. allg. Chem*., 621, **1995**, 1275–1281.

[47] W. Banße, J. Fliegner, S. Sawusch, U. Schilde, E. Uhlemann, *Zeitsch. Für. Natur. B.*, 53, **1998**, 689–693.

[48] R. Dinda, P. Sengupta, S. Ghosh, H. Figge, W.S. Sheldrick , *J. Chem. Sci: Dalton. Trans.*, **2002**, 4434–4439.

[49] S.Y. Ebrahimipour, H. Khabazadeh, J. Castro, I. Sheikhshoaie, A. Crochet, K.M. Fromm, *Inorg. Chim. Acta*., 427, **2015**, 52–61.

[50] N.K. Ngan, K.M. Lo, C.S.R. Wong, *Polyhedron*, 30, **2011**, 2922–2932.

[51] K.C. Agrawal, A.C. Sartorelli, *Prog. Med. Chem*., 15, **1978**, 321–356.

[52] J.R. Dimmock, R.N. Puthucode, J.M. Smith, M. Hetherington, J.W. Quail, U. Pugazhenthi, J. Lechler, J.P. Stables, *J. Med. Chem*., 39, **1996**, 3984–3997.

[53] D.X. West, A.E. Liberta, S.B. Padhye, R.C. Chikate, P.B. Sonawane, A.S. Kumbhar, R.G. Yerande, *Coord. Chem. Rev*., 123, **1993**, 49–71.

[54] R. Takjoo, A. Akbari, M. Ahmadi, H.A. Rudbari, G. Bruno, *Polyhedron*, 55, **2013**, 225–232.

[55] S. Duman, I. Kizilcikli, B. Ulkuseven, *Phosp. Sulf. Silic*., 190, **2015,** 342–351.

[56] B.I. Ceylan, N.G. Deniz, S. Kahraman, B. Ulkuseven, *Spect. Chim. Acta.*, 141, **2015**, 272–277.

[57] M.A. Husseina, T.S. Guan, R.A. Haque, M.B.K. Ahamed, A.M.S. Abdul Majid, *Spect. Chim. Acta*., 136, **2015**, 1335–1348.

[58] N.K. Ngan, C.S. Wong, K.M. Lo, *J. Chem. Crystsllogr*., 41, **2011,** 1700–1706.

[59] M.A. Husseina, T.S. Guan, R.A. Haque, M.B.K. Ahamed, A.M.S. Abdul Majid, *Inorg. Chim. Acta*., 421, **2014**, 270–283.

[60] X. Hu, K. Meyer, *J. Organomet. Chem*., 690, **2005**, 5474–5484.

[61] J.G. Verkade, *Acc. Chem. Res*., 26, **1993**, 483–489.

[62] A.S. Borovik, *Acc. Chem. Res*., 38, **2005**, 54–61.

[63] S. Yamaguchi, H. Masuda, *Sci. Technol. Adv. Mater*., 6, **2005**, 34–47.

[64] B. Kuswandi, Nuriman, W. Verboom, D.N. Reinhoudt, *Sensors*, *6*, **2006**, 978−1017.

[65] C.J. Hinshaw, G. Peng, R. Singh, J.T. Spence, J.H. Enemark, M. Bruck, J. Kristofzski, S.L. Merbs, R.B. Ortega, P.A. Wexler, *Inorg. Chem.*, 28, **1989**, 4483–4491.

[66] Y.L. Wong, L.H. Tong, J.R. Dilworth, D.K.P. Ng, H. K. Lee, *Dalton Trans.*, 39, **2010**, 4602–4611.

[67] F. Madeira, S. Barroso, S. Namorado, P.M. Reis, B. Royo, A.M. Martins, *Inorg. Chim. Acta*., 383, **2012**, 152−156.

[68] X. Lei, N. Chelamalla, *Polyhedron*, 49, **2013**, 244–251.

[69] S. Khatua, H. Stoeckli−Evans, T. Harada, R. Kuroda, M. Bhattacharjee, *Inorg. Chem*., 45, **2006**, 9619–9621.

[70] S. Khatua, T. Harada, R. Kuroda, M. Bhattacharjee, *Chem. Commun*., **2007**, 3927–3929.

[71] L.H. Tong, Y. L. Wong, H.K. Lee, J. R. Dilworth, *Inorg. Chim. Acta*., 383, **2012**, 91–97.

[72] A. Riisioe, A. Lehtonen, M.M. Hanninen, R. Sillanpää, *Eur. J. Inorg. Chem.*, **2013** 1499–1508.

[73] T. Heikkila, R. Sillanpää, A. Lehtonen, *J. Coord. Chem*., 67, **2014**, 1863–1872.

[74] A.E. Martella, R.J. Motekaitis, Y. Sun, R. Ma, M.J. Welch, T. Pajeau, *Inorg. Chimi. Act., 291, **1999**, 238–246.*

[75] P.D. Knight, P. Scott, *Coord. Chem. Rev*., 242, **2003**, 125–143.

[76] M. Kannan, T. Punniyamurthy, *Tetrahedron:Asymmetry*, 25, **2014**, 1331–1339.

[77] M. Vaidyanathan, M. Palaniandavar, *Proc.Indian Acad. Sci., Chem. Sci.*, 112, **2000**, 223–238.

[78] A. Lehtonen, R. Sillanpää, *Polyhedron*, 24, **2005**, 257–265.

[79] A.K Duhme-Klair, G. Vollmer, C. Mars, R. Fröhlich, *Angew. Chem. Int. Ed.*, 39, **2000**, 1626–1628.

[80] H. Yang, H. Wang, Z. Chengjian, *J. Org. Chem*., 72, **2007**, 10029–10034.

[81] C.J. Whiteoak, G.J.P. Britovsek, V.C. Gibson, A.J.P. White, *Dalton Trans.*, **2009**, 2337–2344.

[82] J.E. Ziegler, G. Du, P.E. Fanwick, M.M. Abu-Omar, *Inorg. Chem*., 48, **2009**, 11290–11296.

[83] R. Mayilmurugan, P. Traar, J.A. Schachner, M. Volpe, N.C. Mösch-Zanetti, *Eur. J. Inorg. Chem*., **2013**, 3664–3670.

[84] H. Arzoumanian, *Coord. Chem. Rev*., 178-180, **1998**, 191−202.

[85] T. Punniyamurthy, S. Velusamy, J. Iqbal, *Chem. Rev.*, 105, **2005** 2329−2364.

[86] F. Romano, A. Linden, M. Mba, C. Zonta, G. Licini, *Adv. Synth. Catal*., 352, **2010**, 2937−2942.

[87] R.H. Holm, *Coord. Chem. Rev*., 100, **1990**, 183–221.

[88] S.C.A. Sousa, A.C. Fernandes, *Coord. Chem. Rev*., 284, **2015**, 67–92.

[89] M. Amini, M.M. Haghdoost, M. Bagherzadeh, *Coord. Chem. Rev*., 257, **2013**, 1093–1121.

[90] M.R. Patrícia, C.C. Romao, B. Royo, *Dalton. Trans*., **2006**, 1842–1846.

[91] P.J. Costa, C.C. Rom, A.C. Fernandes, B. Royo, P.M. Reis, M.J. Calhorda, *Chemistry*, 13, **2007**, 3934–3941.

[92] D. Sengupta, S. Gangopadhyay, M.G.B. Drewc, P.K. Gangopadhyay, *Dalton. Trans*., 44, **2015**, 1323–1331.

[93] K.R. Jain, W.A. Herrmann, F.E. Kuhn, *Coord. Chem. Rev*., 252, **2008**, 556–568.

[94] A.J. Burke, *Coord. Chem. Rev*., 252, **2008**, 170–175.

[95] A.G.J. Ligtenbarg, R. Hage, B.L. Feringa, *Coord. Chem. Rev*., 237, **2003**, 89–101.

[96] A. Podgoršek, M. Zupan, J. Iskra, *Angew. Chem. Int. Ed*., 48, **2009**, 8424–8450.

[97] V. Conte, A. Coletti, B. Floris, G. Licini, C. Zonta, *Coord. Chem. Rev*., 255, **2011**, 2165–2177.

[98] D. Wischang, O. Brücher, J. Hartung, *Coord. Chem. Rev*., 255, **2011**, 2204–2217.

[99] J.J. Boruah, S.P. Das, R. Borah, S.R. Gogoi, N.S. Islam, *Polyhedron*, 52, **2013**, 246–254.

[100] M.R. Mauryaa, S. Dhaka, F. Avecilla, *Polyhedron*, 67, **2014**, 145–159.

[101] S. Pasayat, S.P. Dash, S. Roy, R. Dinda, S. Dhaka, M.R. Maurya, W. Kaminsky, Y.P. Patil, M. Nethaji, *Polyhedron*, 67, **2014**, 1–10.

[102] M.R. Maurya, N. Kumar, F. Avecilla, *J. Mol. Catal. A. Chem*., 392, **2014**, 50–60.

Chapter 2

Complexes of *cis*-$\{MoO_2\}^{2+}$ with a series of NNO-donor pyridine based Schiff bases: Syntheses, structures and properties[§]

Dioxomolybdenum(VI) complexes having the general formula *cis*-$[MoO_2(OMe)(L^n)]$ (**1**−**6)** with the tridentate 2-((2-(pyridin-2-yl)hydrazono)-methyl)phenol and its substituted derivatives (HL^n, n = 1−6) have been synthesized. Elemental analysis and various spectroscopic (IR, UV-Vis, ^{1}H NMR and fluorescence) measurements have been used for the characterization of the complexes. X-ray crystal structures of all the complexes except for one have been determined. In each of these analogous complexes, the metal centre is in distorted octahedral N_2O_4 coordination sphere assembled by the meridionally spanning pyridine-N, azomethine-N and phenolate-O donor $(L^n)^-$, the methoxo-O and the two mutually *cis* oriented oxo groups. In the crystal, the complex molecules are involved in intermolecular N−H···O hydrogen bonding interaction involving the hydrazine NH and the metal coordinated methoxo-O. In four structures, discrete dimeric units are formed through a pair of reciprocal N−H···O hydrogen bonds, while N−H···O bridged linear one-dimesional polymeric structure is formed in the fifth structure.

2.1. Introduction

Coordination complexes of high-valent molybdenum are of considerable interest due to their ability to function as catalysts in a variety of organic oxidation reactions [1−7]. Likewise, hydrazones and their complexes have attracted much attention due to the wide variety of reactivities exhibited by them and their applications in various research areas such as structural, biological, pharmaceutical and materials chemistry [8−16]. Interestingly, in

[§] This work has been published in *Polyhedron*, 42, **2012**, 161−167.

the vast literature available on cisdioxomoybdenum(VI) complexes [17−21], structurally characterized complexes of it with hydrazones are not many. Majority of the complexes belonging to this type are with thiosemicarbazones [22−31] and acyl/aroylhydrazones [32−54] and only a handful are with semicarbazones [55] and heterocyclic hydrazones [56,57]. The N,N,O-donor Schiff base 2-((2-(pyridin-2-yl)hydrazono)methyl)phenol and its substituted derivatives (HL^n) are known to exhibit azo-imine tautomerism involving its −NH−N=CH− fragment [58] and also amino-imino tautomerism involving its 2-pyridine−NH− fragment [59]. Among these tautomeric forms, only the imino form can act as dianionic tridentate ligand and the remaining forms are expected to act as monoanionic tridentate ligand. We have explored the coordination chemistry of *cis*-dioxomolybdenum(VI) with HL^n (n = 1−6) and isolated a series of complexes (**1**−**6)** containing the *cis*-$\{MoO_2(OMe)\}^+$ unit (Chart 2.1). In the following sections, the syntheses, characterization, physical properties and crystal structures of these complexes are described.

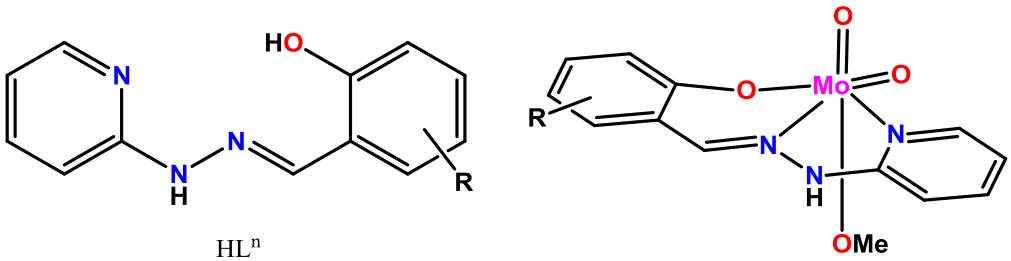

HL^n
(n = 1–5 for R = H, Cl, Br, Me and OMe *para* to OH and n = 6 for R = OMe *para* to azomethine)

cis-$[MoO_2(OMe)(L^n)]$
1–6 (for n = 1-6)

Chart 2.1. Chemical structure diagrams of the Schiff bases and their complexes.

2.2. Experimental

2.2.1. Materials

The Schiff bases (HL^1−HL^6) were prepared from equimolar amounts of 2-hydrazinopyridine and the appropriate substituted salicylaldehyde by following a procedure similar to that reported earlier [60]. Bis(acetylacetonato)dioxomolybdenum(VI) was prepared by following a reported method [61]. All other chemicals and solvents were of analytical grade available commercially and were used as received.

2.2.2. Physical measurements

Elemental (C, H, N) analysis data were obtained with the help of a Thermo Finnigan Flash EA1112 series elemental analyzer. A Shimadzu LCMS 2010 liquid chromatograph mass spectrometer was used for the purity verification. Solution electrical conductivities were measured with the help of a Digisun DI-909 conductivity meter. Magnetic susceptibility measurements were performed with a Sherwood Scientific balance. The infrared spectra were recorded on Jasco-5300 and Nicolet 380 FTIR spectrophotometers. A Shimadzu UV-3600 UV-VIS-NIR spectrophotometer was used to collect the electronic spectra. The fluorescence spectra were recorded using a Horiba Jobin Yvon Fluoromax-4 spectrofluorometer. The ^{1}H NMR spectra were collected with the help of a Bruker 400 MHz NMR spectrometer.

2.2.3. Synthesis of cis-[MoO_2(OMe)(L^n)] (1-6)

All the complexes (**1**−**6**) were prepared by using the following general procedure. Solid [$MoO_2(acac)_2$] (33 mg, 0.1 mmol) was added to a hot methanol solution of the corresponding HL^n (0.1 mmol). The mixture was heated on a steam bath for 45 min. The resulting purple solution was slowly cooled to ambient temperature. After about 12 h the dark crystalline complex

deposited was collected by filtration, washed with ether, hexane and little ice-cold methanol and finally dried in air.

cis-[MoO_2(OMe)(L^1)] (1 (R = H)). Yield: 26 mg (70%). Anal. calcd for $C_{13}H_{13}MoN_3O_4$: C, 42.05; H, 3.53; N, 11.32. Found: C, 42.15; H, 3.58; N, 11.21. Selected IR data (cm^{-1}): 3440 (ν_{N-H}), 1616 ($\nu_{C=N}$), 926 and 910 ($\nu_{cis\text{-}MoO_2}$). ^{1}H NMR data (δ (ppm) (J (Hz))): 7.65 (6) (d, 1H, H^1), 6.11 (7) (t, 1H, H^2), 7.40 (8) (t, 1H, H^3), 6.64 (9) (d, 1H, H^4), 4.12 (s, 1H, NH), 8.42 (s, 1H, H^6), 7.59 (8) (d, 1H, H^8), 7.04 (8) (t, 1H, H^9), 7.28 (8) (t, 1H, H^{10}), 6.90 (8) (d, 1H, H^{11}), 3.20 (s, 3H, $MoOCH_3$).

cis-[MoO_2(OMe)(L^2)] (2 (R = 5-Cl)).Yield: 30 mg (74%). Anal. calcd for $C_{13}H_{12}ClMoN_3O_4$: C, 38.47; H, 2.98; N, 10.36. Found: C, 38.65; H, 2.91; N, 10.21. Selected IR data (cm^{-1}): 3452 (ν_{N-H}), 1616 ($\nu_{C=N}$), 932 and 910 ($\nu_{cis\text{-}MoO_2}$). ^{1}H NMR data (δ (ppm) (J (Hz))): 7.67 (6) (d, 1H, H^1), 6.16 (6) (t, 1H, H^2), 7.32 (8) (t, 1H, H^3), 6.67 (9) (d, 1H, H^4), 4.12 (s, 1H, NH), 8.39 (s, 1H, H^6), 7.71 (s, 1H, H^8), 7.39 (11) (d, 1H, H^{10}), 6.92 (9) (d, 1H, H^{11}), 3.20 (s, 3H, $MoOCH_3$).

cis-[MoO_2(OMe)(L^3)] (3 (R = 5-Br)).Yield: 33 mg (73%). Anal. calcd for $C_{13}H_{12}BrMoN_3O_4$: C, 34.67; H, 2.69; N, 9.34. Found: C, 34.33; H, 2.76; and N, 9.23. Selected IR data (cm^{-1}): 3440 (ν_{N-H}), 1616 ($\nu_{C=N}$), 937 and 904 ($\nu_{cis\text{-}MoO_2}$). ^{1}H NMR data (δ (ppm) (J (Hz))): 7.67 (6) (d, 1H, H^1), 6.16 (6) (t, 1H, H^2), 7.32 (8) (t, 1H, H^3), 6.67 (9) (d, 1H, H^4), 4.13 (s, 1H, NH), 8.39 (s, 1H, H^6), 7.83 (s, 1H, H^8), 7.51 (9) (d, 1H, H^{10}), 6.86 (9) (d, 1H, H^{11}), 3.20 (s, 3H, $MoOCH_3$).

cis-[MoO_2(OMe)(L^4)] (4 (R = 5-Me)). Yield: 32 mg (83%). Anal. calcd for $C_{14}H_{15}MoN_3O_4$: C, 43.63; H, 3.93; N, 10.91. Found: C, 43.56; H, 3.85; N, 10.67. Selected IR data (cm^{-1}): 3458 (ν_{N-H}), 1622 ($\nu_{C=N}$), 931 and 908 ($\nu_{cis\text{-}MoO_2}$). ^{1}H NMR data (δ (ppm) (J (Hz))): 7.64 (5) (d, 1H, H^1), 6.09 (6) (t, 1H, H^2), 7.27 (8) (t, 1H, H^3), 6.62 (9) (d, 1H, H^4), 4.13 (s, 1H, NH), 8.34 (s,

1H, H^6), 7.29 (s, 1H, H^8), 2.30 (s, 3H, CH_3 at C^9), 7.21 (8) (d, 1H, H^{10}), 6.78 (8) (d, 1H, H^{11}), 3.20 (s, 3H, $MoOCH_3$).

cis-[MoO_2(OMe)(L^5)] (5 (R = 5-OMe)). Yield: 32 mg (80%). Anal. calcd for $C_{14}H_{15}MoN_3O_5$: C, 41.89; H, 3.77; N, 10.48. Found: C, 41.55; H, 3.71; and N, 10.31. Selected IR data (cm^{-1}): 3454 (ν_{N-H}), 1622 ($\nu_{C=N}$), 926 and 904 ($\nu_{cis\text{-}MoO_2}$). ^{1}H NMR data (δ (ppm) (J (Hz))): 7.64 (6) (d, 1H, H^1), 6.10 (6) (t, 1H, H^2), 7.27 (7) (t, 1H, H^3), 6.63 (9) (d, 1H, H^4), 4.12 (s, 1H, NH), 8.36 (s, 1H, H^6), 7.18 (s, 1H, H^8), 3.79 (s, 3H, OCH_3 at C^9), 6.82 (9) (d, 1H, H^{10}), 6.98 (9) (d, 1H, H^{11}), 3.20 (s, 3H, $MoOCH_3$).

cis-[MoO_2(OMe)(L^6)] (6 (R = 4-OMe)). Yield: 33 mg (82%). Anal. calcd for $C_{14}H_{15}MoN_3O_5$: C, 41.89; H, 3.77; N, 10.48. Found: C, 41.61; H, 3.71; N, 10.28. Selected IR data (cm^{-1}): 3440 (ν_{N-H}), 1605 ($\nu_{C=N}$), 932 and 899 ($\nu_{cis\text{-}MoO_2}$). ^{1}H NMR data (δ (ppm) (J (Hz))): 7.59 (3) (d, 1H, H^1), 6.00 (6) (t, 1H, H^2), 7.19 (8) (t, 1H, H^3), 6.65 (9) (d, 1H, H^4), 4.14 (s, 1H, NH), 8.36 (s, 1H, H^6), 7.50 (9) (d, 1H, H^8), 6.57 (11) (d, 1H, H^9), 3.82 (s, 3H, OCH_3 at C^{10}), 6.52 (s, 1H, H^{11}), 3.21 (s, 3H, $MoOCH_3$).

2.2.4. X-ray crystallography

Single crystals of **1**−**4** and **6** were collected from the crystalline materials obtained during their synthesis. Despite our several attempts by various ways we were not able to get X-ray quality crystals of **5**. Determination of the unit cell parameters and the collection of the intensity data at 298 K for each of **1**, **4** and **6** were performed using a Bruker-Nonius SMART APEX CCD single crystal diffractometer, equipped with a graphite monochromator and a Mo $K\alpha$ fine-focus sealed tube (λ = 0.71073 Å). The SMART and SAINT-Plus programs were used for data acquisition and data extraction, respectively [62]. The absorption corrections were performed using the SADABS program [63]. The unit cell parameters and the intensity data at 298 K for both **2** and **3** were obtained on an Oxford Diffraction

Table 2.1. Selected crystallographic data.

Complex	**1**	**2**	**3**	**4**	**6**
Empirical formula	$C_{13}H_{13}MoN_3O_4$	$C_{13}H_{12}ClMoN_3O_4$	$C_{13}H_{12}BrMoN_3O_4$	$C_{14}H_{15}MoN_3O_4$	$C_{14}H_{15}MoN_3O_5$
Formula weight	371.20	405.65	450.11	385.23	401.23
Crystal system	Triclinic	Triclinic	Triclinic	Monoclinic	Monoclinic
Space group	$P\bar{1}$	$P\bar{1}$	$P\bar{1}$	$P2_1/n$	Cc
Unit cell dimensions (Å, °)					
a	7.6919(15)	7.6054(4)	7.5944(6)	9.8571(16)	12.262(2)
b	9.6526(19)	9.6711(6)	9.7310(8)	7.6452(12)	16.565(3)
c	10.511(2)	11.2957(6)	11.3063(10)	20.820(3)	7.5212(13)
α	104.833(3)	105.436(5)	105.722(7)	90	90
β	106.809(3)	106.308(5)	105.136(7)	103.016(2)	97.888(3)
γ	90.242(3)	90.597(5)	91.024(7)	90	90
V (Å), Z	719.6(2), 2	765.37(7), 2	772.85(11), 2	1528.7(4), 4	1513.3(4), 4
ρ (g cm^{-3})	1.713	1.760	1.934	1.674	1.761
μ (mm^{-1})	0.930	1.051	3.454	0.879	0.896
Reflections collected	6897	5100	4879	14029	7149
Reflections unique	2530	2701	2717	2681	2652
Reflections [$I \geq 2\sigma(I)$]	2450	2341	2160	2513	2344
Parameters	191	200	200	201	210
$R1$, $wR2$ [$I \geq 2\sigma(I)$]	0.0281, 0.0728	0.0355, 0.0735	0.0417, 0.0733	0.0303, 0.0796	0.0494, 0.0895
$R1$, $wR2$ (all data)	0.0291, 0.0735	0.0444, 0.0778	0.0588, 0.0816	0.0325, 0.0813	0.0581, 0.0928
GOF on F^2	1.109	1.047	1.032	1.098	1.063
Largest peak & hole (e Å^{-3})	0.457 & − 0.690	0.476 & −0.575	0.591 & −0.595	0.564 & −0.464	0.803 & −0.770

Xcalibur Gemini single crystal X-ray diffractometer using graphite monochromated Mo Kα radiation (λ = 0.71073 Å). The CrysAlisPro software [64] was used for data collection, reduction and absorption correction. The structure of each of the five complexes was solved by direct method and refined on F^2 by full-matrix least-squares procedures. The non-hydrogen atoms were refined using anisotropic thermal parameters. The hydrogen atoms were included in the structure factor calculation at idealized positions by using a riding model. Structure solution and refinement were performed using the SHELX-97 programs [65] available in the WinGX package [66]. The Ortex6a [67], Platon [68] and Mercury [69] packages were used for molecular graphics. X-ray crystallographic data (in CIF format) have been deposited with Cambridge Crystallographic Data Center. Deposition nos. are CCDC 873195–873199 for **1**–**4** and **6**, respectively. The selected crystal data and structure refinement summary for **1**–**4** and **6** are listed in Table 2.1.

2.3. Results and discussion

2.3.1. Synthesis and some properties

The complexes **1**−**6** (Chart 2.1) have been synthesized in very good yields (70−83%) by treating the Schiff bases (HL^n) with [$MoO_2(acac)_2$] in hot methanol under aerobic condition. The elemental analysis data are in good agreement with the general formula of the complexes as [$MoO_2(OMe)(L^n)$]. Magnetic susceptibility measurements indicate the diamagnetic character of **1**−**6** and hence the +6 oxidation state of the metal centre in each of them. The purple complexes are insoluble in acetonitrile and chlorinated solvents such as dichloromethane and chloroform, but moderately soluble in methanol and highly soluble in dimethylformamide and dimethylsulfoxide. However, in dimethylformamide the complexes are not stable. In solution, all the complexes behave as non-electrolyte.

2.3.2. Spectroscopic characterization

2.3.2.1. Infrared spectra

Infrared spectra of HL^n and the corresponding complexes were recorded in KBr disks. Spectra of HL^1 and **1** are shown in Fig.2.1 and the remaining spectra are provided in the appendix at the end of the chapter. The spectra of **1**–**6** display a broad band within 3440−3458 cm^{-1} and a large number of bands with various intensities in the range 1625−400 cm^{-1}.

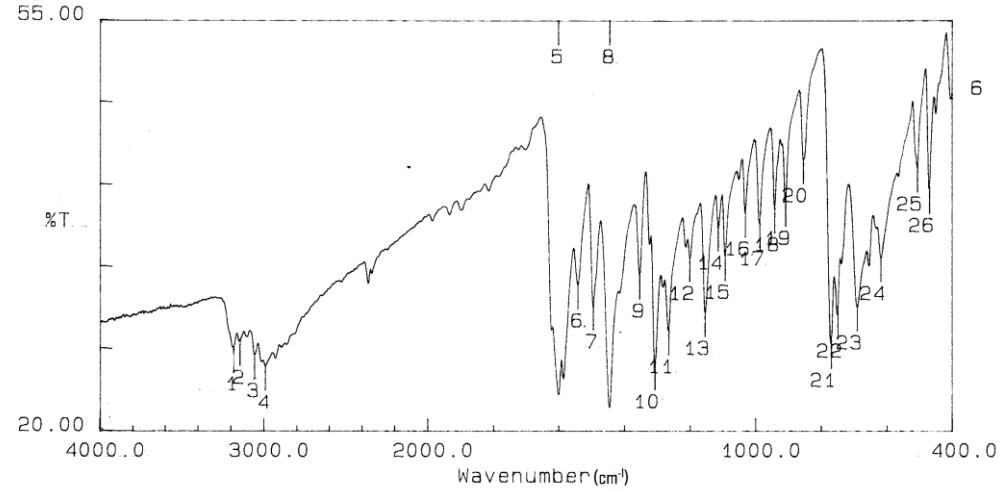

(a)

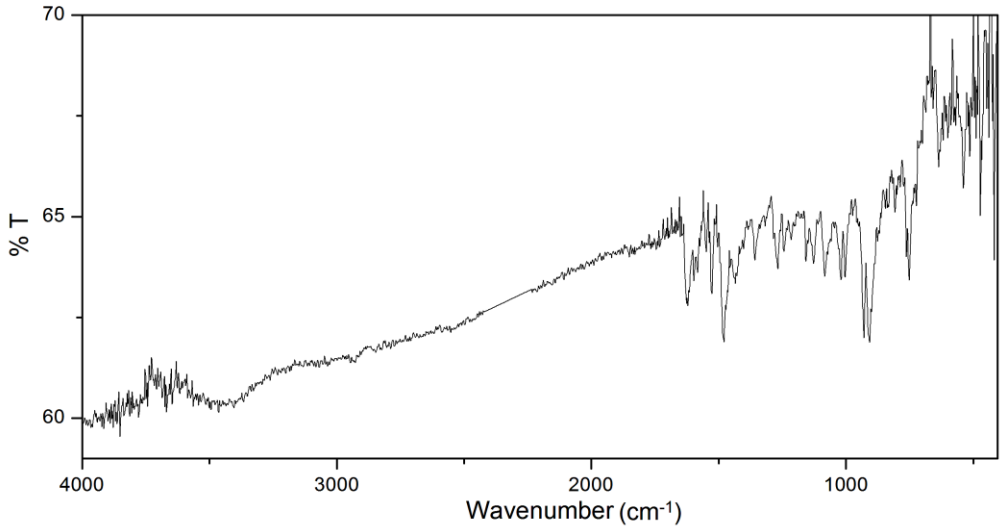

(b)

Fig. 2.1. FTIR spectrum of (a) HL^1 and (b) $[MoO_2(OMe)(L^1)]$ (**1**).

Except for the following we have not tried to assign all the bands. The broad band at ~3450 cm^{-1} is very likely associated with the hydrazine N−H stretch of the ligand $(L^n)^-$. A strong band appeared between 1605−1622 cm^{-1} is attributed to the C=N stretch of $(L^n)^-$ [70]. All the complexes display a pair of strong and sharp bands in the ranges 899−910 and 926−937 cm^{-1} typical of the {*cis*-MoO_2}$^{2+}$ moiety [47,52,53,57,71,72].

2.3.2.2 Electronic and emission spectra

Methanol solutions of Schiff bases and **1**−**6** were used to record the electronic and emission spectra. A representative electronic spectrum is shown in Fig. 2.2. All the spectral data are listed in Table 2.2. The major features in all the spectra are very similar. A broad and moderately strong absorption observed at ~540 nm is followed by a shoulder of similar intensity at ~390 nm and three (**5** and **6**) to four (**1**−**4**) very intense absorptions in the range 350−220 nm. Except for the absorption observed at ~540 nm and small shifts

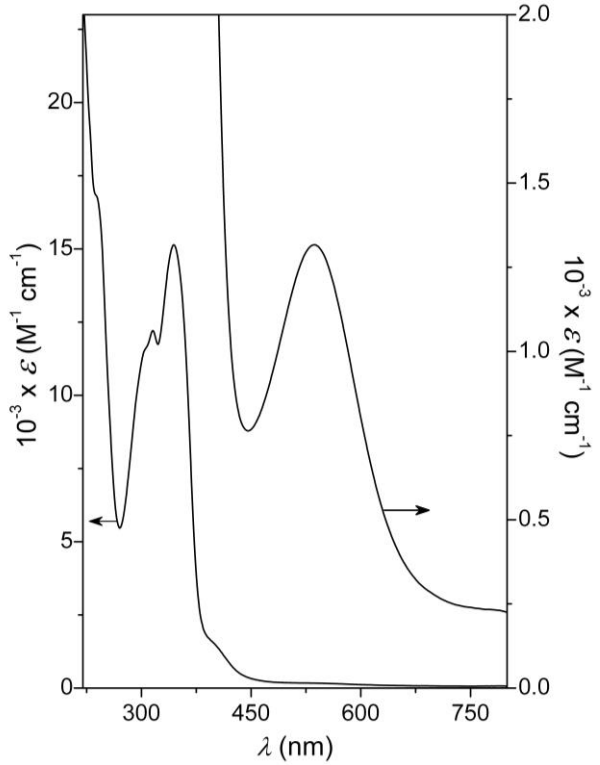

Fig. 2.2. Electronic spectrum of [MoO_2(OMe)(L^2)] (**2**) in methanol.

(by ~5−10 nm) of band positions the spectral profiles of the Schiff bases (HL^1−HL^6) in methanol are very similar with the spectral profiles of **1**−**6**. Thus the lowest energy band is assigned to ligand-to-metal charge transfer transition [24−29,49,53,57] and the remaining absorptions are attributed to ligand centred transitions.

Table 2.2 Electronic[a] and emission[a] spectroscopic data.

Complex	Absorption λ_{max} (nm) ($10^{-3} \times \varepsilon$ (M^{-1} cm^{-1}))	Emission λ_{max} (nm) (excitation at λ nm))
HL^1	390 (2.8),[b] 335 (30.1), 310 (23.1), 298 (20.1),[b] 240 (16.2)	451 (390)
HL^2	395 (4.0),[b] 345 (25.3), 316 (19.6), 305 (18.2),[b] 241 (21.8)	478 (395)
HL^3	395 (3.6),[b] 345 (24.8), 316 (19.6), 305 (11.8),[b] 242 (19.3)	480 (395)
HL^4	395 (1.9),[b] 340 (30.9), 312 (27.3), 302 (25.6),[b] 240 (21.8)	473 (395)
HL^5	410 (1.0),[b] 351 (17.3), 316 (18.3), 310 (18.7),[b] 235 (14.5)	505 (410)
HL^6	395 (2.0),[b] 338 (18.5), 309 (11.8), 245 (10.8)	455 (395)
1	535 (1.6), 385 (6.2),[b] 334 (18.5), 308 (16.3), 297 (16.4), 242 (22.3)[b]	450 (385).
2	537 (1.3), 395 (1.6),[b] 345 (15.1), 317 (12.2), 304 (11.5),[b] 240 (16.7)[b]	460 (395)
3	536 (1.0), 395 (2.2),[b] 345 (10.8), 317 (8.1), 304 (7.4),[b] 240 (10.7)[b]	460 (395)
4	535 (2.6), 395 (3.1),[b] 342 (23.5), 312 (19.9), 304 (19.3),[b] 230 (25.7) [b]	450 (395)
5	538 (1.3), 404 (1.0),[b] 350 (15.2), 312 (16.4), 220 (19.6)[b]	470 (400)
6	545 (1.7), 383 (2.6),[b] 337 (22.1), 308 (13.6),[b] 243 (15.6)	515 (383)

[a] In methanol, [b] Shoulder.

Both Schiff bases and their complexes (Chart 2.1) are emissive in character. Emisssion spectra of HL^1–HL^6 and **1**–**6** were recorded in methanol. Representative spectra are shown in Fig. 2.3. The Schiff bases on excitation at their first absorption (390–410 nm) display a broad emission band in the range 450–505 nm (Fig. 2.3). The emission occurs at the highest energy (450 nm) for the unsubstituted HL^1 and at the lowest energy (505 nm) for HL^5 where the most electron releasing group OMe is at *para* (C^9) to its phenol fragment. However, when the OMe is at *para* to azomethine and *meta* to phenol in HL^6 there is no significant change in the band position (455 nm) when compared with that of the unsubstituted HL^1. For both HL^2 and HL^3 (electron withdrawing Cl and Br at C^9) the emission band appears at 480 nm, while it is observed at 470 nm for HL^4 (electron releasing Me at C^9). Thus

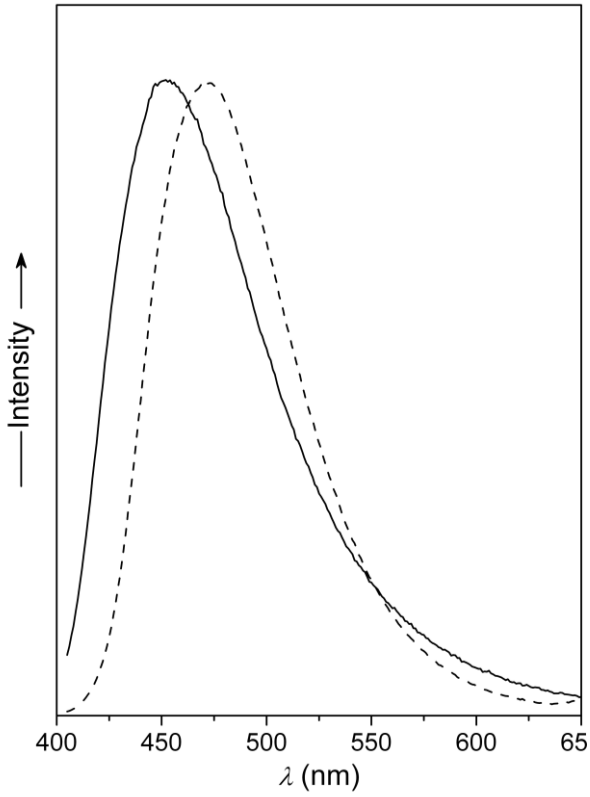

Fig. 2.3. Emission spectra of HL^4 (- - - -) and [MoO_2(L^4)(OMe)] (**4**) (——) in methanol.

there is a definite variation of the band position with the change of the substituent but there is no particular trend in this variation with the electronic nature of the substituent. Interestingly the unchanged pyridine fragment in HL^1–HL^6 is expected to be primarily responsible for their emission behavior. However, the variation of emission band position with the change of substituent on the phenol fragment indicates that, in the excited state, there is a communication between both aromatic parts of these Schiff bases. It may be noted that in the amine form (2-pyridine−NH−) of the pyridine end of HL^n there is no conjugation in the bridge between its two aromatic parts, but the imine form of this end [59] provides the conjugation in the bridge.

In the case of the complexes **1**−**6**, no emission was observed on excitation at the ligand-to-metal charge transfer band position at ~540 nm. As mentioned earlier below 450 nm the electronic spectral profiles and the band positions of the Schiff bases and the corresponding complexes are very similar. Like HL^1–HL^6 on excitation at ~390 nm **1**−**6** also show a broad emission band in the range 450−515 nm (Fig. 2.3). Thus the emission responses of the complexes involve only ligand centred orbitals. The emission occurs at the same position (450 nm) for HL^1 and its complex **1**. However, emission band positions are very different for HL^2–HL^6 and the corresponding complexes **2**−**6**. For each of **2**−**4** there is a blue shift by 20 nm of the emission compared to that of the corresponding Schiff bases HL^2–HL^4, while for **5** the emission is slightly more blue-shifted (by 30 nm) compared to that of HL^5. It may be noted that in **1** the ligand $(L^1)^-$ is unsubstituted and in each of **2**−**5** the substitution is at *para* (C^9) to the phenolate group of the ligand $(L^2)^-$–$(L^5)^-$. This blue shift indicates that perhaps complexation causes more stabilization of the ground state than the excited state and hence a larger energy gap between them in **2**−**5** compared to that in the corresponding Schiff bases. Interestingly for **6** the trend is reversed and the emission is red shifted by 60

nm when compared with the emission of HL^6. Here the most electron releasing substituent OMe is *para* (C^{10}) to the azomethine group. This causes a stronger bonding of the azomethine-N of the ligand $(L^6)^-$ to the metal centre in **6**. The X-ray structure of **6** indeed shows a shorter azomethine-N to Mo bond length compared to that in the other complexes (*vide infra*). This strong bonding may result into increased acidity of the neighboring NH proton and hence its relatively easy dissociation causing a superior conjugated structure of the ligand $(L^6)^-$ in **6** compared to that of the free Schiff base HL^6. Perhaps this increased conjugation in 6 leads to more stabilization of the excited state than the ground state and hence a red-shift of its emission than that of HL^6.

2.3.2 3. NMR spectra

Dimethylsulfoxide-d_6 was used as the solvent in the ^{1}H NMR experiments due to high solubility of **1**−**6** in it. All the spectral data are given under experimental section and the spectra of HL^1 and **1** are illustrated in Fig.2.4. The remaining spectra are given in the appendix at the end of the chapter. As expected none of the complexes display the phenol proton resonance observed for the free Schiff bases (HL^1−HL^6) (Chart 2.1) in the range δ 10.84−11.00 ppm. Overall the spectra of the complexes are very similar indicating same type of coordination of the ligands. Two doublets observed within δ 7.59−7.67 ppm and δ 6.62−6.67 ppm are assigned to the two pyridine ring protons H^1 and H^4. The remaining two pyridine ring protons H^2 and H^3 appear as two triplets at δ 6.00−6.16 ppm and δ 7.19−7.40 ppm, respectively. The proton (H^{11}) *ortho* to the phenolate resonates as a doublet within δ 6.78−6.98 ppm in **1**−**5**, while for 6 the signal for H^{11} appears as a singlet at δ 6.52 due to the presence of the methoxy substituent at C^{10}. In the complex (**1**) containing the unsubstituted ligand $(L^1)^-$, both H^9 and H^{10} resonate as triplet at δ 7.04 and 7.28 ppm, respectively. On the other hand, H^9

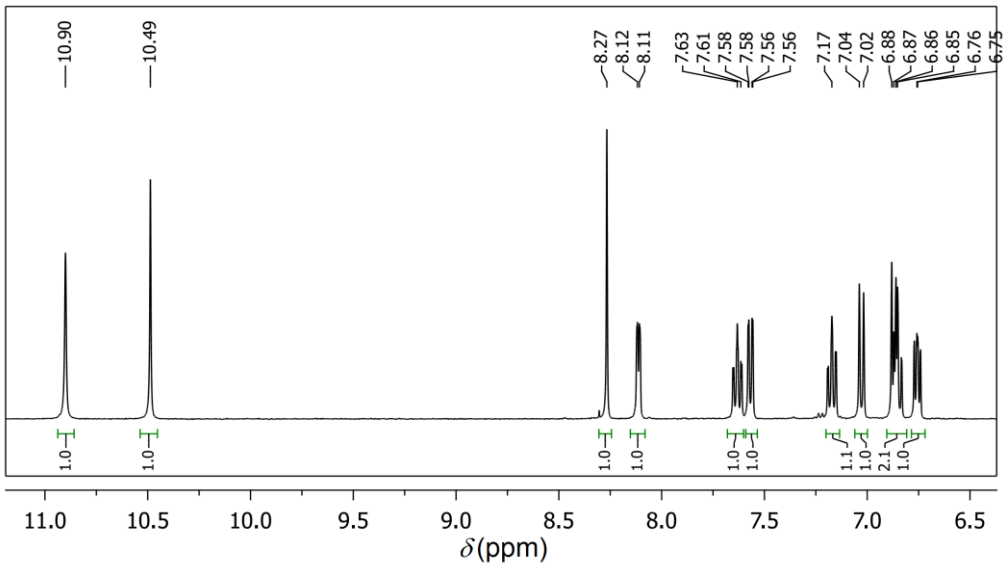

(a)

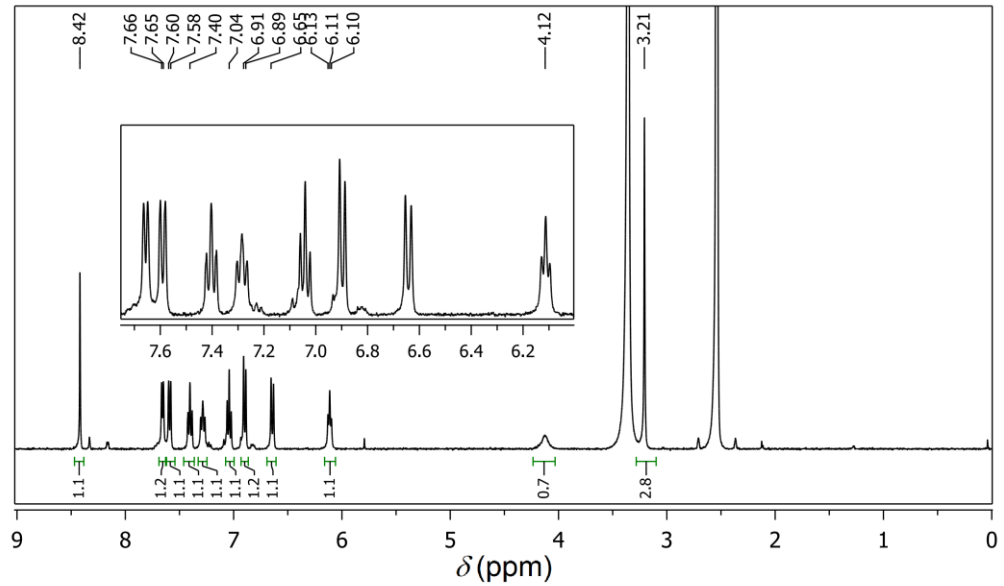

(b)

Fig. 2.4. ^{1}H-NMR spectra of (a) HL^{1} and (b) **1** in dimethylsulfoxide-d_6.

is absent and H^{10} resonates as a doublet in the range δ 6.82−7.51 ppm due to substituent at C^{9} in all of **2**−**5**. In contrast, H^{9} appears as a doublet at δ 6.57 ppm and H^{10} is absent due to the substituent at C^{10} in **6**. In both 1 and 6, H^{8} appears as a doublet at δ 7.59 and 7.50 ppm, respectively, while that in **2**−**5**

resonates as a singlet within δ 7.18−7.83 ppm. The singlet observed in the range δ 8.34−8.42 ppm for all the complexes is attributed to the azomethine (−HC=N−) proton. In HL^1−HL^6 the singlet corresponding to this proton appears within δ 8.21−8.28 ppm. The hydrazine NH proton of HL^1−HL^6 is observed within δ 9.97−10.80 ppm as a singlet. In **1**−**6**, the singlet due to the NH proton shows a significant up-field shift and appears at ~δ 4.13 ppm. In general, the chemical shifts of the aromatic protons in **1**−**6** show an up-field shift but by a much lesser amount (δ 0.50−0.70 ppm) compared to the corresponding chemical shifts observed for the free Schiff bases (HL^1−HL^6). The protons of the methyl substituent at C^9 in HL^4 and in complex 4 are observed as a singlet at δ 2.22 and 2.30 ppm, respectively. The singlet due to the protons of the methoxy substituent at C^9 in HL^5 and at C^{10} in HL^6 appear at δ 3.76 and 3.78 ppm, respectively, while that for their corresponding complexes 5 and 6 is observed at δ 3.79 and 3.82 ppm, respectively. The similar environment around the metal coordinated methoxo methyl group in 1−6 is reflected by the essentially identical chemical shift (δ 3.20 ppm) of the singlet due to its protons.

2.3.4. Description of X-ray structures

Complexes **1**−**4** crystallize in centrosymmetric space groups, while complex **6** crystallizes in the non-centrosymmetric monoclinic *C*c space group (Flack parameter 0.01(6)). The space group for each of **1**−**3** is the triclinic $P\bar{1}$ and for **4** it is monoclinic $P2_1/n$. In all the five structures, the asymmetric unit contains a single complex molecule. The overall molecular structures of **1**−**4** and **6** are very similar. The metal centred bond lengths and angles are listed in Table 2.3. The structures of **1**−**4** are represented in the Figs 2.5 and 2.6. In each complex, the molybdenum atom is in a distorted N_2O_4 coordination sphere. The pyridine-N, the azomethine-N and the phenolate-O donor $(L^n)^-$ is

Table 2.3. Selected bond lengths (Å) and angles (^{o}) for **1**, **2**, **3**, **4** and **6**.

Complex	**1**	**2**	**3**	**4**	**6**
Mo−N1	2.1302	2.1313	2.1293	2.1252	2.1008
Mo−N3	2.2342	2.2433	2.2354	2.2372	2.2125
Mo−O1	1.9192	1.9203	1.9153	1.9132	1.9056
Mo−O2	1.6932	1.6972	1.6963	1.6982	1.6864
Mo−O3	1.6892	1.6983	1.6954	1.6922	1.6755
Mo−O4	2.2942	2.3142	2.3153	2.3112	2.3135
N1−Mo−N3	71.188	71.3810	71.7914	71.378	70.83
N3−Mo−O1	83.138	83.1310	83.2213	83.248	83.62
N1−Mo−O2	93.8210	94.7812	94.5915	93.7810	94.73
N1−Mo−O3	94.9810	94.2713	94.2116	94.4510	92.63
N1−Mo−O4	79.878	79.9911	79.6314	78.838	79.03
N3−Mo−O3	93.939	94.5611	94.2816	93.669	96.33
N3−Mo−O4	76.167	75.849	75.8813	76.427	75.82
O1−Mo−O2	106.21	104.9912	104.7514	105.8410	104.53
O1−Mo−O3	99.0110	99.4613	99.5616	100.1811	101.83
O1−Mo−O4	82.219	82.5310	82.8414	82.729	83.72
O2−Mo−O3	105.1511	105.1312	105.1318	104.8111	104.82
O2−Mo−O4	84.039	83.6911	83.8615	84.049	81.5619
N1−Mo−O1	151.499	151.9010	152.2715	151.439	151.92
N3−Mo−O2	156.849	156.8811	157.2115	157.309	155.02
O3−Mo−O4	169.859	169.9511	169.5914	169.359	170.02

coordinated to the *cis*-$\{MoO_2\}^{2+}$ unit in a meridional fashion. The sixth coordination site is satisfied by the methoxo-O. The conformation of the metal coordinated $(L^n)^-$ is unexceptional and observed before [58,70]. The chelate bite angles for the five- and the six-membered rings are in the ranges 70.8(3)−71.79(14)^o and 83.13(8)−83.6(2)^o, respectively. The remaining *cis* bond angles at the metal centre are within 75.84(9)−106.2(1)^o. The *trans* (phenolate)O−Mo−N(pyridine), (oxo)O−Mo−N(azomethine) and (oxo)O−Mo−O(methoxo) bond angles are in the ranges 151.43(9)−152.27(15)^o, 155.0(2)−157.30(9)^o and 169.35(9)−170.0(2)^o, respectively.

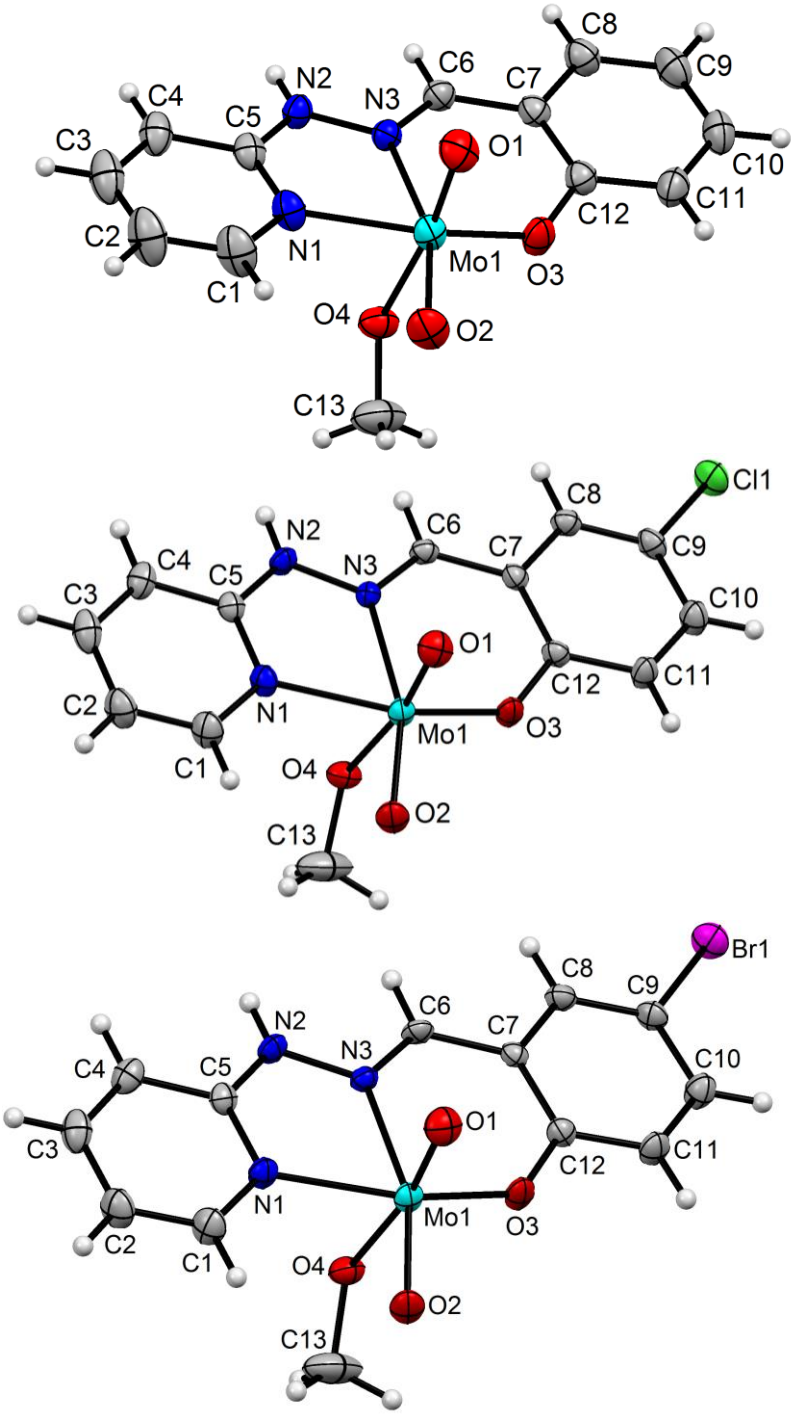

Fig. 2.5. Molecular structures of *cis*-[MoO_2(OMe)(L^1)] (**1**) (top), [MoO_2(OMe)(L^2)] (**2**) (middle) and *cis*-[MoO_2(OMe)(L^3)] (**3**) (bottom) with the atom labeling schemes. All non-hydrogen atoms are represented by their 30% probability thermal ellipsoids.

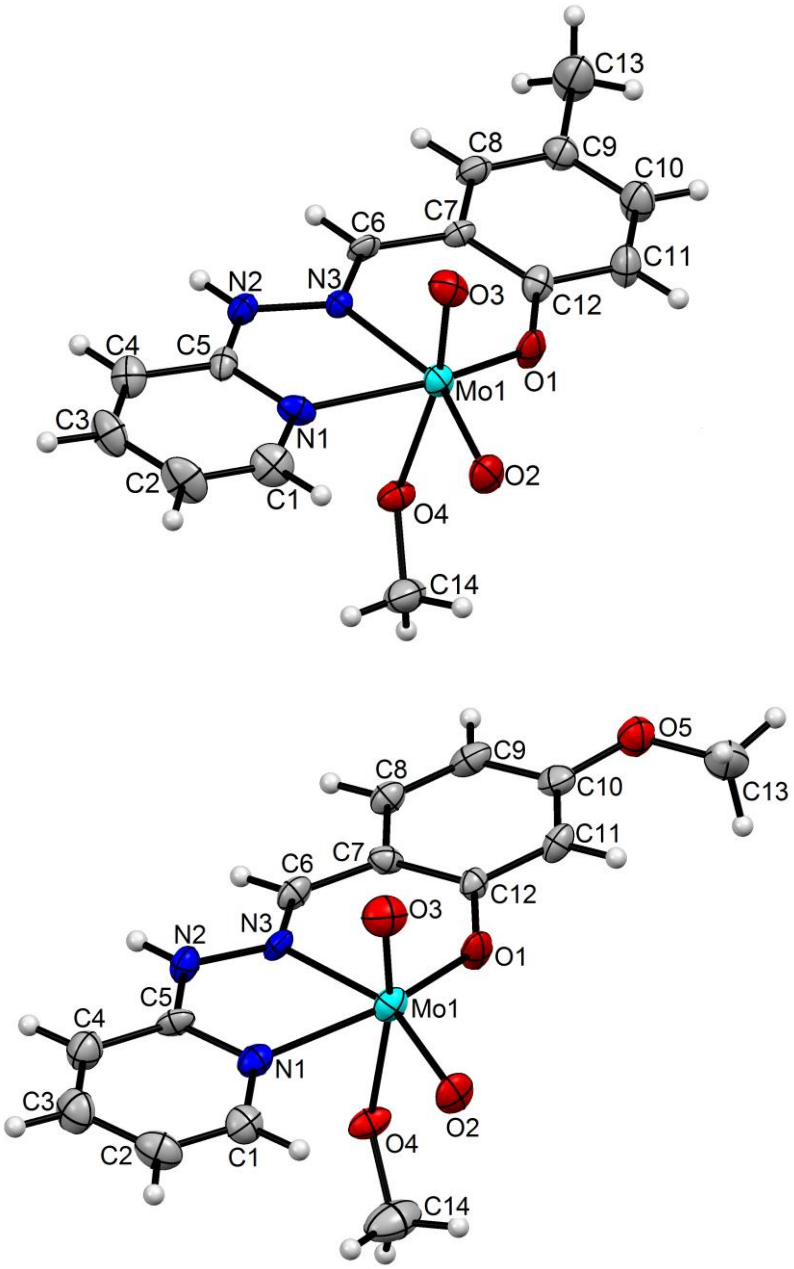

Fig. 2.6. Molecular structures of *cis*-[$MoO_2(OMe)(L^4)$] (**4**) (top) and *cis*-[$MoO_2(OMe)(L^6)$] (**6**) (bottom) with the atom labeling schemes. All non-hydrogen atoms are represented by their 30% probability thermal ellipsoids.

In all the structures, the Mo-atom is shifted from the (ONN)O square-plane (mean deviation 0.02−0.04 Å) constituted by the $(L^n)^-$ and one oxo group (O2) toward the second oxo group (O3) by 0.30−0.32 Å (Table 2.3). The very similar bond lengths associated with the metal centres in **1**−**4** (Table 2.3) indicate that the substituent *para* to the phenolate has no significant influence. Interestingly except for the Mo−O (methoxo) bond the remaining five bond lengths in **6** are shorter than the corresponding bond lengths in **1**−**4** (Table 2.4). It is very likely that the electron releasing OMe group at *para* to the azomethine group makes its N-atom a better donor and hence a shorter Mo−N(azomethine) bond length in **6** than that in **1**−**4**. Perhaps the short middle Mo−N(azomethine) bond forces the terminal phenolate-O and pyridine-N atoms of the rigid tridentate planar $(L^6)^-$ to be closer to the metal and makes the Mo−O(phenolate) and the Mo−N(azomethine) bonds also shorter than the corresponding bonds in **1**−**4**. However, it is not readily apparent why the Mo=O bonds in **6** are shorter than those in **1**−**4**. In general, the bond lengths associated with the Mo-atom in the present series of complexes are within the ranges reported for complexes of *cis*-{MoO_2}$^{2+}$ with similar ligands [22−57].

2.3.5. Hydrogen bonding and self-assembly

Considering the presence of the hydrazine N−H group and several hydrogen bond acceptors in $[MoO_2(OMe)(L^n)]$ we have investigated the intermolecular hydrogen bonding and the ensuing self-assembly pattern for each of **1**−**4** and **6**. During our investigation we have noticed that there is an intermolecular short O···Br contact (3.046(3) Å) in **3** involving one of the two oxo groups (O2) bonded to the metal and the Br substituent of the ligand. The 'checkcif' results show this short contact as 'alert B'. This type of C−Br···O interactions has been called as 'halogen bonding' [73]. However, we have not

considered this interaction or any other non-conventional hydrogen bonding / non-covalent interaction to explore the self-assembled motifs of **1**−**4** and **6**.

Table 2.4. Hydrogen bonding parameters (Å and ^{o}).

Complex	D–H···A	H···A(Å)	D···A(Å)	D–H···A(^{o})
1	N(2)−H(2A)···O(4)^{i}	1.85	2.637(3)	151
2	N(2)−H(2A)···O(4)^{i}	1.91	2.680(3)	148
3	N(2)−H(2A)···O(4)^{ii}	1.91	2.674(5)	148
4	N(2)−H(2A)···O(4)^{iii}	1.89	2.667(3)	149
6	N(2)−H(2A)···O(4)^{iv}	1.84	2.649(8)	155

Symmetry transformations used: (i) −x+1, −y+1, −z+1; (ii) −x, −y+1, −z+1;(iii) −x+1, −y+1, −z; (iv) x, −y+1, z+1/2.

In all the complexes, the metal coordinated methoxo-O is involved in strong charge assisted type hydrogen bond [70,74−76] with the N−H group of the ligand. The N−H···O hydrogen bond parameters for all five complexes are listed in Table 2.4. The molecules of each of **1**−**4** form centrosymmetric dimeric species through a pair of reciprocal N−H···O interactions. The hydrogen bonded dimers of **1**–**4** are depicted in Fig. 2.7 (a–d). Interestingly **6** is also involved in the same N−H···O interaction, but its self-assembly leads to a one-dimensional polymeric structure (Fig. 2.7 (e)) instead of dimeric structure as observed for the rest (**2**−**4**). It may be noted that the $[MoO_2(OMe)(L^n)]$ (**1**−**6**) molecules are asymmetric but only **6** has a non-centrosymmetric space group and **2**−**4** have centrosymmetric space groups. This difference of the space group character is reflected in the two types of self-assembly patterns described above.

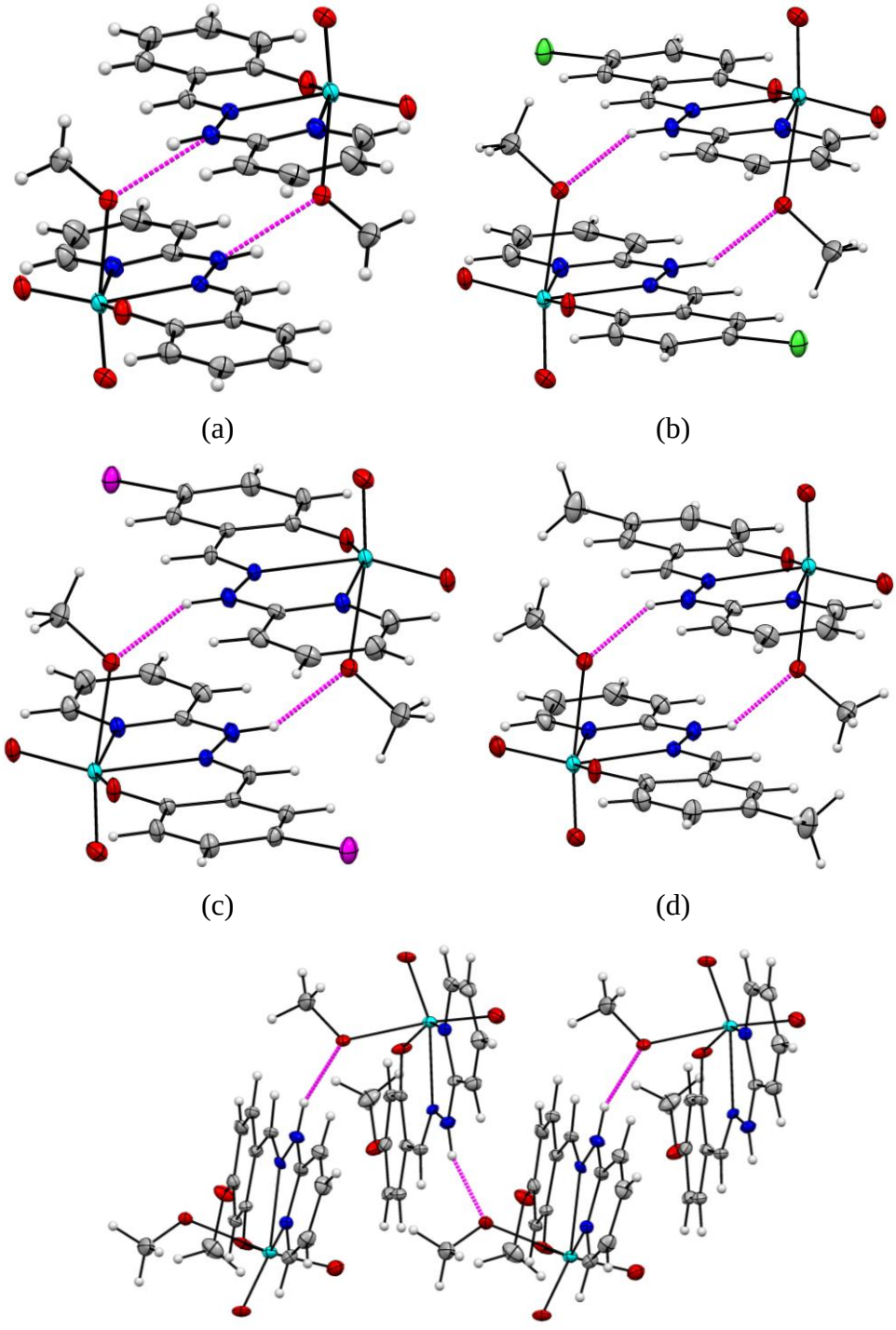

Fig. 2.7. Intermolecular Hydrogen bonding assisted self-assembly patterns of (a) **1**, (b) **2**, (c) **3**, (d) **4** and (e) **6**.

2.4. Conclusions

A series of *cis*-$\{MoO_2\}^{2+}$ complexes with 2-pyridylhydrazones of salicylaldehyde and its derivatives have been reported. IR, UV-Vis, NMR and fluorescence spectroscopic properties and X-ray crystal structures of these new complexes are described. IR and ^{1}H NMR spectra are complementary to the molecular structures determined by X-ray crystallography. Although the purple complexes display a ligand-to-metal charge transfer band near 540 nm, but their emission characteristics involve only the ligand centred orbitals. X-ray structures show a distorted octahedral N_2O_4 coordination sphere assembled by the tridentate hydrazone, one methoxo and two mutually *cis* oriented oxo groups around the molybdenum in each complex. In the crystals, the complex molecules are involved in intermolecular N−H···O hydrogen bond. Crystallization in centrosymmetric space group leads to N−H···O assisted dimeric units, while crystallization in non-centrosymmetric space group results into N−H···O assisted infinite chain structure.

2.5. References

[1] H. Arzoumanian, *Coord. Chem. Rev.*, 178-180, **1998**, 191−202.

[2] T. Punniyamurthy, S. Velusamy, J. Iqbal, *Chem. Rev.*, 105, **2005**, 2329−2364.

[3] F.E. Kühn, A.M. Santos, M. Abrantes, *Chem. Rev.*, 106, **2006**, 2455−2475.

[4] M.R. Maddani, K.R. Prabhu. *J. Indian Inst. Sci.*, 90, **2010**, 287−297.

[5] F. Romano, A. Linden, M. Mba, C. Zonta, G. Licini, *Adv. Synth. Catal.*, 352, **2010**, 2937−2942.

[6] J.A. Brito, B. Royo, M. Gómez, *Catal. Sci. Technol.*, 1, **2011**, 1109−1118.

[7] R.G. de Noronha, A.C. Fernandes, *Curr. Org. Chem.*, 16, **2012**, 33−64.

[8] J.R. Dilworth, *Coord. Chem. Rev.*, 21, **1976**, 29−62.

[9] K.N. Zelenin, L.A. Khorseeva, V.V. Alekseev, *Pharm. Chem. J.*, 26, **1992**, 395−405.

[10] Y. Mizobe, Y. Ishii, M. Hidai, *Coord Chem. Rev.*, 139, **1995**, 281−311.

[11] B.D. Koivisto, R.G. Hicks, *Coord Chem. Rev.*, 249, **2005**, 2612−2630.

[12] L.D. Popov, A.N. Morozov, I.N. Shcherbakov, Y.P. Tupolova, V.V. Lukov, V.A. Kogan, *Russ. Chem. Rev.*, 78, **2009**, 643−658.

[13] C. Manzura, M. Fuentealbaa, J.-R. Hamon, D. Carrillo, *Coord Chem. Rev.*, 254, **2010**, 765−780.

[14] B. Narasimhan, P. Kumar, D. Sharma, *Acta Pharm. Sci.*, 52, **2010**, 169−180.

[15] B.M. Paterson, P.S. Donnelly, *Chem. Soc. Rev.*, 40, **2011**, 3005−3018.

[16] S. Kobayashi, Y. Mori, J.S. Fossey, M.M. Salter. *Chem. Rev.*, 111, **2011**, 2626−2704.

[17] E.I. Stiefel, In: G. Wilkinson, J.A. McCleverty (Eds.), *Comprehensive Coordination Chemistry*, vol. 3, Pergamon, Oxford, **1987**, pp. 1375−1420.

[18] A. Syamal, M.R. Maurya, *Coord. Chem. Rev.*, 95, **1989**, 183−238.

[19] M.J. Morris, *Coord. Chem. Rev.*, 172, **1998**, 181−245.

[20] C.G. Young, In: J.A. McCleverty, T.J. Meyer (Eds.), *Comprehensive Coordination Chemistry II*, vol. 4, Elsevier Pergamon, Amsterdam, **2004**, pp. 415–527.

[21] R.D. Chakravarthy, D.K. Chand, *J. Chem. Sci.*, 123, **2011**, 187−199.

[22] C. Bustos, O. Burckardt, R. Schrebler, D. Carrillo, A.M. Arif, A.H. Cowely, C.M. Nunn, *Inorg. Chem.*, 29, **1990**, 3996−4001.

[23] L. Stelzig, S. Kötte, B. Krebs, *J. Chem. Soc., Dalton Trans.*, **1998**, 2921−2926.

[24] A. Rana, R. Dinda, P. Sengupta, S. Ghosh, L.R. Falvello *Polyhedron*, 21, **2002**, 1023−1030.

[25] N.R. Pramanik, S. Ghosh, T.K. Raychaudhuri, S. Ray, R.J. Butcher, S.S. Mandal, *Polyhedron*, 23, **2004**, 1595−1603.

[26] E.B. Seena, M.R.P. Kurup, *Polyhedron*, 26, **2007**, 3595−3601.

[27] N.R. Pramanik, S. Ghosh, T.K. Raychaudhuri, S. Chaudhuri, M.G.B. Drew, S.S. Mandal, *J. Coord. Chem.*, 60, **2007**, 2177−2190.

[28] H. Kang, W.T. Lim, B.K. Koo, *J. Korean Chem. Soc.*, 52, **2008**, 439−444.

[29] İ. Kizilcikli, S. Eğlence, A. Gelir, B. Ülküseven, *Trans. Met. Chem.*, 33, **2008**, 775−779.

[30] V. Vrdoljak, B. Prugovečki, M. Cindrić, D. Matković-Čalogović, A. Brbot-Šaranović, *Acta Chim. Slov.*, 55, **2008**, 828−833.

[31] D. Milić, V. Vrdoljak, D. Matković-Čalogović, M. Cindrić, *J. Chem. Crystallogr.*, 39, **2009**, 553−557.

[32] Y.-L. Zhai, X.-X. Xu, X. Wang, *Polyhedron*, 11, **1992**, 415−418.

[33] X. Wang, X.-M. Zhang, H.-X. Liu, *J. Coord. Chem.*, 33, **1994**, 223−228.

[34] H.-X. Liu, X.-M. Zhang, X. Wang, *Polyhedron*, 13, **1994**, 441−444.

[35] X. Wang, X.-M. Zhang, H.-X. Liu, *Polyhedron*, 13, **1994**, 2611−2614.

[36] B. Prelesnik, I. Ivanovic, V.M. Leovac, K. Andjelkovic, *Acta Cryst.*, C52, **1996**, 1375−1377.

[37] S.N. Rao, K.N. Munshi, N. N. Rao, M.M. Bhadbhade, E. Suresh, *Polyhedron*, 18, **1999**, 2491−2497.

[38] R. Dinda, P. Sengupta, S. Ghosh, H. Mayer-Figge, W.S. Sheldrick, *J. Chem. Soc., Dalton Trans.*, **2002**, 4434−4439.

[39] C. Zhang, G. Rheinwald, V. Lozan, B. Wu, P.-G. Lassahn, H. Lang, C. Janiak, *Z. Anorg. Allg. Chem.*, 628, **2002**, 1259−1268.

[40] G.S. Sanyal, R. Ganguly, P.K. Nath R.J. Butcher, *J. Indian Chem Soc.*, 79, **2002**, 468−488.

[41] R. Dinda, P. Sengupta, S. Ghosh, W.S. Sheldrick, *Eur. J. Inorg. Chem.*, **2003**, 363−369.

[42] S. Gao, X.-F. Zhang, L.-H. Huo, H. Zhao, *Acta Cryst.*, E60, **2004**, m1731−m1733.

[43] R. Dinda, S. Ghosh, L.R. Falvello, M. Tomás, T.C.W. Mak, *Polyhedron*, 25, **2006**, 2375−2382.

[44] J.-H. Liu, X-Y. Wu, Q.-Z. Zhang, X. He, W.-B. Yang, C.-Z. Lu, *Chin. J. Inorg. Chem.*, 22, **2006**, 1028−1032.

[45] S. Gupta, A.K. Barik, S. Pal, A. Hazra, S. Roy, R.J. Butcher, S.K. Kar, *Polyhedron*, 26, **2007**, 133−141.

[46] M. Mancka, W. Plass, *Inorg. Chem. Commun.*, 10, **2007**, 677−680.

[47] R. Debel, A. Buchholz, W. Plass, *Z. Anorg. Allg. Chem.*, 634, **2008**, 2291−2298.

[48] Y. Lei, C. Fu, *Synth. React. Inorg. Met.-Org. Nano-Met. Chem.*, 41, **2011**, 704−709.

[49] N.K. Ngan, K.M. Lo, C.S.R. Wong, *Polyhedron*, 30, **2011**, 2922−2932.

[50] N.K. Ngan, R.C.S. Wong, K.M. Lo, S.W. Ng, *Acta Cryst.*, E67, **2011**, m747.

[51] N.K. Ngan, K.M. Lo, C.S.R. Wong, *Acta Cryst.*, E67, **2011**, m857.

[52] S.-P. Gao, *J. Coord. Chem.*, 64, **2011**, 2869−2877.

[53] Y. Lei, C. Fu, *Russ. J. Coord. Chem.*, 38, **2012**, 65−70.

[54] N.K. Ngan, K.M. Lo, C.S.R. Wong, *Polyhedron*, 33, **2012**, 235−251.

[55] A.B. Ilyukhin, V.L. Abramenko, V.S. Sergienko, *Koord. Khimiya.*, 20, **1994**, 653−664.

[56] A.B. Ilyukhin, V.S. Sergienko, V.L. Abramenko, *Zhur. Neorg. Khimii*., 39, **1994**, 912−921.

[57] S. Gupta, S. Pal, A.K. Barik, S. Roy, A. Hazra, T.N. Mandal, R.J. Butcher, S.K. Kar. *Polyhedron*, 28, **2009**, 711−720.

[58] S. Mukherjee, C. Basu, S. Chowdhury, A.P. Chattopadhyay, A. Ghorai, U. Ghosh, H. Stoeckli-Evans, *Inorg. Chim. Acta*, 363, **2010**, 2752−2761.

[59] M.F. Zady, J.L. Wong, *J. Org. Chem.*, 41, **1976**, 2491−2495.

[60] M.F. Zady, F.N. Bruscato, J.L. Wong, *J. Chem. Soc., Perkin Trans.*, I, **1975**, 2036−2039.

[61] G.J.-J. Chen, J.W. McDonald, W.E. Newton, *Inorg. Chem.*, 15, **1976**, 2612−2615.

[62] *SMART* version 5.630 and *SAINT-plus* version 6.45, Bruker-Nonius Analytical X-ray Systems Inc., Madison, WI, USA, **2003**.

[63] G.M. Sheldrick, *SADABS*, Program for Area Detector Absorption Correction, University of Göttingen, Göttingen, Germany, **1997**.

[64] *CrysAlisPro version 1.171.33, Oxford Diffraction Ltd.*, Abingdon, Oxfordshire, UK, **2007**.

[65] G.M. Sheldrick, *XHELX-97*, *Structure Determination Software*, University of Göttingen, Göttingen, Germany, **1997**.

[66] L.J. Farrugia, *J. Appl. Crystallogr.*, 32, **1999**, 837−838.

[67] P. McArdle, *J. Appl. Crystallogr.*, 28, **1995**, 65.

[68] A.L. Spek, *Platon, A Multipurpose Crystallographic Tool*, Utrecht University, Utrecht, The Netherlands, **2002**.

[69] C.F. Macrae, I.J. Bruno, J.A. Chisholm, P.R. Edgington, P. McCabe, E. Pidcock, L. Rodriguez-Monge, R. Taylor, J. van de Streek, P.A. Wood, *J. Appl. Cryst.*, 41, **2008**, 466−470.

[70] K. Nagaraju, R. Raveendran, S.N. Pal, S. Pal, *Polyhedron*, 33, **2012**, 52−59.

[71] O.A. Rajan, A. Chakravorty, *Inorg. Chem.*, 20, **1981**, 660-664.

[72] F.R. Sensato, Q.B. Cass, B.R. Lopes, T.C. Lourenço, J. Zukerman-Schpector, E.R.T. Tiekink, E. Longo, J. Andrés, *Inorg Chim. Acta*, 375, **2011**, 41−46.

[73] R.G. Gonnade, M.S. Shashidhar, M.M. Bhadbhade, *J. Indian Inst. Sci.*, 87, **2007**, 149−165 and references therein.

[74] P. Gilli, V. Bertolasi, V. Ferretti, G. Gilli, *J. Am. Chem. Soc.*, 116, **1994**, 909−915.

[75] H.A. Habib, B. Gil-Hernández, K. Abu-Shandi, J. Sanchiz, C. Janiak, *Polyhedron*, 29, **2010**, 2537−2545.

[76] S. Das, S. Maloth, S. Pal, *Eur. J. Inorg. Chem.*, **2011**, 4270–4276.

Appendix

FTIR spectrum of HL^2.

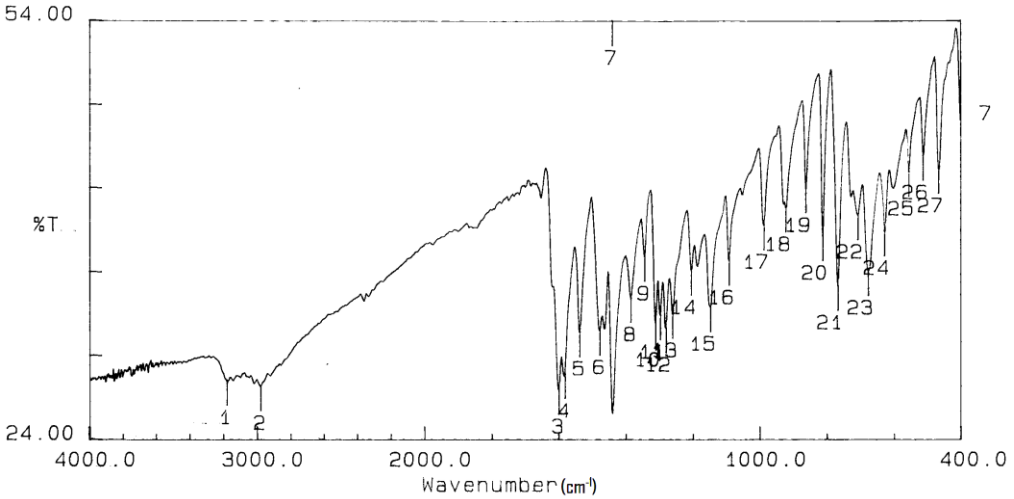

FTIR spectrum of HL^3.

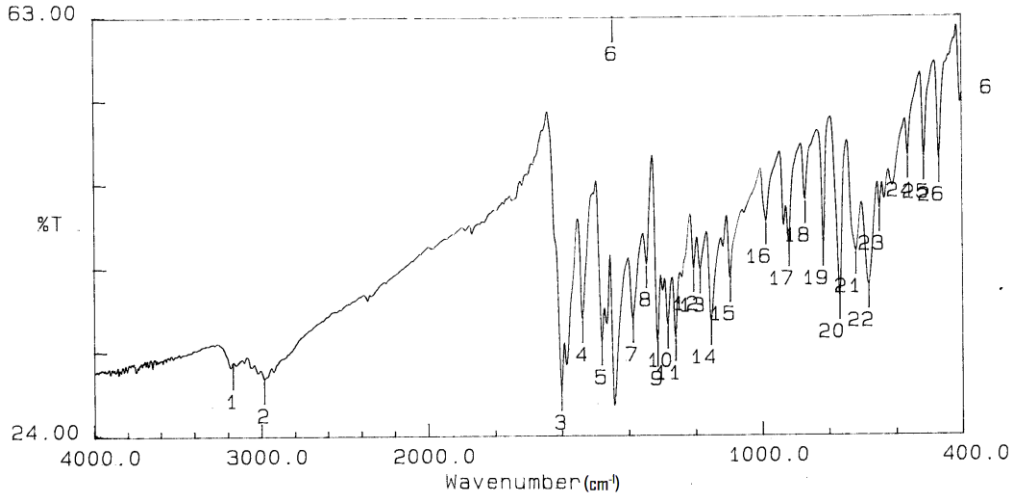

FTIR spectrum of HL^4.

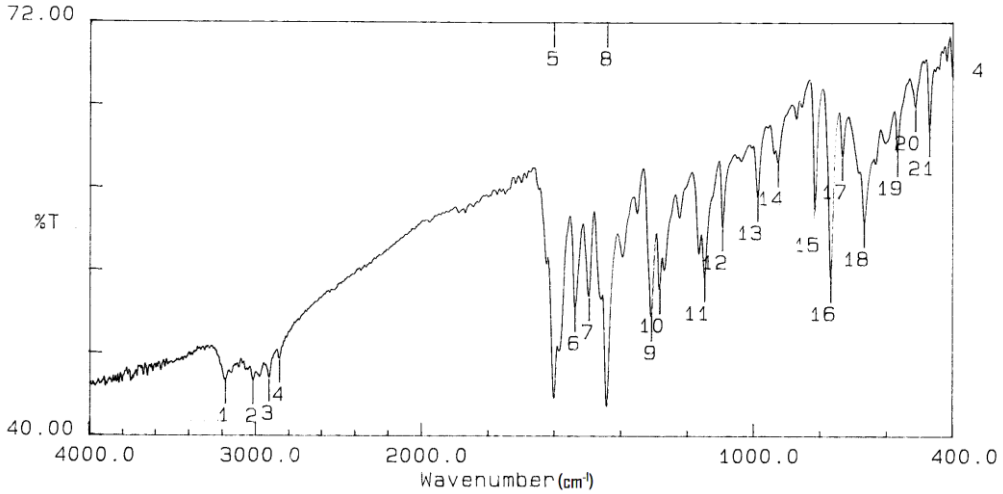

FTIR spectrum of HL^5.

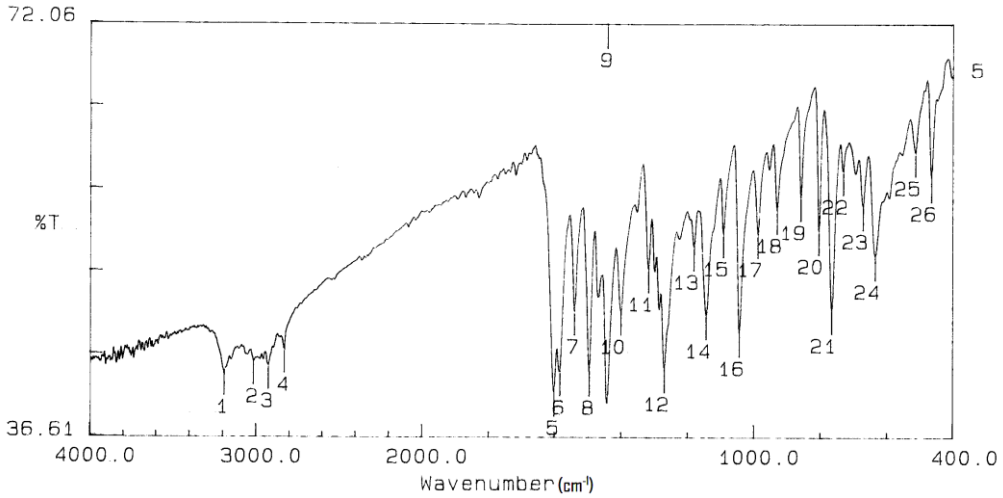

FTIR spectrum of HL^6.

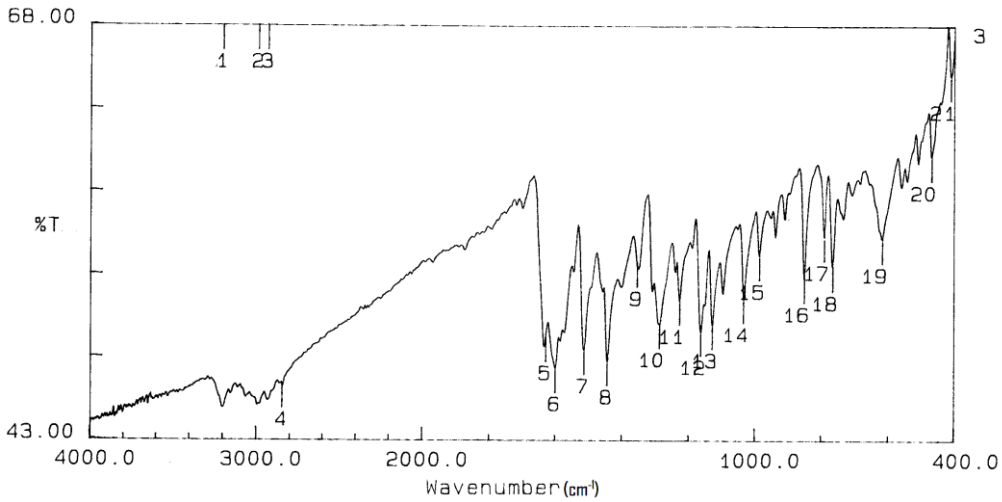

FTIR spectrum of $[MoO_2(OMe)(L^2)]$ (**2**).

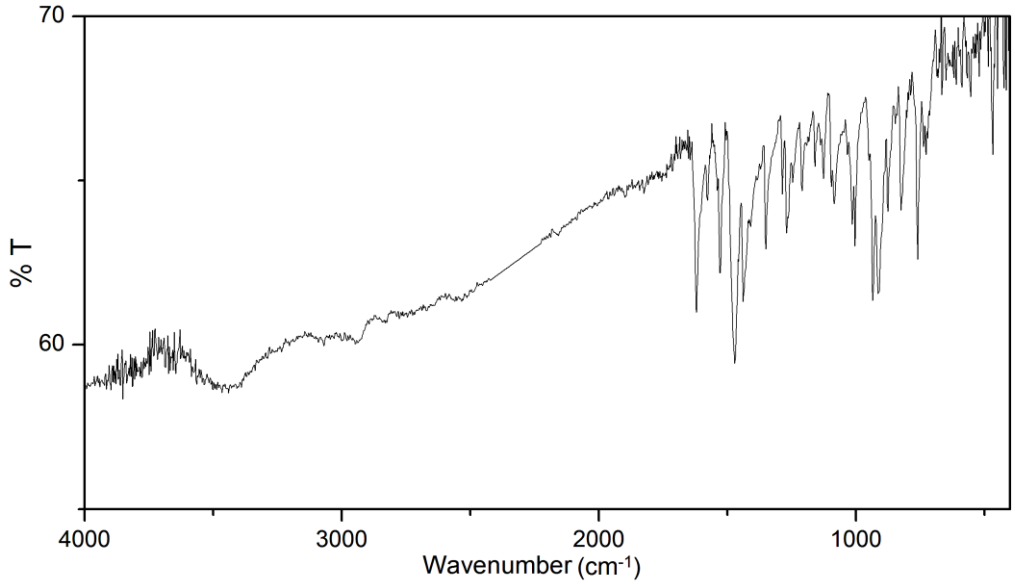

FTIR spectrum of [MoO_2(OMe)(L^3)] (**3**).

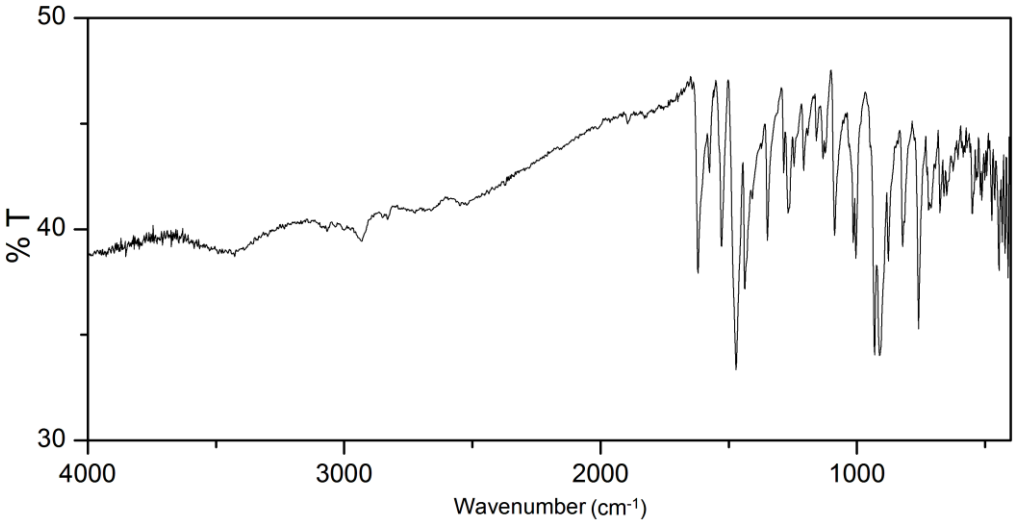

FTIR spectrum of [MoO_2(OMe)(L^4)] (**4**).

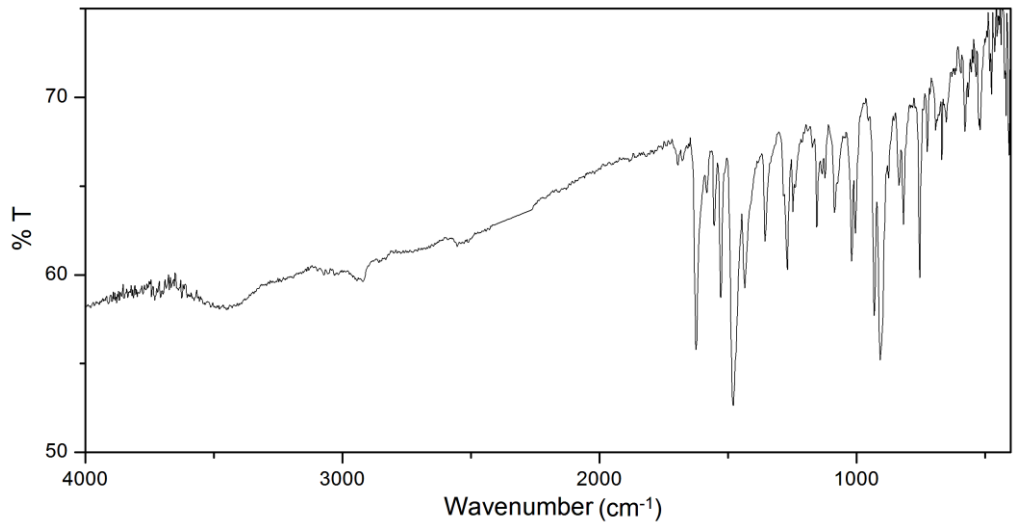

FTIR spectrum of $[MoO_2(OMe)(L^5)]$ (**5**).

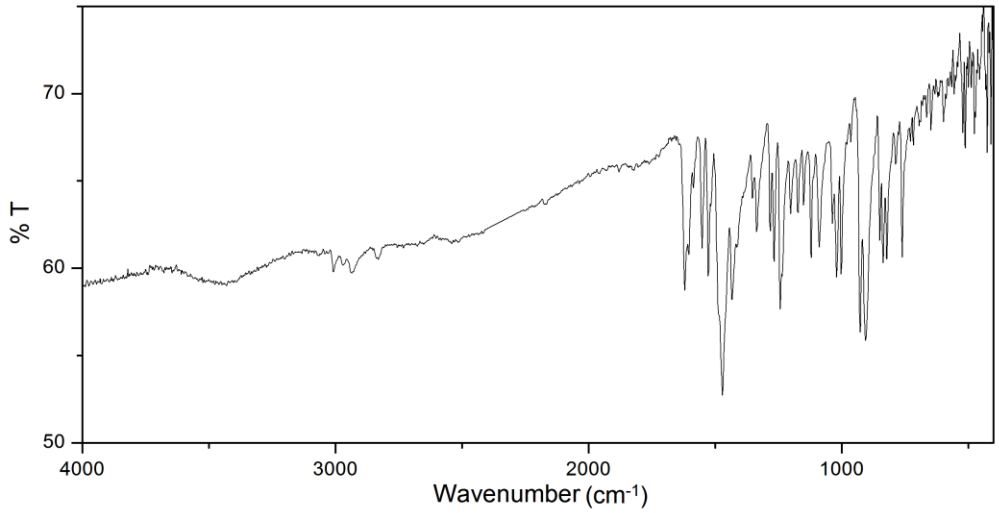

FTIR spectrum of $[MoO_2(OMe)(L^6)]$ (**6**).

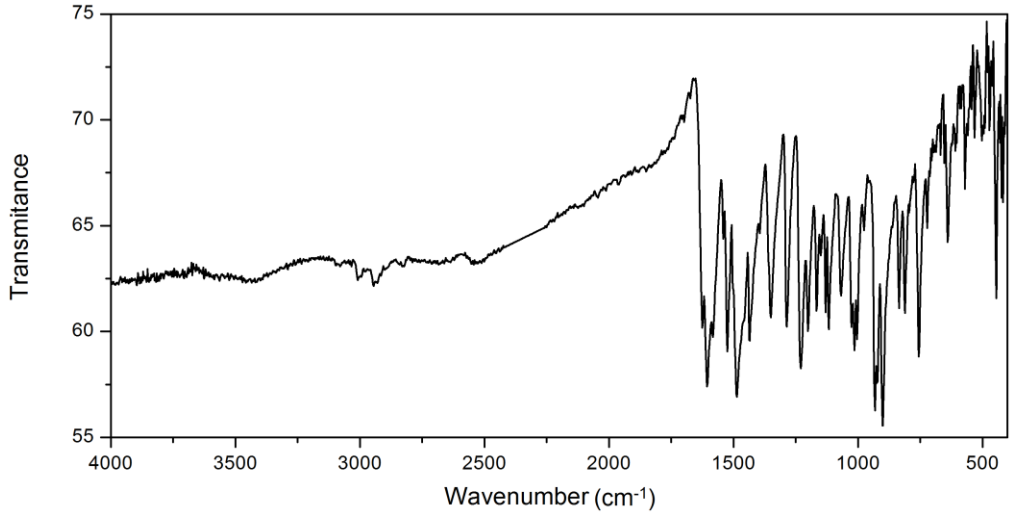

Electronic spectra of $HL^{1–6}$.

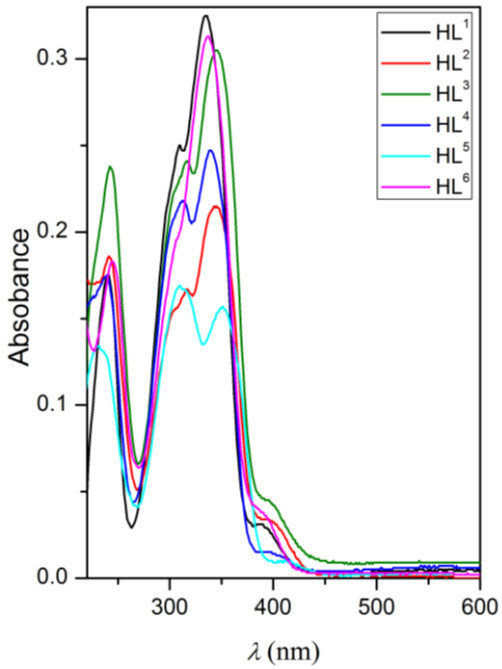

Electronic spectra of **1**–**6**.

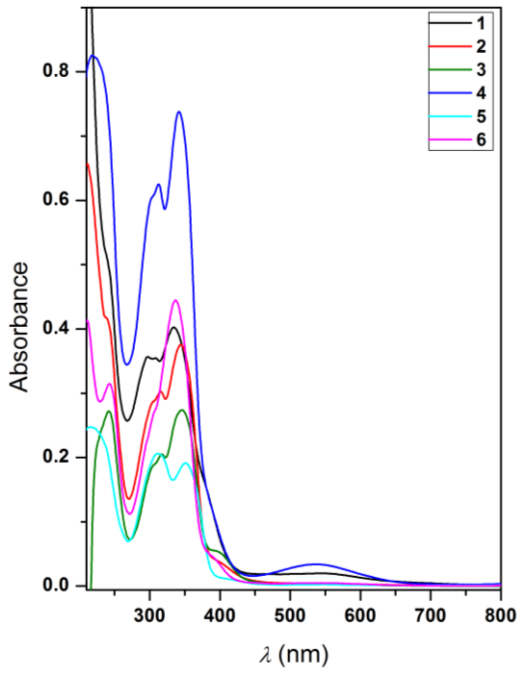

^{1}H-NMR Spectrum of HL^{2}:

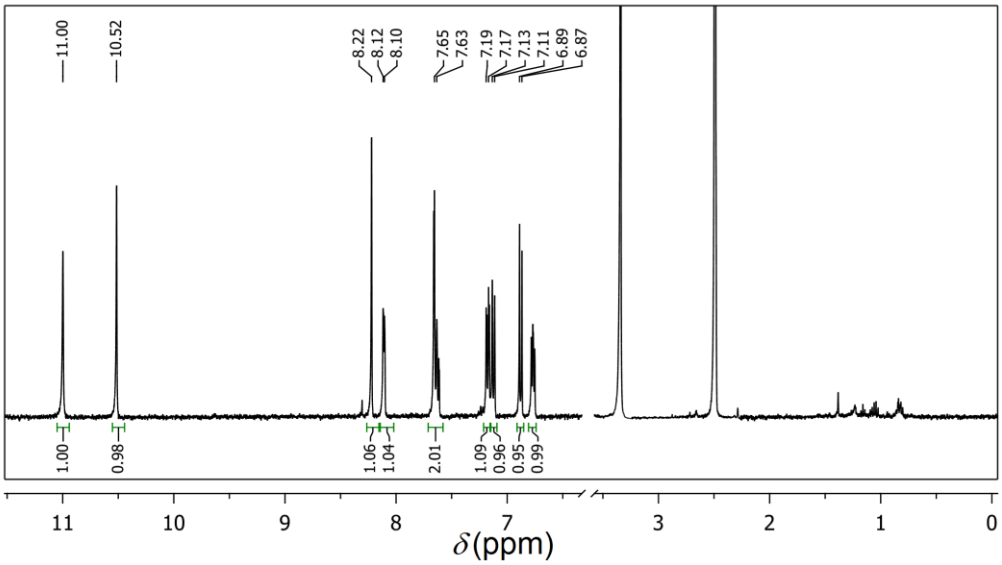

^{1}H-NMR Spectrum of HL^{3}:

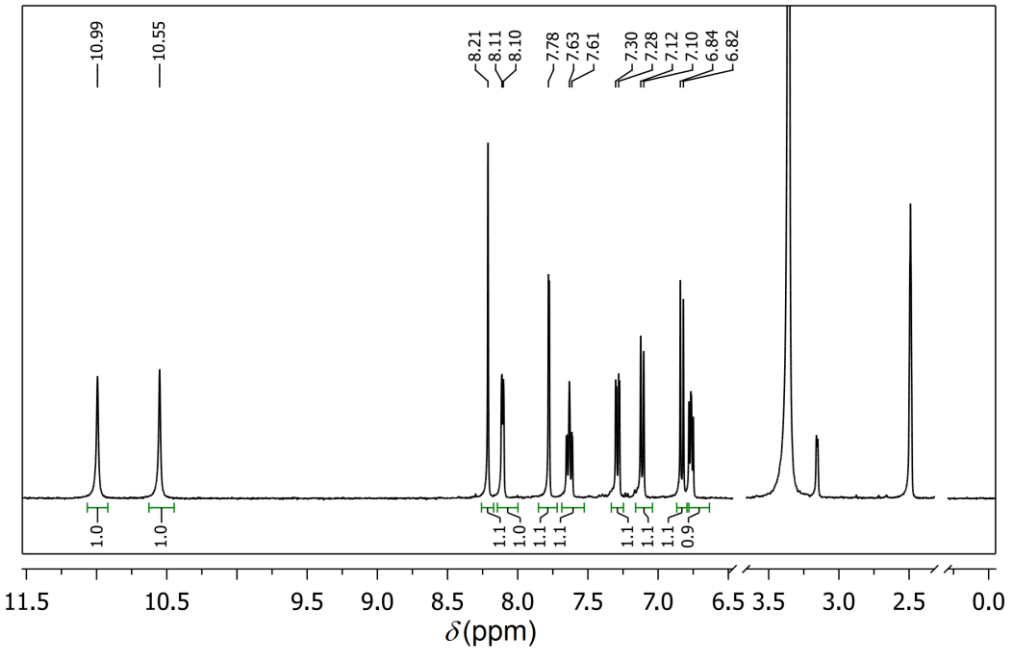

^{1}H-NMR Spectrum of HL^{4}:

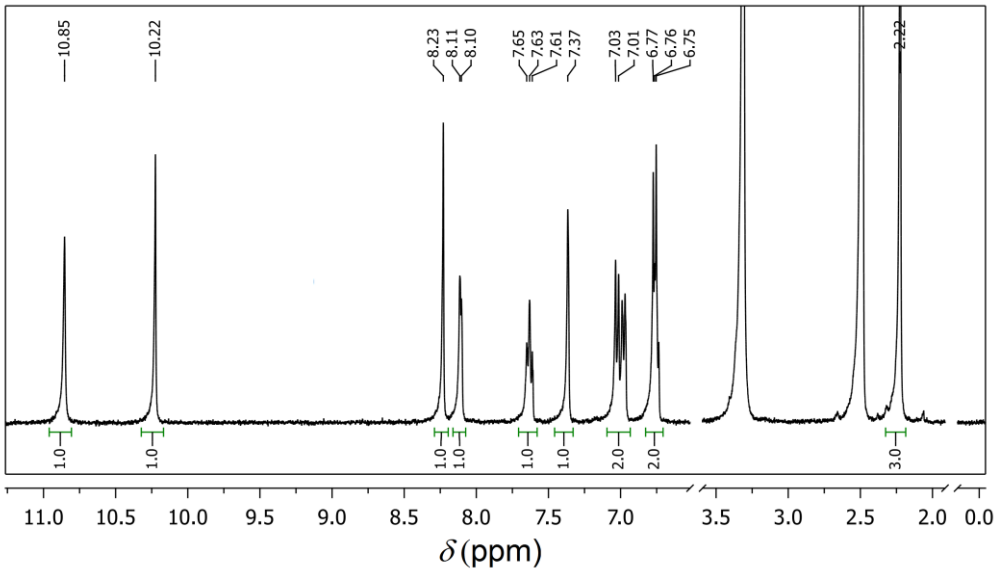

^{1}H-NMR Spectrum of HL^{5}:

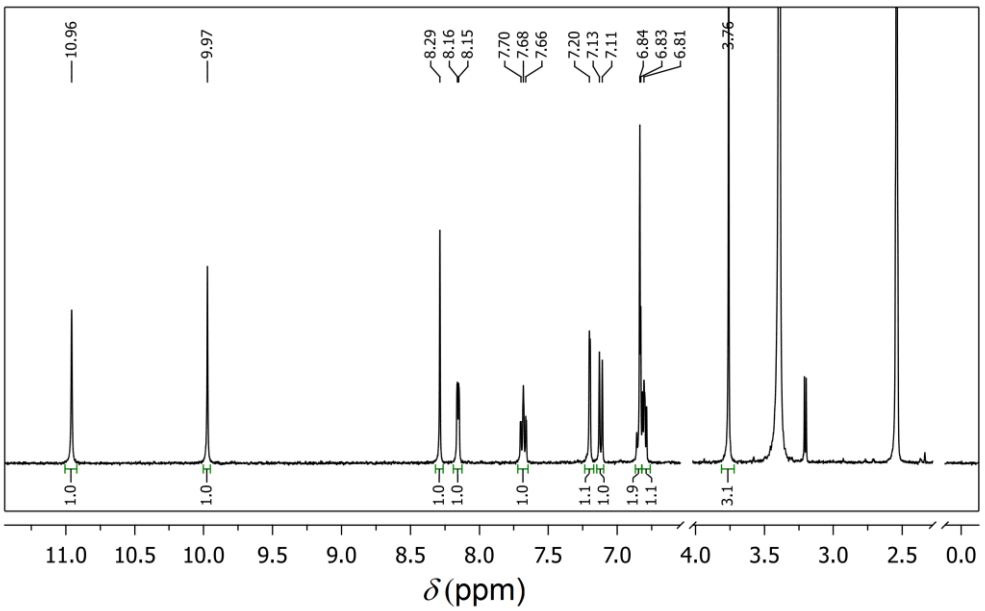

^{1}H-NMR Spectrum of HL^{6}:

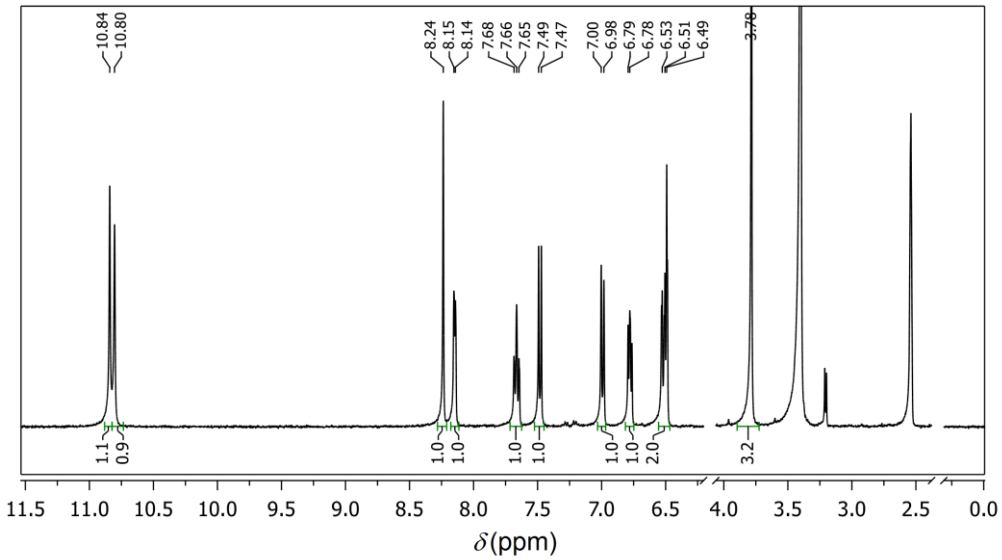

^{1}H-NMR Spectrum of *cis*-[MoO_2(OMe)(L^2)] (**2**):

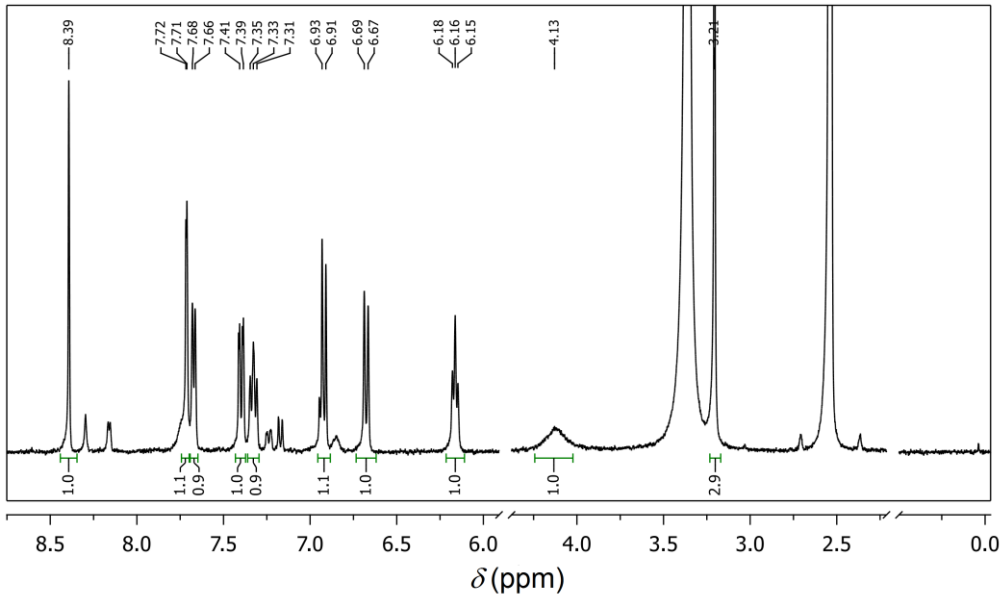

^{1}H-NMR Spectrum of *cis*-[MoO_2(OMe)(L^3)] (**3**):

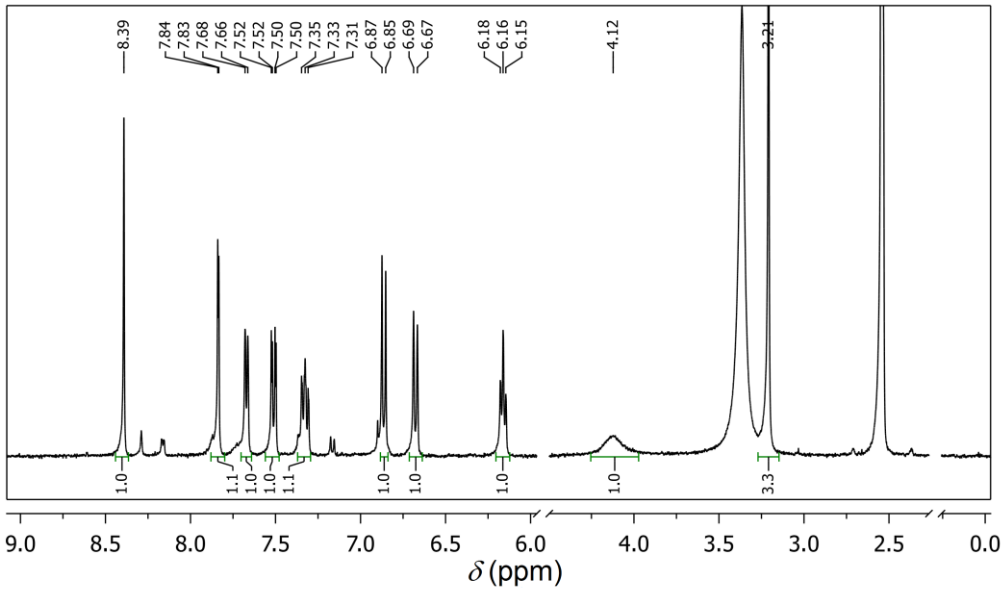

^{1}H-NMR Spectrum of *cis*-[MoO_2(OMe)(L^4)] (**4**):

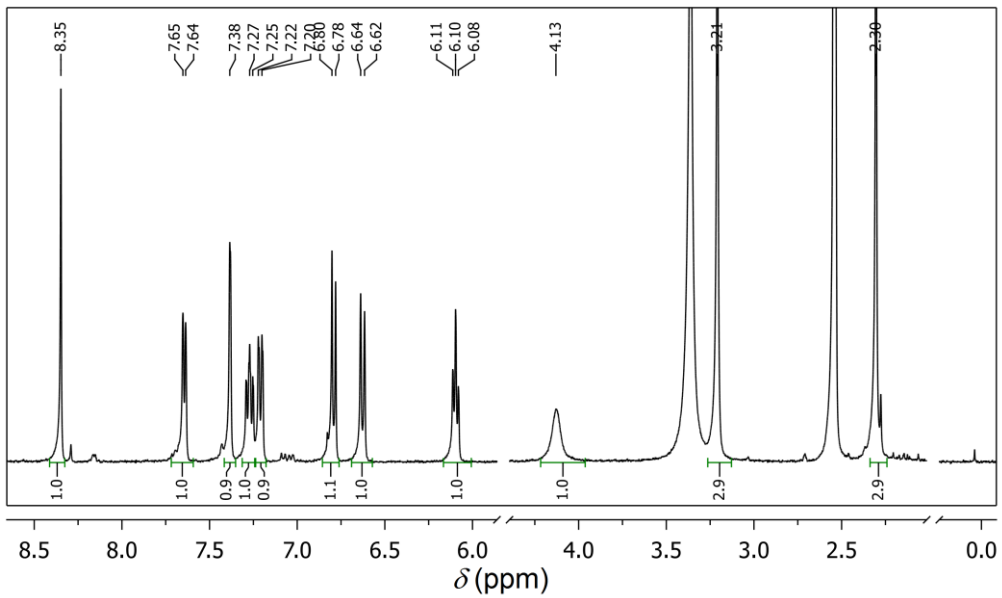

^{1}H-NMR Spectrum of *cis*-[MoO_2(OMe)(L^5)] (**5**):

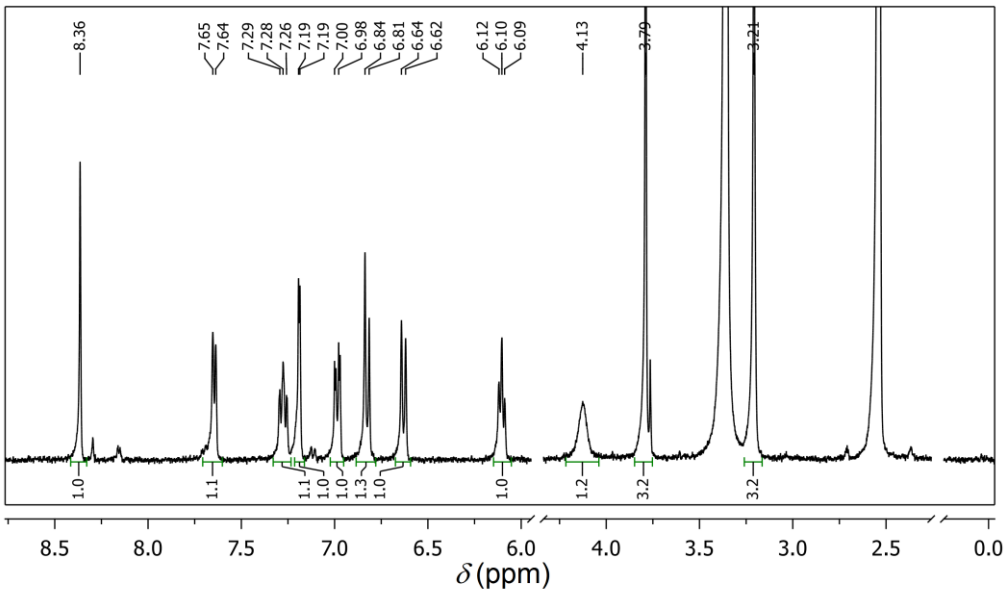

^{1}H-NMR Spectrum of *cis*-[MoO_2(OMe)(L^6)] (**6**):

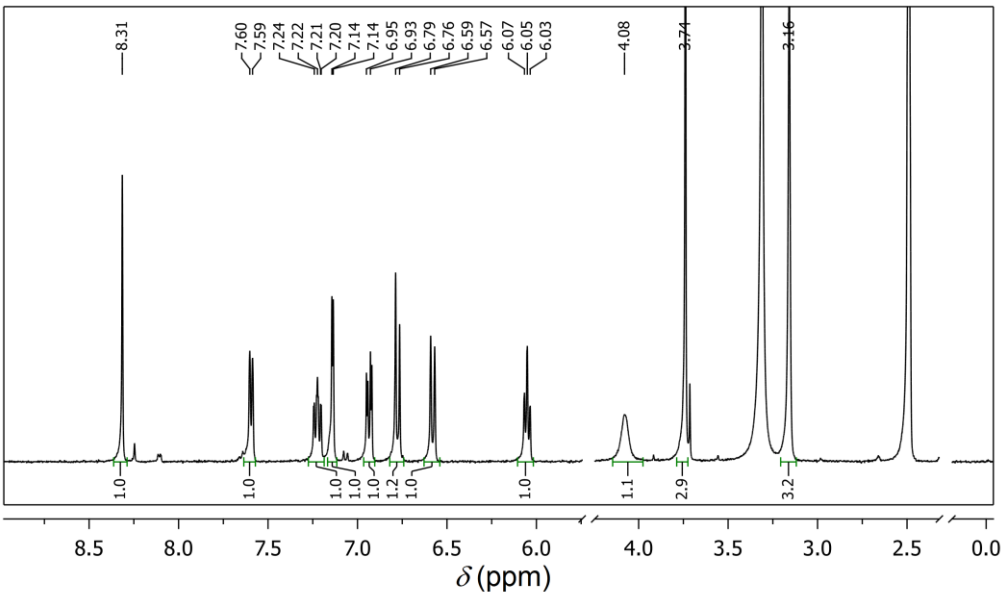

Atomic coordinates (x 104) and equivalent isotropic displacement parameters ($Å^2$ x 103). U(eq) is defined as one third of the trace of the orthogonalized Uij tensor.

Table A 2.1. For *cis*-[MoO_2(OMe)(L^1)] (**1**).

	X	Y	Z	U (eq)
Mo(1)	1737(1)	6828(1)	3248(1)	45(1)
O(1)	1805(3)	8268(2)	4907(2)	56(1)
O(2)	2004(3)	7726(2)	2118(2)	65(1)
O(3)	-500(3)	6260(2)	2709(2)	63(1)
O(4)	4844(2)	7261(2)	4146(2)	53(1)
N(1)	2558(3)	4872(3)	2195(2)	50(1)
N(2)	3054(3)	4094(2)	4184(2)	41(1)
N(3)	2494(3)	5420(2)	4677(2)	37(1)
C(1)	2589(5)	4582(4)	857(3)	74(1)
C(2)	3113(5)	3339(5)	204(3)	85(1)
C(3)	3613(5)	2296(4)	899(3)	73(1)
C(4)	3566(4)	2521(3)	2210(3)	56(1)
C(5)	3044(3)	3852(3)	2884(3)	44(1)
C(6)	2371(3)	5716(3)	5914(3)	41(1)
C(7)	1831(3)	7043(3)	6629(3)	41(1)
C(8)	1653(4)	7146(3)	7942(3)	52(1)
C(9)	1134(4)	8374(4)	8680(3)	62(1)
C(10)	768(4)	9533(3)	8118(3)	61(1)
C(11)	975(4)	9475(3)	6851(3)	55(1)
C(12)	1530(3)	8248(3)	6113(3)	43(1)
C(13)	5957(5)	8233(4)	3874(5)	89(1)

Table A 2.2. For *cis*-[$MoO_2(OMe)(L^2)$] (**2**).

	X	Y	Z	U(eq)
Mo(1)	6841(1)	6911(1)	3368(1)	31(1)
O(1)	8539(4)	6301(3)	2714(3)	48(1)
O(2)	5677(3)	7931(3)	2450(2)	44(1)
O(3)	8290(3)	8270(3)	4925(2)	39(1)
O(4)	4553(3)	7374(3)	4368(2)	38(1)
N(1)	5015(4)	5012(3)	2362(3)	34(1)
N(2)	7226(4)	5415(3)	4617(3)	26(1)
N(3)	6229(4)	4093(3)	4108(3)	32(1)
C(1)	9477(4)	8225(4)	6055(3)	30(1)
C(2)	10626(5)	9452(4)	6801(4)	40(1)
C(3)	11808(5)	9498(4)	7992(4)	42(1)
C(4)	11780(5)	8287(4)	8439(4)	35(1)
C(5)	10703(5)	7058(4)	7710(3)	33(1)
C(6)	9520(4)	6984(4)	6478(3)	29(1)
C(7)	8387(4)	5661(4)	5764(3)	29(1)
C(8)	5118(5)	3914(4)	2924(3)	31(1)
C(9)	4008(5)	2598(4)	2253(4)	42(1)
C(10)	2785(6)	2457(5)	1068(4)	49(1)
C(11)	2656(6)	3608(5)	523(4)	51(1)
C(12)	3775(5)	4830(5)	1172(4)	46(1)
C(13)	3122(7)	8260(6)	4080(6)	83(2)
Cl(2)	13151(1)	8367(1)	9996(1)	52(1)

Table A 2.3. For *cis*-[MoO_2(OMe)(L^3)] (**3**).

	X	Y	Z	U(eq)
Mo(1)	1863(1)	6909(1)	3371(1)	31(1)
O(1)	3299(4)	8265(3)	4910(3)	40(1)
O(2)	726(4)	7924(3)	2470(3)	44(1)
O(3)	3556(4)	6297(3)	2701(4)	49(1)
O(4)	-436(4)	7358(3)	4385(3)	40(1)
N(1)	2233(5)	5425(3)	4602(4)	27(1)
N(2)	1231(5)	4098(4)	4095(4)	34(1)
N(3)	33(5)	5027(4)	2370(4)	34(1)
C(1)	4433(6)	8219(5)	6029(4)	31(1)
C(2)	5555(6)	9456(5)	6795(5)	39(1)
C(3)	6684(7)	9507(5)	7975(5)	41(1)
C(4)	6699(6)	8298(5)	8417(5)	34(1)
C(5)	5629(6)	7062(5)	7664(4)	33(1)
C(6)	4501(5)	6990(4)	6445(4)	25(1)
C(7)	3380(6)	5655(4)	5727(5)	32(1)
C(8)	134(6)	3936(5)	2928(5)	31(1)
C(9)	-979(6)	2623(5)	2260(5)	40(1)
C(10)	-2183(7)	2498(5)	1101(5)	47(1)
C(11)	-2296(7)	3635(5)	556(5)	50(2)
C(12)	-1191(7)	4851(5)	1206(5)	46(1)
C(13)	-1841(9)	8260(7)	4132(8)	87(2)
Br(1)	8106(1)	8380(1)	10091(1)	50(1)

Table A 2.4. For *cis*-[$MoO_2(OMe)(L^4)$] (**4**).

	X	Y	Z	U(eq)
Mo(1)	5277(1)	1724(1)	114(1)	35(1)
O(1)	6693(6)	1741(3)	1198(5)	48(2)
O(2)	5805(6)	1645(3)	-876(5)	49(2)
O(3)	3234(5)	1858(3)	-1225(5)	41(2)
O(4)	4551(6)	943(3)	224(5)	44(2)
N(1)	3888(7)	2677(3)	1016(6)	37(2)
N(2)	5182(7)	2698(3)	18(6)	37(2)
N(3)	4008(6)	2049(3)	934(5)	29(2)
C(1)	3955(8)	695(4)	827(8)	39(2)
C(2)	3861(10)	67(4)	869(8)	48(3)
C(3)	3278(10)	-213(4)	1459(8)	52(3)
C(4)	2733(9)	127(4)	2024(8)	44(2)
C(5)	2839(9)	750(4)	1988(7)	41(2)
C(6)	3442(8)	1047(4)	1418(6)	30(2)
C(7)	3462(8)	1707(4)	1416(6)	34(2)
C(8)	4522(8)	2998(4)	547(7)	35(2)
C(9)	4527(9)	3646(4)	558(8)	46(2)
C(10)	5123(10)	3964(4)	63(10)	56(3)
C(11)	5793(10)	3656(5)	-470(10)	62(3)
C(12)	5784(9)	3049(5)	-450(9)	53(3)
C(13)	3066(10)	1938(5)	-2289(8)	60(3)
C(14)	2098(13)	-185(5)	2714(10)	73(4)

Table A 2.5. For *cis*-[MoO_2(OMe)(L^6)] (**6**)

	X	Y	Z	U(eq)
Mo(1)	6317(1)	6740(1)	9694(1)	38(1)
O(1)	6831(5)	6903(3)	11846(8)	59(2)
O(2)	5955(4)	7663(3)	8865(7)	48(1)
O(3)	5418(4)	6348(3)	6924(6)	44(1)
O(4)	7607(5)	6474(4)	8674(9)	48(2)
O(5)	11025(4)	5360(3)	7638(7)	59(2)
N(1)	6158(5)	5416(3)	9924(8)	29(2)
N(2)	5245(5)	5124(4)	10533(9)	40(2)
N(3)	4745(6)	6462(5)	10349(10)	38(2)
C(1)	8280(7)	5843(5)	8640(11)	31(2)
C(2)	9321(7)	5952(5)	8208(10)	41(2)
C(4)	9605(6)	4523(4)	8255(9)	47(2)
C(3)	9988(6)	5300(4)	8030(9)	43(2)
C(5)	8596(6)	4405(4)	8692(9)	39(2)
C(6)	7900(6)	5057(5)	8936(10)	34(2)
C(7)	6865(6)	4888(4)	9510(9)	37(2)
C(8)	4544(7)	5680(5)	10781(12)	37(2)
C(9)	3547(7)	5529(5)	11483(11)	51(2)
C(10)	2825(7)	6104(6)	11711(12)	59(2)
C(11)	3042(7)	6892(5)	11215(11)	57(2)
C(12)	3976(6)	7052(5)	10580(9)	46(2)
C(13)	11426(7)	6141(6)	7300(13)	74(3)
C(14)	4756(9)	6847(5)	5715(13)	83(3)

Chapter 3

cis-$\{MoO_2\}^{2+}$ assisted transformation of ligands: Mannich-type addition of methine to azomethine[§]

Reactions of $[MoO_2(acac)_2]$ ($acac^-$ = acetylacetonate) with the potentially N_2O-donor 5,5-membered fused chelate rings forming Schiff bases 2-(2-pyridylaldimine)ethanol (HL^1) and 4/5-*R*-2-(2-pyridylaldimine)phenols (HL^n; n = 2–5 for *R* = H, 4-Cl, 4-Me and 5-Me, respectively) lead to facile formation of the racemic complexes of general formula *cis*-$[MoO_2(acacL^{1-5})]$ (**1**–**5**) in 80–85% yields. Here, $(acacL^n)^{2-}$ represents a chiral N_2O_2-donor ligand system formed by a novel Mannich-type reaction that involves acetylacetonate and the azomethine fragment of HL^n both coordinated to the *cis*-$\{MoO_2\}^{2+}$ unit. Characterization of **1**–**5** has been performed with the help of microanalytical (CHN), spectroscopic (ESI-MS, IR, UV-Vis and ^{1}H- and ^{13}C-NMR) and electrochemical measurements. The molecular structures of all the complexes except for **5** are authenticated by single crystal X-ray crystallography. The Mo(VI) center in each of these analogous complexes is in a distorted octahedral N_2O_4 coordination sphere assembled by the chiral N_2O_2-donor transformed ligand $(acacL^n)^{2-}$ and the two mutually *cis*-oriented oxo ligands. In the crystal lattice, each of **1**–**4** exists as centrosymmetric discrete dimer *via* a pair of reciprocal N–H···O hydrogen bonds between its enantiomeric pairs.

3.1. Introduction

Complexes of *cis*-$\{MoO_2\}^{2+}$ unit are generally synthesized by classical ligand exchange reactions between the new ligands of interest and bis(acetylacetonato)dioxomolybdenum(VI) $[MoO_2(acac)_2]$ [1–24]. Such complexes with tridentate meridionally spanning ligands are particularly attractive as these ligands allow the octahedral metal center to have a vacant coordination site *trans* to one of the two strong *trans*-labilizing oxo groups [1–

[§] This work has been published in *Daltan Trans.*, 44, **2015**, 2401−2408.

18]. Complexes with dianionic tridentate ligands either dimerize and form a weakly bridged $\{OMo(\mu\text{-}O)_2MoO\}^{4+}$ core or pick up an ancillary monodentate ligand such as a solvent molecule, pyridine, phosphine, phosphine oxide etc [1–14]. Reports on complexes of *cis*-$\{MoO_2\}^{2+}$ with monoanionic tridentate ligands are rather limited [15–18]. In such complexes, the monodentate conjugate base of the protic synthesis reaction solvent methanol or a halide satisfies the vacant coordination site. In the preceding chapter, we have described the synthesis and physical properties of a series of such *cis*-$\{MoO_2\}^{2+}$ complexes with 5,6-membered fused chelate rings forming N_2O-donor *N*-(2-pyridyl)-*N*'-(salicylidene)hydrazine and its derivatives where the sixth coordination site is occupied by a methoxo group [18]. In the present chapter, we have tried to synthesize analogous complexes with similar but 5,5-membered fused chelate rings forming N_2O-donor Schiff bases 2-(2-pyridylaldimine)ethanol and 4/5-*R*-2-(2-pyridylaldimine)phenols (HL^n (n = 1–5), H represents the dissociable alcohol or phenol proton) using $[MoO_2(acac)_2]$ as the starting material. During our synthesis attempts, we have encountered a *cis*-$\{MoO_2\}^{2+}$ assisted transformation of ligands *via* Mannich-type reaction [25,26] and isolated a series of racemic complexes of *cis*-$\{MoO_2\}^{2+}$ with the chiral tetradentate transformed ligands $(acacL^n)^{2-}$ (Chart 3.1). Ligand transformations via nucleophilic addition reactions involving the coordinated polarized azomethine fragment of various transition metal complexes have been reported before [27–29], but, to the best of our knowledge there is no example of *cis*-$\{MoO_2\}^{2+}$ assisted ligand transformation of the same type. Herein, we describe the synthesis, X-ray crystal structures and physical properties of these complexes.

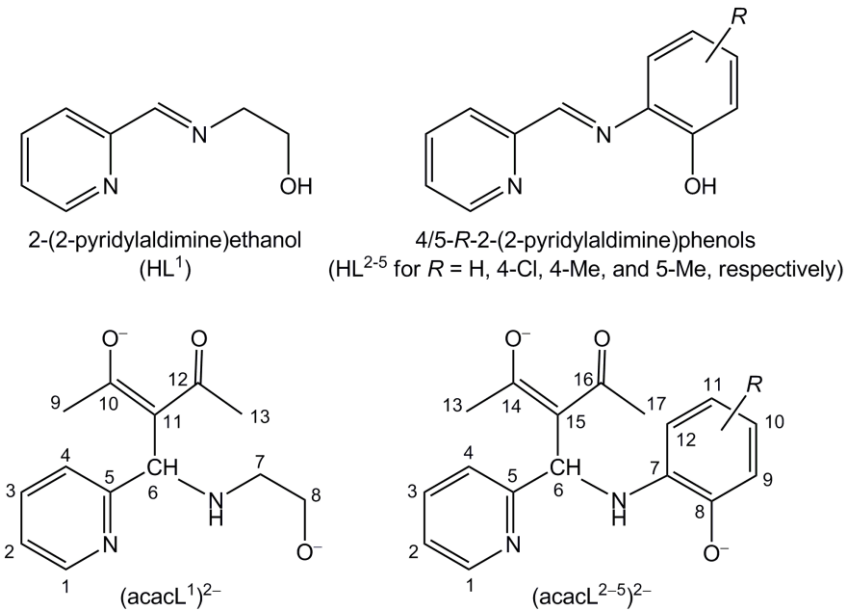

Chart 3.1. Chemical structures of Schiff bases HL$^{1–5}$ and the transformed ligands (acacL$^{1–5}$)$^{2–}$.

3.2. Experimental

3.2.1. Materials

Bis(acetylacetonato)dioxomolybdenum(VI), [$MoO_2(acac)_2$], was prepared using a literature method [30]. The Schiff bases (HL^n) were prepared by condensation reactions of equimolar amounts of 2-pyridylaldehyde and the corresponding amino alcohol/phenols by following reported procedures [31,32]. All other chemicals and solvents used in this work were of analytical grade and were used as procured without further purification.

3.2.2. Physical measurements

Elemental (CHN) analysis data were obtained with the help of a Thermo Finnigan Flash EA1112 series elemental analyzer. Solid state magnetic susceptibility measurements were performed with a Sherwood Scientific balance. A Shimadzu LCMS 2010 liquid chromatography mass

spectrometer was used for the purity verification of the Schiff bases. A Bruker Maxis HRMS (ESI-TOF analyzer) spectrometer was used to record the positive ion mass spectra of the complexes in methanol. The infrared spectra were recorded on Jasco-5300 and Nicolet 380 FTIR spectrophotometers using KBr pellets. A Shimadzu UV-3600 UV-Vis-NIR spectrophotometer was used to collect the electronic spectra. The ^{1}H (400 MHz) and ^{13}C (100 MHz) NMR spectra were collected with the help of a Bruker NMR spectrometer. Solution electrical conductivities were measured with the help of a Digisun DI-909 conductivity meter. A CH Instruments model 620A electrochemical analyzer was used for the cyclic voltammetric measurements under nitrogen atmosphere with a Pt-disk working electrode, a Pt-wire auxiliary electrode and an Ag/AgCl reference electrode.

3.2.3. Synthesis of the complexes [MoO_2(acacL^n)] (1–5)

All five complexes were synthesized using a general method as described next. Solid [$MoO_2(acac)_2$] (33 mg, 0.1 mmol) was added to a solution of the corresponding Schiff base HL^n (0.1 mmol) in 25 mL of methanol and the resulting mixture was heated on a steam bath for 30 min. After cooling to room temperature the reaction mixture was filtered to remove any solid present and then evaporated slowly at room temperature to about 2–3 mL. The complex separated as yellow to light brown crystalline material were collected by filtration, washed with ice-cold methanol, hexane and ether and finally dried in air. The yield was in the range 80–85%.

cis-[MoO_2(acacL^1)] (1). Yield 85%. Anal. Calcd for $C_{13}H_{16}MoN_2O_5$ (378.011): C, 41.50; H, 4.29; N, 7.45. Found C, 41.61; H, 4.42; N, 7.43. ESI-MS *m/z* $(M + H)^+$: 379.019. Selected IR bands (cm^{-1}): $\upsilon_{(MoO2)}$ 926 and 907, $\upsilon_{(C=O)}$ 1639, $\upsilon_{(N-H)}$ 3431. UV-Vis data (λ_{max}

(nm) (10^{-3} x ε (M^{-1} cm^{-1})): 261 (11.2) and 298 (7.1). ^{1}H NMR data (δ (ppm) (J (Hz))): 8.90 (5) (d, 1H, H^1), 7.57 (7) (t, 1H, H^2), 8.04 (8) (t, 1H, H^3), 7.50 (8) (d, 1H, H^4), 5.36 (s, 1H, H^6), 4.40 (m, 2H, H^7), 3.60 (m, 1H, H^{8a}), 2.22 (m, 1H, H^{8b}), 7.05(12) (t, 1H, NH), 2.09 (s, 3H, C^9H_3), 2.35 (s, 3H, $C^{13}H_3$). ^{13}C NMR data (δ(ppm)): 148.06 (C^1), 123.35(C^2), 124.80 (C^3), 141.06 (C^4), 158.11 (C^5), 59.86 (C^6), 53.31 (C^7), 76.25 (C^8), 25.19 (C^9), 175.3 (C^{10}), 114.53 (C^{11}), 195.27 (C^{12}), 31.29 (C^{13}). E_{pc} = –1.40 V.

cis-[MoO$_2$(acacL^2)] (2). Yield 82%. Anal. Calcd for $C_{17}H_{16}MoN_2O_5$ (426.011): C, 48.13; H, 3.80; N, 6.60. Found C, 48.37; H, 4.01; N, 6.56. ESI-MS *m/z* $(M + H)^+$: 427.019. Selected IR bands (cm^{-1}): $\upsilon_{(MoO2)}$ 931 and 909, $\upsilon_{(C=O)}$ 1634, $\upsilon_{(N-H)}$ 3451. UV-Vis data (λ_{max} (nm) (10^{-3} x ε (M^{-1} cm^{-1})): 260 (14.5) and 285 (11.8). ^{1}H NMR data (δ (ppm) (J (Hz))): 8.85 (6) (d, 1H, H^1), 7.54 (6.4) (t, 1H, H^2), 7.93 (7) (t, 1H, H^3), 7.43 (8) (d, 1H, H^4), 5.80 (s, 1H, H^6), 6.63 (8) (d, 1H, H^9), 6.86 (8) (t, 1H, H^{10}), 7.07 (8) (t, 1H, H^{11}), 7.40 (8) (d, 1H, H^{12}), 8.66 (s, 1H, NH), 2.21 (s, 3H, $C^{13}H_3$), 2.49 (s, 3H, $C^{17}H_3$). ^{13}C NMR data (δ(ppm)): 148.51 (C^1), 125.51(C^2), 126.38 (C^3), 141.49 (C^4), 157.45 (C^5), 63.73 (C^6), 133.35 (C^7), 162.03 (C^8), 117.32 (C^9), 129.55 (C^{10}), 121.17 (C^{11}), 122.50 (C^{12}), 24.42 (C^{13}), 173.66 (C^{14}), 116.31 (C^{15}), 195.89 (C^{16}), 31.40(C^{17}). E_{pc} = –1.0 V.

cis-[MoO$_2$(acacL^3)] (3). Yield 80%. Anal. Calcd for $C_{17}H_{15}ClMoN_2O_5$ (459.972): C, 44.51; H, 3.30; N, 6.11. Found C, 44.52; H, 3.71; N, 6.23. ESI-MS *m/z* $(M + H)^+$: 460.980. Selected IR bands (cm^{-1}): $\upsilon_{(MoO2)}$ 922 and 906, $\upsilon_{(C=O)}$ 1638, $\upsilon_{(N-H)}$ 3438. UV-Vis data (λ_{max} (nm) (10^{-3} x ε (M^{-1} cm^{-1})): 240 (11.4) and 293 (9.5). ^{1}H NMR data (δ (ppm) (J (Hz))): 8.85 (5) (d, 1H, H^1), 7.57 (6) (t, 1H, H^2), 7.97 (8) (t, 1H, H^3), 7.50 (8) (d, 1H, H^4), 5.80 (s, 1H, H^6), 6.66 (9) (d, 1H, H^9), 7.13 (9) (d, 1H, H^{10}), 7.48 (s, 1H, H^{12}), 8.78 (s, 1H, NH), 2.19 (s, 3H, $C^{13}H_3$),

2.51 (s, 3H, $C^{17}H_3$). ^{13}C NMR data (δ(ppm)): 148.60 (C^1), 123.70 (C^2), 126.38 (C^3), 141.66 (C^4), 157.11 (C^5), 63.73 (C^6), 134.30 (C^7), 161.13 (C^8), 118.69 (C^9), 129.62 (C^{10}), 123.91 (C^{11}), 122.74 (C^{12}), 24.21 (C^{13}), 173.33 (C^{14}), 116.14 (C^{15}), 195.13 (C^{16}), 31.44(C^{17}). E_{pc} = –0.93 V.

cis-[MoO₂(acacL⁴)] (4). Yield 85%. Anal. Calcd for $C_{18}H_{18}MoN_2O_5$ (440.026): C, 49.33; H, 4.14; N, 6.39. Found C, 49.45; H, 4.27; N, 6.31. ESI-MS *m/z* $(M + H)^+$: 441.035. Selected IR bands (cm^{-1}): $\upsilon_{(MoO_2)}$ 922 and 904, $\upsilon_{(C=O)}$ 1632, $\upsilon_{(N-H)}$ 3434. UV-Vis data (λ_{max} (nm) (10^{-3} x ε (M^{-1} cm^{-1})): 258 (8.4) and 289 (7.1). ^1H NMR data (δ (ppm) (J (Hz))): 8.85 (5) (d, 1H, H^1), 7.54 (7) (t, 1H, H^2), 7.93 (8) (t, 1H, H^3), 7.53 (8) (d, 1H, H^4), 5.78 (s, 1H, H^6), 6.51 (5) (d, 1H, H^9), 6.88 (5) (d, 1H, H^{10}), 7.19 (s, 1H, H^{12}), 8.59 (s, 1H, NH), 2.20 (s, 6H, $C^{13}H_3$ and CH_3 on ^{11}C of phenolate), 2.48 (s, 3H, $C^{17}H_3$). ^{13}C NMR data (δ(ppm)): 148.46 (C^1), 125.44 (C^2), 126.29 (C^3), 141.46 (C^4), 157.52 (C^5), 63.60 (C^6), 133.01 (C^7), 159.78 (C^8), 116.83 (C^9), 130.34 (C^{10}), 130.10 (C^{11}), 122.52 (C^{12}), 24.49 (C^{13}), 173.72 (C^{14}), 116.31 (C^{15}), 195.90 (C^{16}), 31.43(C^{17}), 20.59(CH_3 on C^{11} of phenolate). E_{pc} = –1.05 V.

cis-[MoO₂(acacL⁵)] (5). Yield 82%. Anal. Calcd for $C_{18}H_{18}MoN_2O_5$ (440.026): C, 49.33; H, 4.14; N, 6.39. Found C, 49.41; H, 4.25; N, 6.31. ESI-MS *m/z* $(M + H)^+$: 441.035. Selected IR bands (cm^{-1}): $\upsilon_{(MoO_2)}$ 931 and 913, $\upsilon_{(C=O)}$ 1623, $\upsilon_{(N-H)}$ 3432. UV-Vis data (λ_{max} (nm) (10^{-3} x ε (M^{-1} cm^{-1})): 260 (15.5) and 285 (11.5). ^1H NMR data (δ (ppm) (J (Hz))): 8.85 (5) (d, 1H, H^1), 7.54 (6) (t, 1H, H^2), 7.93 (8) (t, 1H, H^3), 7.42 (8) (d, 1H, H^4), 5.75 (s, 1H, H^6), 6.43 (s, 1H, H^9), 6.67 (8) (d, 1H, H^{11}), 7.26 (8) (d, 1H, H^{12}), 8.54 (s, 1H, NH), 2.199 (s, 3H, $C^{13}H_3$), 2.48 (s, 3H, $C^{17}H_3$), 2.12 (s, 3H, CH_3 on ^{10}C of phenolate). ^{13}C NMR data (δ(ppm)): 148.48 (C^1), 125.46 (C^2), 125.76 (C^3), 141.48 (C^4), 157.35 (C^5), 63.65 (C^6), 139.28 (C^7), 161.85 (C^8), 117.59 (C^9), 130.79 (C^{10}), 121.94 (C^{11}), 122.51 (C^{12}), 24.44 (C^{13}), 173.63 (C^{14}), 116.28

(C^{15}), 195.89 (C^{16}), 31.40(C^{17}), 20.59(CH_3 on C^{10} of phenolate). E_{pc} = –1.09 V and E_{pa} = –0.52 V.

3.2.4. X-ray crystallography

Single crystals of **1**–**4** were collected from the crystalline materials obtained from their synthesis reaction mixtures. All our attempts to grow X-ray quality crystals of **5** using various methods were unsuccessful. A Bruker-Nonius SMART APEX CCD single crystal diffractometer equipped with a graphite monochromator and a Mo Kα fine-focus sealed tube (λ = 0.71073 Å) was used for unit cell determination and intensity data collection for both **1** and **3** at 298 K. The SMART and SAINT-PLUS software packages [33] were used for data acquisition and data extraction, respectively. The absorption corrections were performed using the SADABS program [34]. The unit cell parameters and the intensity data at 298 K for both **2** and **3** were determined on an Oxford Diffraction Xcalibur Gemini single crystal X-ray diffractometer using graphite monochromated Mo Kα radiation (λ = 0.71073 Å). The CrysAlisPro software package [35] was used for data collection, reduction and absorption correction. The structures were solved by direct methods and refined on F^2 by full-matrix least-squares procedures. In all the structurers, the non-hydrogen atoms were refined using anisotropic thermal parameters. The hydrogen atoms were included in the structure factor calculations at idealized positions using a riding model. SHELX-97 programs [36] accessed through the WinGX package [37] were used for structure solution and refinement. The Platon [38] and the Mercury [39] packages were used for molecular graphics. X-ray crystallographic data (in CIF format) have been deposited with the Cambridge Crsystallographic Data Centre. The deposition nos. are CCDC 1029376–1029379 for **1**–**4**, respectively. The selected crystal data and structure refinement summary for **1**–**4** are listed in Table 3.1.

Table 3.1. Selected crystallographic data.

Complex	**1**	**2**	**3**	**4**
Empirical formula	$C_{13}H_{16}MoN_2O_5$	$C_{17}H_{16}MoN_2O_5$	$C_{17}H_{15}ClMoN_2O_5$	$C_{18}H_{18}MoN_2O_5$
Formula weight	376.22	424.26	458.70	438.28
Crystal system	Monoclinic	Triclinic	Triclinic	Triclinic
Space group	$P2_1/n$	$P\bar{1}$	$P\bar{1}$	$P\bar{1}$
a (Å)	7.3971(5)	8.1423(7)	7.8674(5)	7.9031(5)
b (Å)	13.1764(9)	10.2929(11)	8.4723(5)	8.4137(7)
c (Å)	14.2217(9)	11.0127(12)	13.9072(8)	14.0404(9)
α (°)	90	112.944(10)	76.819(1)	75.991(6)
β (°)	91.405(1)	93.302(8)	84.328(1)	83.346(5)
γ (°)	90	99.329(8)	77.558(1)	78.967(6)
V (Å^3)	1385.73(16)	831.25(15)	880.16(9)	886.72(11)
Z	4	2	2	2
ρ (g cm^{-3})	1.803	1.695	1.731	1.642
μ (mm^{-1})	0.970	0.820	0.928	0.771
Reflections collected	14117	5724	8471	6338
Reflections unique	2725	3368	3093	3621
Reflections [$I \geq 2\sigma(I)$]	2597	3224	2916	2933
Parameters	190	228	235	238
$R1$, $wR2$ [$I \geq 2\sigma(I)$]	0.0238, 0.0649	0.0340, 0.0763	0.0269, 0.0711	0.0454, 0.0847
$R1$, $wR2$ (all data)	0.0250, 0.0657	0.0410, 0.0818	0.0287, 0.0724	0.0631, 0.0942
GOF on F^2	1.063	1.095	1.054	1.041
$\Delta\rho_{max}$, $\Delta\rho_{min}$ (e Å^{-3})	0.400, −0.444	0.515, −0.297	0.541, −0.424	0.517, −0.356

3.3. Results and discussion

3.3.1. Synthesis and some properties

The complexes **1**–**5** were synthesized in 80–85% yields by reacting [$MoO_2(acac)_2$] with the corresponding HL^n in hot methanol. The elemental (CHN) analysis and ESI-mass spectral data are consistent with the general formulation of **1**–**5** as [$MoO_2(acacL^n)$] where $(acacL^n)^{2-}$ represents a chiral tetradentate ligand (Chart 3.1). Magnetic susceptibility measurements indicate the diamagnetic character of **1**–**5** and hence the +6 oxidation state of the metal center in each of them. The yellow to light brown complexes are highly soluble in dimethylformamide and dimethylsulfoxide, moderately soluble in methanol and acetonitrile and sparingly soluble in chloroform and dichloromethane. In solution, all the complexes behave as non-electrolyte.

3.3.2. Description of X-ray structures

The crystal structure of **1** has been solved in the monoclinic $P2_1/n$ space group, whereas that of each of **2**–**4** has been solved in the triclinic $P\bar{1}$ space group. The asymmetric unit in each structure comprises a single complex molecule. The metal centered bond parameters are listed in Table 3.2 and the molecular structures of **1**–**4** are illustrated in Figs. 3.1 and 3.2. The molecular structures and the bond parameters of all four complexes are very similar and hence suggest no significant influence of the ligand substituents on the overall structure. In general, the metal to coordinating atom bond lengths are comparable with the bond lengths reported for similar *cis*-$\{MoO_2\}^{2+}$ complexes with O,N-donor tri- or tetradentate ligands [1–24]. The intraligand bond parameters are unexceptional and consistent with the corresponding chemical structure. In each complex, the transformed ligand $(acacL^n)^{2-}$ is coordinated to the metal centre through the alcoholate- or the phenolate-O, the

amine-N, the pyridine-N and the enolate-O with the formation of one six-membered and two five-membered chelate rings. The tetradentate $(acacL^n)^{2-}$ and the two mutually *cis*-oriented oxo groups assemble a distorted octahedral N_2O_4 coordination sphere around the metal centre.

Table 3.2. Selected bond lengths (Å) and angles (°) for **1**–**4**.

Complex	**1**	**2**	**3**	**4**
Mo1–O1	1.7015(16)	1.702(2)	1.695(2)	1.693(3)
Mo1–O2	1.7055(15)	1.688(2)	1.7001(19)	1.696(3)
Mo1–O3	1.9089(15)	1.948(2)	1.9410(18)	1.941(2)
Mo1–O4	2.0037(14)	1.938(2)	1.9729(17)	1.970(2)
Mo1–N1	2.3750(17)	2.317(2)	2.333(2)	2.336(3)
Mo1–N2	2.2955(16)	2.323(2)	2.323(2)	2.315(3)
O1–Mo1–O2	108.68(9)	107.71(11)	107.54(11)	107.56(15)
O1–Mo1–O3	99.65(8)	98.41(11)	99.67(9)	99.52(13)
O1–Mo1–O4	95.30(8)	96.80(11)	96.04(9)	96.44(13)
O1–Mo1–N1	162.32(7)	162.79(10)	161.84(9)	162.39(12)
O1–Mo1–N2	94.35(7)	92.59(9)	92.93(9)	93.60(12)
O2–Mo1–O3	98.04(7)	96.37(10)	96.84(9)	96.91(12)
O2–Mo1–O4	97.95(7)	100.57(10)	99.36(9)	99.12(12)
O2–Mo1–N1	87.85(7)	89.50(9)	90.14(9)	89.60(13)
O2–Mo1–N2	156.95(7)	159.44(10)	159.30(9)	158.63(13)
O3–Mo1–O4	153.29(8)	152.56(9)	152.84(8)	152.77(11)
O3–Mo1–N1	83.70(7)	79.37(9)	81.81(8)	81.83(11)
O3–Mo1–N2	76.58(6)	76.92(9)	76.19(7)	76.09(10)
O4–Mo1–N1	75.67(6)	79.35(9)	76.52(7)	76.44(10)
O4–Mo1–N2	80.34(6)	79.71(9)	81.03(7)	81.04(9)
N1–Mo1–N2	69.38(5)	70.25(8)	69.72(7)	69.55(10)

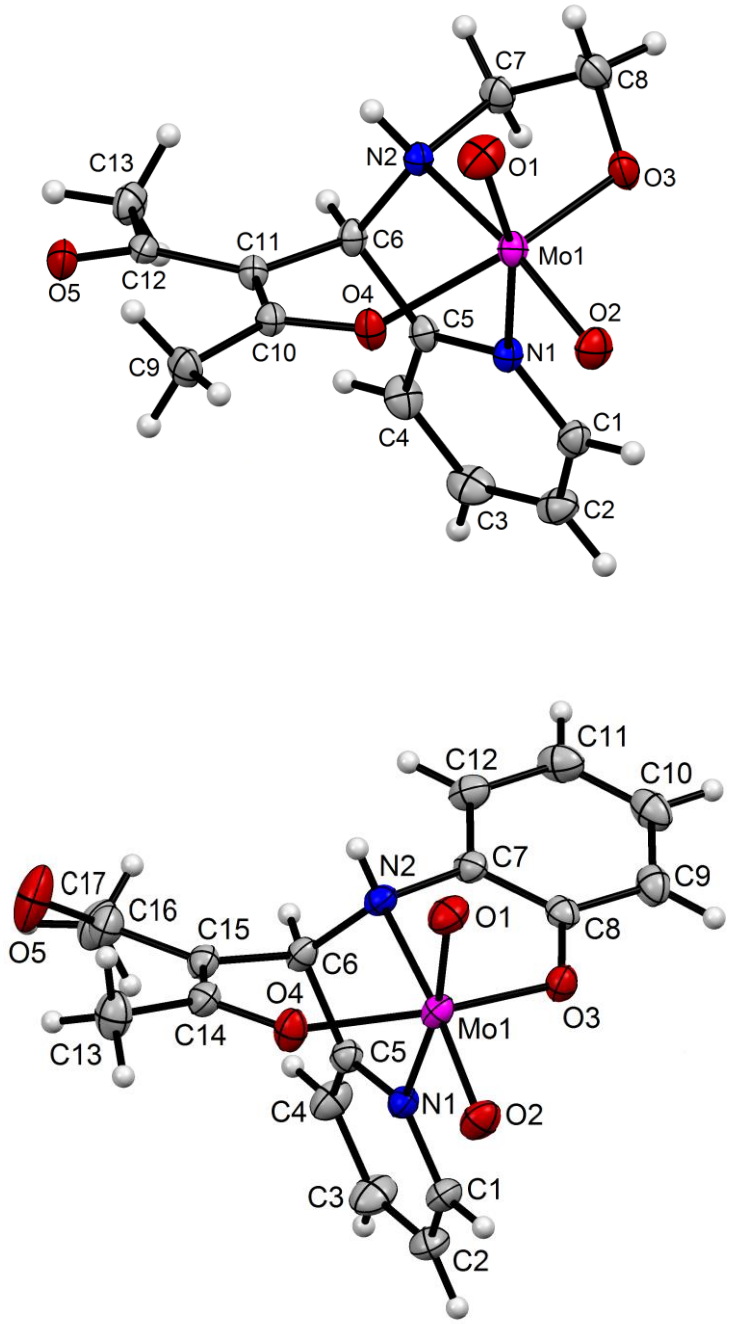

Fig. 3.1. Molecular structures of [MoO_2(acacL^1)] (**1**) (top) and [MoO_2(acacL^2)] (**2**) (bottom) with the atom labeling schemes. All non-hydrogen atoms are represented by their 30% probability thermal ellipsoids.

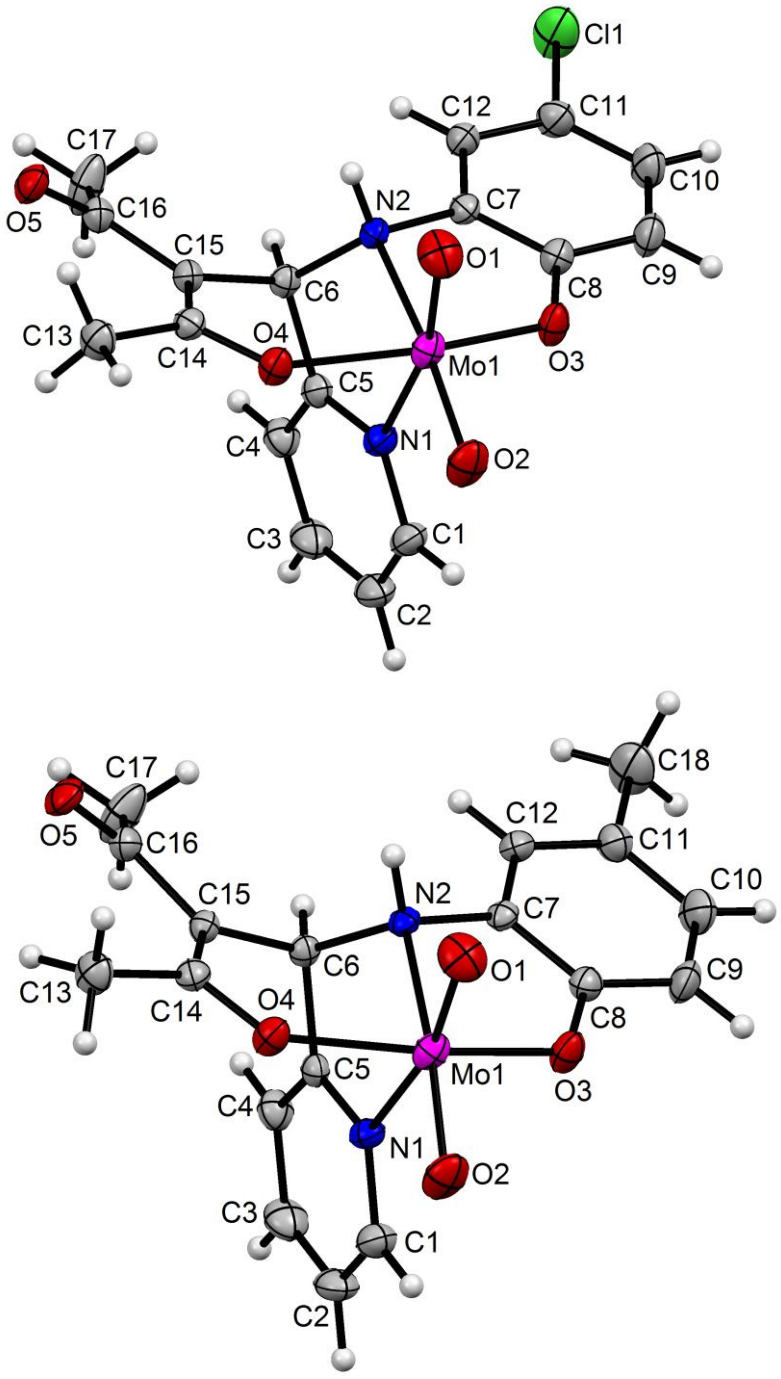

Fig. 3.2. Molecular structures of $[MoO_2(acacL^3)]$ (**3**) (top) and $[MoO_2(acacL^4)]$ (**4**) (bottom) with the atom labeling schemes. All non-hydrogen atoms are represented by their 30% probability thermal ellipsoids.

The alcoholate- or the phenolate-O, the amine-N and the pyridine-N are facially coordinated, while the enolate-O and the two oxo groups occupy the opposite face of the distorted octahedron. The structure of (acacL^n)$^{2-}$ clearly indicates Mannich-type addition of the central =CH– of (acac)$^-$ across the azomethine bond of (L^n)$^-$ (Chart 3.1, Fig. 3.1 and Fig 3.2). Consequently, both carbon atom and the metal coordinated N-atom of the reduced azomethine in the transformed ligand become chiral.

3.3.3. Hydrogen bonding and self-assembly

For each of **1**, **3** and **4**, the enantiomers of the chiral complex molecule are involved in a pair of reciprocal N5–H···O5 hydrogen bonds involving the N–H group and the free carbonyl O-atom of the acetylacetonate fragment of (acacL^n)$^{2-}$. However, in the case of **2**, the enantiomers are involved in a similar pair of reciprocal N5–H···O2 hydrogen bonds involving the N–H group of (acacL^n)$^{2-}$ and one metal coordinated oxo group. The N···O distances are in the range 2.842(2)–2.894(3) Å and the N–H···O angles are either 152 or 153° (Table 3.3.). The dimers of **1**–**4** are shown in Fig. 3.3. As a consequence of the formation of these centrosymmetric hydrogen bonded dimers involving the enantiomeric pair of molecules, each of the chiral **1**–**4** crystallizes in the centrosymmetric space group and is isolated in racemic form.

Table 3.3. Hydrogen bonding parameters (Å and ^{o})

Complex	D−H···A	D···A (Å)	D−H···A (°)
1	N(2)−H(2A)···O(5)^{i}	2.842(2)	153
2	N(2)−H(2A)···O(1)^{ii}	2.894(3)	153
3	N(2)−H(2A)···O(5)^{iii}	2.850(3)	152
4	N(2)−H(2A)···O(5)^{iv}	2.854(4)	152

Symmetry transformations used: (i) –x+1, –y, –z+1. (ii) –x+1, –y+1, –z+2. (iii) –x+1, –y+1, –z+1. (iv) –x–1, –y+1, –z+2.

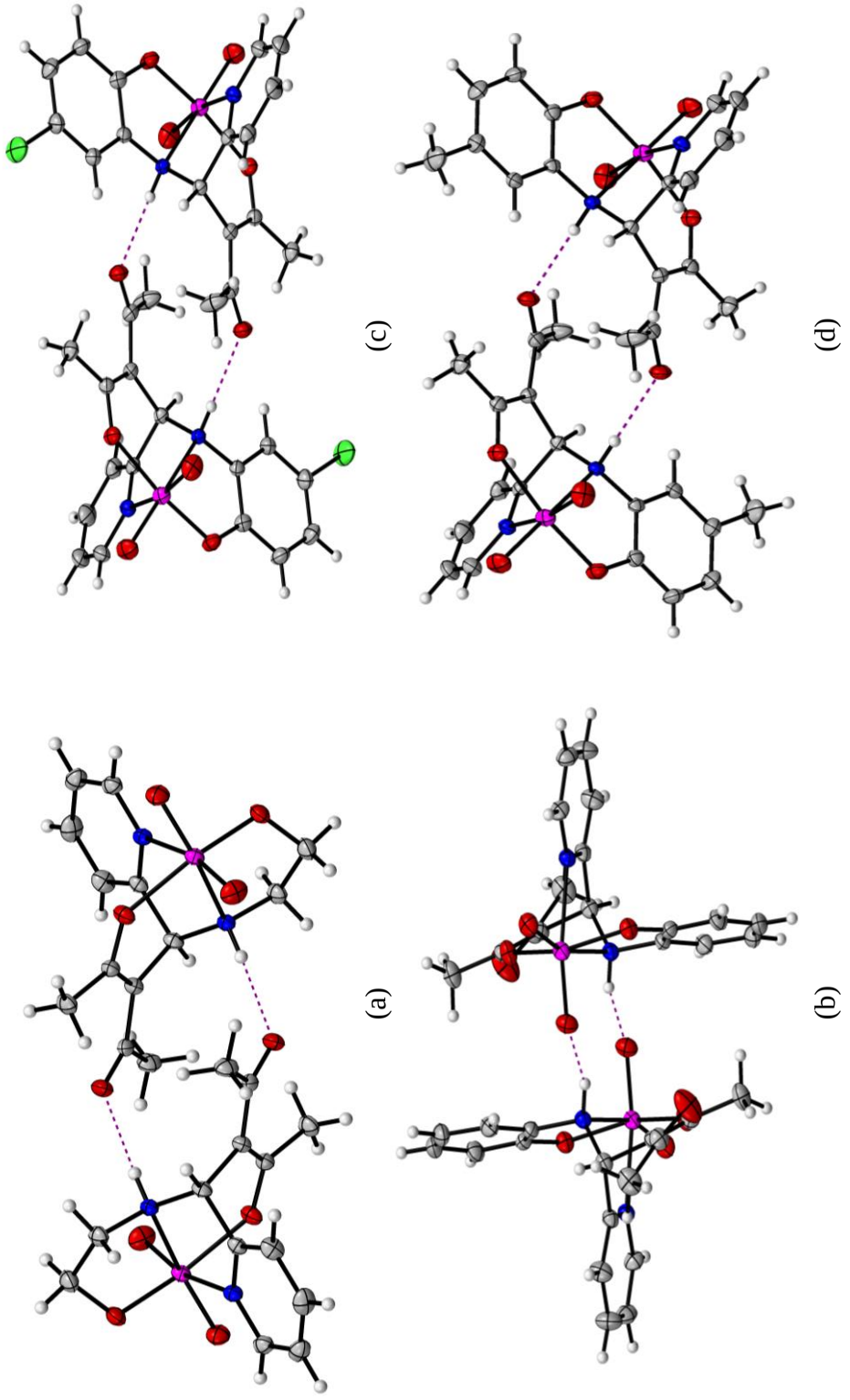

Fig. 3.3. Intermolecular hydrogen bonding assisted self-assemby of (a) **1**, (b) **2**, (c) **3** and (d) **4**.

3.3.4. Spectroscopic characterization

3.3.4.1. Infrared spectra

Infrared spectra of the complexes have been recorded in KBr pellets. A representative spectrum is shown in Fig. 3.4 and the remaining spectra are provided in the appendix at the end of the chapter. All of **1**–**5** display a broad band centered at ~3440 cm^{-1} and a sharp strong band in the range 1623–1639 cm^{-1} in the infrared spectra. These bands are attributed to the N–H and C=O groups, respectively of $(acacL^n)^{2-}$ that are involved in mutual intermolecular hydrogen bonds. The peaks observed in the range 3150–2830 are likely to be due to the C–H stretchings. The typical Mo=O stretches of the *cis*-{MoO_2}$^{2+}$ unit are observed as two sharp and intense bands in the ranges 904–913 and 922–931 cm^{-1} [1–22].

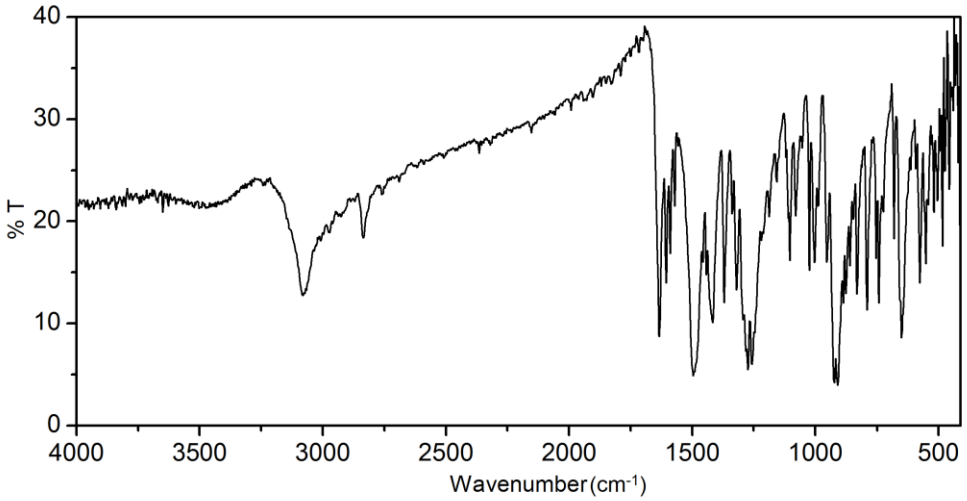

Fig. 3.4. FTIR spectrum of [MoO_2($acacL^2$)] (**2**).

3.3.4.2 Electronic spectra

The electronic spectra were recorded using methanol solutions of **1**–**5**. The spectral profiles of all the complexes are very similar. The electronic spectra of **1**–**5** are illustrated in Fig. 3.5. None of the complexes display any absorption band in the visible region. Only two intense absorption maxima

have been observed in the wavelength ranges 285–300 and 240–260 nm. Similar absorption bands observed for *cis*-$\{MoO_2\}^{2+}$ complexes with somewhat analogous tetradentate N,O-donor ligands have been assigned as ligand-to-metal charge transfer and intraligand transitions, respectively [40].

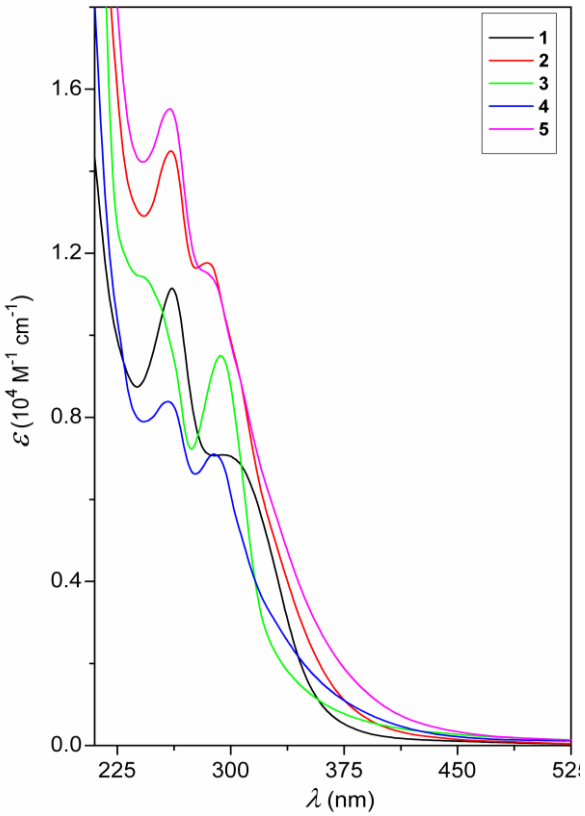

Fig. 3.5. Electronic spectra of $[MoO_2(acacL^{1–5})]$ (**1**–**5**) in methanol.

3.3.4 3. NMR spectra

The ^{1}H- and ^{13}C-NMR spectra of **1**–**5** were recorded in dimethylsulfoxide-d_6 solutions. The chemical shift values are given in the experimental section. The representative ^{1}H- and ^{13}C-NMR spectra are given in Fig. 3.6 and the remaining spectra are provided in the appendix of this chapter. The NH proton in **2**–**4** resonates as a singlet in the range δ 8.54–8.78 ppm, while that for **1** appears as a triplet at δ 7.05 ppm due to the coupling

with the adjacent methylene group protons. For all the complexes the proton at the chiral carbon center (C^6) of $(acacL^n)^{2-}$ (Chart 3.1) appears as a singlet within δ 5.36–5.80 ppm. The methine proton of the enol form of Hacac and $acac^-$ of $[MoO_2(acac)_2]$ resonates at δ ~5.52 ppm. In **1**–**4**, the bond distances from the central carbon atom (C^{11} in **1** and C^{15} in **2**–**4**) of the acetylacetonate fragment to the enolate carbon (C^{10} in **1** and C^{14} in **2**–**4**), the keto carbon (C^{12} in **1** and C^{16} in **2**–**4**) and the chiral carbon (C^6 in **1**–**4**) centres are in the ranges 1.355(4)–1.369(3), 1.461(3)–1.478(4) and 1.512(4)–1.521(3) Å, respectively. These bond lengths and the sum of the three bond angles (~359.8°) at the central carbon of the acetylacetonate fragment of $(acacL^{1-4})^{2-}$ clearly establish its sp^2 nature and hence the absence of any proton attached to it. Thus, the assignment of the signal in the range δ 5.36–5.80 ppm to the C^6 proton is very appropriate. Further the azomethine proton of free HL^n resonates as a singlet within δ 8.49–8.82 ppm. An upfield shift by ~3.08 ppm in **1**–**5** is not unexpected due to the reduction of the azomethine to amine in $(acacL^n)^{2-}$. The pyridine ring protons at C^1 and C^4 resonate as doublets at δ ~8.88 and ~7.48 ppm, respectively and at C^2 and C^3 appear as triplets at δ ~7.56 and ~7.95 ppm, respectively. In contrast to the two signals for the two methylene groups as displayed by 2-aminoethanol and HL^1, **1** shows three sets of signals due to diastereotopicity of the protons at C^8. The two protons multiplet appeared at δ 4.40 ppm is assigned to the methylene protons at C^7, while the two separate multiplets each of single proton observed at δ 3.60 and 2.22 ppm are attributed to the two methylene protons at C^8. A doublet for **2**-**4** and a singlet for **5** observed within δ 6.43–6.66 ppm is assigned to the phenolate ring *ortho*-proton at C^9. The proton at C^{10} appears as a triplet at δ 6.86 ppm for **2**, whereas it is observed as a doublet at δ 7.23 and 6.88 ppm for **3** and **4**, respectively. A triplet at δ 7.07 ppm and a doublet at δ 6.67 ppm observed for **2** and **5** respectively are attributed to the proton at C^{11}. A doublet observed for

2 and **5** and a singlet observed for **3** and **4** in the range δ 7.19–7.48 ppm are attributed to the proton at C^{12}. In general, for **1**–**5** except for the proton at C^4 which shows an upfield shift by 0.5 ppm, all other aromatic ring protons show a downfield shift when compared with that for HL^n, 2-pyridylaldehyde and the corresponding 2-aminophenols. The exception observed for C^4 proton which is *ortho* to the azomethine in HL^n is perhaps due to the reduction of the azomethine to amine in **1**–**5**. A three protons singlet observed in the range δ 2.09–2.21 ppm is assigned to the methyl group protons of the metal coordinated enolate end of the acetylacetonate fragment of $(acacL^n)^{2-}$ in **1** (at C^9), **2**, **3** and **5** (at C^{13}). A six protons singlet observed at δ 2.20 ppm for **4** is attributed to the protons of the enolate end methyl (C^{13}) and the methyl *para* to the phenolate fragment. The methyl protons at the uncoordinated keto end of the acetylacetonate fragment of the ligand in **1** (at C^{13}) and **3** (at C^{17}) appears as a singlet at δ 2.35 and 2.51 ppm, respectively. However, the corresponding signals for **2**, **4** and **5** overlaps with the solvent signal at δ 2.49 ppm. It may be noted that the symmetric free Hacac shows a single signal for the protons of the two methyl groups at δ 2.24 and 2.04 ppm for its diketo and enol forms, respectively. The corresponding signals for the chelating $acac^-$ in $[MoO_2(acac)_2]$ are also very closely spaced (δ 2.14 and 2.16 ppm). The protons of the methyl group at *meta* position of the phenolate ring in **5** resonates as a singlet at δ 2.20 ppm.

In the ^{13}C NMR spectra of **1**–**5**, the signal observed within δ 59.86–63.68 ppm has been assigned to the chiral carbon C^6 of $(acacL^n)^{2-}$. The significant upfield shift of this signal with respect to the signal observed within δ 155.67–163.22 ppm for the azomethine carbon of HL^n is attributed to its conversion to amine in $(acacL^n)^{2-}$. The C^1–C^5 of the pyridine ring fragment of $(acacL^n)^{2-}$ in **1**–**5** resonate at δ ~148.3, ~125.6, ~141.4, ~124.5 and ~157.6 ppm, respectively. Two resonances observed at δ 76.25 and 53.41 ppm for **1**

have been assigned to the two methylene carbons of (acacL^1)$^{2-}$ adjacent to O$^-$ and NH, respectively. The signals corresponding to the carbons (C^7–C^{12}) of the phenolate fragment of (acacL$^{2-5}$)$^{2-}$ in **2**–**5** are observed in the ranges δ 133.01–139.28, 159.78–162.02, 116.83–118.69, 129.55–130.79, 121.17–130.10 and 122.50–122.74 ppm, respectively. The methyl carbons at *para* to the phenolate in **4** and *meta* to the phenolate in **5** resonate at δ 20.59 and 21.17 ppm, respectively. Overall the resonances associated with the aromatic carbons in **1**–**5** show a downfield shift when compared with that for HL^n, 2-pyridylaldehyde and the corresponding 2-aminophenols. The methyl carbon at the enolate end (C^9 in **1** and C^{13} in **2**–**5**) and that of the dangling keto end (C^{13} in **1** and C^{17} in **2**–**5**) of the acetylacetonate fragment of (acacL^n)$^{2-}$ resonate at δ ~24.7 and ~31.4 ppm, respectively. The methyl carbon signals for the charge delocalised chelating acac$^-$ in [MoO$_2$(acac)$_2$] are relatively more closely spaced (δ 24.96 and 27.04 ppm), while the symmetric free Hacac displays only one signal (at δ 30.82 (keto form) or 24.80 (enol form) ppm) for its methyl carbons. The coordinated enolate carbon (C^{10} in **1** and C^{14} in **2**–**5**), free carbonyl carbon (C^{12} in **1** and C^{16} in **2**–**5**) and the central carbon (C^{11} in **1** and C^{15} in **2**–**5**) of the acetylacetonate fragment of (acacL^n)$^{2-}$ appear at δ ~173.5, ~196.0 ppm and ~116.2 ppm, respectively. The signals for the corresponding carbons in acac$^-$ of [MoO$_2$(acac)$_2$] appear at δ 191.76, 203.92 and 102.98 ppm respectively. The central carbon of free Hacac appears at δ 58.52 and 100.48 ppm for the keto and enol forms, respectively. In contrast to **1**–**5** and [MoO$_2$(acac)$_2$], free Hacac shows only one signal for the oxygen bearing two carbons at δ 202.09 and 191.25 ppm for the keto and enol forms, respectively. Overall the NMR characteristics of **1**–**5** are consistent with the chemical structure of (acacL^n)$^{2-}$ and the lone enolate end bound coordination mode of its acetylacetonate fragment.

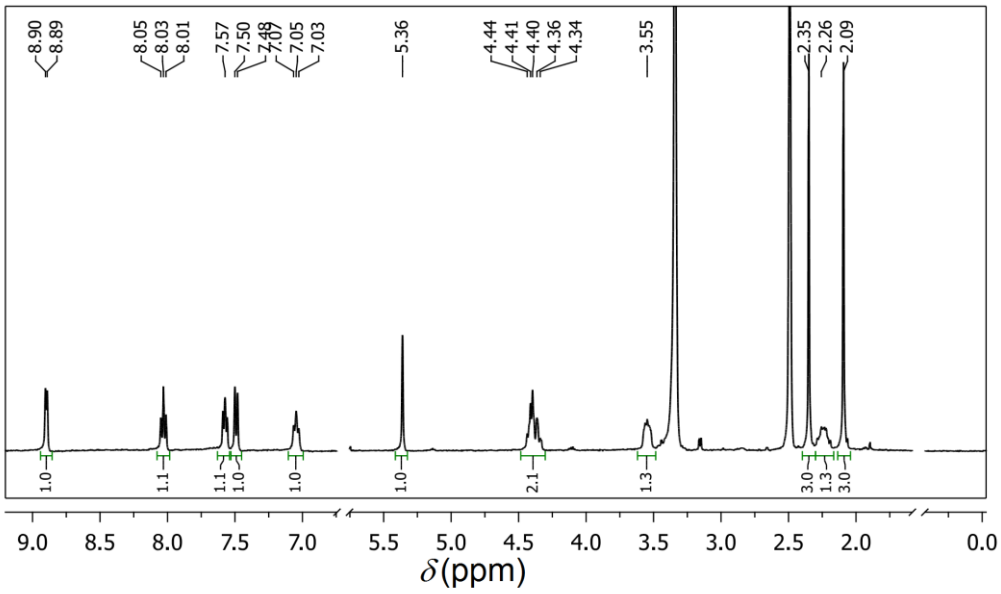

(a)

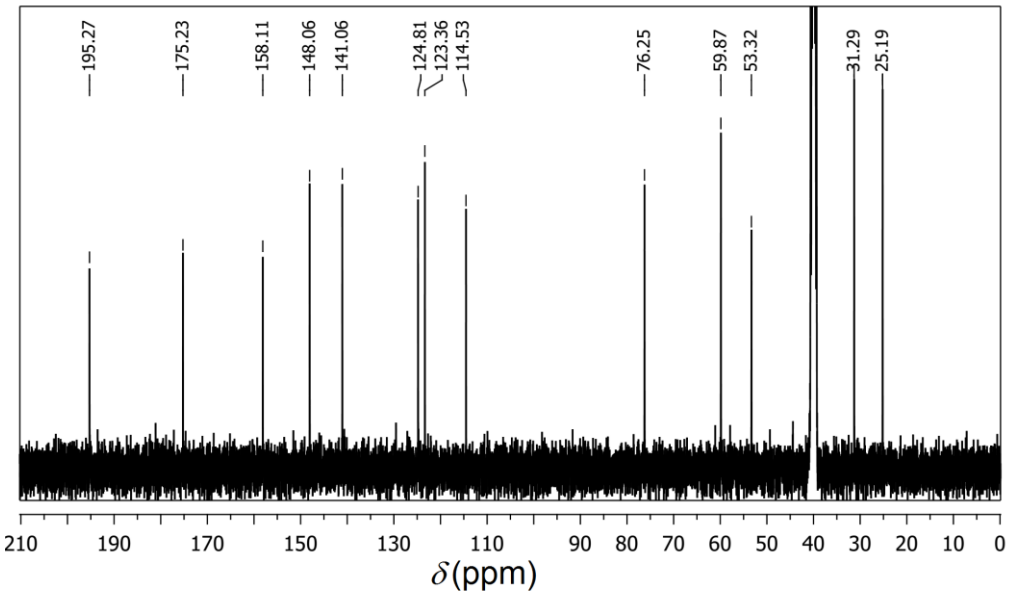

(b)

Fig. 3.6. (a) ^{1}H– and (b) ^{13}C–NMR spectra of [MoO_2(acacL^1)] (**1**) in dimethylsulfoxide–d_6.

3.3.5. Redox properties

Cyclic voltammograms of **1**–**5** were recorded using the corresponding ~10^{-3} M dimethylformamide solutions containing tetrabutylammonium perchlorate as the supporting electrolyte. The measurements were carried out at 298 K under nitrogen atmosphere with a Pt-disk working electrode, a Pt-wire auxiliary electrode and an Ag/AgCl reference electrode. Under identical condition the ferrocenium/ferrocene (Fc^+/Fc) couple was observed at $E_{1/2}$ = 0.66 V. All the complexes display an irreversible cathodic response (Fig. 3.7). The E_{pc} is –1.40 V for **1**, while for **2**–**5** it is in the range –0.93 to –1.09 V. The

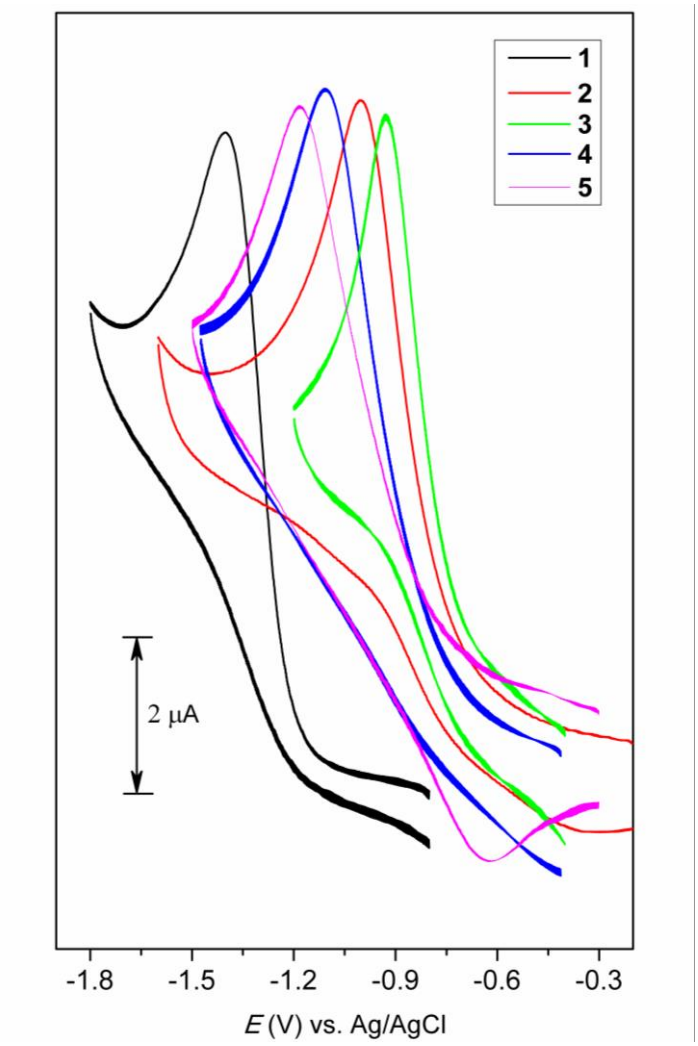

Fig. 3.7. Cyclic voltammograms of **1**–**5** in dimethylformamide.

one-electron nature of this electron transfer process has been conjectured by comparing the current heights with Fc^{+}/Fc and other known one-electron transfer processes [41,42]. On reverse scan except **5** no other complex shows any anodic response (Fig. 3.7). For **5**, the E_{pa} and the ΔE_p (= $E_{pa} - E_{pc}$) values are –0.52 V and 570 mV, respectively and the ratio of the cathodic peak current to the anodic peak current is ~5. These irreversible responses indicate the decomposition of the reduced species for all the complexes. Similar irreversible reductions observed in comparable potential ranges for complexes of *cis*-$\{MoO_2\}^{2+}$ with O,N-donor tri- and tetradentate ligands are attributed to Mo(VI) to Mo(V) reduction [5,8,14,15,19,20]. The reduction potential of **1** is significantly more cathodic than that of **2**–**5**. This is most likely due to better σ-donor ability of alcoholate-O in **1** than that of the phenolate-O in **2**–**5**. The trend in the reduction potentials of **2**–**5** is also consistent with the inductive effect of the substituent on the phenolate ring.

3.3.6. Plausible mechanism

X-ray structural characterization of **1**–**4** confirms their similar molecular structures and formation of the chiral tetradentate ligands $(acacL^{1-4})^{2-}$, the combined form of $(acac)^{-}$ and $(L^{n})^{-}$ in all four complexes. Considering the similarities in the synthetic methods for the preparation of **1**–**5** and their comparable physical properties, the same molecular structure of **5** and hence similar structure and coordination mode of the $(acacL^{5})^{2-}$ have been inferred. In control experiments without $[MoO_2(acac)_2]$, the observed transformation has not been observed. Thus, a possible *cis*-$\{MoO_2\}^{2+}$ coordination assisted Mannich-type [25,26] reaction mechanism for the formation of $(acacL^{n})^{2-}$ during the synthesis of **1**–**5** from $[MoO_2(acac)_2]$ and HL^{n} is suggested (Scheme 3.1).

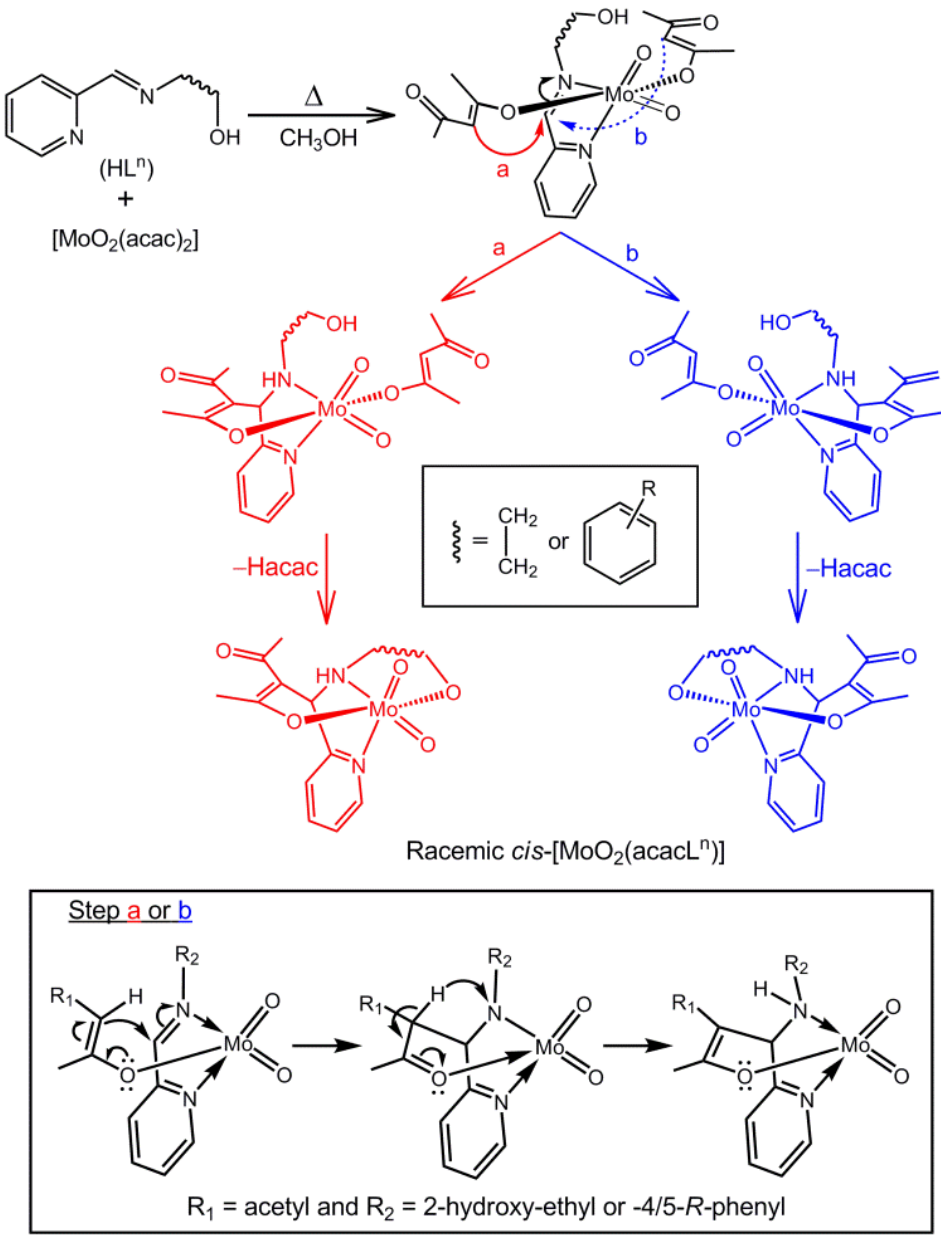

Scheme 3.1. Proposed mechanism for the formation of racemic *cis*-[MoO$_2$(acacL^n)] (n = 1–5).

In the very beginning, one O-atom of each of the two (acac)$^-$ ligands *trans* to the two strong *trans* labilising oxo groups in [MoO$_2$(acac)$_2$] dissociates and the two mutually *cis*-oriented vacant coordination sites thus created are occupied by the Schiff base HL^n through its pyridine-N and

azomethine-N atoms. In the resulting new species *cis*(O),*trans*(acac)-[$MoO_2(\eta^1$-acac$)_2(HL^n)$], nucleophilic attack on the polarized azomethine-C by the central carbon atom of one of the two *trans*-oriented $(\eta^1$-acac$)^-$ ligands is followed by a 1,3-proton shift from the attacking carbon atom to the azomethine-N atom (pathway 'a' or 'b'). As both 'a' and 'b' paths are equally probable, this step is expected to be the key step for the racemization of the product. The final step involves coordination and deprotonation of the dangling hydroxyl group of HL^n and elimination of the remaining $(\eta^1$-acac$)^-$ as Hacac.

3.4. Conclusions

In conclusion, *cis*-$\{MoO_2\}^{2+}$ assisted transformation of ligands and isolation of its complexes with the transformed chiral tetradentate ligands in their racemic forms have been described. It is very apparent that the transformation occurs due to intramolecular Mannich-type nucleophilic addition of the central =CH– of the coordinated acetylacetonate $(acac)^-$ across the N-coordinated polarized azomethine of the Schiff base system HL^n (= 2-(2-pyridyl-aldimine)ethanol and 4/5-*R*-2-(2-pyridylaldimine)phenols). The molecular structures of the complexes *cis*-$[MoO_2(acacL^n)]$ where $(acacL^n)^{2-}$ represents the transformed ligands determined by X-ray crystallography are consistent with their spectroscopic characteristics.

3.5. References

[1] Lang, C. Janiak, *Z. Anorg. Allg. Chem.*, 628, **2002**, 1259–1268.

[2] R. Dinda, P. Sengupta, S. Ghosh, H. Mayer-Figge, W.S. Sheldrick, J. Chem. Soc., *Dalton Trans.*, **2002**, 4434–4439.

[3] M. Cindrić, N. Strukan, V. Vrdoljak, B. Kamenar, *Z. Anorg. Allg. Chem.*, 630, **2004**, 585–590.

[4] A. Lehtonen, R. Sillanpää, *Polyhedron*, 24, **2005**, 257–265.

[5] N.R. Pramanik, S. Ghosh, T.K. Raychaudhuri, S. Chaudhuri, M. G. B. Drew, S.S. Mandal, *J. Coord. Chem.*, 60, **2007**, 2177–2190.

[6] D. Agustin, C. Bibal, B. Neveux, J.–C. Daran, R. Poli, *Z. Anorg. Allg. Chem.*, 635, **2009**, 2120–2125.

[7] C. Bibal, J.–C. Daran, S. Deroover, R. Poli, *Polyhedron*, 29, **2010**, 639–647.

[8] N.K. Ngan, K. M. Lo, C.S.R. Wong, *Polyhedron*, 30, **2011**, 2922–2932.

[9] K. Užarević, M. Rubčić, M. Radić, A. Puškarić, M. Cindrić, *Cryst.Eng.Comm.*, 13, **2011**, 4314–4323.

[10] R.D. Chakravarthy, D.K. Chand, *J. Chem. Sci.*, 123, **2011**, 187–199.

[11] K. Užarević, G. Pavlović, M. Cindrić, *Polyhedron*, 52, **2013**, 294–300.

[12] R. Takjoo, A. Akbari, M. Ahmadi, R.H. Amiri, G. Bruno, *Polyhedron*, 55 **2013**, 225–232.

[13] R. Takjoo, A. Hashemzadeh, H.A. Rudbari, F. Nicolo, *J. Coord. Chem.*, 66, **2013**, 345–357.

[14] S. Pasayat, S.P. Dash, S. Roy, R. Dinda, S. Dhaka, M.R. Maurya, W. Kaminsky, Y.P. Patil, M. Nethaji, *Polyhedron*, 67, **2014**, 1–10.

[15] S. Gupta, S. Pal, A.K. Barik, S. Roy, A. Hazra, T.N. Mandal, R.J. Butcher, S.K. Kar, *Polyhedron*, 28, **2009**, 711–720.

[16] M.E. Judmaier, A. Wallner, G.N. Stipicic, K. Kirchner, J. Baumgartner, F. Belaj, N.C. Mösch-Zanetti, *Inorg. Chem.*, 48, **2009**, 10211–10221.

[17] T. Arumuganathan, R. Mayilmurugan, M. Volpe, N.C. Mösch-Zanetti, *Dalton Trans.*, 40, **2011**, 7850–7857.

[18] S.K. Kurapati, U. Ugandhar, S. Maloth, S. Pal, *Polyhedron*, 42, **2012**, 161–167.

[19] Y.–L. Wong, Y.Yan, E.S.H. Chan, Q. Yang, T.C.W. Mak, D.K.P. Ng, J. Chem. Soc., *Dalton Trans*., **1998**, 3057–3064.

[20] A. Lehtonen, M. Wasberg, R. Sillanpää, *Polyhedron*, 25, **2006**, 767–775.

[21] M. Cindrić G. Galin, D. Matković-Čalogović, P. Novak, T. Hrenar, I. Ljubić, T. K. Novak, *Polyhedron*, 28, **2009**, 562–568.

[22] E. Zamanifar, F. Farzaneh, J. Simpson, M. Maghami, *Inorg. Chim. Acta.*, 414, **2014**, 63–70.

[23] R.J. Cross, L.J. Farrugia, P.D. Newman, R.D. Peacock, D. Stirling, *Inorg. Chem.*, 38, **1999**, 1186–1192.

[24] A. Riisiö, A. Lehtonen, M. M. Hänninen, R. Sillanpää, *Eur. J. Inorg. Chem.*, **2013**, 1499–1508.

[25] M. Arend, B. Westermann, N. Risch, *Angew. Chem. Int. Ed.*, 37, **1998**, 1044–1070.

[26] S.G. Subramaniapillai, *J. Chem. Sci.*, 125, **2013**, 467–482.

[27] M. Menon, S. Choudhuri, A. Pramanik, A. K. Deb, S.K. Chandra, N. Bag, S. Goswami, A. Chakravorty, *J Chem. Soc., Chem. Commun.*, **1994**, 57–58.

[28] N.R. Sangeetha, S.N. Pal, S. Pal, *Polyhedron*, 19, **2000**, 2713–2717.

[29] T. Birkle, A. Carbayo, J.V. Cuevas, G. García-Herbosa, A. Muñoz, *Eur. J. Inorg. Chem.*, **2012**, 2259–2266 and references therein.

[30] G.J.J. Chen, J.W. McDonald, W.E. Newton, *Inorg. Chem.*, 15, **1976**, 2612−2615.

[31] S. Striegler, M. Dittel, *Inorg. Chem.*, 44, **2005**, 2728–2733.

[32] N. Gomez-Blanco, J.J. Fernandez, A. Fernandez, D. Vazquez-Garcia, M. Lopez-Torres, J.M. Vila, *Eur. J. Inorg. Chem.*, **2009**, 3071−3083.

[33] *SMART* version 5.630 and *SAINT-plus* version 6.45, Bruker-Nonius Analytical X-ray Systems Inc., Madison, WI, USA, **2003**.

[34] G.M. Sheldrick, *SADABS,* Program for Area Detector Absorption Correction, University of Gottingen, Gottingen, Germany, **1997**.

[35] *CrysAlisPro v1.171.36.28, Agilent Technologies*, Yarnton, Oxfordshire, UK, **2013**.

[36] G.M. Sheldrick, *Acta Crystallogr., Sect. A.*, 64, **2008**, 112−122.

[37] L.J. Farrugia, *J. Appl. Crystallogr.*, 32, **1999**, 837−838.

[38] A.L. Spek, *Platon., A Multipurpose Crystallographic Tool*, Utrecht University, Utrecht, The Netherlands, **2002**.

[39] C.F. Macrae, I.J. Bruno, J.A. Chisholm, P.R. Edgington, P. McCabe, E. Pidcock, L. Rodriguez-Monge, R. Taylor, J. van de Streek, P. A. Wood, *J. Appl. Crystallogr.*, 41, **2008**, 466–470.

[40] X. Lei, N. Chelamalla, *Polyhedron*, 49, **2013**, 244–251.

[41] K. Nagaraju, S. Pal, *J. Organomet. Chem.*, 745-746, **2013**, 404–408.

[42] A.R.B. Rao, S. Pal, *J. Organomet. Chem.*, 762, **2014**, 58–66.

Appendix

FTIR spectrum of [MoO_2(acacL^1)] (**1**).

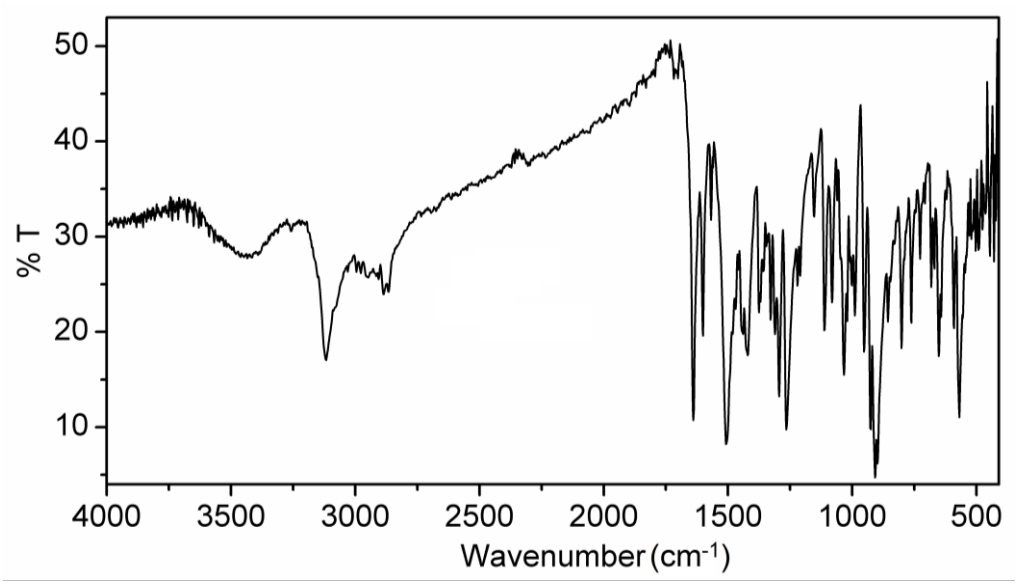

FTIR spectrum of [MoO_2(acacL^3)] (**3**)

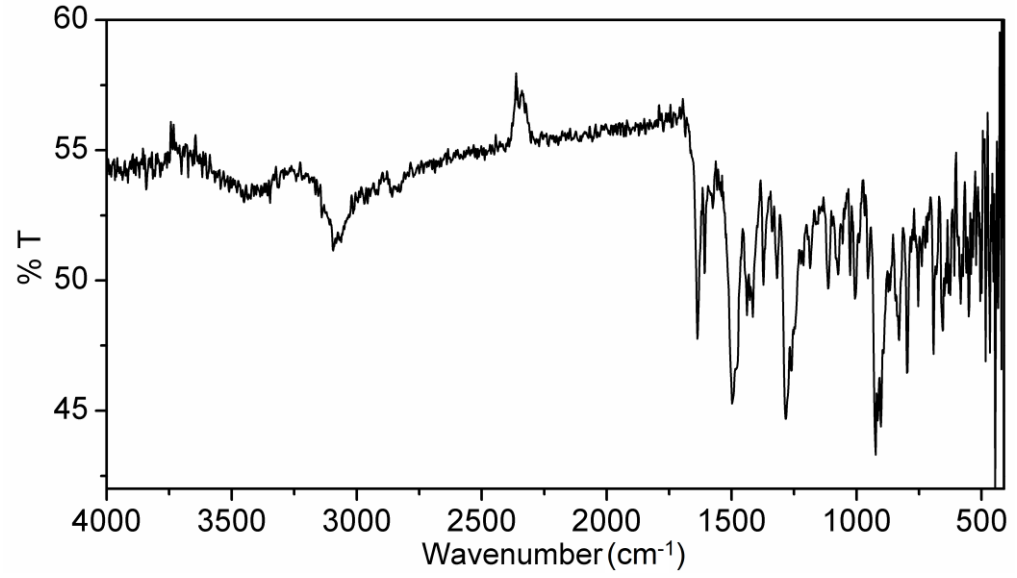

FTIR spectrum of [MoO_2(acacL^4)] (**4**)

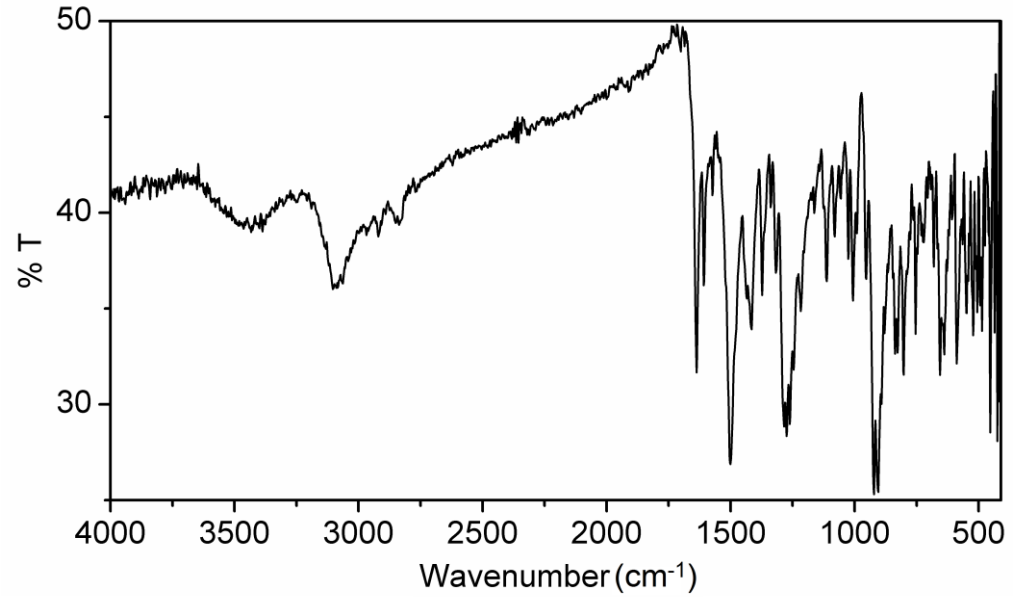

FTIR spectrum of [MoO_2(acacL^5)] (**5**)

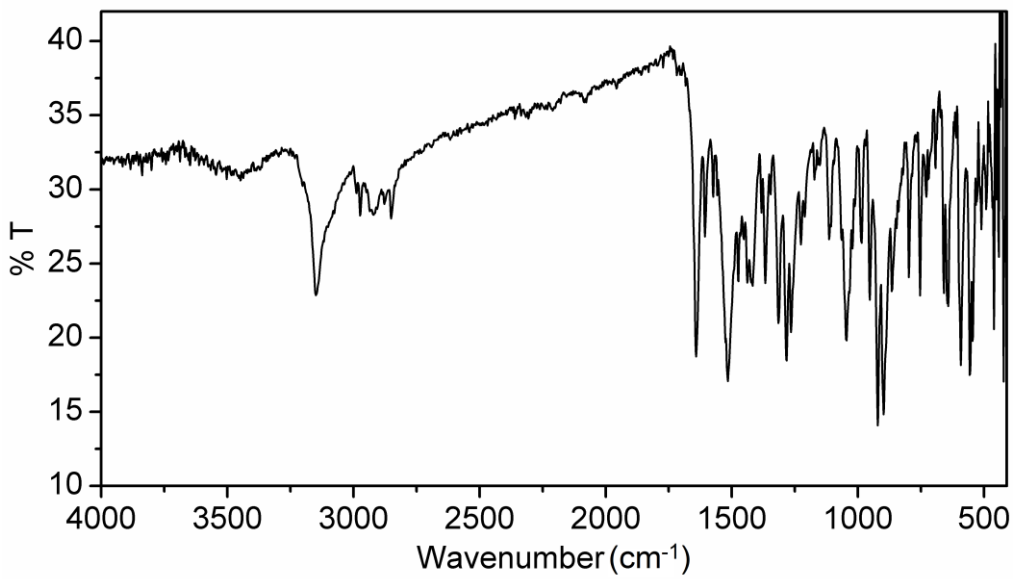

^{1}H-NMR Spectrum of [MoO(acacL^{2})] (**2**)

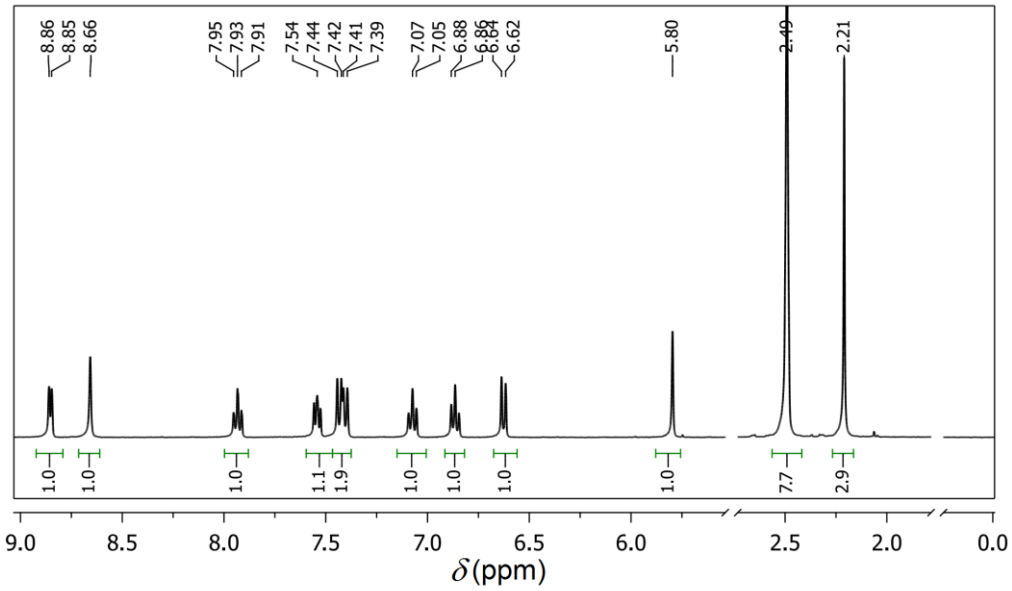

^{13}C-NMR Spectrum of [MoO(acacL^{2})] (**2**)

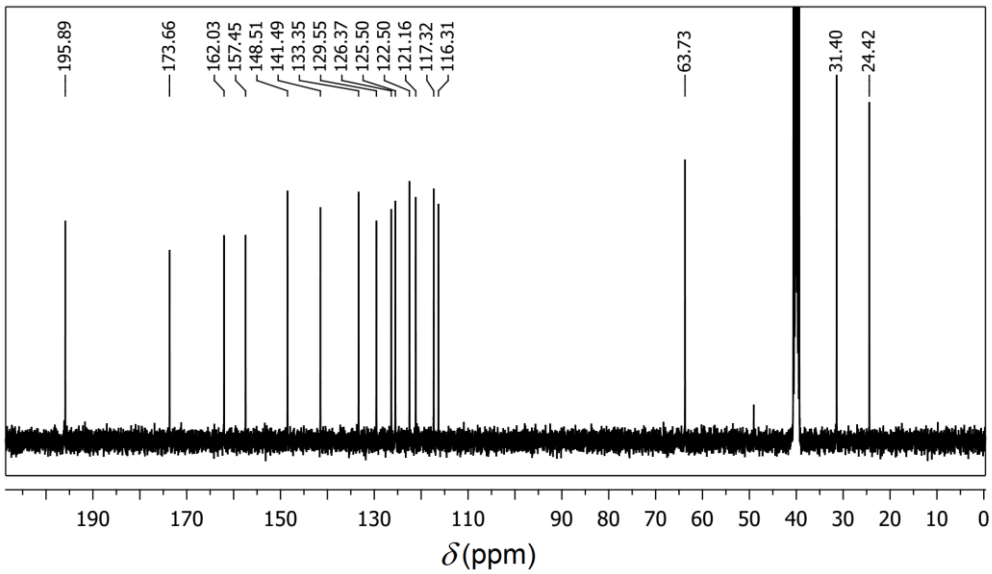

^{1}H-NMR Spectrum of [MoO(acacL^{3})] (3)

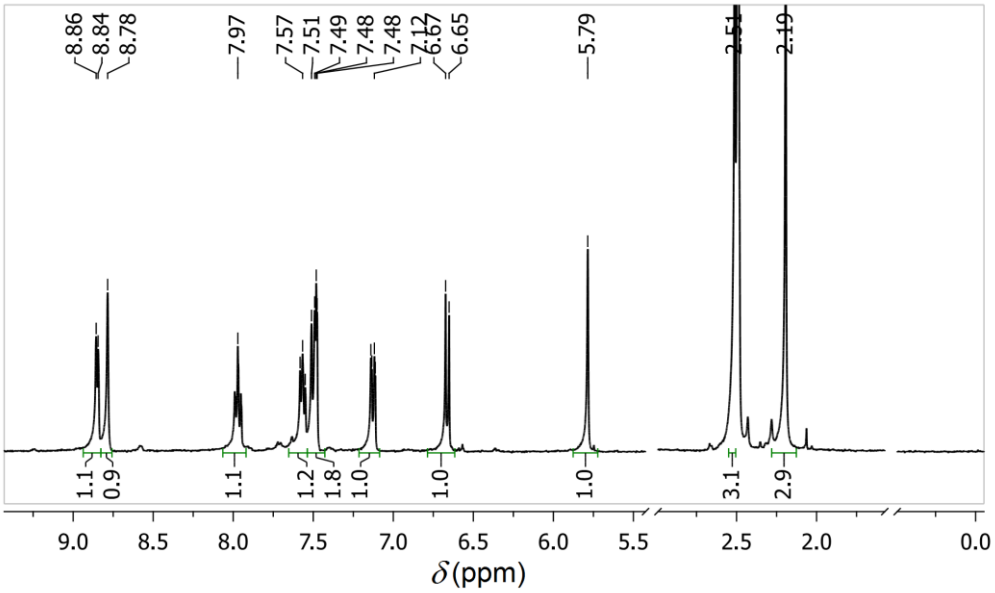

^{13}C-NMR Spectrum of [MoO(acacL^{3})] (**3**)

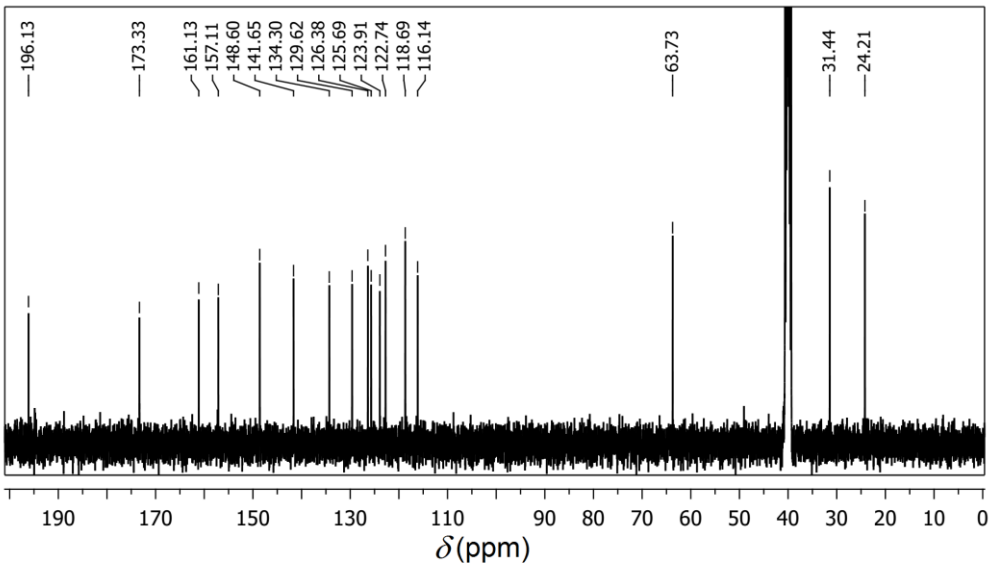

^{1}H-NMR Spectrum of [MoO(acacL^{4})] (**4**)

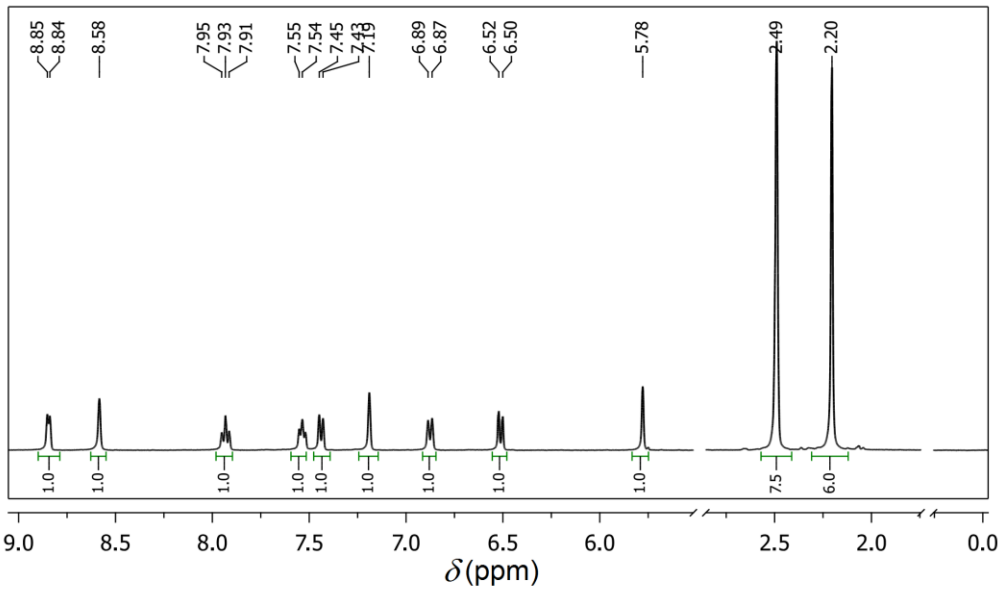

^{13}C-NMR Spectrum of [MoO(acacL^{4})] (**4**)

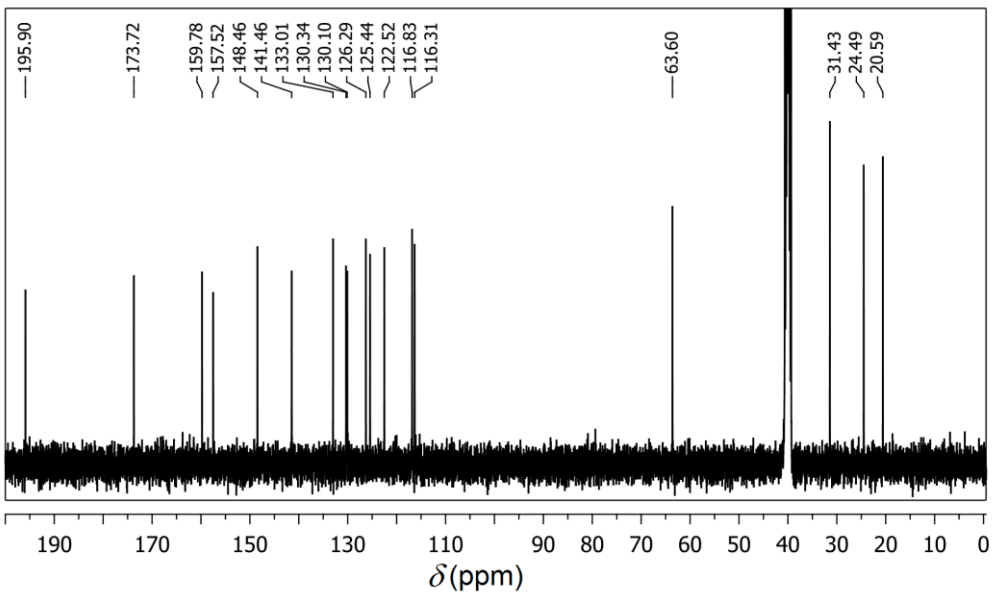

^{1}H-NMR Spectrum of [MoO(acacL^{5})] (**5**)

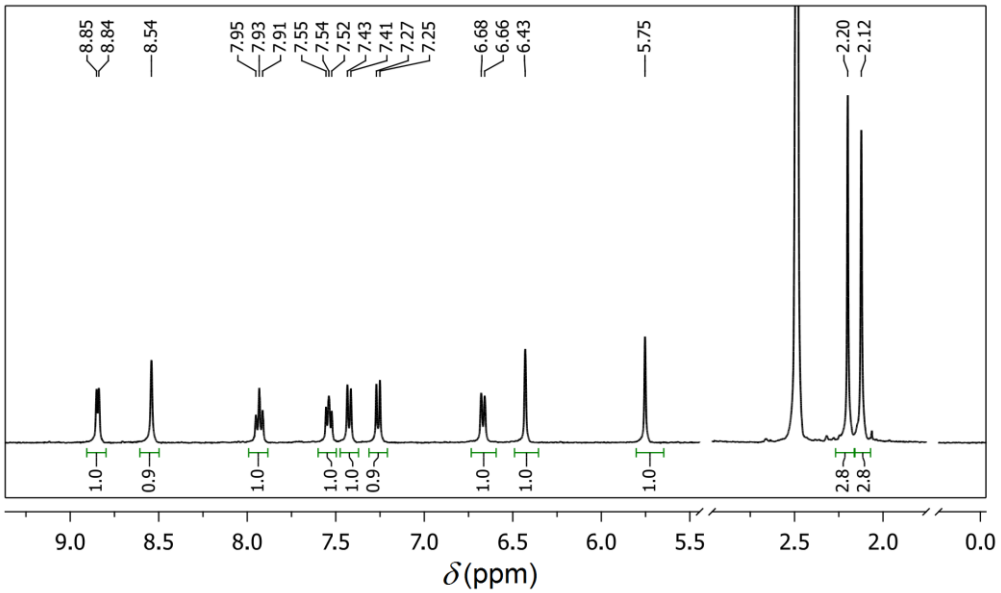

^{13}C-NMR Spectrum of [MoO(acacL^{5})] (**5**)

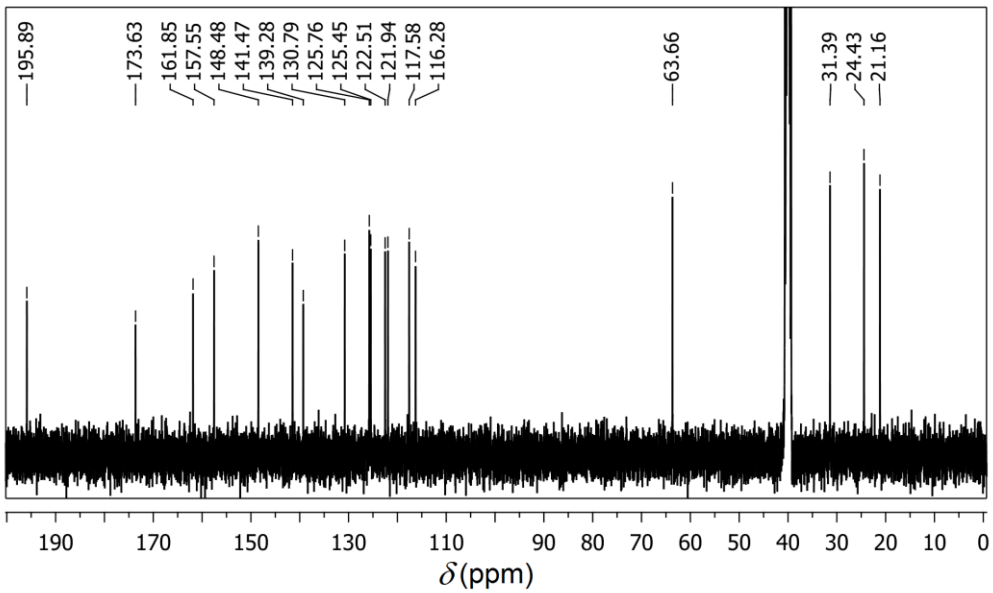

Atomic coordinates (x 10^4) and equivalent isotropic displacement parameters (Å^2 x 10^3). U(eq) is defined as one third of the trace of the orthogonalized Uij tensor.

Table A 3.1. For [MoO(acacL^1)] (**1**)

	X	Y	Z	U (eq)
Mo(1)	10786(1)	2366(1)	7543(1)	28(1)
O(1)	11774(2)	2991(1)	6643(1)	49(1)
O(2)	9860(2)	3237(1)	8276(1)	41(1)
O(3)	12888(2)	2048(1)	8292(1)	39(1)
O(4)	8530(2)	1999(1)	6810(1)	33(1)
O(5)	7414(2)	-259(1)	4835(1)	42(1)
N(1)	9421(2)	1081(1)	8456(1)	28(1)
N(2)	11591(2)	785(1)	7022(1)	26(1)
C(1)	8698(3)	1222(2)	9307(1)	35(1)
C(2)	7711(3)	480(2)	9746(2)	42(1)
C(3)	7465(3)	-439(2)	9302(2)	46(1)
C(4)	8218(3)	-595(2)	8432(2)	39(1)
C(5)	9189(3)	183(2)	8027(1)	28(1)
C(6)	10027(3)	81(1)	7070(1)	27(1)
C(7)	13217(3)	445(2)	7567(2)	35(1)
C(9)	6543(3)	1637(2)	5541(2)	39(1)
C(8)	14183(3)	1391(2)	7901(2)	43(1)
C(10)	7987(2)	1278(2)	6219(1)	29(1)
C(11)	8676(2)	315(1)	6275(1)	27(1)
C(12)	8267(2)	-456(2)	5563(1)	30(1)
C(13)	8982(3)	-1516(2)	5697(2)	40(1)

Table A 3.2. For [MoO(acacL^2)] (**2**)

	X	Y	Z	U (eq)
Mo(1)	5780(1)	2478(1)	8158(1)	33(1)
O(1)	7049(4)	4103(3)	9101(3)	48(1)
O(2)	7027(3)	1305(3)	7439(3)	47(1)
O(3)	5184(3)	2848(3)	6602(2)	38(1)
O(4)	5220(3)	1946(3)	9612(3)	43(1)
O(5)	1534(5)	2665(5)	12147(3)	81(1)
N(1)	3444(4)	658(3)	7126(3)	33(1)
N(2)	3356(4)	3397(3)	8616(3)	33(1)
C(1)	3482(5)	-571(4)	6071(4)	39(1)
C(2)	2069(6)	-1566(4)	5416(4)	48(1)
C(3)	538(6)	-1308(5)	5816(5)	56(1)
C(4)	498(5)	-53(5)	6897(4)	47(1)
C(5)	1966(4)	896(4)	7537(3)	34(1)
C(6)	2045(4)	2279(4)	8738(3)	34(1)
C(7)	2913(5)	3844(4)	7562(3)	35(1)
C(8)	3918(4)	3536(4)	6551(4)	35(1)
C(9)	3605(5)	3928(4)	5501(4)	45(1)
C(10)	2355(6)	4679(4)	5515(4)	51(1)
C(11)	1382(6)	5010(5)	6530(4)	52(1)
C(12)	1647(5)	4579(4)	7555(4)	44(1)
C(13)	4635(6)	1845(6)	11629(4)	54(1)
C(14)	4027(5)	2015(4)	10399(4)	38(1)
C(15)	2474(4)	2175(4)	10054(3)	35(1)
C(16)	1179(5)	2284(5)	10959(4)	45(1)
C(17)	-622(6)	1876(6)	10382(5)	60(1)

Table A 3.3. For [MoO(acacL^3)] (**3**)

	X	Y	Z	U (eq)
Mo(1)	4883(1)	3757(1)	2740(1)	34(1)
O(1)	5270(3)	5432(3)	3089(2)	55(1)
O(2)	6842(3)	2595(3)	2474(2)	54(1)
O(3)	4282(2)	4750(2)	1381(1)	41(1)
O(4)	4403(2)	2516(2)	4090(1)	39(1)
O(5)	61(3)	3093(2)	6003(1)	45(1)
N(1)	3483(3)	1747(2)	2476(1)	35(1)
N(2)	1878(3)	4656(2)	2856(1)	28(1)
C(1)	4260(4)	479(3)	2036(2)	43(1)
C(2)	3416(5)	-708(3)	1943(2)	51(1)
C(3)	1703(5)	-628(3)	2284(2)	52(1)
C(4)	888(4)	660(3)	2743(2)	41(1)
C(5)	1829(3)	1801(3)	2835(2)	31(1)
C(6)	1065(3)	3213(3)	3343(2)	28(1)
C(7)	1315(3)	5426(3)	1868(2)	30(1)
C(8)	2647(3)	5480(3)	1133(2)	35(1)
C(9)	2263(4)	6271(3)	173(2)	47(1)
C(10)	574(4)	6998(4)	-52(2)	52(1)
C(11)	-749(4)	6929(3)	693(2)	46(1)
C(12)	-399(3)	6156(3)	1655(2)	36(1)
C(13)	3636(4)	1758(3)	5775(2)	43(1)
C(14)	3055(3)	2415(3)	4735(2)	32(1)
C(15)	1382(3)	2798(3)	4447(2)	30(1)
C(16)	-95(3)	2942(3)	5166(2)	35(1)
C(17)	-1888(4)	2979(5)	4875(2)	64(1)
Cl(1)	-2877(1)	7852(1)	392(1)	76(1)

Table A 3.4. For [MoO(acacL^4)] (**4**)

Mo(1)	-107(1)	3817(1)	7755(1)	33(1)
O(1)	319(5)	5496(5)	8090(3)	54(1)
O(2)	1817(5)	2651(6)	7490(3)	53(1)
O(3)	-644(4)	4828(5)	6404(2)	41(1)
O(4)	-646(4)	2547(4)	9099(2)	37(1)
O(5)	-5006(5)	3087(5)	10996(2)	44(1)
N(1)	-3069(5)	4691(4)	7871(3)	26(1)
N(2)	-1533(5)	1779(5)	7498(3)	32(1)
C(1)	-3185(6)	1842(5)	7843(3)	28(1)
C(2)	-4152(7)	710(6)	7721(4)	39(1)
C(3)	-3380(8)	-536(7)	7259(4)	51(1)
C(4)	-1679(8)	-621(7)	6937(4)	50(1)
C(5)	-787(7)	553(6)	7054(4)	41(1)
C(6)	-3926(5)	3239(5)	8359(3)	26(1)
C(7)	-1473(7)	1742(7)	10770(4)	43(1)
C(8)	-1997(6)	2420(6)	9742(3)	31(1)
C(9)	-3651(6)	2792(5)	9447(3)	28(1)
C(10)	-5138(6)	2924(6)	10173(3)	33(1)
C(12)	-2269(6)	5550(6)	6154(3)	33(1)
C(13)	-3604(6)	5475(5)	6891(3)	26(1)
C(14)	-5288(6)	6158(6)	6674(3)	33(1)
C(15)	-5667(7)	6940(6)	5721(4)	40(1)
C(16)	-4321(8)	7002(7)	4991(4)	50(1)
C(17)	-2631(8)	6331(7)	5199(4)	47(1)
C(11)	-6900(7)	2914(11)	9884(4)	66(2)
C(18)	-7497(8)	7681(10)	5470(5)	68(2)

Chapter 4

Complexes of *cis*-$\{MoO_2\}^{2+}$ with unsymmetrical tetradentate tripodal NO_3-donor ligands: syntheses, characterization and catalytic applications[§]

A series of *cis*-dioxomolybdenum(VI) complexes of general formula *cis*-$[MoO_2(HL^n)]$ (**1**−**4**) have been synthesized in 80−85% yields by reacting equimolar amounts of $[MoO_2(acac)_2]$ ($acac^-$ = acetylacetonate) with 2,2'-(2-hydroxy-3,5-R_1,R_2-benzylazanediyl)diethanols (H_3L^n, n = 1−4) in methanol. Characterization of the complexes has been performed by elemental analysis, spectroscopic (IR, UV-Vis, ^{1}H- and ^{13}C-NMR) and electrochemical measurements. The molecular structures of all four complexes have been determined by single-crystal X-ray diffraction studies. In each of these analogous complexes, the metal centre is in a distorted octahedral NO_5 coordination sphere assembled by the single edge shared 5,5,6-membered chelate rings forming NO_3-donor $(HL^n)^{2-}$ and two *cis* oriented oxo groups. Crystal structures of the complexes reveal formation of discrete centrosymmetric dimeric species via a pair of reciprocal intermolecular O−H···O hydrogen bonding interactions. Spectroscopic data of all the complexes are consistent with their molecular structures. In the cyclic voltammograms, the redox-active complexes display a quasi-reversible to irreversible metal centred reduction with the cathodic peak potential in the range –0.92 to –1.12 V (vs. Ag/AgCl). All the complexes have been evaluated for their catalytic activities in oxidative bromination reactions of styrene and salicylaldehyde and in benzoin oxidation reaction.

4.1. Introduction

A vast number of *cis*-$\{MoO_2\}^{2+}$ complexes with a variety of ligands are available in the literature [1–5] and as mentioned in chapters 1 and 2, the majority of these complexes are with bi- and tridentate ligands. Reports on *cis*-

[§] This work has been published in *Inorg. Chim. Acta*, 430, **2015**, 67−73.

$\{MoO_2\}^{2+}$ complexes with tetradentate tripodal ligands are rather limited [6−16]. Tripodal ligands are structurally and electronically easily tunable and they create a pocket to hold the metal ion leaving one side open for ancillary ligands. Compared to bi- or tridentate ligands tetradentate tripodal ligands are expected to bind metal ions more strongly and provide more stable complexes due to their increased denticity and hence greater chelate effect.

In this chapter, we have explored the coordination chemistry of unsymmetrical tripodal tetradentate NO_3-donor 2,2'-(2-hydroxy-3,5-R_1,R_2-benzylazanediyl)diethanols (H_3L^n, n = 1–4) with $\{cis\text{-}MoO_2\}^{2+}$ and synthesized a series of complexes having the formula *cis*-$[MoO_2(HL^n)]$ (**1**−**4**) (Chart 4.1). The catalytic abilities of the isolated complexes in oxidative bromination reactions of styrene and salicylaldehyde and benzoin oxidation reaction were also assessed. In recent times, because of the convenient and eco-friendly nature, oxidative bromination with bromoperoxidases and their mimics have drawn considerable attention over traditional bromination using Br_2 [17–28]. Brominated organic compounds are of interest due to their applications as flame retardants, pharmaceuticals, biocides and pesticides [29–31]. Vanadium(V) based bromoperoxidases are most widespread amongst all the naturally occurring bromoperoxidases [17–24]. As a result complexes of oxovanadium(V) have been studied extensively as structural and functional models for bromoperoxidases [18, 32–35]. As mentioned in chapter 1, the reports on bromoperoxidase activities of *cis*-dioxomolybdenum(VI) complexes are rather limited [36–41], even though they are known to efficiently catalyze various organic oxidation reactions [42–47] and these catalytically active complexes are with mostly bi- and tridentate ligands than with tetradentate ligands [36–47]. α-Dicarbonyls belong to an important class of organic compounds in the context of their applications in synthetic organic chemistry. Hence, selective catalytic oxidation of benzoin to benzil is an

important key reaction [48–50]. However, not many reports on benzoin oxidation reaction catalyzed by oxomolybdenum(VI) species are available in literature [39,40,51,52]. Herein, we describe the details of synthesis, X-ray structures, physicochemical properties and catalytic behaviours of *cis*-[MoO$_2$(HL^n)] (**1**–**4**).

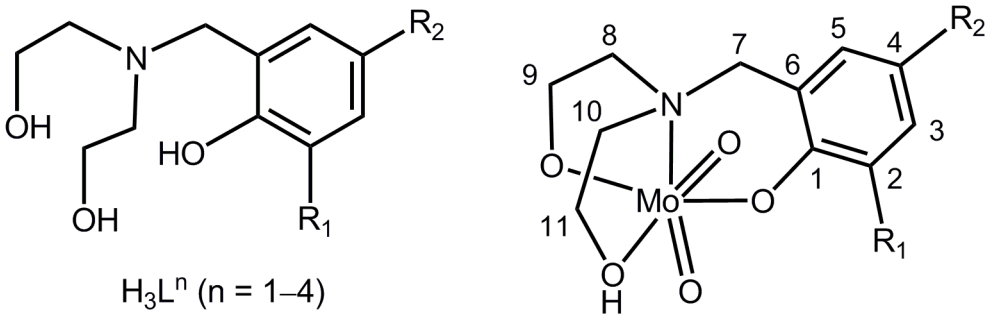

H_3L^n (n = 1–4)
n = 1 for R_1 = H and R_2 = Me
n = 2 for R_1 = H, R_2 = Et
n = 3 for R_1 = H and R_2 = ^{t}Bu
n = 4 for R_1 = ^{t}Bu and R_2 = ^{t}Bu

cis-[MoO$_2$(HL^n)]
1 (n = 1), **2** (n = 2),
3 (n = 3) and **4** (n = 4)

Chart 4.1. Chemical structures of N-caped tripodal ligands H_3L^{1-4} and their corresponding complexes *cis*-[MoO$_2$(HL$^{1–4}$)] (**1**–**4**).

4.2. Experimental

4.2.1. Materials

Bis(acetylacetonato)dioxomolybdenum(VI), [MoO$_2$(acac)$_2$], was prepared according to a literature procedure [53]. 2,2'-(2-hydroxy-3,5-R_1,R_2-benzylazanediyl)diethanols (H_3L^n) were synthesized using a procedure very similar to that reported earlier [54,55]. A general synthetic procedure and some characterization (LC-MS and NMR) data for H_3L^n have been provided in the supplementary material. All other chemicals were of analytical grade available commercially and used as received. Solvents were purified by standard procedures [56].

4.2.2. Physical measurements

A Thermo Finnigan Flash EA1112 series elemental analyzer was used to obtain the elemental (C, H, N) analysis data. A Shimadzu LCMS 2010 liquid chromatograph mass spectrometer was used for the purity verification of H_3L^n. Room temperature magnetic susceptibility measurements were performed with a Sherwood Scientific balance. Solution electrical conductivities were measured using a Digisun DI-909 conductivity meter. The infrared spectra were obtained with the help of a Thermo Scientific Nicolet 380 FT-IR spectrophotometer. The electronic spectra were collected with the help of a Shimadzu UV-3600 UV-Vis-NIR spectrophotometer. The ^1H (400 MHz) and ^{13}C (100 MHz) NMR spectra were recorded using tetramethylsilane as internal standard on a Bruker NMR spectrometer. The cyclic voltammetric measurements were performed on a CH Instruments model 620A electrochemical analyzer. Gas chromatographic measurements were performed with the help of Shimadzu GC-2010 Plus equipped with FID and Shimadzu GCMS-QP2010 instruments.

4.2.3. Synthesis of $H_3L^{1–4}$

A mixture of 10 mmol of paraformaldehyde, 10 mmol of diethanolamine and 10 mmol of phenol (*p*-cresol, 4-ethylphenol, 4-*t*-Bu-phenol, 2,4 di-*t*-Bu-phenol) in 25 ml of methanol was stirred under reflux condition for 24 h. Then the reaction mixture was cooled to room temperature and solvent was evaporated on a rotary evaporator. The residue obtained was dissolved in 5 ml of dichloromethane and excess of hexane was added. $H_3L^{1,2}$ were separated as pale yellow oils in about 5-10 minutes, while $H_3L^{3,4}$ were precipitated as white crystalline materials in about 1 h. $H_3L^{1,2}$ were collected by decanting the solvents and $H_3L^{3,4}$ were isolated by filtration. The products obtained after drying under vacuum were of

sufficient purity for the synthesis of the *cis*-dioxomolybdenum(VI) complexes in high yields. NMR quality samples of H_3L^n were obtained by flash column chromatographic purification using acetonitrile-dichloromathane (1:19) mixture as eluent.

***H_3L^1*.** Yellow oil, 75% yield. m/z = 226.20, ^{1}H NMR data in $CDCl_3$ (δ (ppm) (*J* (Hz))): 7.00 (8) (d, 1H), 6.82 (s, 1H), 6.76 (8) (d, 1H), 5.32 (br, s, 3H), 3.85 (s, 2H), 3.79 (4) (t, 4H), 2.81 (4) (t, 4H), 2.26 (s, 3H). ^{13}C NMR data in $CDCl_3$ (δ (ppm)): 154.78 (1C), 129.36 (1C), 129.15 (1C), 128.33 (1C), 122.17 (1C), 115.86 (1C), 59.60 (2C), 58.80 (1C), 55.81 (2C), 20.40 (1C).

***H_3L^2*.** Yellow oil, 78% yield. m/z = 240.15, ^{1}H NMR data in $CDCl_3$ (δ (ppm) (*J* (Hz))): 7.02 (8) (d, 1H), 6.83(s, 1H), 6.77 (8) (d, 1H), 5.20 (br, s, 3H), 3.85 (s, 2H), 3.78 (4) (t, 4H), 2.79 (4) (t, 4H), 2.56 (8) (q, 2H), 1.21 (8) (t, 3H). ^{13}C NMR data in $CDCl_3$ (δ (ppm)): 155.02 (1C), 135.08 (1C), 128.20 (1C), 128.04 (1C), 122.20 (1C), 116.01 (1C), 59.75 (2C), 59.08 (1C), 55.96 (2C), 27.96 (1C), 15.93 (1C).

***H_3L^3*.** White crystalline material, 82% yield. m/z = 268.15, ^{1}H NMR data in $CDCl_3$ (δ (ppm) (*J* (Hz))): 7.22 (8) (d, 1H), 7.01 (s, 1H), 6.79 (8) (d, 1H), 5.19 (br, s, 3H), 3.88 (s, 2H), 3.79 (4) (t, 4H), 2.81 (4) (t, 4H), 1.30 (s, 9H). ^{13}C NMR data in $CDCl_3$ (δ (ppm)): 154.68 (1C), 142.08 (1C), 125.68 (1C), 125.57 (1C), 121.60 (1C), 115.72 (1C), 59.93 (2C), 59.60 (1C), 56.02 (2C), 34.00 (1C), 31.64 (3C).

***H_3L^4*.** White crystalline material, 85% yield. m/z = 324.50, ^{1}H NMR data in $CDCl_3$ (δ (ppm) (*J* (Hz))): 7.25(s, 1H), 6.87 (s, 1H), 5.21 (br, s, 3H), 3.87 (s, 2H), 3.78 (4) (t, 4H), 2.81 (4) (t, 4H), 1.44 (s, 9H), 1.31 (s, 9H). ^{13}C NMR data in $CDCl_3$ (δ (ppm)): 153.80 (1C), 140.97 (1C), 135.90 (1C), 123.58 (1C), 123.15 (1C), 121.68 (1C), 60.39 (1C), 60.36 (2C), 56.46 (2C), 34.88 (1C), 34.19 (1C), 31.73 (3C), 29.66 (3C).

4.2.4. Synthesis of complexes cis-[$MoO_2(HL^{1-4})$] (1−4)

All the complexes were synthesized by using the following general procedure: 65 mg (0.2 mmol) of solid [$MoO_2(acac)_2$] was added to a hot methanol solution (30 ml) of 0.2 mmol of the corresponding H_3L^n (n = 1–4). The resulting mixture was boiled at reflux for 1 h. Then the reaction mixture was cooled to room temperature, filtered to remove suspended particles if any and allowed to evaporate slowly in air. After about a day the yellow microcrystalline material separated was collected by filtration, washed first with cold methanol and then with dichloromethane and hexane (1:1) mixture and finally dried in air.

cis-[$MoO_2(HL^1)$] (1). Yield 81%. Anal. calcd for $C_{12}H_{17}MoNO_5$: C, 41.04; H, 4.88; N, 3.99. Found C, 41.28; H, 4.56; N, 4.12 %. Selected IR data (cm^{-1}): 2947 (ν_{C-H} of CH_3), 2837−2668 (ν_{C-H} of $-CH_2-$), 908 and 881 (*cis*-$\{MoO_2\}^{2+}$). UV-Vis data (λ_{max} (nm) (10^{-3} x ε (M^{-1} cm^{-1})): 320sh (4.0), 285sh (6.7). ^{1}H NMR (δ (ppm) (*J* (Hz))): 9.03 (s, 1H, Mo-OH), 6.92 (8) (d, 1H, H^3), 6.89 (s, 1H, H^5), 6.56 (8) (d, 1H, H^2), 4.77 (15) (d, 1H, H^{7a}), 4.56 (m, 1H, H^{10a}), 4.40 (m, 1H, H^{10b}), 4.00 (15) (d, 1H, H^{7b}), 3.66 (m, 1H, H^{8a}), 3.58 (m, 1H, H^{8b}), 3.26 (m, 1H, H^{11a}), 3.19 (m, 1H, H^{11b}), 2.76 (m, 1H, H^{9a}), 2.55 (m, 1H, H^{9b}), 2.20 (s, 3H, 4-Me). ^{13}C NMR (δ (ppm)): 160.50 (1C, C^1), 132.18 (1C, C^4), 131.30 (1C, C^6), 131.03 (1C, C^2), 124.66 (1C, C^5), 120.62 (1C, C^3), 74.52 (1C, C^7), 64.16 (1C, C^{10}), 62.32 (1C, C^8), 59.47 (1C, C^{11}), 57.83 (1C, C^9) and 22.75 (1C, 4-Me). $E_{1/2}$ (V) (ΔE_p (mV)): –0.74 (360).

cis-[$MoO_2(HL^2)$] (2). Yield 80%. Anal. calcd for $C_{13}H_{19}MoNO_5$: C, 42.75; H, 5.24; N, 3.83. Found C, 42.68; H, 4.91; N, 3.95 %. Selected IR data (cm^{-1}): 2964 (ν_{C-H} of CH_3), 2854−2662 (ν_{C-H} of $-CH_2-$), 914 and 892 (*cis*-$\{MoO_2\}^{2+}$). UV-Vis data (λ_{max} (nm) (10^{-3} x ε (M^{-1} cm^{-1})): 321sh (2.6), 282sh (4.5). ^{1}H NMR (δ (ppm) (*J* (Hz))): 9.03 (s, 1H, Mo-

OH), 6.95 (8) (d, 1H, H^3), 6.91 (s, 1H, H^5), 6.59 (8) (d, 1H, H^2), 4.82 (15) (d, 1H, H^{7a}), 4.57 (m, 1H, H^{10a}), 4.40 (m, 1H, H^{10b}), 4.03 (15) (d, 1H, H^{7b}), 3.67 (m, 1H, H^{8a}), 3.58 (m, 1H, H^{8b}), 3.26 (m, 1H, H^{11a}), 3.19 (m, 1H, H^{11b}), 2.77 (m, 1H, H^{9a}), 2.56 (m, 1H, H^{9b}), 2.49 (2H, CH_2 of 4-Et), 1.13 (8) (t, 3H, CH_3 of 4-Et). ^{13}C NMR (δ (ppm)): 158.47 (1C, C^1), 135.38 (1C, C^4), 128.73 (1C, C^6), 127.85 (1C, C^2), 122.44 (1C, C^5), 118.43 (1C, C^3), 72.34 (1C, C^7), 62.04 (1C, C^{10}), 60.10 (1C, C^8), 57.22 (1C, C^{11}), 57.65 (1C, C^9), 27.74 (1C, CH_2 of 4-Et) and 16.28 (1C, CH_3 of 4-Et). $E_{1/2}$ (V) (ΔE_p (mV)): –0.77 (440).

cis-[MoO₂(HL³)] (3). Yield 83%. Anal. calcd for $C_{15}H_{23}MoNO_5$: C, 45.81; H, 5.89; N, 3.56. Found C, 45.86; H, 5.68; N, 3.51 %. Selected IR data (cm^{-1}): 2958 (ν_{C-H} of CH_3), 2859−2670 (ν_{C-H} of $-CH_2-$), 925 and 886 (*cis*-{MoO_2}$^{2+}$). UV-Vis data (λ_{max} (nm) (10^{-3} x ε (M^{-1} cm^{-1})): 320sh (2.7), 275sh (5.0). ^{1}H NMR (δ (ppm) (*J* (Hz))): 9.05 (s, 1H, Mo-OH), 7.14 (8) (d, 1H, H^3), 7.08 (s, 1H, H^5), 6.60 (8) (d, 1H, H^2), 4.80 (15) (d, 1H, H^{7a}), 4.59 (m, 1H, H^{10a}), 4.40 (m, 1H, H^{10b}), 4.07 (15) (d, 1H, H^{7b}), 3.68 (m, 1H, H^{8a}), 3.60 (m, 1H, H^{8b}), 3.27 (m, 1H, H^{11a}), 3.20 (m, 1H, H^{11b}), 2.77 (m, 1H, H^{9a}), 2.55 (m, 1H, H^{9b}), 1.23 (s, 9H, CH_3 of 4-*t*-Bu). ^{13}C NMR (δ (ppm)): 158.19 (1C, C^1), 142.37 (1C, C^4), 126.01 (1C, C^6), 125.38 (1C, C^2), 121.93 (1C, C^5), 118.11 (1C, C^3), 72.40 (1C, C^7), 62.24 (1C, C^{10}), 60.01 (1C, C^8), 57.17 (1C, C^{11}), 55.70 (1C, C^9), 34.19 (1C, 4-*t*-Bu) and 31.82 (3C, 4-*t*-Bu). E_{pc} (V): –0.96.

cis-[MoO₂(HL⁴)] (4). Yield 85%. Anal. calcd for $C_{19}H_{31}MoNO_5$: C, 50.78; H, 6.95; N, 3.12. Found C, 50.72; H, 6.71; N, 3.32 %. Selected IR data (cm^{-1}): 2953 (ν_{C-H} of CH_3), 2848−2660 (ν_{C-H} of $-CH_2-$), 903 and 881 (*cis*-{MoO_2}$^{2+}$). UV-Vis data (λ_{max} (nm) (10^{-3} x ε (M^{-1} cm^{-1})): 332 (3.6), 278sh (5.7). ^{1}H NMR δ ((ppm) (*J* (Hz))): 8.81 (s, 1H, Mo-OH), 7.12 (s, 1H, H^5), 6.95 (s, 1H, H^3), 4.75 (14) (d, 1H, H^{7a}), 4.54 (m,

1H, H^{10a}), 4.40 (m, 1H, H^{10b}), 4.04 (14) (d, 1H, H^{7b}), 3.65 (m, 1H, H^{8a}), 3.47 (m, 1H, H^{8b}), 3.31 (m, 1H, H^{11a}), 3.17 (m, 1H, H^{11b}), 2.81 (m, 1H, H^{9a}), 2.58 (m, 1H, H^{9b}), 1.31 (s, 9H, CH_3 of 2-*t*-Bu) 1.23 (s, 9H, CH_3 of 4-*t*-Bu). ^{13}C NMR (δ (ppm)): 159.42 (1C, C^1), 143.51 (1C, C^4), 139.34 (1C, C^2), 126.34 (1C, C^6), 124.56 (1C, C^5), 124.28 (1C, C^3), 73.77 (1C, C^7), 64.91 (1C, C^{10}), 62.62 (1C, C^8), 59.59 (1C, C^{11}), 57.62 (1C, C^9), 36.55 (1C, 2-*t*-Bu), 32.32 (3C, 2-*t*-Bu), 37.42 (1C, 4-*t*-Bu) and 34.12 (3C, 4-*t*-Bu). $E_{1/2}$ (V) (ΔE_p (mV)): –0.71 (830).

4.2.5. Procedure for oxidative bromination of styrene

A 10 ml round bottom flask containing 4 ml of 1:1 acetonitrile and water mixture was charged with 0.01 mmol of *cis*-[$MoO_2(HL^n)$], 520 μl (5 mmol) of styrene, 1.2 ml of 30% w/w aqueous solution (10 mmol) of H_2O_2, 1.2 g (10 mmol) of KBr and 1.2 ml of 60% aqueous (10 mmol) $HClO_4$. The mixture was stirred at 60° C for 4 h and then cooled to room temperature. After cooling it was diluted with 15 ml of water and extracted with dichloromethane (2 x 4 ml). The combined dichloromethane extracts were dried over anhydrous sodium sulphate and then subjected to GC analysis for calculation of yields from the areas under the peaks. The products were identified by GC-MS.

4.2.6. Procedure for oxidative bromination of salicylaldehyde

0.01 mmol of *cis*-[$MoO_2(HL^n)$], 530 μl (5 mmol) of salicylaldehyde, 1.2 ml of 30% w/w aqueous solution (10 mmol) of H_2O_2, 1.2 g (10 mmol) of KBr and 1.2 ml of 60% aqueous (10 mmol) $HClO_4$ were added to 4 ml of 1:1 acetonitrile and water mixture in a 10 ml round bottom flask. The mixture was stirred at 60°C for 1 h. After cooling to room temperature the mixture was diluted with 15 ml of water and then extracted with dichloromethane (2 x 4 ml). The

dichloromethane extracts were combined, dried over anhydrous sodium sulphate and then subjected to GC-MS analysis for identification of the products and calculation of yields from the areas under the peaks.

4.2.7. Procedure for benzoin oxidation

0.01 mmol of *cis*-[$MoO_2(HL^n)$] and 1.2 ml of 30% w/w aqueous solution (10 mmol) of H_2O_2 were added to 1.07 g (5 mmol) of benzoin taken in 3 ml of methanol. The resulting mixture was stirred at 60° C for 4 h. The reaction progress was monitored with TLC. After completion of the reaction the mixture was diluted with 15 ml of water and then extracted with dichloromethane (2 x 4 ml). After drying over anhydrous sodium sulphate the combined dichloromethane extracts were analyzed by GC-MS to identify the products and calculate the yields from the areas under the peaks.

4.2.8. X-ray crystallography

Single crystals of **1** and **3** were obtained by recrystallization of the corresponding complexes from hot acetonitrile and that of **2** and **4** were collected from the crystalline materials obtained during their synthesis. Selected crystallographic data for **1**−**4** are listed in Table 4.1. The unit cell parameters and the intensity data at 298 K for **1**, **3** and **4** were obtained with the help of an Oxford Diffraction Xcalibur Gemini single crystal X-ray diffractometer equipped with a graphite monochromator and a Mo Kα fine-focus sealed tube (λ = 0.71073 Å). The CrysAlisPro software [57] was used for data collection, reduction and absorption correction. Some residual absorption effects in the dataset of **4** were treated with XABS2 program [58]. Determination of the unit cell parameters and the collection of the intensity data at 298 K for **2** were performed on a Bruker-Nonius SMART APEX CCD single crystal diffractometer using graphite monochromated Mo Kα radiation

Table 4.1. Selected crystallographic data.

Complex	**1**	**2**	**3**·2CH_3CN	**4**
Empirical formula	$C_{12}H_{17}MoNO_5$	$C_{13}H_{19}MoNO_5$	$C_{19}H_{29}MoN_3O_5$	$C_{19}H_{31}MoNO_5$
Formula weight	351.21	365.23	475.39	449.39
Crystal system	Monoclinic	Monoclinic	Triclinic	Monoclinic
Space group	$P2_1/c$	$P2_1/c$	$P\bar{1}$	$P2_1/c$
a (Å)	6.582(4)	13.9819(9)	7.0365(5)	22.232(3)
b (Å)	32.2225(12)	6.9127(4)	11.8658(8)	7.3594(14)
c (Å)	7.0812(9)	15.0916(10)	14.0224(10)	12.894(2)
α (°)	90	90	70.158(6)	90
β (°)	119.653(6)	94.6510(10)	77.337(6)	90.071(17)
γ (°)	90	90	86.791(5)	90
V (Å^3)	1340.09(19)	1453.84(16)	1074.27(13)	2109.6(6)
Z	4	4	2	4
ρ (g cm^{-3})	1.741	1.669	1.47	1.415
μ (mm^{-1})	0.994	0.920	0.644	0.648
Reflections collected	4886	13382	6862	5203
Reflections unique	2349	2567	3780	3251
Reflections [$I \geq 2\sigma(I)$]	2217	2342	3134	2121
Parameters	172	182	255	241
$R1$, $wR2$ [$I \geq 2\sigma(I)$]	0.0613, 0.1064	0.0242, 0.0650	0.0504, 0.1171	0.0832, 0.1585
$R1$, $wR2$ (all data)	0.0663, 0.1081	0.0269, 0.0663	0.0640, 0.1281	0.1263, 0.1778
GOF on F^2	1.449	1.083	1.042	1.056
$\Delta\rho_{max}$, $\Delta\rho_{min}$ (e Å^{-3})	0.663 / −1.107	0.360 / −0.313	0.913 / −0.886	1.662 / −1.174

(λ = 0.71073 Å).The SMART and the SAINT-Plus [59] programs were used for data acquisition and data extraction, respectively. An empirical absorption correction was applied using the SADABS program [60]. The structure of each of **1**−**4** was solved by direct method and refined on F^2 by full−matrix least-squares procedures. All non-hydrogen atoms were refined using anisotropic thermal parameters. All hydrogen atoms were included in the structure factor calculations at idealized positions by using a riding model. The SHELX-97 programs [61] provided in the WinGX package [62] were used for structure solution and refinement. The Platon [63] and the Mercury [64] packages were used for molecular graphics. X-ray crystallographic data (in CIF format) have been deposited with Cambridge Crystallographic Data Centre. The deposition nos. are CCDC 1042110–1042113 for **1**–**4**, respectively.

4.3. Results and discussion

4.3.1. Synthesis and some properties

The tripodal 2,2'-(2-hydroxy-3,5-R_1,R_2-benzylazanediyl)diethanols (H_3L^n) (Chart 4.1) were synthesized in 75–85% yields by Mannich condensation reactions of equimolar amounts of bis(2-hydroxyethyl)amine, corresponding substituted phenols and formaldehyde in methanol under reflux condition. The complexes *cis*-[$MoO_2(HL^n)$] (**1**−**4**) were synthesized by reacting the appropriate H_3L^n and [$MoO_2(acac)_2$] in refluxing methanol. All four complexes were isolated as yellow microcrystalline materials in very good yields (80−85%). The elemental analysis data are in good agreement with those calculated for **1**−**4**. Magnetic susceptibility measurements indicate the diamagnetic character of all the complexes. The diamagnetic behaviour is consistent with the +6 oxidation state of the metal centre in each of the four complexes. All the complexes are highly soluble in dimethylformamide and

dimethylsulfoxide, moderately soluble in methanol, ethanol, acetonitrile, chloroform and dichloromethane and insoluble in diethylether, hexane and toluene. In solution, each of the four complexes is electrically non-conducting.

4.3.2. Spectroscopic characterization

4.3.2.1. Infrared spectra

Infrared spectra of H_3L^n and the corresponding complexes (**1**−**4**) were recorded in KBr pellets. Representative spectra are illustrated in Fig. 4.1. The remaining spectra are provided in the appendix at the end of the chapter. All the spectra show a large number of bands of various intensities in the range 4000–400 cm^{-1}. However, except for the following selected few we have not attempted to assign the remaining bands. The spectra of H_3L^n show a strong and broad band around 3350 cm^{-1} corresponding to its three hydroxyl functionalities. In contrast, the complexes display a very weak broad band centred at ~3420 cm^{-1}. The disappearance of the strong broad band is consistent with deprotonation of two out of three hydroxyl groups of the ligand due to complexation. The weak band at ~3420 cm^{-1} is perhaps due to the lone hydrogen bonded metal coordinated OH group in the complexes. The bands corresponding to the symmetric and asymmetric stretches of the *cis*-$\{MoO_2\}^{2+}$ core in **1**−**4**, are observed in the ranges 925−903 and 892−881 cm^{-1}, respectively [6–8,11,14,16,65–71].

4.3.2.2 Electronic spectra

The electronic spectra of **1**–**4** were recorded in dimethylsulfoxide solutions. The spectral profiles are very similar. The spectra of **1**–**4** have been shown in Fig. 4.2. All the complexes display two strong absorptions in the ranges 332–317 and 285–280 nm. Comparable absorptions observed for complexes of *cis*-dioxomolybdenum(VI) with ligands having similar

coordinating atoms have been assigned to ligand-to-metal charge transfer and ligand centred transitions, respectively [14,34,65–71].

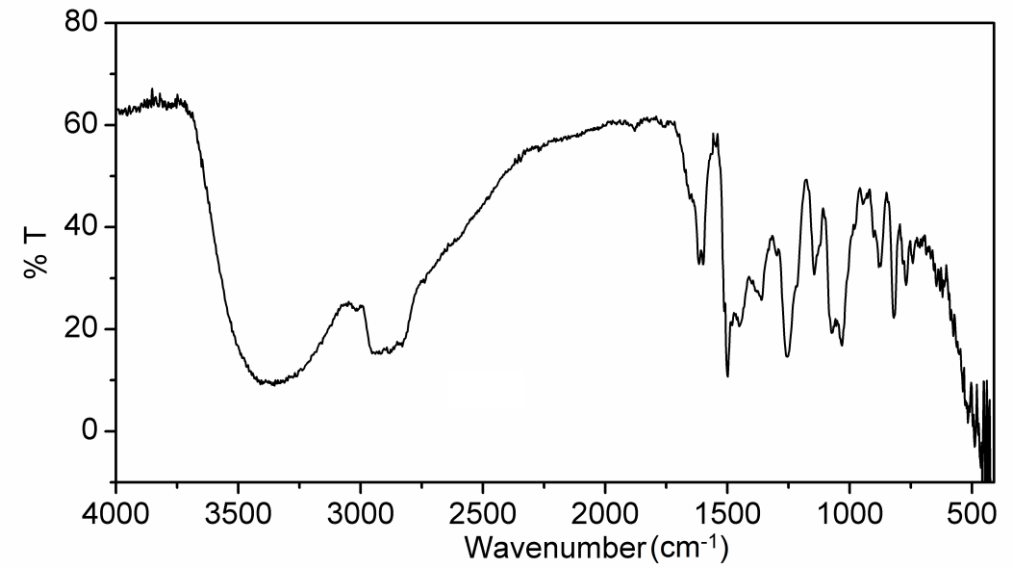

(a)

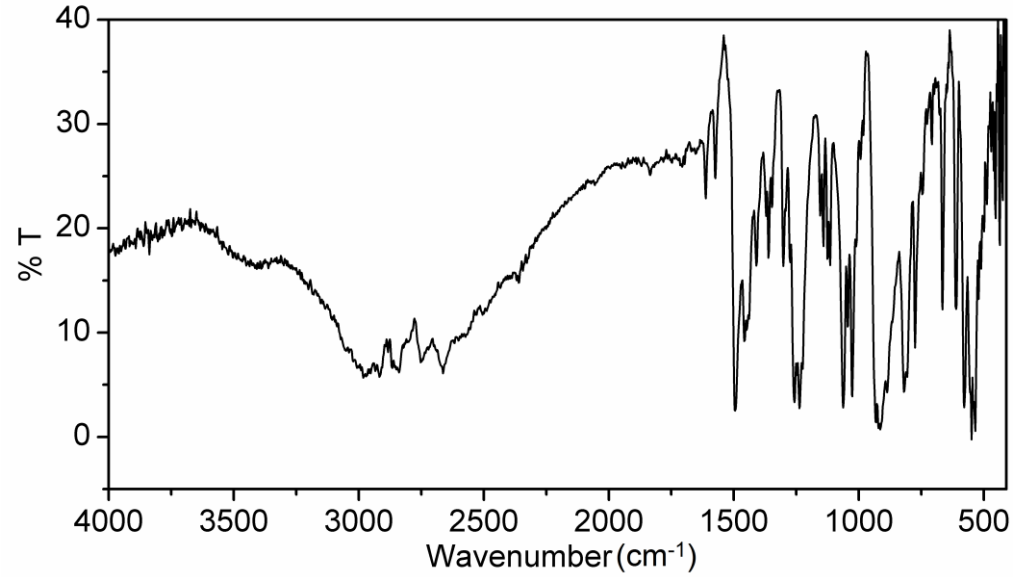

(b)

Fig. 4.1. FTIR spectrum of (a) H_3L^1 and (b) *cis*-[$MoO_2(HL^1)$] (**1**).

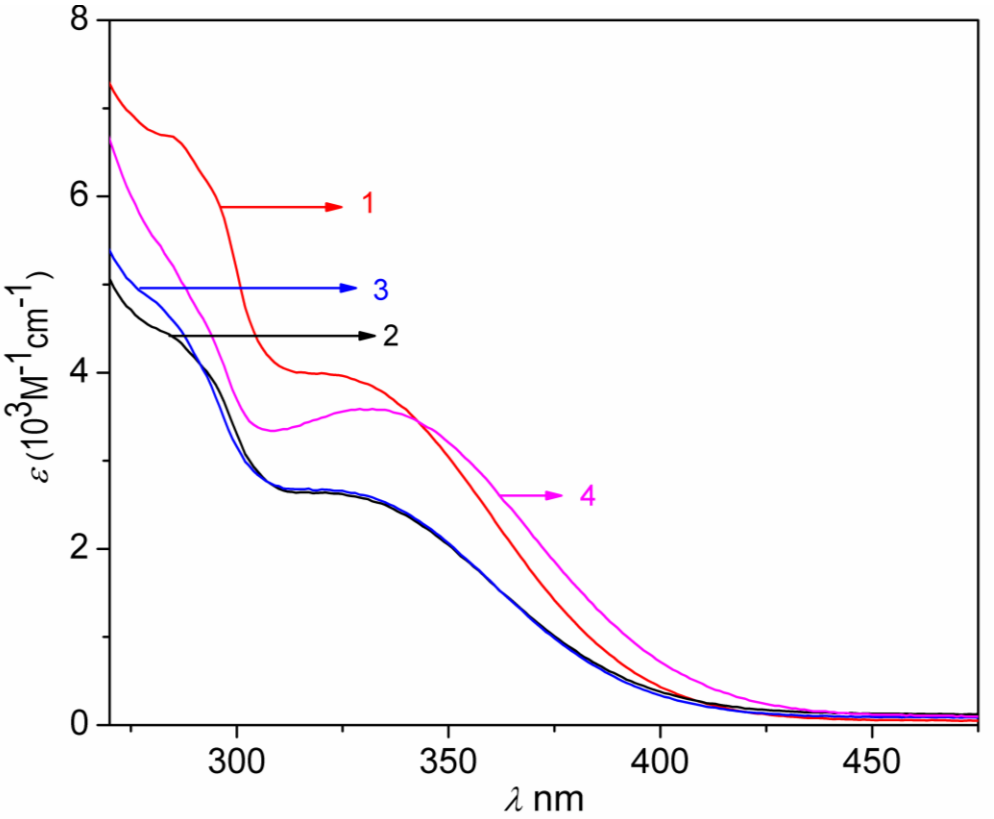

Fig. 4.2. Electronic spectra of *cis*-[$MoO_2(HL^{1–4})$] (**1**–**4**) in dimethylsulfoxide.

4.3.2 3. NMR spectra

^{1}H-, ^{13}C- and ^{13}C-DEPT NMR spectroscopic measurements with DMSO-d_6 solutions of **1**–**4** have been performed. Representative spectra are illustrated in Fig. 4.3 and the remaining spectra are provided in the appendix at the end of the chapter. The spectral data of all four complexes are consistent with the corresponding molecular structures as established by X-ray crystallography. The ^{1}H-NMR spectra of **1**–**3** show two doublets in the ranges δ 6.56–6.60 and 6.92–7.14 ppm for the protons at C^2 and C^3, respectively (Chart 4.1). The singlet observed at δ 7.12 ppm in the spectrum of **4** is assigned to the proton at C^3. The C^5 proton of **1**–**4** resonates as a singlet within δ 6.89–7.08 ppm. Each signal corresponding to the protons at C^3 and C^5 show a small splitting due to the spatial interaction with protons of the

alkyl substituent. The methyl group (at C^4) protons of **1** are observed as a singlet at δ 2.19 ppm, while the *t*-butyl group (at C^4) protons of each of **3** and **4** appear as singlet at δ 1.23 ppm. In the case of **2**, the methyl protons of the ethyl group (at C^4) resonate as a triplet at δ 1.13 ppm, while the signal corresponding to the methylene protons of the same ethyl substituent coincides with the residual DMSO signal at 2.49 ppm. The tertiary butyl group (at C^2) protons of **4** resonate as a singlet at δ 1.31 ppm. A relatively broad signal observed within δ 8.81–9.05 ppm for **1**–**4** is attributed to the metal coordinated hydroxyl group proton. Because of diastereotopicity, the five methylene group protons of each complex show ten signals in the range δ 2.5–5.0 ppm. The methylene group (*ortho* to the phenolate) protons (at C^7) show two clear doublets at δ ~4.79 and ~4.04 ppm. The protons at C^{10}, the methylene group (bonded to N) of the protonated arm of $(HL^n)^{2-}$ appear as two multiplets at δ ~4.57 and ~4.40 ppm. On the other hand, the corresponding methylene group (bonded to N) protons at C^8 of the deprotonated arm of $(HL^n)^{2-}$ are observed as two multiplets at δ ~3.67 and ~3.53 ppm. The methylene group (bonded to coordinated OH) protons at C^{11} show two multiplets at δ ~3.29 and 3.19 ppm. In contrast, the multiplets corresponding to the methylene group (bonded to the ethanolate-O) protons at C^9 are observed at δ ~2.79 and ~2.57 ppm.

The ^{13}C-NMR spectra of **1**–**4** display the resonances corresponding to the aromatic carbons C^1–C^6 in the ranges δ 158.2–160.5, 125.4–139.3, 118.1–124.4, 132.2–143.5, 121.9–124.7 and 126.0–131.3 ppm, respectively. The methylene carbon (C^7) attached to the phenolate ring resonates within δ 72.3–74.5 ppm. Two signals observed in the ranges δ 60.0–62.6 and 55.7–57.8 ppm are attributed to the methylene carbon atoms C^8 and C^9, respectively of the ethanolate arm of $(HL^n)^{2-}$. Two more signals appeared within δ 62.0–64.9 and 55.7–59.6 ppm are assigned to the methylene carbon atoms C^{10} and C^{11} of the ethanol arm of $(HL^n)^{2-}$. The carbon atom of the methyl substituent in **1**

resonates at δ 22.75 ppm, while the primary and the secondary carbon atoms of the ethyl substituent in **2** are observed at δ 16.28 and 27.74 ppm,

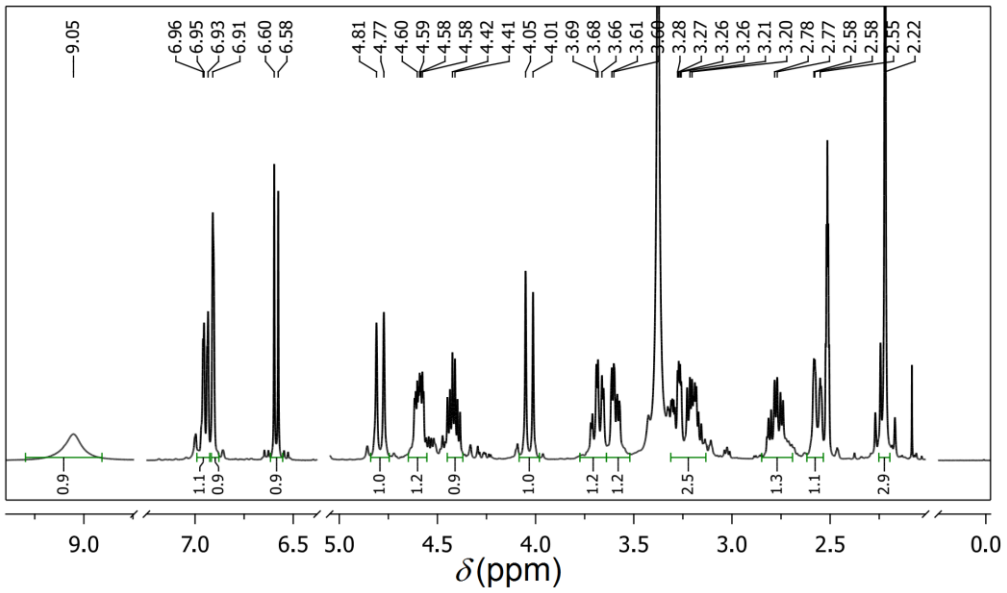

(a)

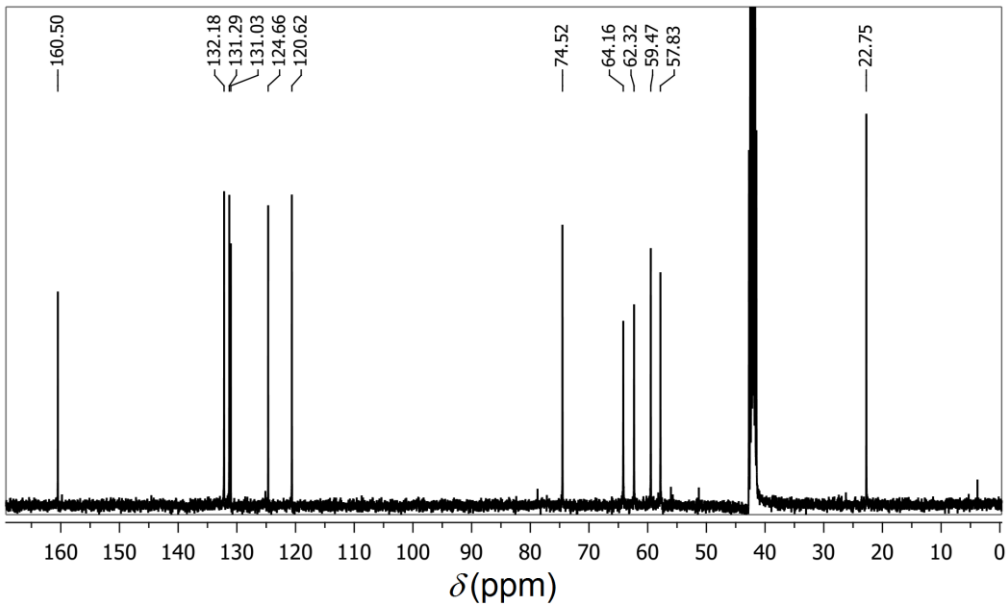

(b)

Fig. 4.3. (a) ^{1}H– and (b) ^{13}C–NMR spectra of [MoO_2(HL^1)] (**1**) in dimethylsulfoxide-d_6.

respectively. The quaternary carbon atom of the *t*-butyl group at *para* position of the phenolate ring appears at δ 34.19 and 37.42 ppm for **3** and **4**, respectively. The primary carbon atoms of the same *t*-butyl substituent in **3** and **4** are observed at δ 31.82 and 34.12 ppm, respectively. The resonances for the quaternary and the primary carbon atoms of the *t*-butyl group at *ortho* position of the pehenolate ring in **4** are observed at δ 36.55 and 32.32 ppm, respectively.

4.3.3. Description of X-ray structures

Complexes **1**, **2** and **4** crystallize in the monoclinic $P2_1/c$ space group without any lattice solvent molecule, while **3** crystallizes in the triclinic $P\bar{1}$ space group with acetonitrile molecules (Table 4.1). Asymmetric unit of each of **1**, **2** and **4** contains one complex molecule and that of **3** contains one complex and two acetonitrile molecules. The bond lengths and angles related to the metal centres are listed in Table 4.2. The molecular structures of **1**–**4** are illustrated in Figs. 4.4 and 4.5. Overall molecular structures of all the complexes are very similar. In each complex, the dianionic tripodal ligand $(HL^n)^{2-}$ coordinates the metal centre through the amine-N, the ethanol-O, the ethanolate-O and the phenolate-O atoms. The intraligand bond parameters are unexceptional. The phenolate-O, the amine-N and the ethanolate-O atoms span meridionally, while the ethanol-O and the two mutually *cis* oxo groups occupy the other meridian and complete a distorted octahedral NO_5 coordination sphere around the metal centre. The Mo−O(3) (2.287(6)−2.292(4) Å) and the Mo−N(1) (2.320(8)−2.364(4) Å) bonds, which are *trans* to the two oxo groups (O(4) and O(5)), are significantly longer compared to the Mo−O(1) (1.922(6)−1.941(4) Å) and Mo−O(2) (1.958(6)−1.967(3) Å) bonds. It is very likely that the *trans* lengthening of the Mo(1)–O(3) facilitates the proton to be on O(3) rather than on the more

strongly metal bound O(1) or O(2), where it will be more acidic and hence easily dissociable. There is no effect of the single substituent at *para* to the phenolate-O (O(1)) on the Mo–O(1) bond lengths in **1**–**3**. However, the Mo–O(1) bond length is shorter by ~0.02 Å in **4** compared to the corresponding bond lengths in **1**–**3** (Table 4.2). This shortening indicates that the Mo–O(1) bond is relatively stronger in **4** than in **1**–**3**.

Table 4.2. Selected bond lengths (Å) and angles (^{o}) for **1**–**4**.

Complex	**1**	**2**	**3**.2CH_3CN	**4**
Mo−O(1)	1.941(4)	1.9406(17)	1.941(3)	1.922(6)
Mo−O(2)	1.960(4)	1.9639(16)	1.967(3)	1.958(6)
Mo−O(3)	2.292(4)	2.2932(17)	2.288(3)	2.287(6)
Mo−O(4)	1.693(4)	1.6938(18)	1.693(3)	1.686(6)
Mo−O(5)	1.704(5)	1.7009(17)	1.698(4)	1.724(6)
Mo−N(1)	2.361(5)	2.3422(18)	2.364(4)	2.320(8)
O(1)−Mo−O(2)	153.01(19)	153.26(7)	152.45(15)	152.8(3)
O(1)−Mo−O(3)	80.29(17)	80.66(7)	80.20(11)	80.6(2)
O(1)−Mo−O(4)	94.5(2)	94.05(9)	94.94(14)	96.0(3)
O(1)−Mo−O(5)	103.3(2)	104.07(9)	104.35(14)	104.1(3)
O(1)−Mo−N(1)	78.69(18)	78.73(6)	78.45(12)	78.6(3)
O(2)−Mo−O(3)	84.94(16)	85.69(7)	85.39(11)	85.1(3)
O(2)−Mo−O(4)	95.1(2)	95.03(9)	94.58(14)	93.7(3)
O(2)−Mo−O(5)	87.4(2)	96.82(8)	97.11(15)	96.9(3)
O(2)−Mo−N(1)	75.24(2)	75.17(6)	74.77(13)	75.0(3)
O(3)−Mo−O(4)	167.1(2)	168.51(8)	168.35(16)	169.1(3)
O(3)−Mo−O(5)	84.12(19)	82.89(8)	83.45(14)	83.1(3)
O(3)−Mo−N(1)	71.55(17)	71.53(6)	71.69(12)	71.4(2)
O(4)−Mo−O(5)	108.6(2)	108.36(9)	108.08(18)	107.8(3)
O(4)−Mo−N(1)	96.0(2)	97.53(8)	97.02(15)	97.8(3)
O(5)−Mo−N(1)	155.0(2)	153.57(8)	154.26(14)	153.7(3)

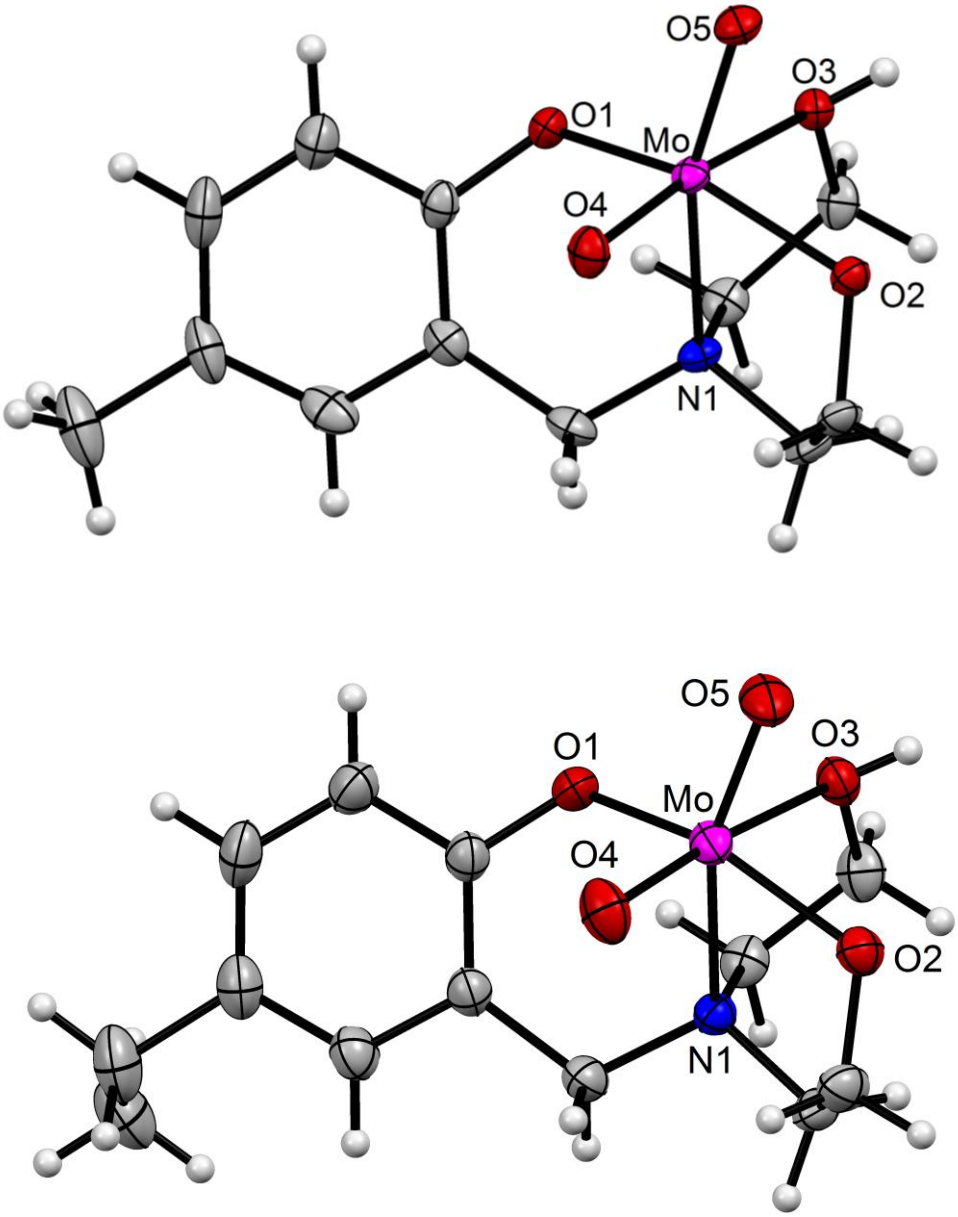

Fig 4.4. Molecular structures of *cis*-[$MoO_2(HL^1)$] (**1**) (top) and *cis*-[$MoO_2(HL^2)$] (**2**) (bottom). All non-hydrogen atoms are represented by their 30% probability thermal ellipsoids.

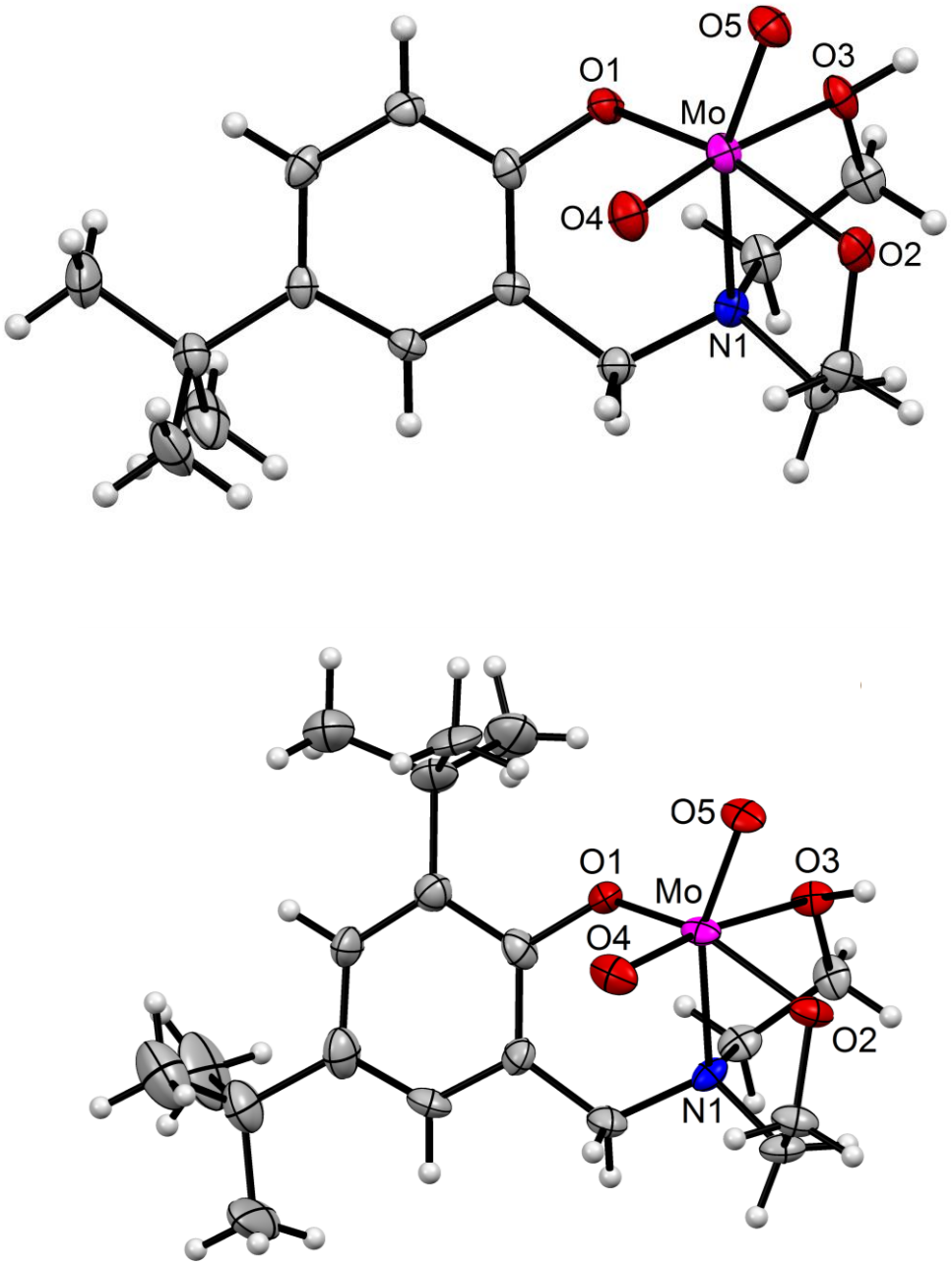

Fig 4.5. Molecular structures of *cis*-[$MoO_2(HL^3)$] (**3**) (top) and *cis* -[$MoO_2(HL^4)$] (**4**) (bottom). All non-hydrogen atoms are represented by their 30% probability thermal ellipsoids.

This is very likely due to the combined positive inductive effect of the two *t*-butyl groups at both *ortho* and *para* positions with respect to the phenolate-O (O(1)) in **4**. Overall, the bond lengths and the bond angles associated with the metal centres in all four complexes are within the ranges reported for *cis*-dioxomolybdenum(VI) complexes with ligands bearing similar coordinating atoms [6–16,40,65–72].

4.3.4. Hydrogen bonding and self-assembly

Considering the presence of one protonated ethanol arm of $(HL^n)^{2-}$ and several hydrogen bond acceptors in *cis*-[$MoO_2(HL^n)$] (**1**−**4**), we have searched for the conventional intermolecular hydrogen bonding interaction and the subsequent self-assembled supramolecular structure for all four complexes. Indeed the metal coordinated ethanol-OH (O(3)–H) participates in a strong O−H···O interaction involving the metal coordinated ethanolate-O (O(2)) of another molecule. The O(3)···O(2) distances vary within the range 2.586(4)–2.606(2) Å, while the O(3)−H···O(2) angles are ~175° for this interaction in **1**−**4** (Table 4.3). In the crystal lattice, the molecules of each of the four complexes dimerise via two such reciprocal O(3)−H···O(2) interactions [71]. The dimers of **1**–**4** are represented in Fig. 4.6.

Table 4.3. Hydrogen bonding parameters (Å and °) for **1**–**4**.

Complex	D−H···A	D···A (Å)	D−H···A (°)
1	O(3)−H(3A)···O(2)^{i}	1.77	2.586(6)
2	O(3)−H(3A)···O(2)^{ii}	1.79	2.606(2)
3	O(3)−H(3A)···O(2)^{iii}	1.77	2.586(4)
4	O(3)−H(3A)···O(2)^{iv}	1.78	2.594(9)

Symmetry transformations used: (i) –x + 2, –y, –z + 2; (ii) –x, –y + 2, –z + 2; (iii) –x, –y + 2, –z + 1; (iv) –x + 1, –y, –z + 1.

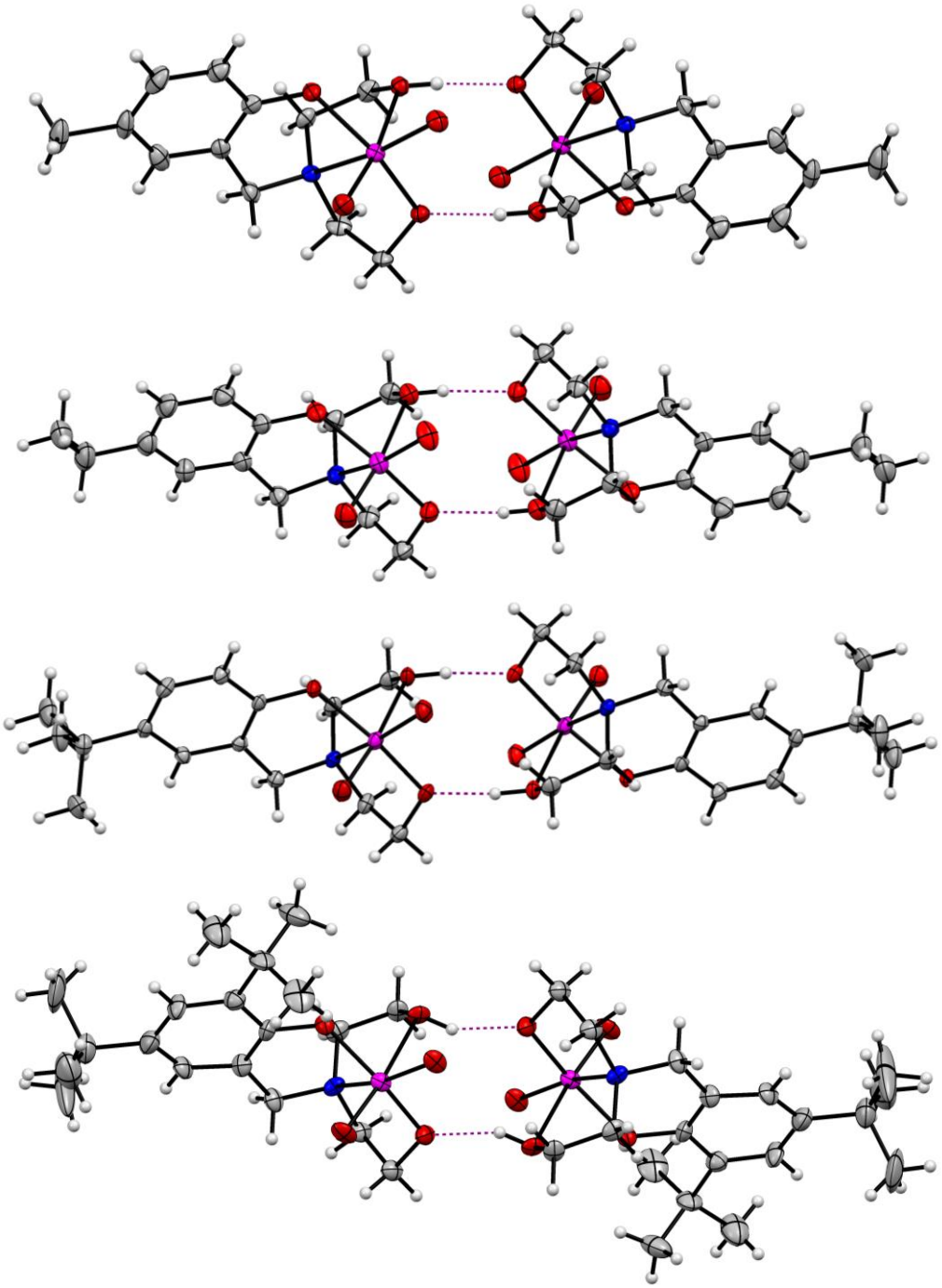

Fig 4.6. Intermolecular Hydrogen bonding directed dimers of **1**–**4** (from top to bottom, respectively).

4.3.5. Powder X-Ray diffraction patterns

The powder X-ray diffraction patterns using the crystalline samples of all the complexes were also collected. The experimental diffraction patterns have been compared with the corresponding simulated diffraction patterns generated from the single crystal X-ray diffraction data (Fig. 4.7).

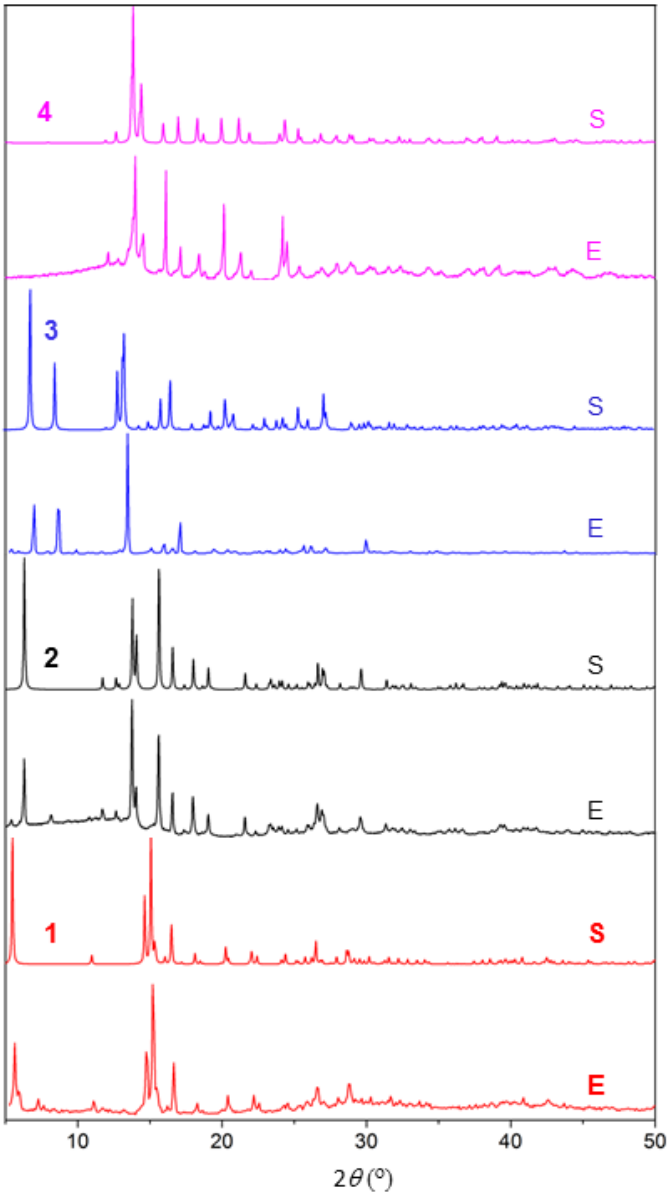

Fig. 4.7. Simulated (S) and experimental (E) powder X-ray diffraction patterns for *cis*-[MoO_2($HL^{1–4}$)] (**1**–**4**).

The satisfactory agreement between the simulated and the experimental diffraction patterns indicates the bulk purity of sample and phase for each of **1**, **2** and **4**. However, the experimental curve is somewhat different than the simulated curve for **3**·2CH_3CN (Fig. 4.7). In all probability, this difference is due to the loss of some of the lattice acetonitrile molecules during grinding of the sample.

4.3.6. Redox properties

Electron-transfer properties of **1**–**4** have been investigated by cyclic voltammetry using their ~10^{-3} M solutions in acetonitrile-dimethylformamide (9:1) containing tetrabutylammonium perchlorate as the supporting electrolyte. The measurements were carried out under nitrogen atmosphere at 298 K with the three electrode setup comprised of a Pt-disk working electrode, a Pt-wire auxiliary electrode and an Ag/AgCl reference electrode. The ferrocenium/ferrocene (Fc^+/Fc) couple appeared at $E_{1/2}$ = 0.63 V under identical condition. The cyclic voltammograms of **1**–**4** have been illustrated in Fig. 4.8. All the complexes display a quasi-reversible to irreversible reduction response on the cathodic side of the Ag/AgCl reference electrode. The E_{pc} values of this reduction span the range –0.92 to –1.12 V. The reduction is irreversible for **3** while the E_{pa} values for the remaining three complexes (**1**, **2** and **4**) are within –0.29 to –0.56 V. The ratio of peak currents (i_{pc}/i_{pa}) for the quasi-reversible responses varies from 2 to 4. The cathodic peak currents are comparable with that of Fc^+/Fc couple and other known one electron-transfer processes [68,73]. Similar electron-transfer responses observed for *cis*-dioxomolybdenum(VI) complexes with ligands containing comparable donor atoms have been assigned to Mo(VI) → Mo(V) process [7,8,40,68–70].

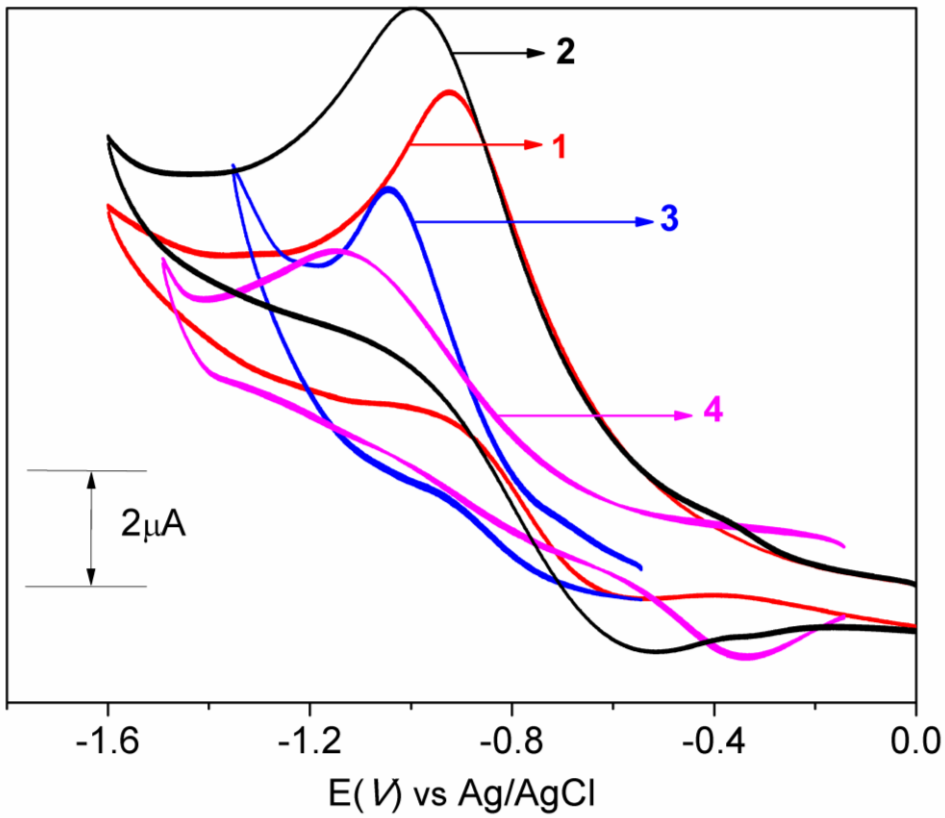

Fig. 4.8. Cyclic voltammograms (scan rate 100 mVs^{-1}) of *cis*-[$MoO_2(HL^{1–4})$] (**1**–**4)** in CH_3CN-$(CH_3)_2NC(O)H$ (1:1).

4.3.7. Catalytic studies

The catalytic behaviours of **1**–**4** in oxidative bromination reactions of styrene and salicylaldehyde and in benzoin oxidation reaction have been investigated (Scheme 4.1). Various solvents, different temperatures and catalyst loadings have been screened using **1** as the catalyst for optimization of all the three reaction conditions. In each reaction, irrespective of the types of the products and their selectivities, only complete or nearly complete conversion of the substrate has been considered during the optimization. These optimized reaction conditions have been used for scrutiny of the remaining three complexes (**2**–**4**) as catalysts. The details of the yields, selectivity and TOF values are summarized in Table 4.4.

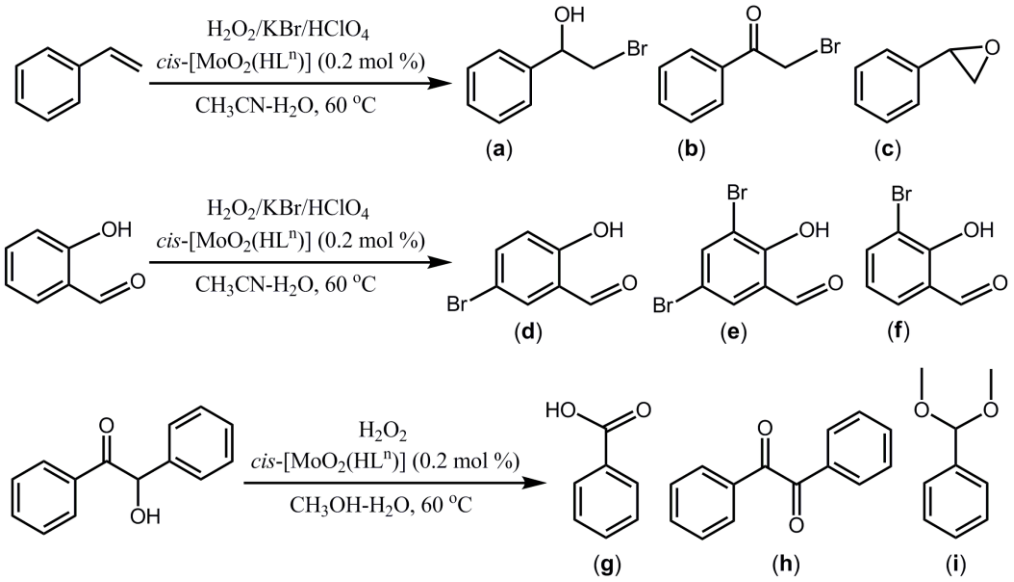

Scheme 4.1. Substrates and the products obtained using *cis*-[$MoO_2(HL^{1–4})$] (**1**–**4**) as catalysts.

Table 4.4. Catalysis data.

Reaction and catalyst	Conversion (%)	TOF (h^{-1})	Product selectivity (%)		
Bromination of styrene			(**a**)	(**b**)	(**c**)
1	99	124	15	73	11
2	98	123	23	68	7
3	96	120	10	73	11
4	95	119	15	68	10
Bromination of salicyladehyde			(**d**)	(**e**)	(**f**)
1	99.5	497	74	19	7
2	99.8	499	70	26	4
3	99.6	498	67	28	5
4	99.7	499	62	34	4
Benzoin oxidation			(**g**)	(**h**)	(**i**)
1	99.9	125	59	29	12
2	99.9	125	57	28	15
3	99.9	125	53	30	17
4	99.9	125	60	33	7

Generally in the present catalytic studies less number of significant products has been detected when compared with earlier studies on the same reactions in presence of *cis*-dioxomolybdenum(VI) complexes with various tridentate ligands as catalysts [39–41]. However, for all the three reactions the TOF values obtained with **1**–**4** as catalysts are lower than the corresponding values reported earlier.

4.3.7.1. Oxidative bromination of styrene

The catalyst *cis*-[$MoO_2(HL^n)$], styrene, H_2O_2, KBr and $HClO_4$ in the mole ratio of 0.01:5:10:10:10 in acetonitrile-water (1:1) mixture at 60 °C have been found as the best condition for maximum conversion of the substrate in about 4 h. Under this condition, three products 2-bromo-1-phenylethane-1-ol (**a**), 2-bromo-1-phenylethane-1-one (**b**) and styrene oxide (**c**) have been identified (Scheme 4.1) for each of the four catalysts (**1**–**4**). The yield of **b** is significantly higher than that of the other two products (**a** and **c**). It is important to note that the formation of **b** has occurred most likely through the oxidation of **a**. The change of the catalyst from **1** to **4** does not affect too significantly the percentage substrate conversion and product selectivity. Under specified condition as mentioned above the control experiment without catalyst has been carried out. The control experiment shows only 10% conversion of the substrate to 2-bromo-1-phenylethane-1-ol (**a**) as the major product. The product selectivities observed here are slightly different than that reported for the bromination reaction of the same substrate catalyzed by *cis*-dioxomolybdenum(VI) complexes [39–41]. In the previous studies, with **a** and **c** formation of 1,2-diol and 1,2-dibromo derivatives instead of **b** have been observed. We could detect a trace amount (< 1%) of the dibromo product but no diol.

4.3.7.2.Oxidative bromination of salicylaldehyde

The optimized reaction condition for oxidative bromination of salicylaldehyde using *cis*-[$MoO_2(HL^n)$] as catalyst is same as described above for oxidative bromination of styrene. But here the maximum conversion of the substrate has been realized within 1 h. The catalytic behaviours of **1**–**4** in this reaction are comparable (Table 4.4). In all the cases, 5-bromosalicylaldehyde (**d**), 3,5-dibromosalicylaldehyde (**e**) and 3-bromosalicylaldehyde (**f**) have been identified as the products (Scheme 4.1). The 5-bromosalicylaldehyde (**d**) has been produced more selectively than the other two products with essentially complete conversion of the substrate. In the control experiment without any catalyst, only 30% of substrate conversion with 100% selectivity for 5-bromosalicylaldehyde (**d**) has been observed in 4 h of reaction time. In earlier studies on bromination of salicylaldehyde using *cis*-dioxomolybdenum(VI) complexes as catalysts [39,40], **d** was the major product as observed here. However, unlike the present observation 2,4,6-tribromo phenol was also reported with **e** and **f** as a minor product.

4.3.7.3. Benzoin oxidation

The *cis*-[$MoO_2(HL^n)$] catalyzed benzoin oxidation reactions have been carried out in methanol employing H_2O_2 as the oxidant. The mole ratio of catalyst, substrate and oxidant used for the reaction is 0.01:5:10. It may be noted that comparable results were obtained when acetonitrile or ethanol was used instead of methanol as the reaction solvent. In all the cases, benzoic acid (**g**), benzil (**h**) and α,α-dimethoxytoluene (**i**) have been detected as the products with complete conversion of benzoin (Scheme 4.1, Table 4.4). Benzoic acid (**g**) is preferentially formed as the major product followed by benzil (**h**) and then α,α-dimethoxytoluene (**i**). A trace amount (< 1%) of methylbenzoate was also detected. As observed in the preceding two catalytic

reactions, here also the catalytic efficiencies of **1**–**4** do not vary in a significant way. Previous studies on benzoin oxidation reactions employing cis-dioxomolybdenum(VI) complexes as catalysts have demonstrated benzoic acid (**g**) to be the major product as found here, but along with (**h**) and (**i**) a comparable amount of methylbenzoate has been also reported as an additional minor product [39,40].

4.4. Conclusions

The N-capped unsymmetrical tripodal tetradentate 2,2'-(2-hydroxy-3,5-R_1,R_2-benzylazanediyl)diethanols (H_3L^n) afford complexes of general molecular formula *cis*-[$MoO_2(HL^n)$] (**1**−**4**) in very good yields. X-ray crystallographic studies reveal the same gross molecular structure for all the complexes. In each complex, the ligand $(HL^n)^{2-}$ acts as 5,5,6-membered chelate rings forming NO_3-donor towards the *cis*-{MoO_2}$^{2+}$ unit. In the crystal lattice, the molecules of each complex form discrete dimers via two reciprocal intermolecular O−H···O interactions involving the ethanol-OH and the ethanolate-O both being metal coordinated. The spectroscopic (IR, UV-Vis and NMR) features of **1**−**4** complement their molecular structures very well. The redox-active complexes are also catalytically active in oxidative bromination reactions of styrene and salicylaldehyde and in benzoin oxidation reaction. The overall catalytic performances of **1**−**4** in these reactions are generally invariant to the type and number of substituents on the phenolate moiety of the ligands.

4.5. References

[1] J.A. Brito, B. Royo, M. Gómez, *Catal. Sci. Technol.*, 1, **2011**, 1109–1118.

[2] R.G. de Noronha, A.C. Fernandes, *Curr. Org. Chem.*, 16, **2012**, 33–64.

[3] A. Syamal, M.R. Maurya, *Coord. Chem. Rev.*, 95, **1989**, 183–238.

[4] M.J. Morris, *Coord. Chem. Rev.*, 172, **1998**, 181−245.

[5] R.D. Chakravarthy, D.K. Chand, *J. Chem. Sci.*, 123, **2011**, 187−199.

[6] C.J. Hinshaw, G. Peng, R. Singh, J.T. Spence, J.H. Enemark, M. Bruck, J. Kristofzski, S.L. Merbs, R.B. Ortega, P.A. Wexler, *Inorg. Chem.*, 28, **1989**, 4483−4491.

[7] Y.–L. Wong, Y. Yan, E.S.H. Chan, Q. Yang, T.C.W. Mak, D.K.P. Ng, J. Chem. Soc., *Dalton Trans.*, **1998**, 3057–3064.

[8] A. Lehtonen, M. Wasberg, R. Sillanpää, *Polyhedron*, 25 (2006) 767−775.

[9] S. Khatua, H. Stoeckli−Evans, T. Harada, R. Kuroda, M. Bhattacharjee, *Inorg. Chem.*, 45, **2006**, 9619−9621.

[10] S. Khatua, T. Harada, R. Kuroda, M. Bhattacharjee, *Chem. Commun.*, **2007**, 3927−3929.

[11] Y.L. Wong, L.H. Tong, J.R. Dilworth, D.K.P. Ng, H. K. Lee, *Dalton Trans.*, 39, **2010**, 4602−4611.

[12] L. H. Tong, Y. L. Wong, H. K. Lee, J. R. Dilworth, *Inorg. Chim. Acta.*, 383, **2012**, 91−97.

[13] F. Madeira, S. Barroso, S. Namorado, P.M. Reis, B. Royo, A.M. Martins, *Inorg. Chim. Acta.*, 383, **2012**, 152−156.

[14] X. Lei, N. Chelamalla, *Polyhedron*, 49, **2013**, 244−251.

[15] A. Riisioe, A. Lehtonen, M.M. Hanninen, R. Sillanpää, *Eur. J. Inorg. Chem.*, **2013**, 1499−1508.

[16] T. Heikkila, R. Sillanpää, A. Lehtonen, *J. Coord. Chem.*, 67, **2014**, 1863−1872.

[17] A. Butler, J. N. Carter-Franklin, *Nat. Prod. Rep.*, 21, **2004**, 180−188.

[18] D. C. Crans, J. J. Smee, E. Gaidamauskas, L. Yang, *Chem. Rev.*, 104, **2004**, 849−902.

[19] J. Hartung, Y. Dumont, M. Greb, D. Hach, F. Köhler, H. Schulz, M. Časný, D. Rehder, H. Vilter, *Pure Appl. Chem.*, 81, **2009**, 1251–1264.

[20] J. M. Winter, B. S. Moore, *J. Biol. Chem.*, 284, **2009**, 18577–18581.

[21] D. Wischang, O. Brücher, J. Hartung, *Coord. Chem. Rev.*, 255, **2011**, 2204–2217.

[22] R. Wever, M. A. van der Horst, *Dalton Trans.*, 42, **2013**, 11778–11786.

[23] D. Rehder, *Oceanography*, 2, **2014**, doi:10.4172/2332-2632.1000121.

[24] C. Leblanc, H. Vilter, J. -B. Fournier, L. Delage, P. Potin, E. Rebuffet, G. Michel, P. L. Solari, M. C. Feiters, M. Czjzek, *Coord. Chem. Rev.*, **2015**, http://dx.doi.org/10.1016/j.ccr.2015.02.013.

[25] A. Podgoršek, M. Zupan, J. Iskra, *Angew. Chem. Int. Ed.*, 48, **2009**, 8424–8450.

[26] J. Jie, G. Jian-Rong, L. Yu-Jin, *Chinese J. Appl. Chem.*, 27, **2010**, 621–625.

[27] V.V. K. M. Kandepi, N. Narender, *Synthesis*, 44, **2012**, 15–26.

[28] Z. Huang, F. Li, B. Chen, T. Lu, Y. Yuan, G. Yuan, *ChemSusChem*, 6, **2013**, 1337–1340.

[29] *Bromine Compounds. Chemistry and Applications*, eds. D. Price, B. Iddon, B. J. Wakefield, Elsevier, New York, **1988**.

[30] L. S. Birnbaum, D. F. Staskal, *Environ. Health Perspect.*, 112, **2004**, 9–17.

[31] D. Ioffe, R. Frim, *Bromine, Organic Compounds* in *Kirk-Othmer Encyclopedia of Chemical Technology*, Wiley, New York, **2011**, pp. 1–26.

[32] A. G. J. Ligtenbarg, R. Hage, B. L. Feringa, *Coord. Chem. Rev.*, 237, **2003**, 89–101.

[33] M. R. Maurya, *J Chem. Sci.*, 118, **2006**, 503–511.

[34] V. Conte, A. Coletti, B. Floris, G. Licini, C. Zonta, *Coord. Chem. Rev.*, 255, **2011**, 2165–2177.

[35] V. Kraehmer, D. Rehder, *Dalton Trans.*, 41, **2012**, 5225–5234.

[36] M. R. Maurya, S. Sikarwar, T. Joseph, P. Manikandan, S. B. Halligudi, *React. Funct. Polym.*, 63, **2005**, 71–83.

[37] M. R. Maurya, U. Kumara, P. Manikandan, *Dalton Trans.*, **2006**, 3561–3575;

[38] J. J. Boruah, S. P. Das, R. Borah, S. R. Gogoi, N. S. Islam, *Polyhedron*, 52, **2013**, 246–254.

[39] M. R. Maurya, S. Dhaka, F. Avecilla, *Polyhedron*, 67, **2014**, 145–159.

[40] S. Pasayat, S. P. Dash, S. Roy, R. Dinda, S. Dhaka, M. R. Maurya, W. Kaminsky, Y. P. Patil, M. Nethaji, *Polyhedron*, 67, **2014**, 1–10.

[41] M. R. Maurya, N. Kumar, F. Avecilla, *J. Mol. Catal. A. Chem.*, 392, **2014**, 50–60.

[42] F. E. Kühn, A. M. Santos, M. Abrantes, *Chem. Rev.*, 106, **2006**, 2455−2475.

[43] R. Sanz, M. R. Pedrosa, *Curr. Org. Synth.*, 6, **2009**, 239–263.

[44] M. R. Maddani, K. R. Prabhu, *J. Indian Inst. Sci.*, 90, **2010**, 287−297.

[45] J. A. Brito, B. Royo, M. Gómez, *Catal. Sci. Technol.*, 1, **2011**, 109−1118.

[46] R. D. Chakravarthy, D. K. Chand, *J. Chem. Sci.*, 123, **2011**, 187–199.

[47] R. G. de Noronha, A. C. Fernandes, *Curr. Org. Chem.*, 16, **2012**, 33−64.

[48] M. Kirihara, Y. Ochiai, S. Takizawa, H. Takahata, H. Nemoto, *Chem. Commun.*, **1999**, 1387–1388.

[49] K.A. Al-Sou'od, B.F. Ali, R. Abu-El-Halawa, A.-A.-H.H. Abu-Nawas, *Int. J. Chem. Kinet.*, 37, **2005**, 444–449.

[50] C. Joo, S. Kang, S.M. Kim, H.Han, J.W. Yang, *Tetrahedron Lett.*, 51, **2010**, 6006–6007.

[51] N. Ueyama, N. Yoshinaga, A. Nakamura, *J. Chem. Soc. Dalton. Trans.*, **1990**, 387–394.

[52] R.K. Bhatia, G.N. Rao, *J. Mol. Catal. A. Chem.*, 121, **1997**, 171–178.

[53] G.J.J. Chen, J.W. McDonald, W.E. Newton, *Inorg. Chem.*, 15, **1976**, 2612−2615.

[54] P.–P. Yang, H.–B. Song, X.–F. Gao, L.–C. Li, D.–Z. Liao, *Cryst. Grow. Des.*, 9, **2009**, 4064−4069.

[55] A. Joohuan, M. Yanyan, R. Chris, C. Rodolphe, B. Colette, *Aust. J. Chem.*, 62, **2009**, 1124−1129.

[56] D.D. Perrin, W.L.F. Armarego, D.P. Perrin, *Purification of Laboratory Chemicals, 2nd ed.*, Pergamon, Oxford, **1983**.

[57] *CrysAlisPro version 1.171.36, Agilent Technologies*, Yarnton, Oxfordshire, UK, 2013.

[58] S. Parkin, B. Moezzi, H. Hope, *J. Appl. Crystallogr.*, 28, **1995**, 53–56.

[59] *SMART version 5.630* and *SAINT−plus version 6.45*, Bruker−Nonius Analytical X−ray Systems Inc., Madison, WI, USA, **2003**.

[60] G.M. Sheldrick, *SADABS, Program for Area Detector Absorption Correction*, University of Göttingen, Göttingen, Germany, **1997**.

[61] G.M. Sheldrick, *Acta Crystallogr., Sect. A.*, 64, **2008**, 112–122.

[62] L.J. Farrugia, *J. Appl. Crystallogr.*, 45, **2012**, 849−854.

[63] A.L. Spek, *Platon, A Multipurpose Crystallographic Tool*, Utrecht University, Utrecht, The Netherlands, **2002**.

[64] C.F. Macrae, I.J. Bruno, J.A. Chisholm, P.R. Edgington, P. McCabe, E. Pidcock, L. Rodriguez-Monge, R. Taylor, J. van de Streek, P.A. Wood, *J. Appl. Cryst.*, 41, **2008**, 466−470.

[65] A. Lymberopoulou-Karaliota, D. Hatzipanayioti, M. Kamariotaki, M. Potamianou, C. Litos, V. Aletras, *Inorg. Chim. Acta*., 358, **2005**, 2975–2995.

[66] Y. Zhu, W. Yan, Y. Zhang, *J. Coord. Chem.*, 64, **2011**, 1104−1112.

[67] S.K. Kurapati, U. Ugandhar, S. Maloth, S. Pal, *Polyhedron*, 42, **2012**, 161−167.

[68] S.K. Kurapati, S. Pal, *Dalton Trans.*, 44, **2015**, 2401−2408.

[69] S. Gupta, S. Pal, A.K. Barik, S. Roy, A. Hazra, T.N. Mandal, R.J. Butcher, S.K. Kar, *Polyhedron*, 28, **2009**, 711−720.

[70] N.K. Ngan, K.M. Lo, C.S.R. Wong, *Polyhedron*, 30, **2011**, 2922–2932.

[71] M. Bagherzadeh, M.M. Haghdoost, A. Ghanbarpour, M. Amini, H.R. Khavasi, E. Payab, A. Ellern, L.K. Woo, *Inorg. Chim. Acta*., 411, **2014**, 61–66.

[72] S.K. Kurapati, *Acta Crystallogr. Sect. E*., 69, **2013**, m460–m461.

[73] S. Pal, R.N. Mukherjee, M. Tomas, L.R. Falvello, A. Chakravorty, *Inorg. Chem.*, 25, **1986**, 200–207.

Appindex

FTIR spectrum of HL^2

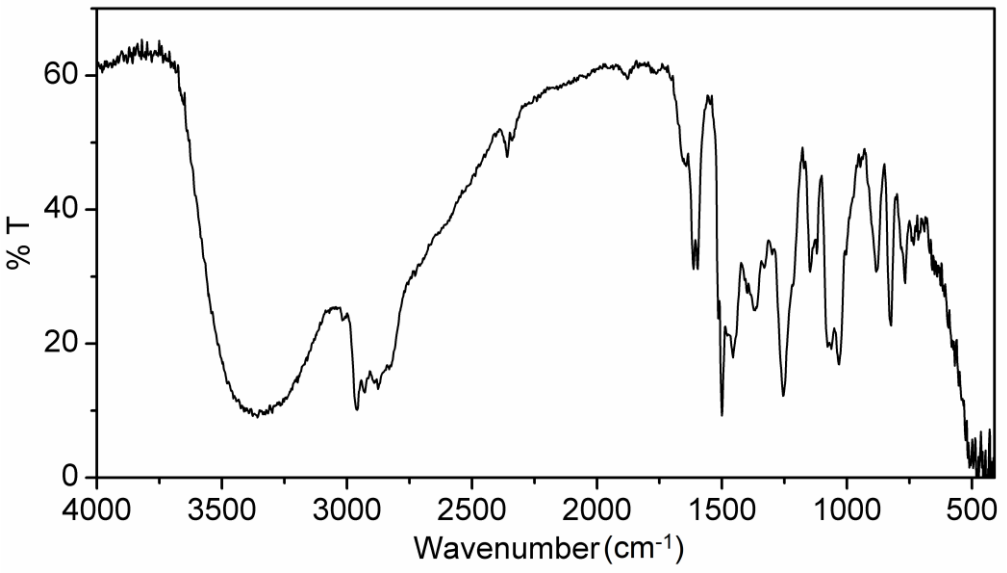

FTIR spectrum of HL^3.

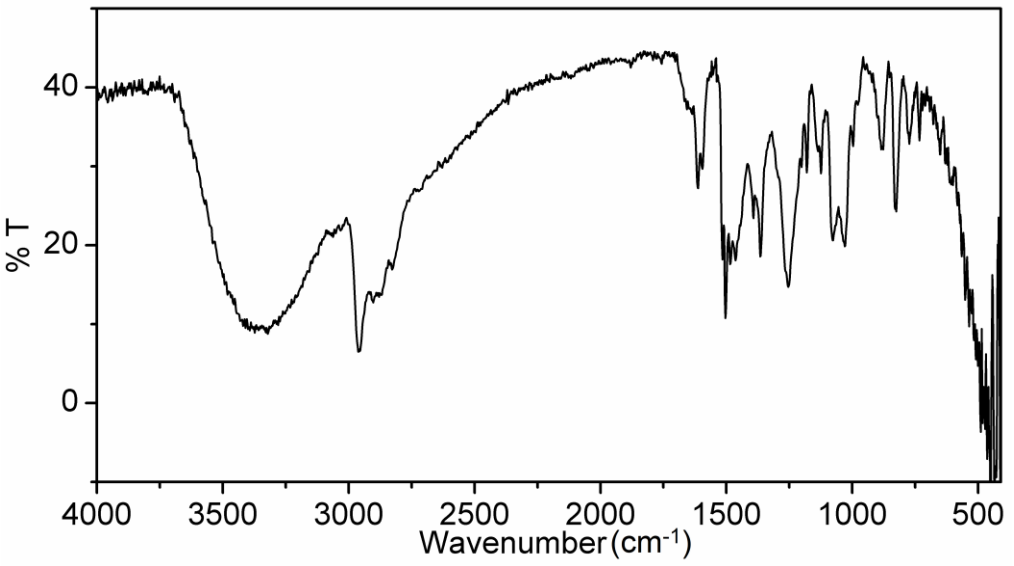

FTIR spectrum of HL^4.

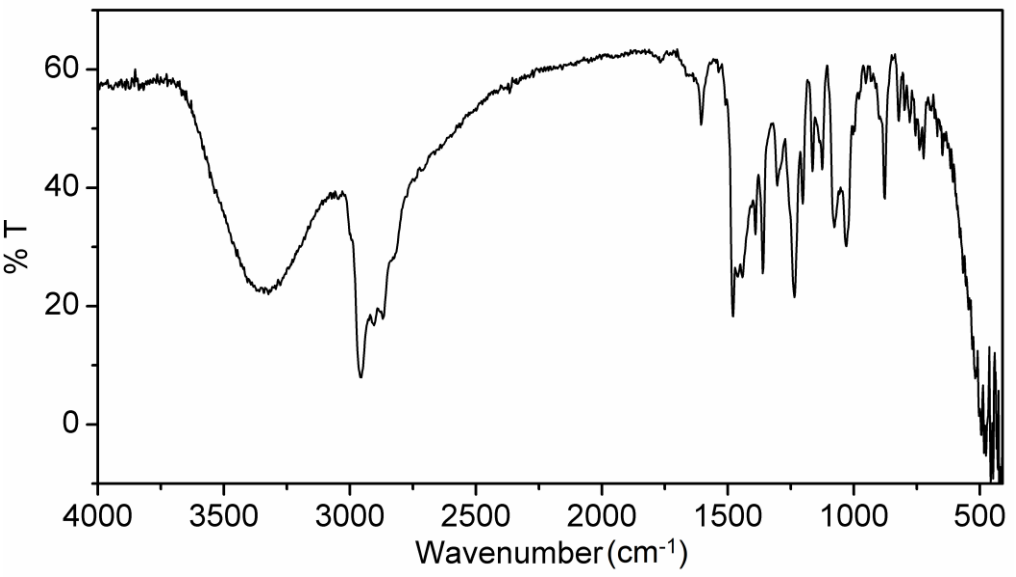

FTIR spectrum of *cis*-[$MoO_2(HL^2)$].(**2**)

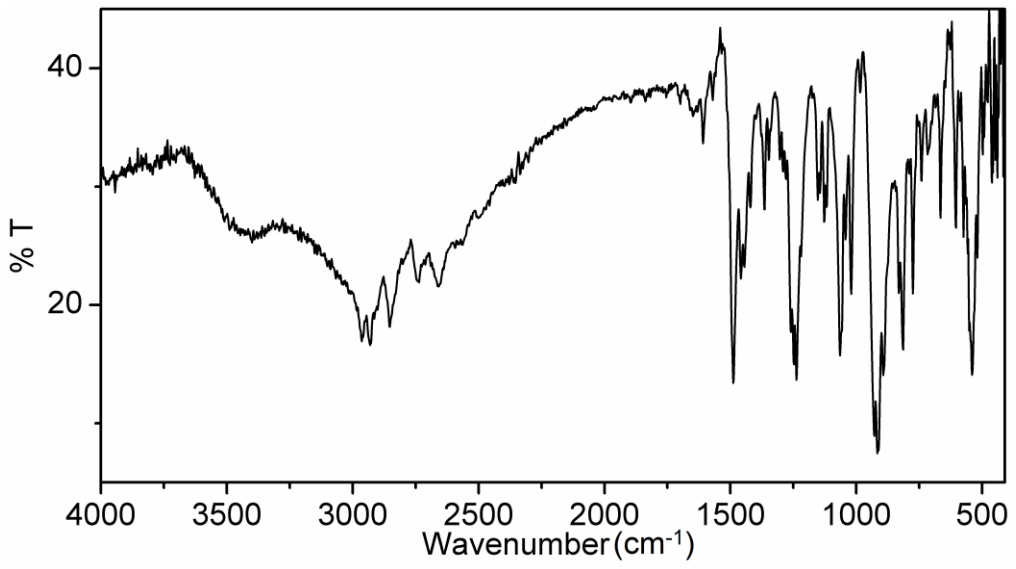

FTIR spectrum of *cis*-[$MoO_2(HL^3)$].(**3**)

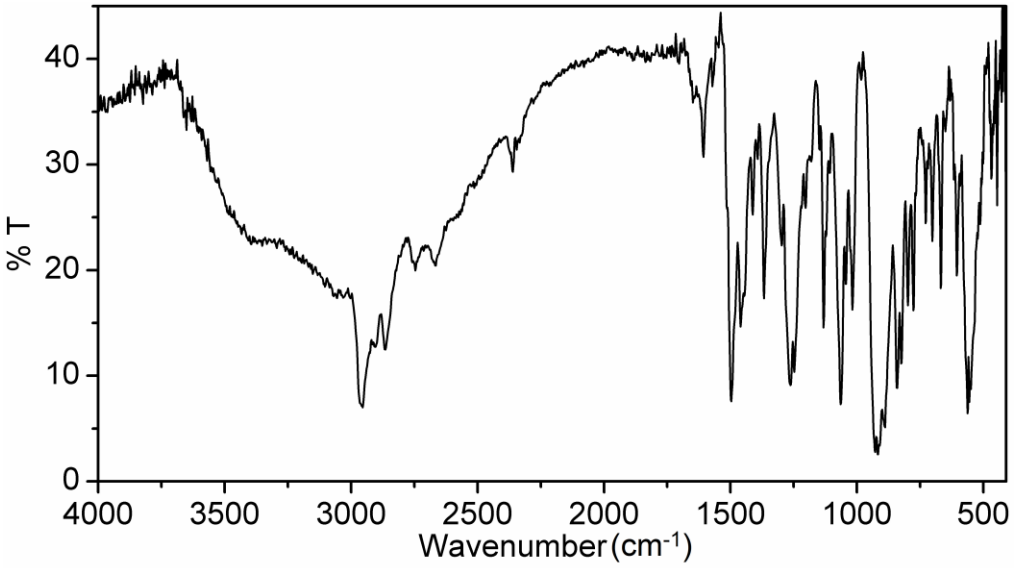

FTIR spectrum of *cis*-[$MoO_2(HL^4)$].(**4**)

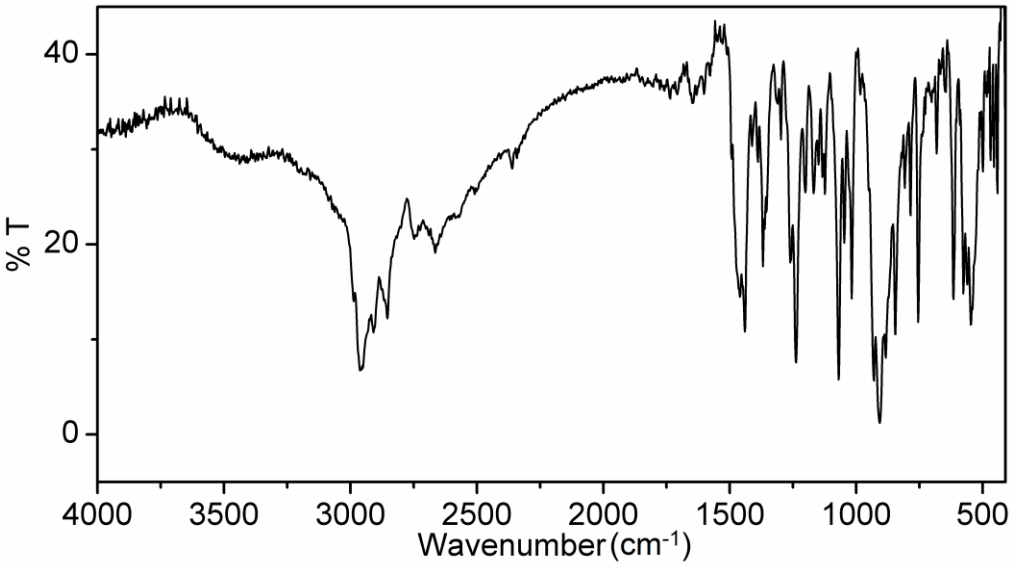

^{1}H-NMR Spectrum of H_3L^1:

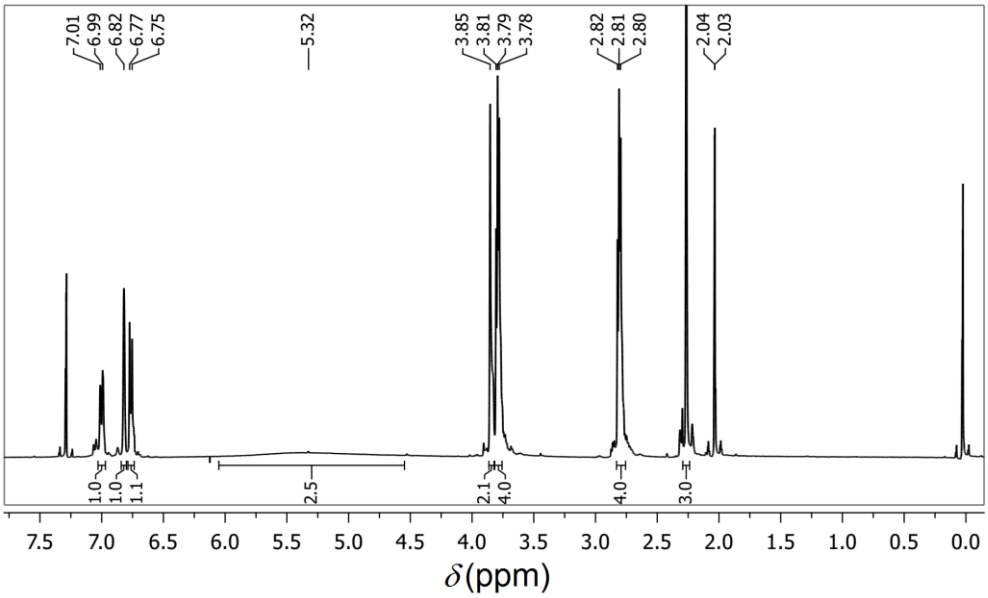

^{13}C-NMR Spectrum of H_3L^1:

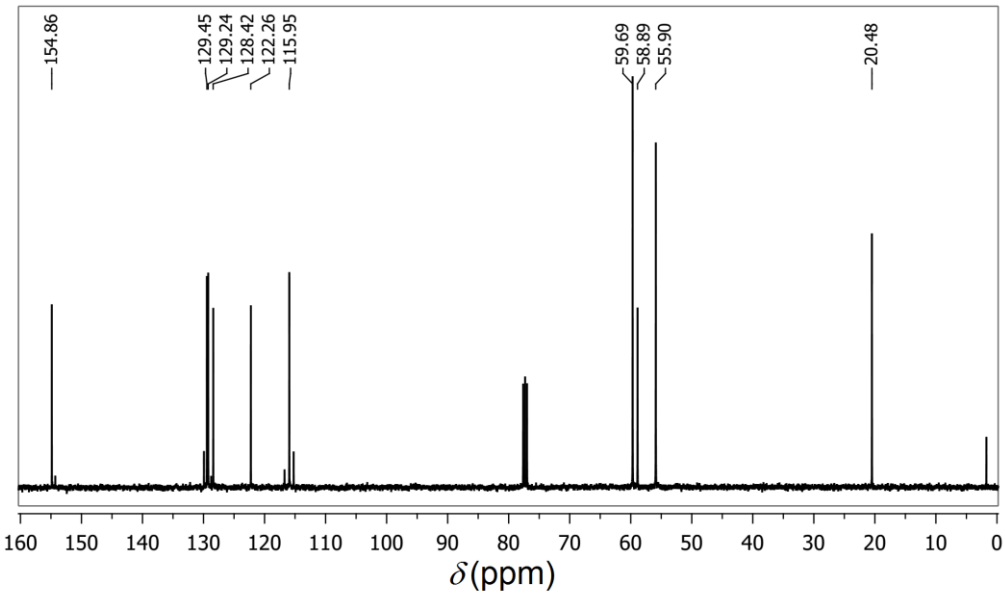

^{13}C-DEPT135 NMR Spectrum of H_3L^1:

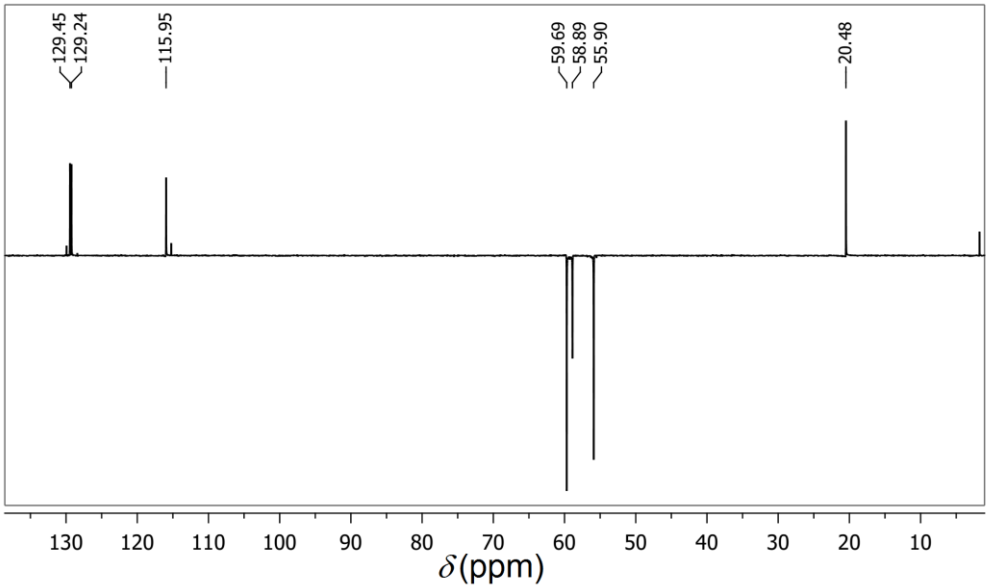

^{1}H-NMR Spectrum of H_3L^2:

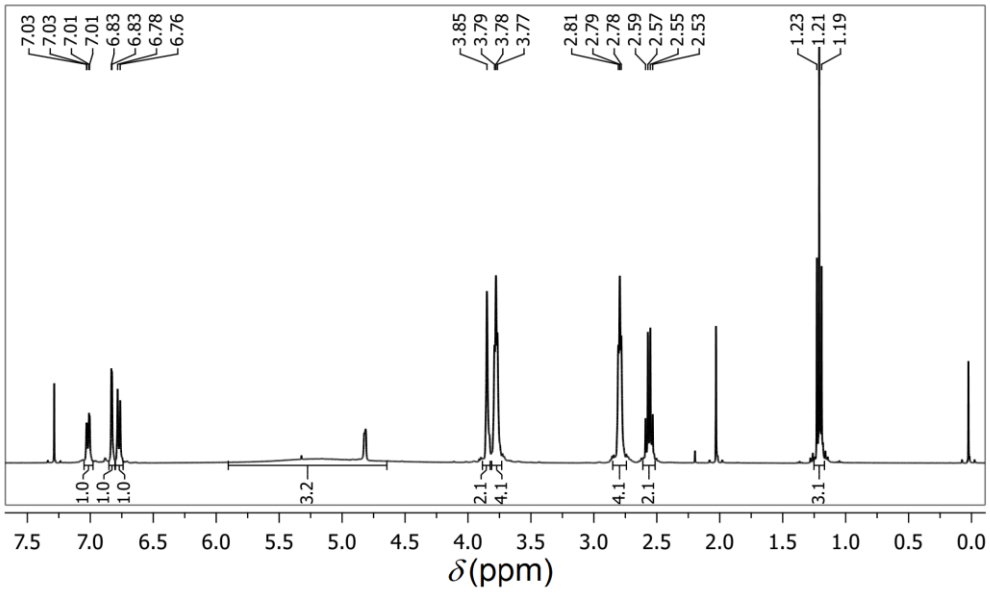

^{13}C-NMR Spectrum of H_3L^2:

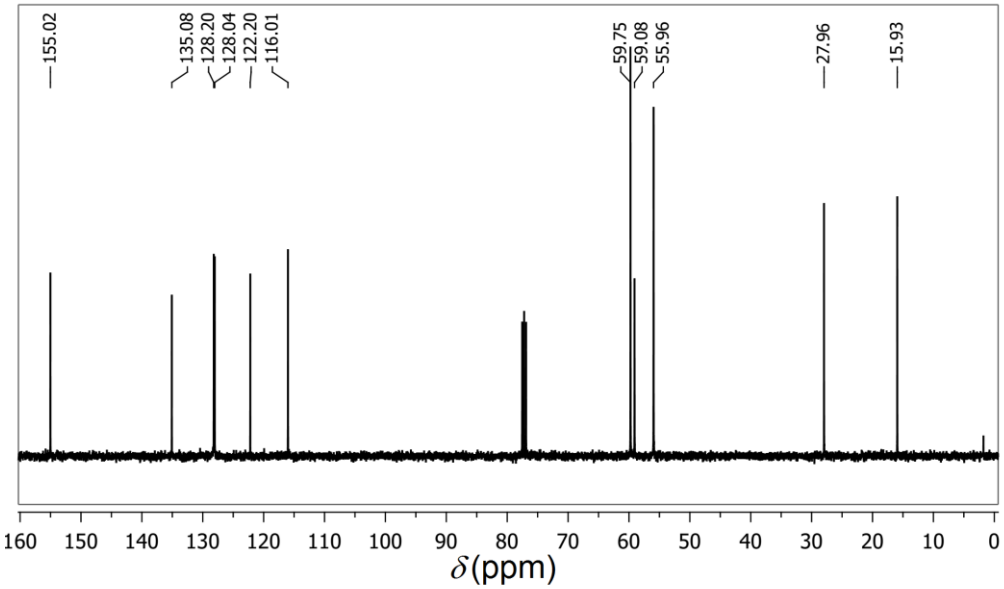

^{13}C-DEPT135 NMR Spectrum of H_3L^2:

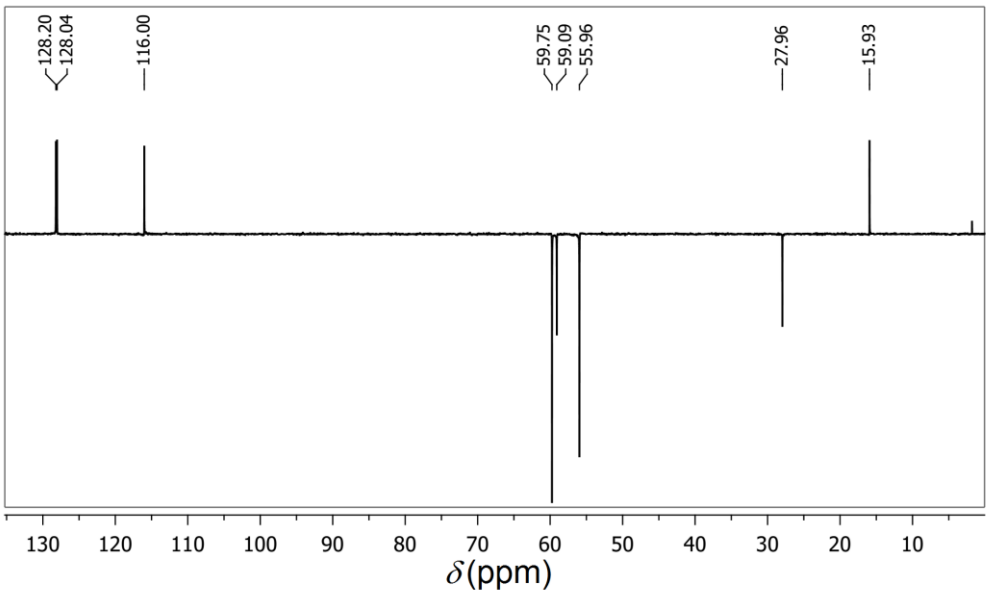

^{1}H-NMR Spectrum of H_3L^3:

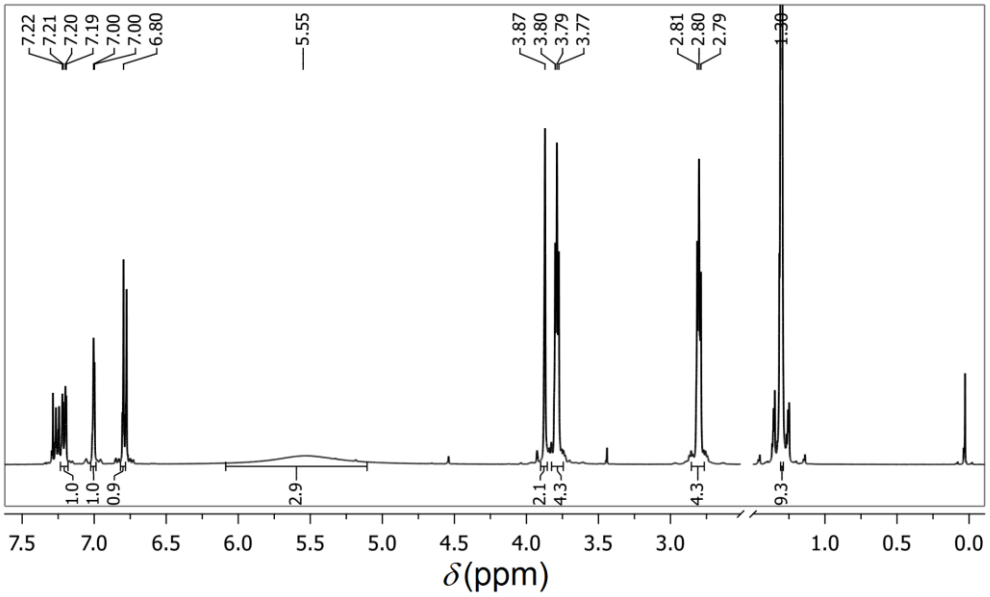

^{13}C-NMR Spectrum of H_3L^3:

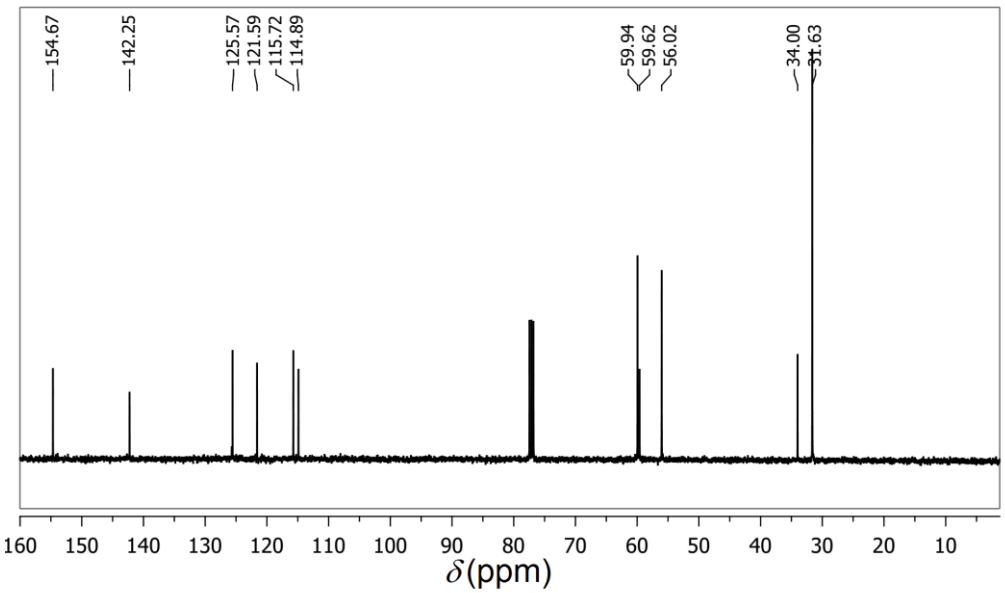

^{13}C-DEPT135 NMR Spectrum of H_3L^3:

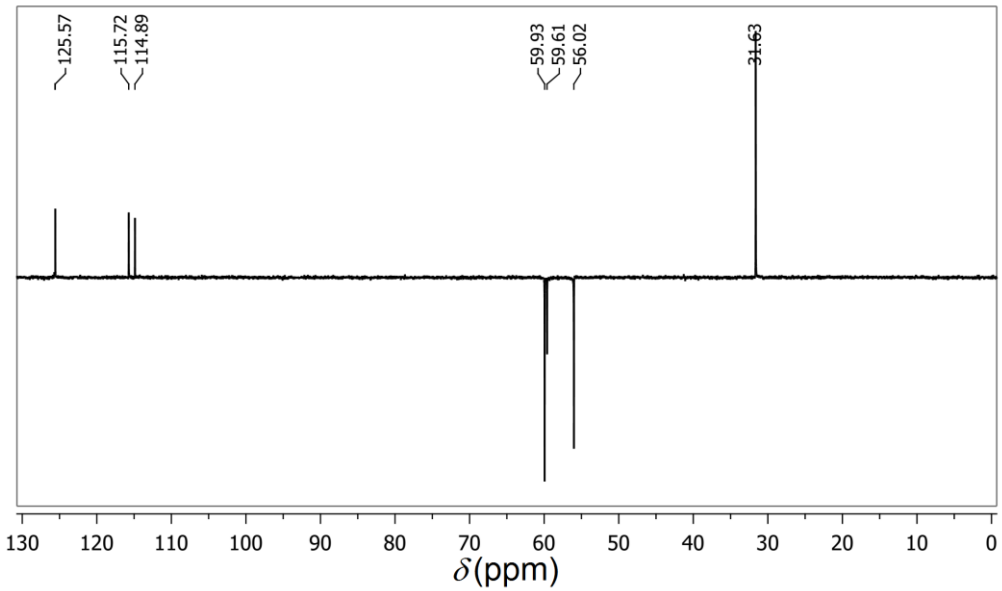

^{1}H-NMR Spectrum of H_3L^4:

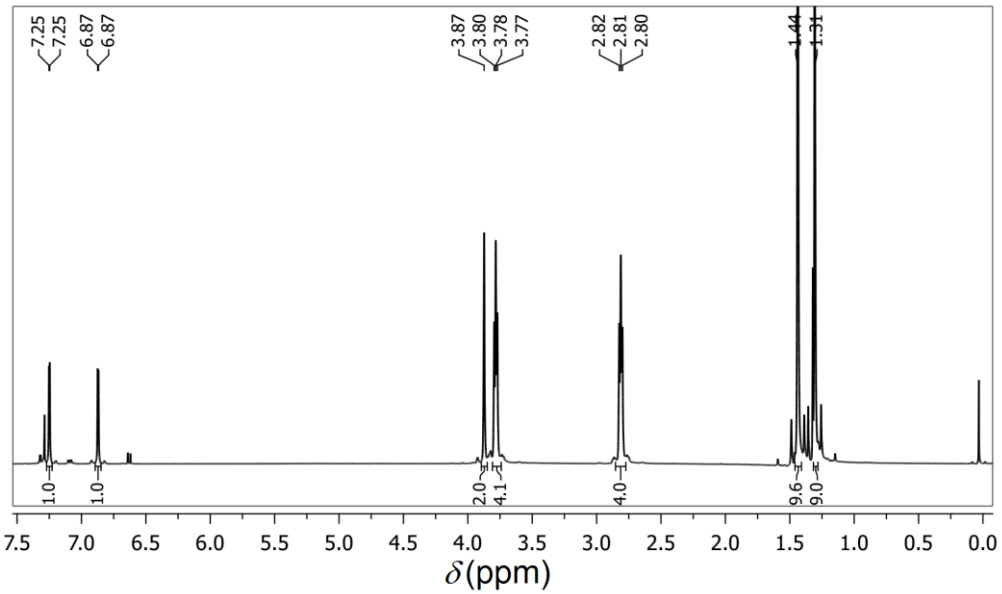

^{13}C-NMR Spectrum of H_3L^4:

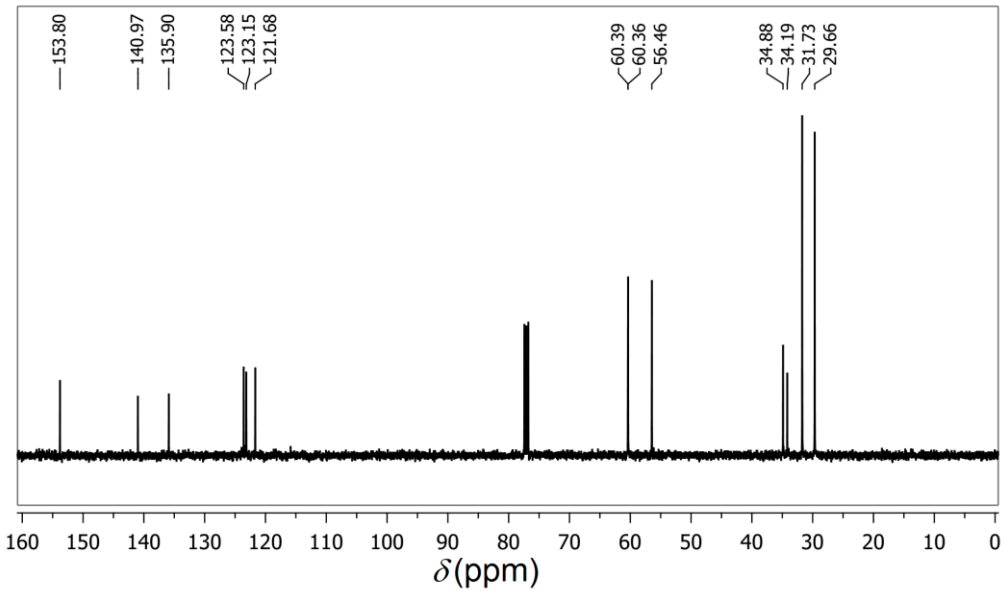

^{13}C-DEPT135 NMR Spectrum of H_3L^3:

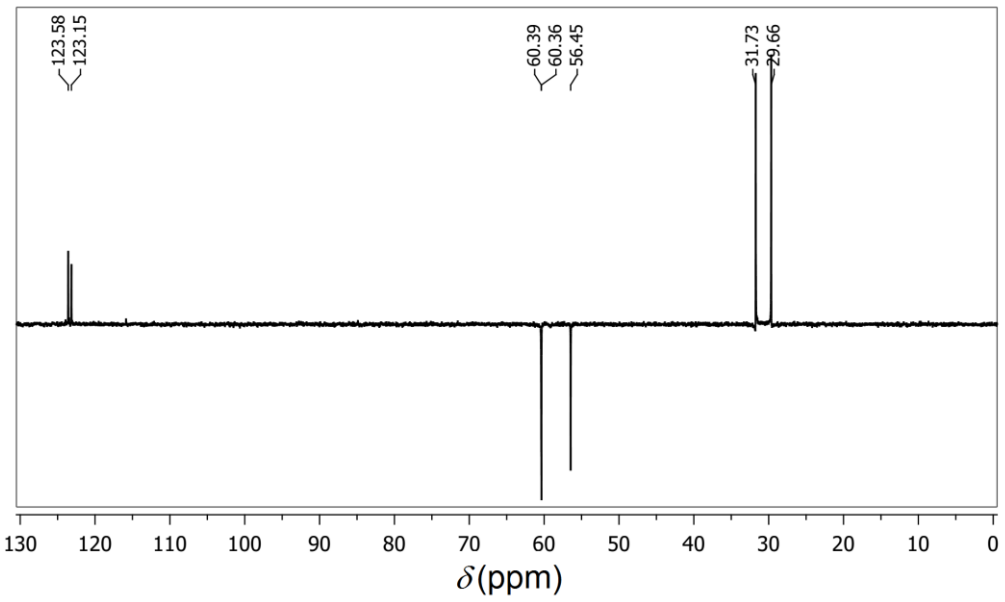

^{13}C-DEPT135 NMR Spectrum of *cis*-[MoO_2(HL^1)] (**1**)

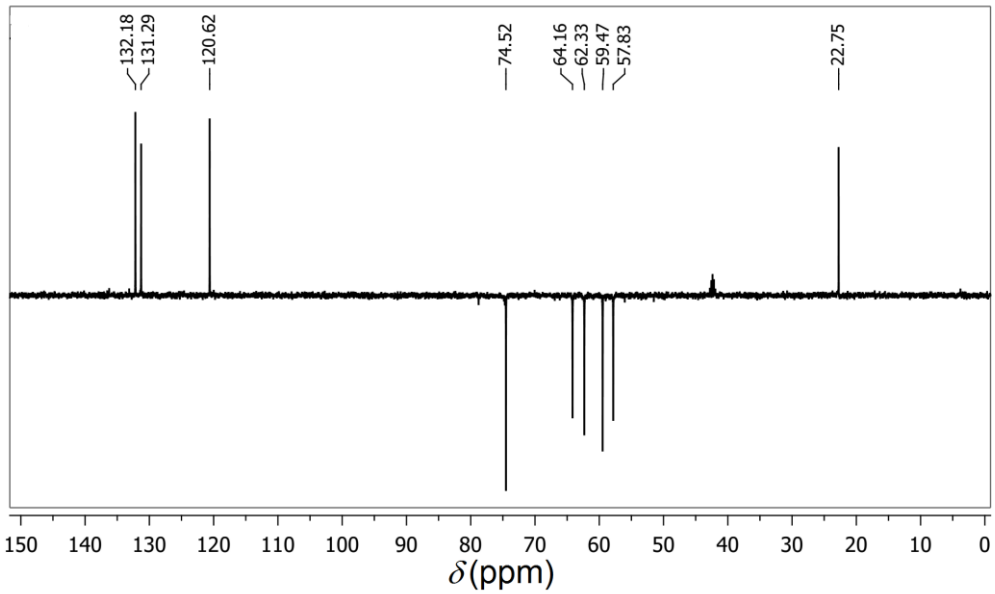

^{1}H-NMR Spectrum of *cis*-[MoO_2(HL^2)] (**2**)

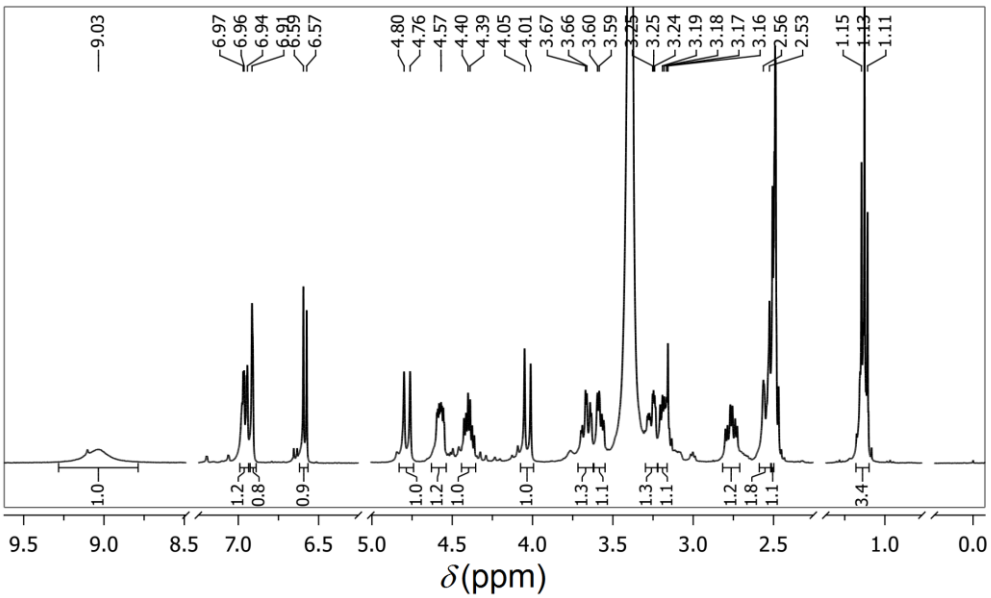

^{13}C-NMR Spectrum of *cis*-[$MoO_2(HL^2)$] (**2**)

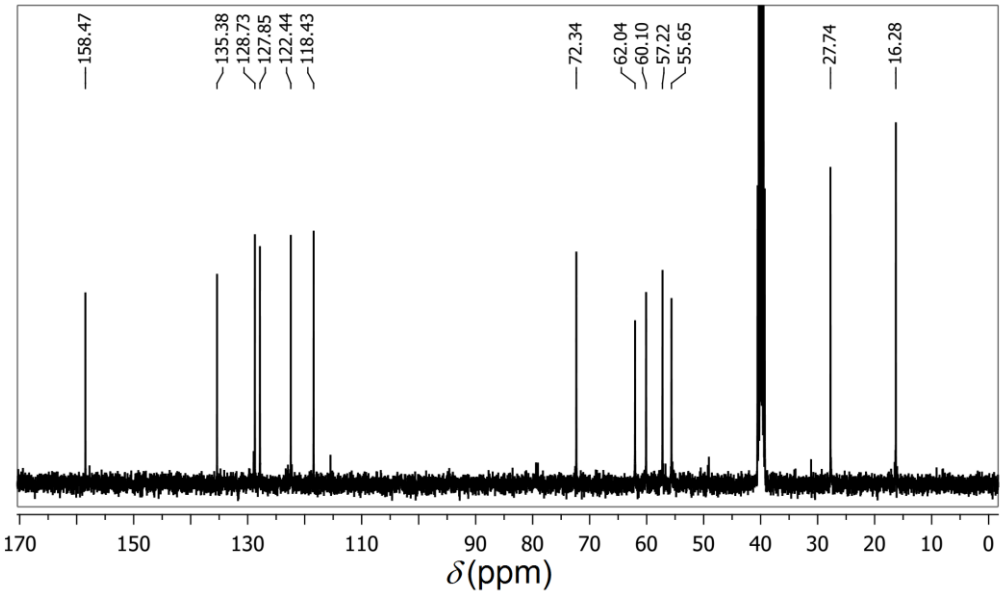

^{13}C-DEPT135 NMR Spectrum of *cis*-[$MoO_2(HL^2)$] (**2**)

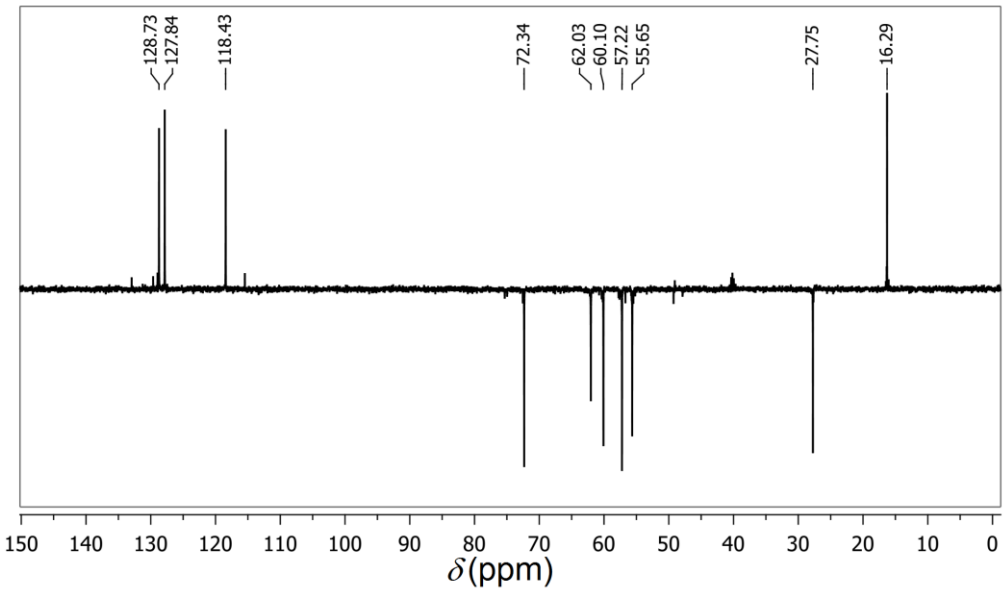

^{1}H-NMR Spectrum of *cis*-[$MoO_2(HL^3)$] (**3**)

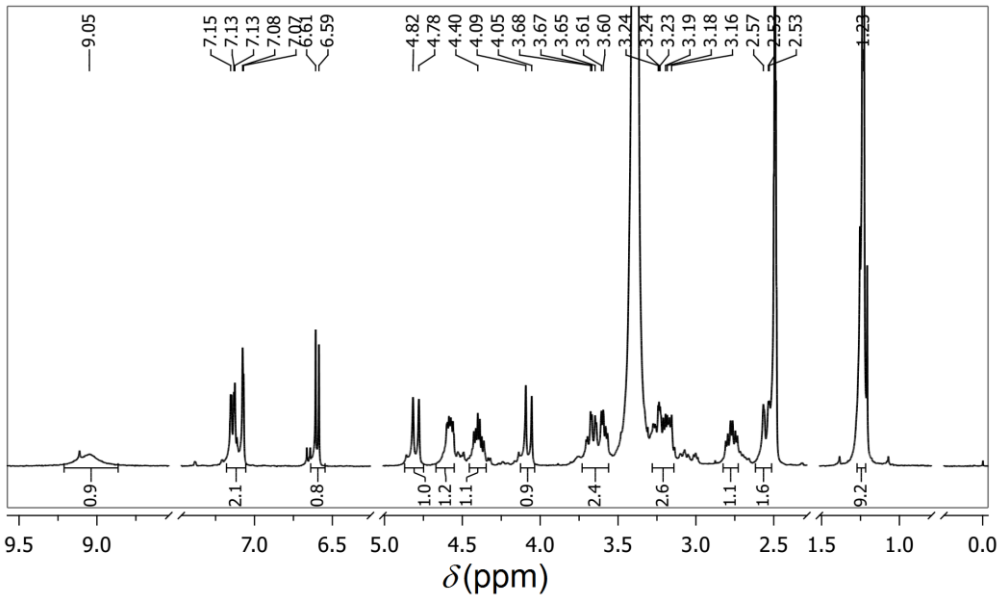

^{13}C-NMR Spectrum of *cis*-[$MoO_2(HL^3)$] (**3**)

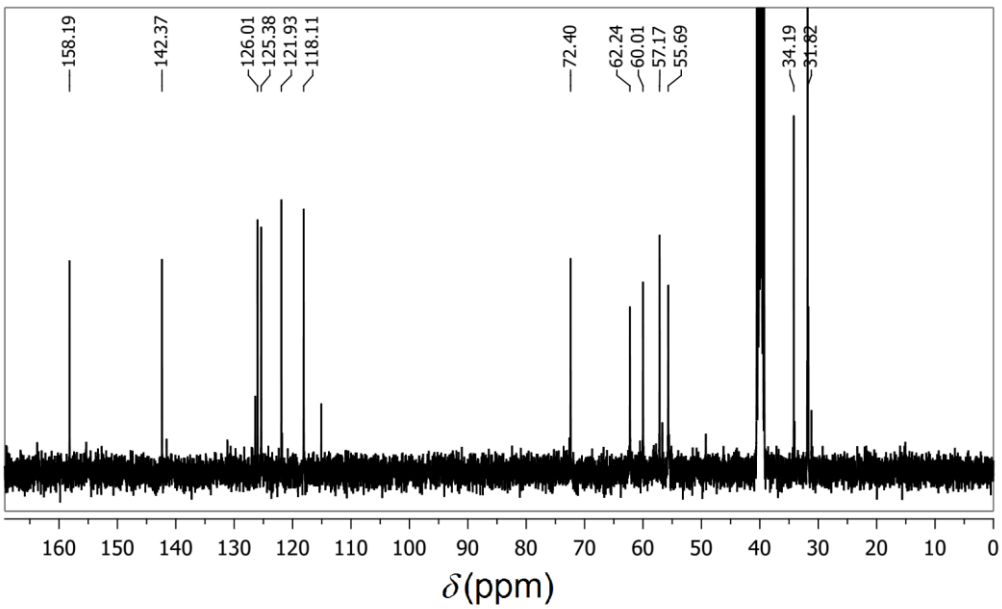

^{13}C-DEPT135 NMR Spectrum of *cis*-[$MoO_2(HL^3)$] (**3**)

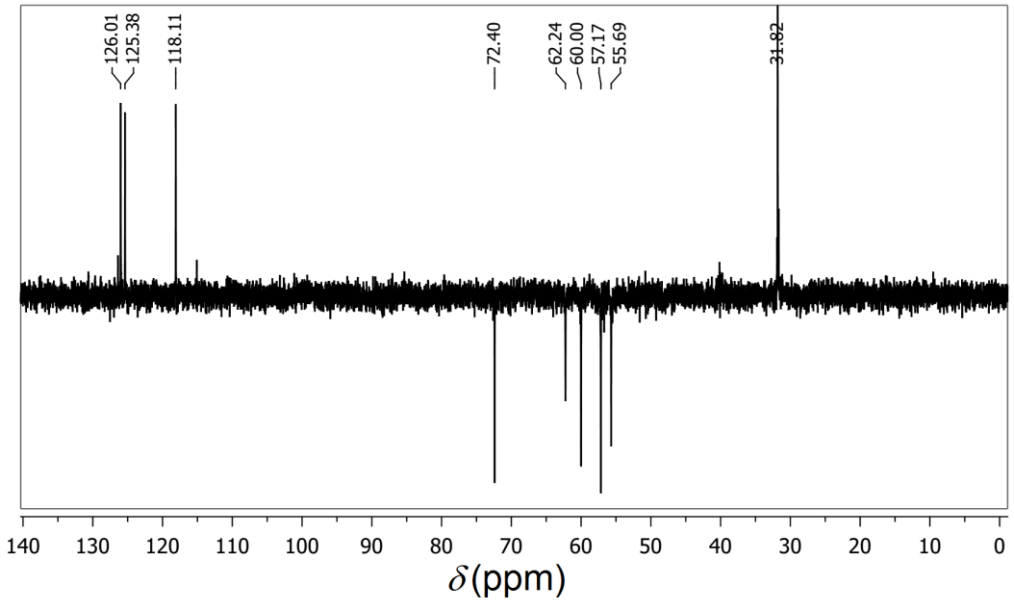

^{1}H-NMR Spectrum of *cis*-[$MoO_2(HL^4)$] (**4**)

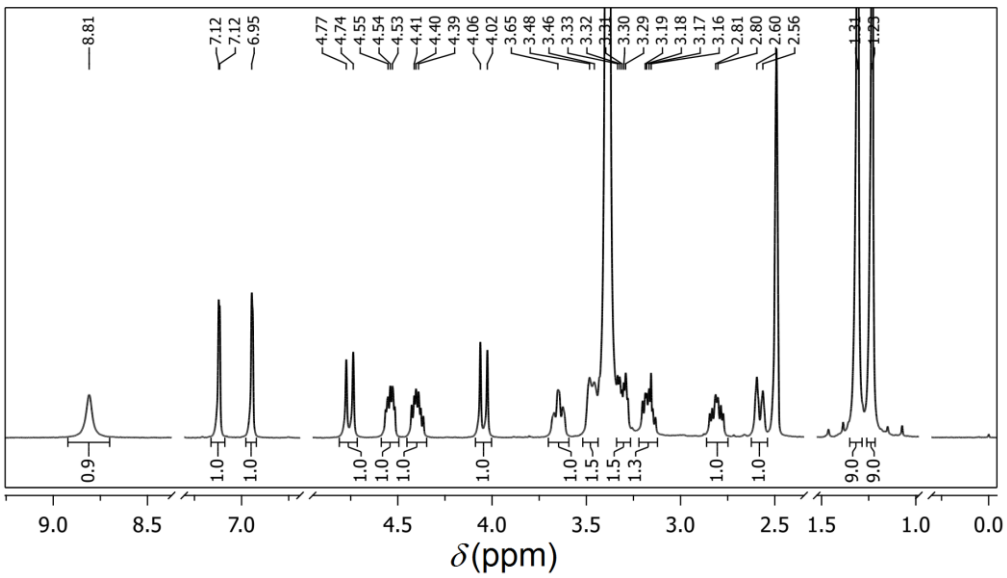

^{13}C-NMR Spectrum of *cis*-[MoO_2(HL^4)] (**4**)

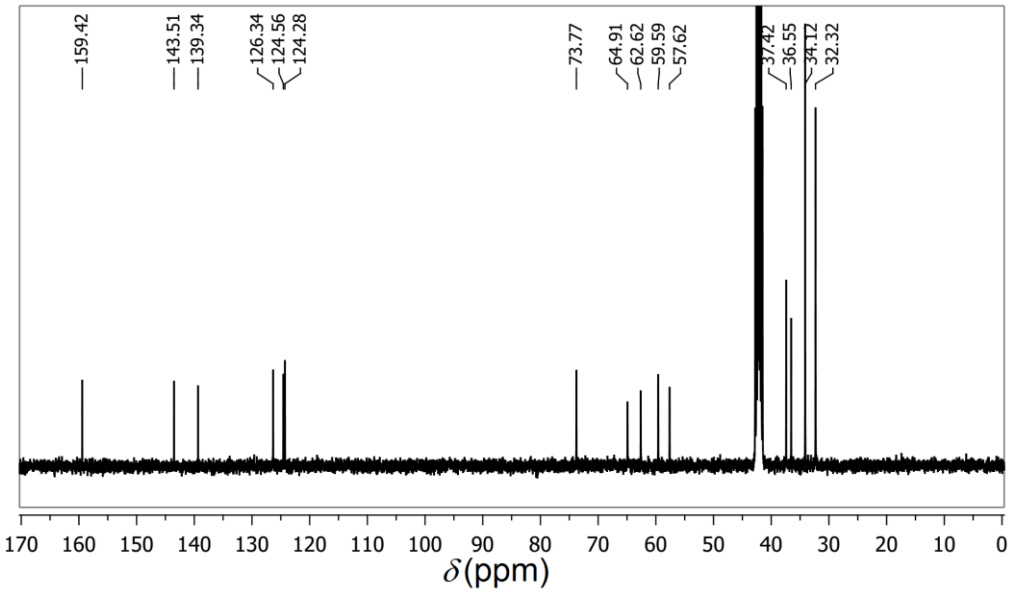

^{13}C-DEPT135 NMR Spectrum of *cis*-[MoO_2(HL^4)] (**4**)

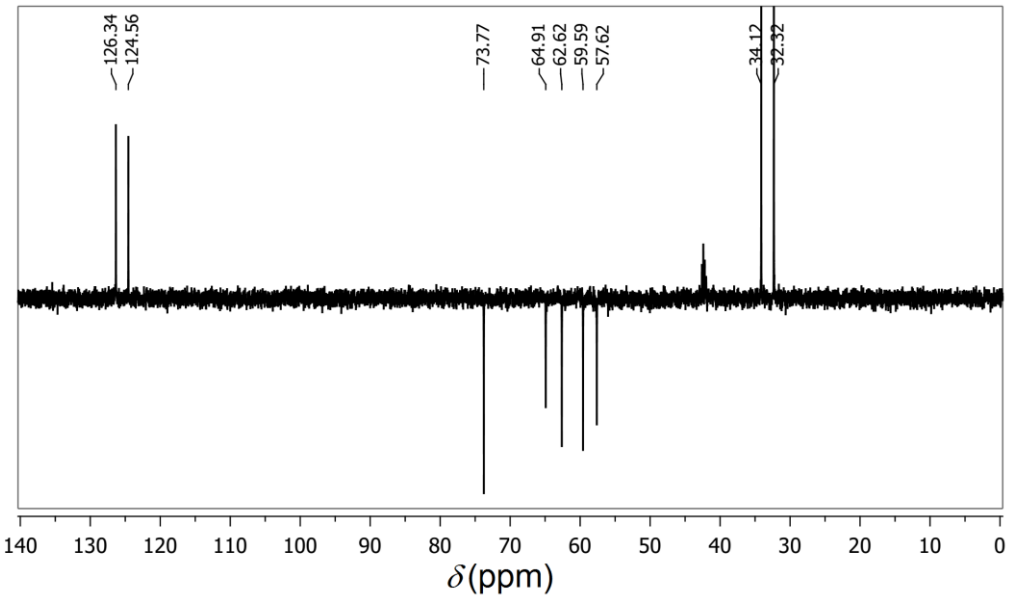

Atomic coordinates (x 10^4) and equivalent isotropic displacement parameters ($Å^2$ x 10^3). U(eq) is defined as one third of the trace of the orthogonalized Uij tensor.

Table A 4.1. For *cis*-[$MoO_2(HL^1)$] (**1**)

	X	Y	Z	U (eq)
Mo	11289(1)	741(1)	11459(1)	26(1)
O(1)	12715(8)	1154(1)	10525(7)	32(1)
O(2)	8744(8)	384(1)	11012(7)	29(1)
O(3)	10998(7)	412(1)	8464(7)	30(1)
O(4)	11089(8)	1061(2)	13257(7)	38(1)
O(5)	13422(8)	394(2)	12867(7)	37(1)
N(1)	8104(9)	1012(2)	8338(8)	28(1)
C(1)	12226(12)	1565(2)	10291(11)	32(2)
C(2)	14019(14)	1844(2)	10955(13)	46(2)
C(3)	13646(17)	2264(2)	10747(13)	54(2)
C(4)	11486(17)	2430(2)	9898(13)	48(2)
C(5)	9734(15)	2145(2)	9241(11)	45(2)
C(6)	10028(12)	1720(2)	9387(10)	33(2)
C(7)	7904(12)	1457(2)	8692(12)	38(2)
C(8)	6047(11)	787(2)	8070(11)	39(2)
C(9)	6608(11)	592(2)	10201(11)	33(2)
C(10)	8397(12)	951(2)	6424(10)	33(2)
C(11)	9143(13)	512(2)	6359(11)	36(2)
C(12)	11115(19)	2891(2)	9755(14)	68(3)

Table A 4.2. For *cis*-[$MoO_2(HL^2)$] (**2**)

	X	Y	Z	U (eq)
Mo	1469(1)	11076(1)	9211(1)	38(1)
O(1)	1699(1)	11074(2)	7960(1)	46(1)
O(2)	1259(1)	9800(2)	10342(1)	44(1)
O(3)	123(1)	9453(3)	8651(1)	44(1)
O(4)	2582(1)	11892(3)	9547(1)	60(1)
O(5)	676(1)	12917(3)	9306(1)	59(1)
N(1)	1878(1)	7833(3)	8999(1)	36(1)
C(1)	2504(2)	10500(4)	7583(2)	43(1)
C(2)	2761(2)	11485(4)	6839(2)	55(1)
C(3)	3579(2)	10942(5)	6429(2)	60(1)
C(4)	4139(2)	9418(5)	6739(2)	55(1)
C(5)	3862(2)	8426(4)	7466(2)	51(1)
C(6)	3052(2)	8923(3)	7901(2)	42(1)
C(7)	2869(2)	7759(4)	8715(2)	45(1)
C(8)	1844(2)	6814(4)	9867(2)	47(1)
C(9)	1921(2)	8297(4)	10598(2)	51(1)
C(10)	1192(2)	6956(4)	8308(2)	43(1)
C(11)	175(2)	7407(4)	8497(2)	50(1)
C(12)	5050(2)	8771(5)	6311(2)	75(1)
C(13)	4940(2)	6927(6)	5834(3)	85(1)

Table A 4.3. For *cis*-[$MoO_2(HL^1)$] . $2CH_3CN$ (**3** . $2CH_3CN$)

	X	Y	Z	U (eq)
Mo	567(1)	7748(1)	5736(1)	30(1)
O(1)	-1024(5)	6400(2)	5861(2)	32(1)
O(2)	1049(5)	9157(3)	6093(3)	37(1)
O(3)	-2118(4)	8742(3)	5231(3)	35(1)
O(4)	2242(5)	6895(3)	6347(3)	45(1)
O(5)	1588(5)	8317(3)	4450(3)	44(1)
N(1)	-1835(5)	7624(3)	7242(3)	27(1)
N(2)	3679(14)	1083(8)	7432(8)	141(4)
N(3)	2824(10)	5478(6)	9054(5)	100(2)
C(1)	-1363(6)	5370(4)	6691(4)	29(1)
C(2)	-1350(7)	4295(4)	6499(4)	33(1)
C(3)	-1659(7)	3215(4)	7303(4)	35(1)
C(4)	-2003(6)	3166(4)	8330(4)	29(1)
C(5)	-2049(6)	4251(4)	8505(4)	29(1)
C(6)	-1723(6)	5356(4)	7708(3)	25(1)
C(7)	-1710(7)	6442(4)	8041(4)	32(1)
C(8)	-1414(7)	8594(4)	7624(4)	35(1)
C(9)	698(7)	8972(4)	7168(4)	38(1)
C(10)	-3781(6)	7772(4)	6969(4)	36(1)
C(11)	-3769(7)	8838(4)	6011(4)	40(1)
C(12)	-2337(7)	1996(4)	9253(4)	39(1)
C(13)	-4328(9)	1983(5)	9947(5)	67(2)
C(14)	-2197(10)	892(4)	8924(5)	66(2)
C(15)	-808(10)	1908(5)	9901(5)	70(2)
C(16)	3811(12)	1915(10)	6732(9)	88(3)
C(17)	4073(11)	2965(8)	5836(6)	86(2)
C(18)	2981(9)	4945(6)	8523(5)	57(2)

Table A 4.4. For *cis*-[$MoO_2(HL^4)$] (**4**)

	X	Y	Z	U (eq)
Mo	6112(1)	-662(1)	4595(1)	34(1)
O(1)	6828(2)	700(9)	4907(5)	39(2)
O(2)	5403(3)	-2080(9)	4991(6)	45(2)
O(3)	5701(3)	1578(8)	5597(5)	38(2)
O(4)	6469(3)	-2463(9)	4071(5)	51(2)
O(5)	5779(3)	535(9)	3599(5)	43(2)
N(1)	6262(3)	-1393(11)	6326(6)	35(2)
C(1)	7373(4)	50(14)	5248(9)	45(3)
C(2)	7897(4)	845(14)	4831(9)	46(3)
C(3)	8438(4)	141(16)	5183(9)	54(3)
C(4)	8493(5)	-1259(17)	5896(11)	62(4)
C(5)	7972(5)	-1902(14)	6315(8)	49(3)
C(6)	7405(4)	-1344(15)	5985(8)	41(3)
C(7)	6867(4)	-2293(14)	6441(8)	47(3)
C(8)	5788(4)	-2708(14)	6669(8)	45(3)
C(9)	5524(5)	-3544(14)	5706(8)	46(3)
C(10)	6260(4)	267(14)	6943(8)	44(3)
C(11)	5720(4)	1398(15)	6696(8)	44(3)
C(12)	9113(5)	-1980(20)	6223(13)	76(4)
C(13)	9074(6)	-3490(30)	7010(20)	225(15)
C(14)	9504(6)	-430(30)	6658(14)	142(8)
C(15)	9428(6)	-2660(20)	5257(13)	120(7)
C(16)	7862(5)	2394(15)	4041(11)	60(4)
C(17)	8507(5)	3031(19)	3702(12)	96(5)
C(18)	7553(6)	1700(20)	3055(10)	85(5)
C(19)	7542(6)	4010(16)	4500(12)	85(5)

Chapter 4

Chapter 5

Complexes of *cis*-$\{MoO_2\}^{2+}$ with unsymmetrical linear tetradentate ONNO-donor ligands: synthesis, characterization and catalytic applications [§]

Reactions of $[MoO_2(acac)_2]$ ($acac^-$ = acetylacetonate), 2-((2-(2-hydroxyethylamino)-ethylamino)methyl)-4-*R*-phenols (H_2L^n, n = 1–5 for *R* = H, Me, OMe, Cl and Br, respectively) and KOH in 1:1:2 mole ration in methanol afford a series of complexes having the general formula *cis*-$[MoO_2(L^n)]$ (**1**−**5**) in 81−86% yields. The complexes have been characterized by elemental analysis, spectroscopic (IR, UV-Vis, ^{1}H-, ^{13}C- and ^{13}C-DEPT NMR) and electrochemical measurements. The molecular structures of **1**−**4** have been determined by single crystal X-ray crystallography. In each of **1**−**4**, the ONNO-donor 6,5,5-membered fused chelate rings forming $(L^n)^{2-}$ and the two mutually *cis* oxo groups assemble a distorted octahedral N_2O_4 coordination sphere around the metal centre. In the crystal lattice, each of **1**−**4** forms one dimensional infinite chain structure via intermolecular N−H···O hydrogen bonding interactions. In cyclic voltammograms, the diamagnetic redox active complexes display an irreversible metal centred reduction in the potential range –0.73 to –0.88 V (vs. Ag/AgCl). The physicochemical data are consistent with a very similar gross molecular structure for all of **1**−**5**. All the complexes exhibit decent bromoperoxidase activities and are also able to effectively catalyze benzoin and methyl(phenyl)sulfide oxidation reactions.

5.1. Introduction

In the preceding chapter, we have described the synthesis and characterization of a series of *cis*-dioxomolybdenum(VI) complexes with an unsymmetrical tripodal tetradentate NO_3-donor ligand system and evaluated their catalytic efficiencies in oxidative bromination and benzoin oxidation

[§] This work has been communicated.

reactions [1]. In the present chapter, we have used unsymmetrical linear tetradentate ONNO-donor 2-((2-(2-hydroxyethylamino)ethylamino)methyl)-4-*R*-phenols (H_2L^nR = H, Me, OMe, Cl and Br) (Chart 5.1) to synthesize complexes of cis-$\{MoO_2\}^{2+}$. In this effort, we have isolated a new series of *cis*-dioxomolybdenum(VI) complexes having the general formula cis-$[MoO_2(L^n)]$. The complexes have been also evaluated for their catalytic efficiencies in oxidative bromination reactions as well as in benzoin and methyl(phenyl)sulfide oxidation reactions. In the following sections, we have described the details of synthesis, characterization, X-ray structures and catalytic behaviours of these complexes.

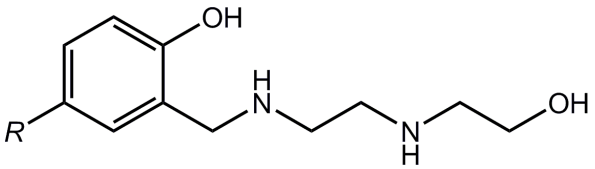

H_2L^n

(n = 1–5 for *R* = H, Me, OMe, Cl and Br, respectively)

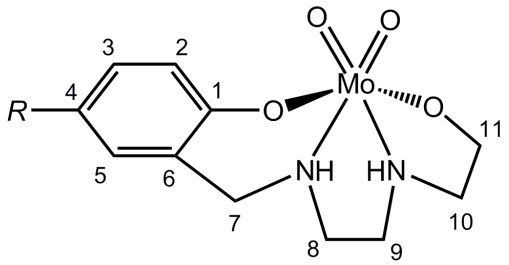

cis-$[MoO_2(L^n)]$

(**1**–**5** for n = 1–5, respectively)

Chart 5.1. Chemical structures of tetradentate linear ligands $H_2L^{1\text{-}5}$ and their complexes *cis*-$[MoO_2(L^{1–5})]$ (**1**–**5**).

5.2. Experimental

5.2.1. Materials

[$MoO_2(acac)_2$] was prepared according to a literature procedure [2]. The hydrochloride salts of 2-((2-(2-hydroxyethylamino)ethylamino)methyl)-4-*R*-phenols (H_2L^n·2HCl) were synthesized by following a reported procedure [3]. All other chemicals and solvents used in this work were of reagent grade and used as received without further purification.

5.2.2. Physical measurements

Elemental (CHN) analysis data were obtained with the help of a Thermo Finnigan Flash EA1112 series elemental analyzer. Magnetic susceptibility measurements were performed with a Sherwood Scientific balance. A Shimadzu LCMS 2010 liquid chromatograph mass spectrometer was used for verification of the compound purity. Solution electrical conductivities were measured with the help of a Digisun DI−909 conductivity meter. Infrared spectra were collected by using KBr pellets on a Thermo Scientific Nicolet 380 FT-IR spectrophotometer. A Shimadzu UV-3600 UV-VIS-NIR spectrophotometer was used to record the electronic spectra. The ^{1}H (400 MHz) and ^{13}C (100 MHz) NMR spectra were recorded with the help of a Bruker NMR spectrometer using tetramethylsilane as internal standard. A CH-Instruments model 620A electrochemical analyzer was used for cyclic voltammetric experiments. Shimadzu GC-2010 Plus equipped with FID and Shimadzu GCMS-QP2010 instruments were used for gas chromatographic measurements.

5.2.3. A general procedure for the synthesis of cis-[$MoO_2(L^{1-5})$] (1−5)

Solid [$MoO_2(acac)_2$] (0.3 mmol) was added to a solution of the corresponding H_2L^n·2HCl (0.3 mmol) and KOH (0.6 mmol) in methanol (25

mL). The resulting bright yellow reaction mixture was boiled under reflux for 0.5 h and then cooled to room temperature under ambient conditions. The pale yellow to bright yellow microcrystalline solid separated were collected by gravity filtration and washed with water, methanol and diethyl ether and finally dried in air.

cis-[MoO$_2$(L^1)] (1). Yield 83%. Anal. Calcd for $C_{11}H_{16}MoN_2O_4$ (336.20): C, 39.30; H, 4.80; N, 8.33. Found C, 39.46; H, 4.71; N, 8.45. Selected IR bands (cm^{-1}): 3238 and 3155 (ν_{N-H}), 2964−2865 (ν_{C-H}), 925 and 876 (νMoO_2). UV-Vis (λ_{max} (nm) (ε (10^3 M^{-1} cm^{-1}))): 313 (4.6), 273 (6.5). ^{1}H NMR (δ (ppm) (*J* (Hz))): 7.12 (8) (t, 1H, H^3), 7.08 (8) (d, 1H, H^5), 6.74 (8) (t, 1H, H^4), 6.65 (8) (d, 1H, H^2), 5.77 (s, 1H, N^{1}H), 5.39 (s, 1H, N^{2}H), 4.59 (16) (d, 1H, H^{7a}), 4.51 (m, 1H, H^{8a}), 4.41 (m, 1H, H^{8b}), 3.78 (16) (d, 1H, H^{7b}), 3.57 (m, 1H, H^{9a}), 2.96 (m, 1H, H^{9b}), 2.66 (m, 1H, H^{10a}), 2.59 (m, 1H, H^{10b}), 2.40 (m, 2H, H^{11}). ^{13}C NMR (δ (ppm)): 161.15 (C^1), 130.66 (C^3), 129.34 (C^5), 123.89 (C^6), 120.08 (C^2), 119.58 (C^4), 73.74 (C^7), 53.83 (C^8), 52.05 (C^9), 47.59 (C^{10}), 47.26 (C^{11}). E_{pc} (V): –0.79

cis-[MoO$_2$(L^2)] (2). Yield 85%. Anal. Calcd for $C_{12}H_{18}MoN_2O_4$ (350.22): C, 41.15; H, 5.18; N, 8.00. Found C, 41.34; H, 5.09; N, 8.12. Selected IR bands (cm^{-1}): 3205 and 3150 (ν_{N-H}), 2930−2840 (ν_{C-H}), 926 and 882 (νMoO_2). UV-Vis (λ_{max} (nm) (ε (10^3 M^{-1} cm^{-1}))): 324 (4.0), 275 (5.2). ^{1}H NMR (δ (ppm) (*J* (Hz))): 6.94 (8) (d, 1H, H^3), 6.90 (s, 1H, H^5), 6.57 (8) (d, 1H, H^2), 5.77 (s, 1H, N^{1}H), 5.35 (s, 1H, N^{2}H), 4.56 (12) (d, 1H, H^{7a}), 4.49 (m, 1H, H^{8a}), 4.38 (m, 1H, H^{8b}), 3.72 (16) (d, 1H, H^{7b}), 3.55 (m, 1H, H^{9a}), 2.95 (m, 1H, H^{9b}), 2.60 (m, 2H, H^{10}), 2.41 (m, 2H, H^{11}), 2.22 (s, 3H, 4-Me). ^{13}C NMR (δ (ppm)): 158.95 (C^1), 130.98 (C^3), 129.77 (C^5), 128.67 (C^6), 123.52 (C^4), 119.28 (C^2), 73.67 (C^7), 53.88 (C^8), 51.98 (C^9), 47.63 (C^{10}), 47.27 (C^{11}), 21.05 (4-Me). E_{pc} (V): –0.73.

cis-[$MoO_2(L^3)$] (3). Yield 86%. Anal. Calcd for $C_{12}H_{18}MoN_2O_5$ (366.22): C, 39.36; H, 4.95; N, 7.65. Found C, 39.25; H, 4.91; N, 7.58 %. Selected IR bands (cm^{-1}): 3210 and 3150 (ν_{N-H}), 2940−2832 (ν_{C-H}), 915 and 887 (νMoO_2). UV-Vis (λ_{max} (nm) (ε (10^3 M^{-1} cm^{-1}))): 340 (4.5), 301 (6.5). ^{1}H NMR (δ (ppm) (*J* (Hz))): 6.70 (d, 1H, H^3), 6.69 (s, 1H, H^5), 6.58 (8) (d, 1H, H^2), 5.73 (s, 1H, N^1H), 5.32 (s, 1H, N^2H), 4.56 (16) (d, 1H, H^{7a}), 4.48 (m, 1H, H^{8a}), 4.38 (m, 1H, H^{8b}), 3.74 (16) (d, 1H, H^{7b}), 3.68 (s, 3H, 4-OMe), 3.54 (m, 1H, H^{9a}), 2.95 (m, 1H, H^{9b}), 2.60 (m, 2H, H^{10}), 2.41 (m, 2H, H^{11}). ^{13}C NMR (δ (ppm)): 155.13 (C^1), 153.07 (C^4), 124.44 (C^6), 119.92 (C^2), 115.56 (C^5), 114.57 (C^3), 73.51 (C^7), 53.88 (C^8), 51.98 (C^9), 47.63 (C^{10}), 47.27 (C^{11}), 56.23 (4-OMe). E_{pc} (V): –0.80.

cis-[$MoO_2(L^4)$] (4). Yield 81%. Anal. Calcd for $C_{11}H_{15}ClMoN_2O_4$ (370.64): C, 35.65; H, 4.08; N, 7.56. Found C, 35.48; H, 4.13; N, 7.51 %. Selected IR data (cm^{-1}): 3205 and 3140 (ν_{N-H}), 2960−2850 (ν_{C-H}), 931 and 887 (νMoO_2). UV-Vis (λ_{max} (nm) (ε (10^3 M^{-1} cm^{-1}))): 314 (5.4), 287 (7.1). ^{1}H NMR (δ (ppm) (*J* (Hz))): 7.16 (s, 1H, H^5), 7.13 (12) (d, 1H, H^3), 6.65 (12) (d, 1H, H^2), 5.80 (s, 1H, N^1H), 5.48 (s, 1H, N^2H), 4.52 (16) (d, 1H, H^{7a}), 4.50 (m, 1H, H^{8a}), 4.41 (m, 1H, H^{8b}), 3.80 (16) (d, 1H, H^{7b}), 3.59 (m, 1H, H^{9a}), 2.96 (m, 1H, H^{9b}), 2.68 (m, 1H, H^{10a}), 2.60 (m, 1H, H^{10b}), 2.41 (m, 2H, H^{11}). ^{13}C NMR (δ (ppm)): 160.21 (C^1), 130.07 (C^3), 128.94 (C^5), 125.95 (C^6), 123.07 (C^4), 121.31 (C^2), 73.87 (C^7), 53.28 (C^8), 52.14 (C^9), 47.55 (C^{10}), 47.29 (C^{11}). E_{pc} (V): –0.83.

cis-[$MoO_2(L^5)$] (5). Yield 82%. Anal. Calcd for $C_{11}H_{15}BrMoN_2O_4$ (415.09): C, 31.83; H, 3.64; N, 6.75. Found C, 31.96; H, 3.58; N, 6.83 %. Selected IR bands (cm^{-1}): 3205 (ν_{N-H}), 2925−2843 (ν_{C-H}), 914 and 876 (νMoO_2). UV-Vis (λ_{max} (nm) (ε (10^3 M^{-1} cm^{-1}))): 317 (5.6), 285 (7.5). ^{1}H NMR (δ (ppm) (*J* (Hz))): 7.30 (s, 1H, H^5), 7.27 (8) (d, 1H, H^3), 6.62 (8) (d, 1H, H^2), 5.83 (s, 1H, N^1H), 5.50 (s, 1H, N^2H), 4.54 (16) (d, 1H, H^{7a}), 4.51 (m,

1H, H^{8a}), 4.41 (m, 1H, H^{8b}), 3.80 (16) (d, 1H, H^{7b}), 3.59 (m, 1H, H^{9a}), 2.96 (m, 1H, H^{9b}), 2.69 (m, 1H, H^{10a}), 2.60 (m, 1H, H^{10b}), 2.41 (m, 2H, H^{11}). ^{13}C NMR (δ (ppm)): 160.65 (C^1), 132.89 (C^3), 131.82 (C^5), 126.55 (C^6), 121.82 (C^2), 110.73 (C^4), 73.87 (C^7), 53.17 (C^8), 52.12 (C^9), 47.53 (C^{10}), 47.27 (C^{11}). E_{pc} (V): –0.88.

5.2.4. Catalysis measurements

Catalytic activities of **1**–**5** in oxidative bromination of various olefinic compounds and in oxidation of benzoin and methyl(phenyl)sulfide were examined. The details of optimized reaction conditions are described below.

5.2.4.1. Oxidative bromination.

10 mmol of substrate, 15 mmol of H_2O_2 (1.8 mL of 30% w/w aqueous solution), 20 mmol of KBr, 20 mmol of $HClO_4$ (2.4 mL of 60% aqueous $HClO_4$ solution) and 0.01 mmol of the catalyst *cis*-[$MoO_2(L^n)$] were taken in 6 mL of the mixed solvent water-methanol (1:1). The resulting mixture was stirred at room temperature for ¼ h to 2½ h (substrate-dependent). Then the reaction mixture was diluted with 50 mL of water and extracted with two 10 mL portions of dichloromethane. The dichloromethane extracts were combined, dried over anhydrous sodium sulfate and finally diluted to 40 mL with dry dichloromethane. This diluted solution was analyzed by GC-MS for identification and yields determination (from the areas under the peaks) of the products.

5.2.4.2. Benzoin oxidation.

20 mmol of H_2O_2 (2.4 mL of 30% w/w aqueous solution) and 0.01 mmol of the catalyst *cis*-[$MoO_2(L^n)$] were added to a methanol (6 mL) solution of 10 mmol of bezoin. The reaction mixture was stirred at room temperature for 1 h, diluted with 40 mL of water and finally

extracted with two 10 mL portions of dichloromethane. The combined dichloromethane extracts were dried over anhydrous sodium sulfate, diluted to 40 mL with dry dichloromethane and subjected to GC-MS analysis to identify the products and determine (using the peak-areas) their yields.

5.2.4.3. Oxidation of methyl(phenyl)sulfide.

10 mmol of methyl(phenyl)sulfide, 15 mmol of H_2O_2 (1.2 mL of 30% w/w aqueous solution) and 0.01 mmol of the catalyst *cis*-[$MoO_2(L^n)$] were stirred at room temperature for 1 h. The reaction mixture was then extracted with two 10 mL portions of dichloromethane. After drying over anhydrous sodium sulfate, the combined dichloromethane extracts were diluted to 40 mL with dry dichloromethane and analyzed by GC-MS for identification of the products and determination of their yields from the peak-areas.

5.2.5. X-ray crystallography

Single crystals of **1**−**4** were obtained by heating a mixture of [$MoO_2(acac)_2$] (0.05 mmol), the corresponding H_2L^n·2HCl (0.05 mmol) and KOH (0.1 mmol) in 25 mL of methanol on a digital water bath at 90° C for 10 minutes and then uniformly cooling (by ~30° C per hour) the reaction mixture to room temperature in about 2 h. We have tried to grow X-ray quality crystals of **5** using various crystallization techniques, but none of them was successful. Determination of the unit cell parameters and the collection of the intensity data at 298 K for each of **1** and **3** were performed on a Bruker-Nonius SMART APEX CCD single crystal diffractometer using graphite monochromated Mo Kα radiation (λ = 0.71073 Å). The SMART and the SAINT-Plus [4] packages were used for data acquisition and data extraction, respectively. Absorption correction was done using the SADABS program [5].

Table 5.1. Selected crystallographic data.

Complex	**1**	**2**	**3**·2CH_3CN	**4**
Empirical formula	$C_{11}H_{16}MoN_2O_4$	$C_{12}H_{18}MoN_2O_4$	$C_{12}H_{18}MoN_2O_5$	$C_{11}H_{15}ClMoN_2O_5$
Formula weight	336.20	350.22	366.22	370.64
Crystal system	Orthorhombic	Triclinic	Triclinic	Triclinic
Space group	$Pca2_1$	$P\bar{1}$	$P\bar{1}$	$P\bar{1}$
a (Å)	10.176(5)	7.1224(11)	7.1472(6)	7.0918(6)
b (Å)	6.880(4)	10.1493(14)	10.1444(9)	10.0620(7)
c (Å)	17.762(9)	10.3743(17)	10.6134(9)	10.3407(8)
α (°)	90	106.585(13)	101.026(1)	106.480(7)
β (°)	90	104.050(13)	108.748(1)	104.952(7)
γ (°)	90	100.195(12)	98.481(1)	98.345(6)
V (Å^3)	1243.5(11)	672.32(16)	696.93(10)	664.36(9)
Z	4	2	2	2
ρ (g cm^{-3})	1.796	1.730	1.745	1.853
μ (mm^{-1})	1.063	0.987	0.962	1.199
Reflections collected	11787	4574	7307	4557
Reflections unique	2435	2744	2731	2443
Reflections [$I \geq 2\sigma(I)$]	2392	2377	2445	1919
Parameters	163	173	181	172
$R1$, $wR2$ [$I \geq 2\sigma(I)$]	0.0178, 0.0439	0.0408, 0.0873	0.0316, 0.0729	0.0525, 0.1315
$R1$, $wR2$ (all data)	0.0181, 0.0443	0.0496, 0.0918	0.0369, 0.0759	0.0682, 0.1400
GOF on F^2	1.165	1.071	1.045	1.036
$\Delta\rho_{max}$, $\Delta\rho_{min}$ (e Å^{-3})	0.405 / −0.682	0.772 / −0.585	0.460 / −0.378	1.750 / −0.543

The unit cell parameters and the intensity data at 298 K for both **2** and **4** were obtained with the help of an Oxford Diffraction Xcalibur Gemini single crystal X-ray diffractometer using graphite monochromated Mo Kα radiation (λ = 0.71073 Å). The CrysAlisPro[6] package was used for data collection, reduction and absorption correction. The structure of each of **1**−**4** was solved by direct method and refined on F^2 by full-matrix least-squares procedures. All non-hydrogen atoms were refined anisotropically, while all hydrogen atoms were included in the structure factor calculation by using a riding model. Structure solution and refinement were done using the SHELX-97 programs[7] as provided in the WinGX package [8]. All the molecular graphic figures were made using either the Platon[9] or the Mercury[10] packages. X-ray crystallographic data (in CIF format) have been deposited with the Cambridge Crystallogrphic Date Centre. The deposition nos. are CCDC 1062701–1062704 for **1**–**5**, respectively. Selected crystal and refinement data for **1**−**4** are listed in Table 5.1.

5.3. Results and discussion

5.3.1. Synthesis and some properties

The complexes *cis*-[$MoO_2(L^n)$] (**1**−**5**) have been synthesized by reacting one mole equivalent each of [$MoO_2(acac)_2$] and the corresponding H_2L^n·2HCl in presence of two mole equivalents of KOH in refluxing methanol. They have been obtained as air stable yellow microcrystalline materials in 81–86% yields. The elemental (CHN) analysis data are in good agreement with those calculated for the molecular formulas of **1**−**5**. The diamagnetic nature of **1**–**5** clearly establishes the +6 oxidation state of molybdenum center in each complex. All the complexes are highly soluble in dimethylsulfoxide and dimethylformamide, sparingly soluble in methanol, ethanol and acetonitrile and insoluble in dichloromethane, chloroform, toluene and hexane. In solutions, all of **1**–**5** behave as non-electrolytes.

5.3.2. Spectroscopic characteristics

5.3.2.1. Infrared spectra

The infrared spectra of **1**–**5** were recorded using KBr pellets. The spectra of **1** and **2** are illustrated in Fig. 5.1 and those of **3**–**5** are provided in the appendix of this chapter. A few selected bands out of a large no of bands

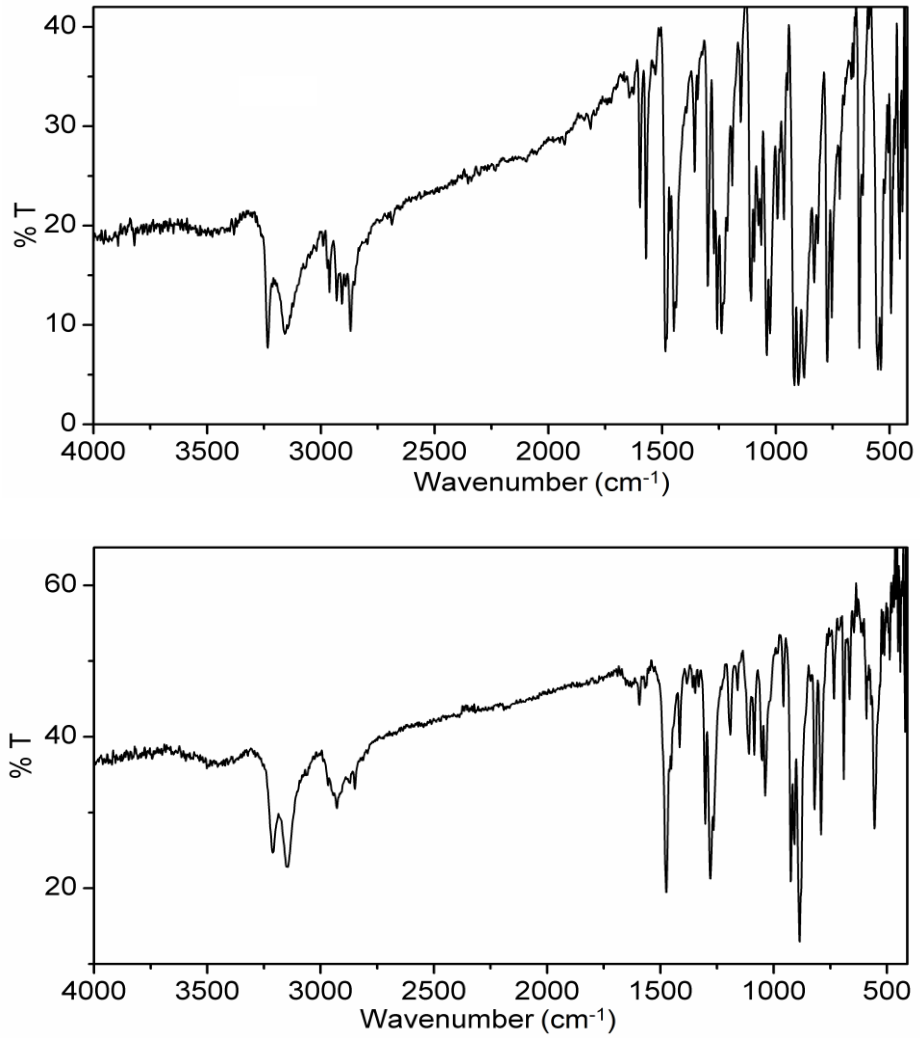

Fig 5.1. FTIR spectra of *cis*-[$MoO_2(L^1)$] (**1**) (top) and *cis*-[$MoO_2(L^2)$] (**2**) (bottom).

observed in the range 4000–400 cm^{-1} have been assigned. **1**–**4** display two broad bands at ~3215 and ~3150 cm^{-1}, while **5** shows a single broad band at 3205 cm^{-1}. These bands are attributed to the two metal coordinated NH

fragments of $(L^n)^{2-}$. The aromatic and aliphatic C–H stretches appear as multiple bands in the range 2970–2830 cm^{-1}. The symmetric and asymmetric stretches of the {*cis*-MoO_2}$^{2+}$ core were observed as two strong and sharp bands in the ranges 926–914 and 887–876 cm^{-1}, respectively [1,11–21].

5.3.2.2. Electronic spectra

Electronic absorption spectra of **1**–**5** were recorded using their dimethylsulfoxide solutions. The spectral profiles of all the complexes are quite similar (Fig. 5.2). Each complex displays two major absorption bands

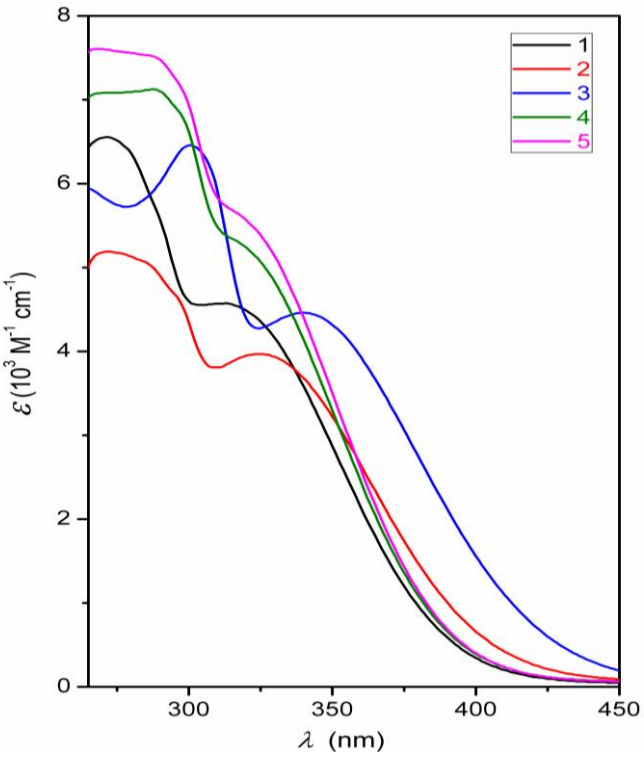

Fig. 5.2. Electronic spectra of *cis*-[$MoO_2(L^{1–5})$] (**1**–**5**) in methanol.

below 350 nm. The first band appears in the range 340–313 nm, while the second band is observed within 301–273 nm. In comparison, free $H_2L^{1–5}$ in methanol display a strong band in the wavelength range 297–276 nm. Thus for **1**–**5** the first low energy band is assigned to ligand-to-metal charge transfer transition, while the second higher energy band is attributed to a ligand

centred transition. Similar pair of absorption bands observed for complexes of *cis*-dioxomolybdenum(VI) with ligands having comparable donor atoms are reported to be due to ligand-to-metal charge transfer and ligand centred transitions, respectively [1,11–19].

5.3.2 3. NMR spectra

^{1}H-, ^{13}C- and ^{13}C-DEPT NMR spectra of **1**–**5** in dimethylsulfoxide-d_6 were recorded. The spectra (^{1}H and ^{13}C) of **1** are depicted in Fig. 5.3. The spectra of **2**–**5** are given in the appendix at the end of the chapter. The ^{1}H-NMR spectra of **1**–**5** are consistent with the same gross molecular structure for all (Chart 5.1, Figs. 5.4 and 5.5). A doublet appeared in the range δ 6.57–6.65 ppm is due to the proton at C^2, whereas the proton at C^3 resonates as a triplet for **1** and as a doublet for **2**–**5** in the range δ 6.70–7.27 ppm. The proton attached to C^5 appears as a doublet for **1** and as a singlet for **2**–**5** within δ 6.69–7.30 ppm. The triplet observed at δ 6.74 ppm for **1** is assigned to the proton at C^4. The protons of the Me and OMe substituents at C^4 in **2** and **3** appear as a singlet at δ 2.22 and 3.68 ppm, respectively. The diastereotopicity of the methylene protons is exhibited by the spectrum of each of **1**–**5**. The protons of the methylene group (C^7H_2) *ortho* to phenolate are observed as two doublets in the range δ 4.52–4.59 and 3.72–3.80 ppm. The C^8H_2 protons show two multiplets at δ ~4.50 and ~4.40 ppm. However, H^{7a} and H^{8a} provide overlapping signals in the cases of **4** and **5**. The methylene protons at C^9 appear as two multiplets at δ ~3.57 and ~2.96 ppm. The $C^{10}H_2$ protons of **1**, **4** and **5** resonate as two multiplets at δ ~2.68 and ~2.60 ppm, while those of **2** and **3** show a single two proton multiplet at δ ~2.62 ppm. A single multiplet observed at δ ~2.41 ppm is assigned to the methylene protons at C^{11}. The protons at the nitrogen atoms of the benzylamine fragment and diethyleneamine fragment are observed as two singlets in the ranges δ 5.73–5.83 and 5.32–5.50 ppm, respectively. Overall trends in the proton chemical

shifts are consistent with the electronic nature of the *para*-substituents of the phenolate moiety of $(L^n)^{2-}$ in **1**–**5**.

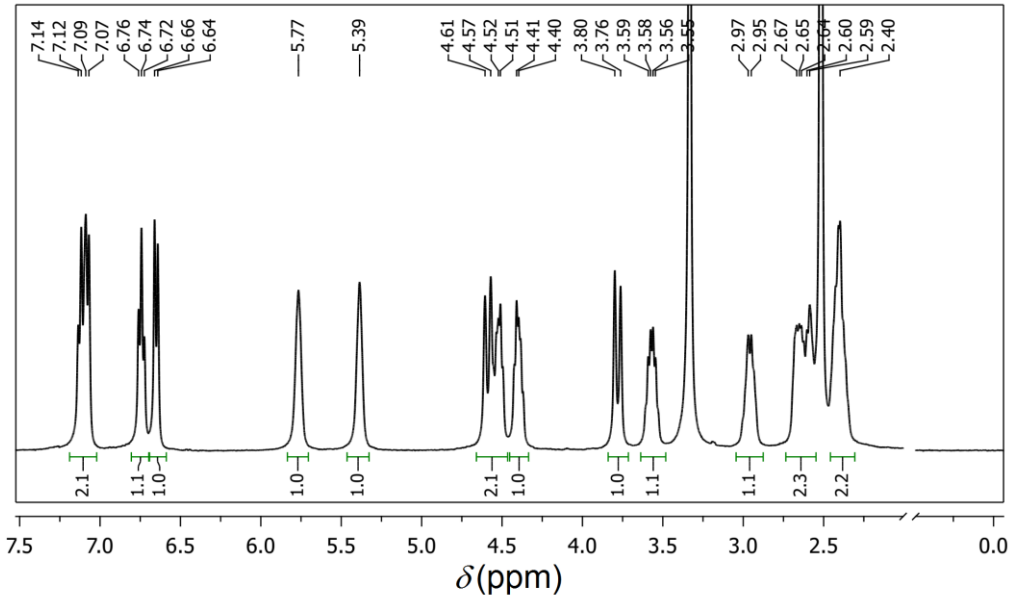

(a)

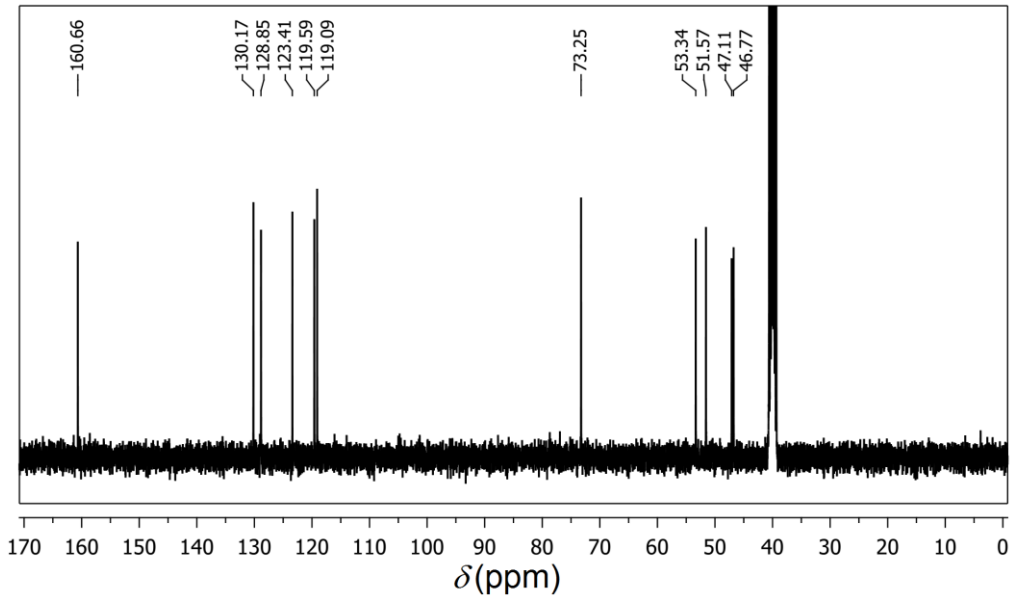

(b)

Fig. 5.3. (a) ^{1}H– and (b) ^{13}C–NMR spectra of [$MoO_2(L^1)$] (**1**) in dimethylsulfoxide–d_6.

The ^{13}C NMR spectra of **1**–**5** are also in good agreement with their similar molecular structures (Chart 5.1). Generally the chemical shifts of the individual carbon atoms of the phenolate ring vary significantly with the change of its *para* substituent, whereas there is essentially no change in the chemical shift of each of the five methylene carbon atoms in the remaining aliphatic skeleton of $(L^n)^{2-}$. The phenolate ring carbons C^1–C^6 resonate in the ranges δ 155.13–161.15, 119.28–121.82, 114.57–132.98, 110.73–153.07, 115.56–131.82 and 123.89–128.67 ppm, respectively. The resonances due to the methylene carbons C^7–C^{11} appear at δ ~73.73, ~53.60, ~52.05, ~47.59 and ~47.26 ppm, respectively. The signals corresponding to the carbons of the Me and the OMe substituents at *para* position of the phenolate ring of $(L^n)^{2-}$ in **2** and **3** are observed at δ 21.05 and 56.23 ppm, respectively. The spectral assignments described above are also consistent with the ^{13}C-DEPT NMR spectra of **1**–**4**.

5.3.3. Description of X-ray structures

Complex **1** crystallizes in the non-centrosymmetric orthorhombic space group *P*ca2_1, whereas the remaining three complexes (**2**−**4**) crystallize in the centrosymmetric triclinic space group $P\bar{1}$. In each structure, the asymmetric unit is comprised of a single complex molecule. The bond parameters related to the metal centres are listed in Table 5.2. Fig. 5.4 illustrates the molecular structures of **1** and **2**, while Fig. 5.5 provides the molecular structures of **3** and **4**. On the whole, the molecular structures of **1**−**4** are very similar. In each complex molecule, the ligand $(L^n)^{2-}$ coordinates to the metal centre through a phenolate-O, two secondary amine-N and an ethanolate-O atoms and forms 6,5,5-membered fused chelate rings. The unsymmetrical ONNO-donor $(L^n)^{2-}$ and the two mutually *cis*-oriented oxo groups form a distorted octahedral N_2O_4 coordination geometry around the

molybdenum. In all of **1**−**4**, the Mo–N(amine) (Mo–N(1) (2.323(5)−2.365(2) Å) and Mo−N(2) (2.318(2)−2.353(3) Å)) bond lengths are significantly longer than the Mo–O(phenolate) (Mo−O(1) (1.939(2)−1.9816(17) Å)) and Mo–O(ethanolate) (Mo−O(2) (1.942(3)−1.946(4) Å)) bond lengths. This lengthening of the Mo–N bonds is due to the strong *trans* effects imposed by the oxo groups (O(3) and O(4)) on the secondary amine-N atoms (N(1) and N(2)). It is worth noting that the Mo–O(ethanolate) bond lengths are very similar but the Mo–O(phenolate) bond lengths vary significantly with the change of the substituent (*R*) at *para* position of the phenolate fragment of $(L^n)^{2-}$ (Table 5.2). Although the variation of the Mo–O(phenolate) bond length does not reflect a systematic trend with the change of the electronic nature of *R*, but for the electron releasing groups (*R* = Me and OMe) the bond lengths are shorter than for *R* = H or electron withdrawing Cl. The bond angles in the five-membered chelate rings are in the range 72.63(7)–74.52(7)° and those in the six-membered chelate rings are within 76.30(7)–81.25(11)°. In contrast, the *cis*-MoO_2 bond angles (108.75(12)–109.1(2)°) are very similar and significantly larger. The remaining *cis* bond angles span the broad range of 82.01(9)–103.51(15)°, while the *trans* bond angles are within a relatively narrow range of 155.51(10)–163.82(10)°. In general, the bond lengths and bond angles within the metal ion coordination spheres of **1**−**4** (Table 5.2) lie in the range reported for *cis*-dioxomolybdenum(VI) complexes with ligands coordinating through comparable donor atoms [1,11–20,27–29].

It may be noted that metal coordination to the secondary amine-N atoms (N(1) and N(2)) of $(L^n)^{2-}$ makes them asymmetric centers and hence molecules of all the complexes are chiral. However, crystallizations of **2**–**4** in the centrosymmetric space group $P\bar{1}$ clearly suggest that in each case, the crystals as well as the bulk sample are racemic in nature.In view of the fact that **1** crystallizes in the non-centrosymmetric space group *P*ca2_1, we have

recorded the solid state circular dichroism (CD) spectrum of its bulk sample. No signal in the CD spectrum of **1** indicates that like **2**–**4** here also the bulk sample contains both the enantiomers in 1:1 ratio and hence it is optically inactive. Thus there is a spontaneous resolution of **1** during the course of its crystallization.

Table 5.2. Selected bond lengths (Å) and angles (^{o}) for **1**–**4**.

Complex	**1**	**2**	**3**	**4**
Mo–O(1)	1.9816(17)	1.939(3)	1.939(2)	1.946(5)
Mo–O(2)	1.9451(15)	1.942(3)	1.942(2)	1.946(4)
Mo–O(3)	1.7063(16)	1.704(3)	1.712(2)	1.709(4)
Mo–O(4)	1.7134(16)	1.690(3)	1.708(2)	1.691(4)
Mo–N(1)	2.365(2)	2.329(3)	2.334(2)	2.323(5)
Mo–N(2)	2.318(2)	2.353(3)	2.336(3)	2.353(5)
O(1)–Mo–O(2)	156.09(7)	155.77(12)	155.51(10)	155.8(2)
O(1)–Mo–O(3)	93.62(8)	93.59(13)	94.05(10)	93.6(2)
O(1)–Mo–O(4)	99.68(9)	103.51(15)	102.62(11)	103.2(2)
O(1)–Mo–N(1)	76.30(7)	81.25(11)	81.03(9)	80.93(18)
O(1)–Mo–N(2)	86.54(7)	84.36(12)	84.19(10)	84.0(2)
O(2)–Mo–O(3)	101.22(8)	96.96(13)	97.38(10)	96.6(2)
O(2)–Mo–O(4)	93.19(8)	93.61(13)	94.11(10)	94.1(2)
O(2)–Mo–N(1)	84.08(7)	82.43(12)	82.01(9)	83.04(19)
O(2)–Mo–N(2)	74.52(7)	73.88(12)	74.15(9)	73.98(19)
O(3)–Mo–O(4)	108.84(9)	108.92(14)	108.75(12)	109.1(2)
O(3)–Mo–N(1)	161.53(7)	163.24(11)	163.82(10)	163.3(2)
O(3)–Mo–N(2)	91.58(8)	90.24(12)	90.58(10)	90.6(2)
O(4)–Mo–N(1)	88.32(8)	87.82(12)	87.40(10)	87.6(2)
O(4)–Mo–N(2)	158.07(7)	158.49(13)	158.74(10)	158.3(2)
N(1)–Mo–N(2)	72.63(7)	73.44(11)	73.64(9)	73.26(19)

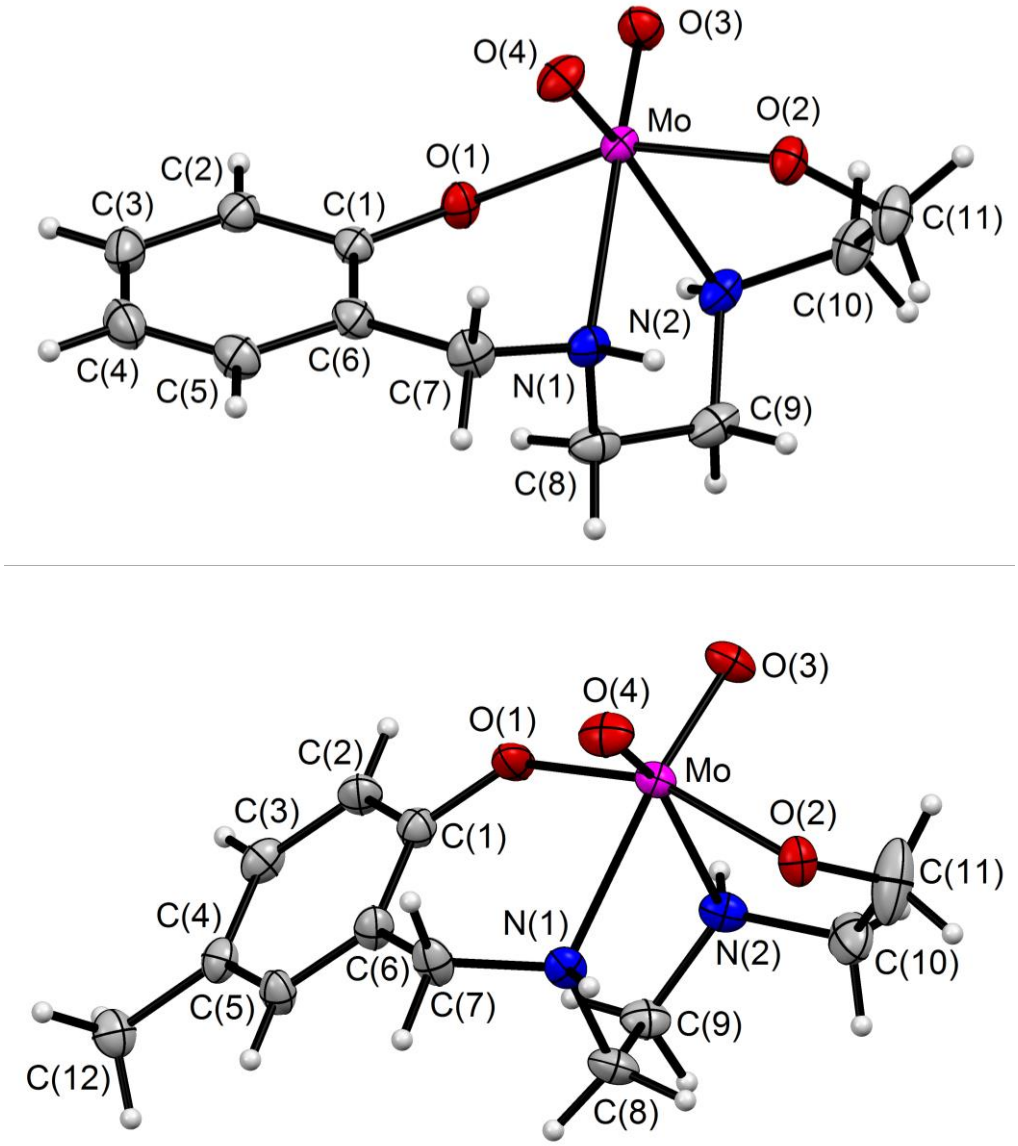

Fig. 5.4. Molecular structures of *cis*-[$MoO_2(L^1)$] (**1**) (top) and *cis*-[$MoO_2(L^2)$] (**2**) (bottom). All non-hydrogen atoms are represented by their 30% probability thermal ellipsoids.

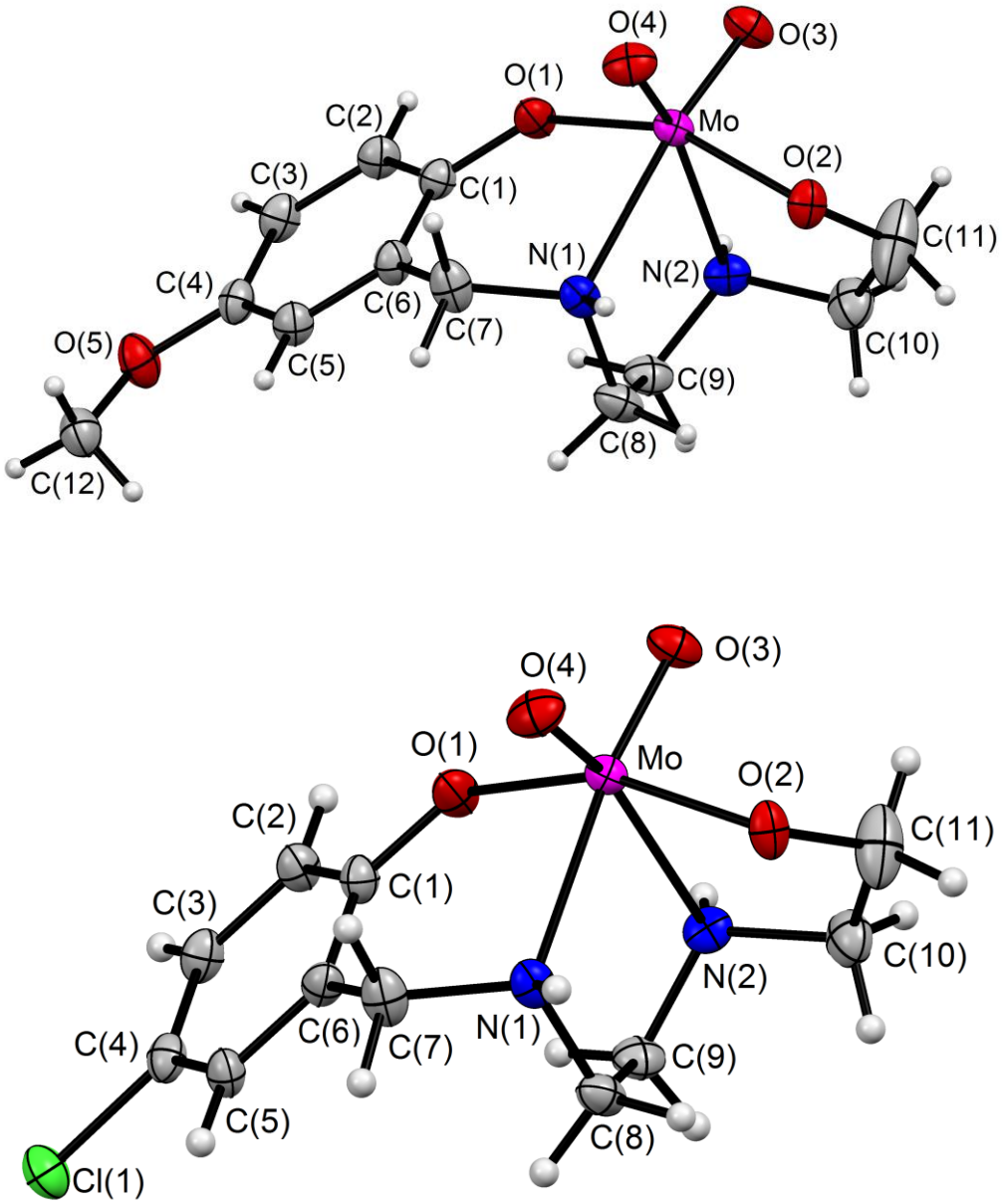

Fig. 5.5. Molecular structures of *cis*-[$MoO_2(L^3)$] (**3**) (top) and *cis*-[$MoO_2(L^4)$] (**4**) (bottom). All non-hydrogen atoms are represented by their 30% probability thermal ellipsoids.

5.3.4. Hydrogen bonding and self-assembly

The presence of two secondary amine functionalities in each of **1**–**4** have led us to search for the intermolecular conventional hydrogen bonding assisted self-assembled supramolecular structures, if any. Indeed, both N–H functionalities in all of **1**–**4** are involved in intermolecular hydrogen bonding with metal bound O-atoms. Both the phenolate- and the ethanolate-O atoms (O(1) and O(2), respectively) in **1**, while the ethanolate-O and one oxo group (O(2) and O(3), respectively) in each of **2**–**4** act as donors in these N–H···O interactions. The geometrical parameters for all three types of N–H···O hydrogen bonds are summarized in Table 5.3. Self-assembly of the molecules of **1**–**4** via these interactions leads to one-dimensional chain structures in the corresponding crystal lattices. The self-assembled structures of **1**–**3** are depicted in Fig. 5.6, while that of **4** is provided in Fig. 5.7. In the case of **1**, the one-dimensional chain formed by the N(1)–H···O(1) and N(2)–H···O(2) interactions propagates along the *a*-axis of the non-centrosymmetric lattice.

Table 5.3. Hydrogen bonding parameters (Å and ^{o}) in **1**–**4**.

Complex	D–H···A	H···A (Å)	D···A (Å)	D–H···A (°)
1	N(1)–H(1A)···O(1)^{i}	2.42	3.316(3)	167.6
	N(2)–H(2A)···O(2)^{ii}	2.04	2.931(3)	164.3
2	N(1)–H(1A)···O(2)^{iii}	1.98	2.880(4)	171.8
	N(2)–H(2A)···O(3)^{iv}	2.03	2.917(4)	163.5
3	N(1)–H(1A)···O(2)^{v}	1.99	2.890(3)	171.2
	N(2)–H(2A)···O(3)^{vi}	2.02	2.924(3)	169.4
4	N(1)–H(1A)···O(2)^{vii}	1.96	2.866(6)	176.1
	N(2)–H(2A)···O(3)^{viii}	2.03	2.920(6)	165.1

Symmetry transformations used: (i) x – 1/2, –y + 1, z; (ii) x + 1/2, –y + 1, z; (iii) –x, –y + 2, –z; (iv) –x, –y + 1, –z; (v) –x, –y + 1, –z + 1; (vi) –x, –y, –z + 1; (vii) –x + 1, –y + 2, –z + 1; (viii) –x + 1, –y + 1, –z + 1

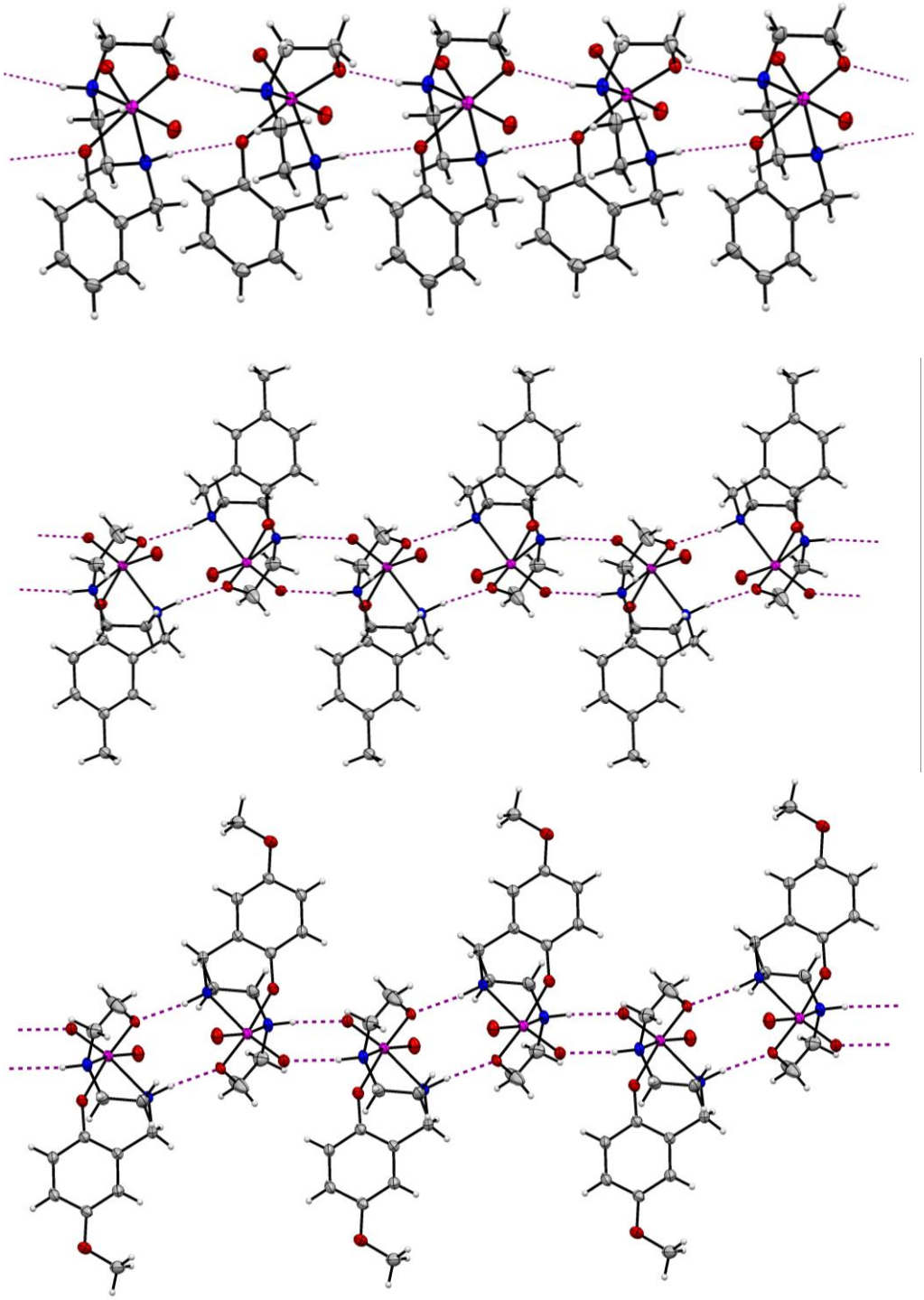

Fig. 5.6. One dimensional chains of **1** (top), **2** (middle) and **3** (bottom).via intermolecular hydrogen bonding.

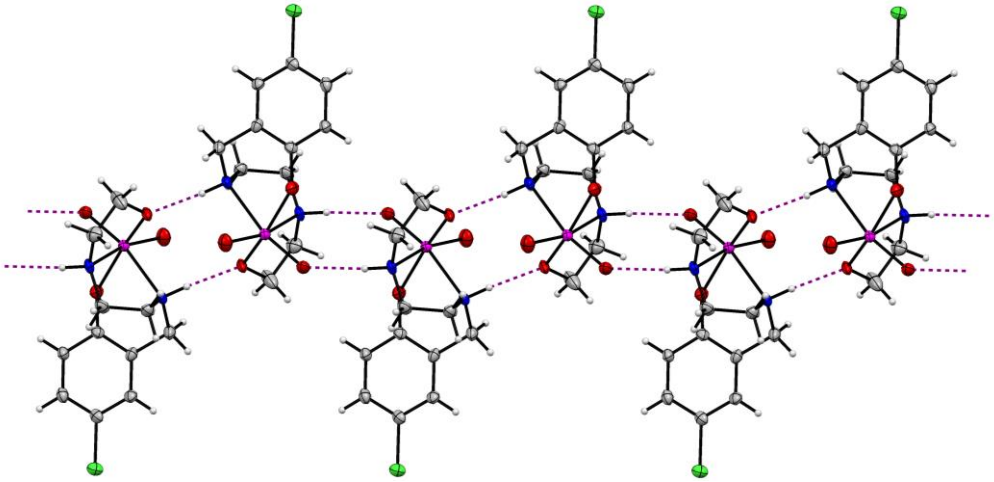

Fig. 5.7. One dimensional chain of **4** via intermolecular hydrogen bonding.

On the other hand, for **2**–**4** the one-dimensional chain structures lie along the *b*-axis of the centrosymmetric lattices. In the chain, each enantiomer is flanked by two opposite enantiomers. One of the two opposite enantiomers is connected by a pair of reciprocal N(1)–H···O(2) interactions, while the other one is connected by a pair of reciprocal N(2)–H···O(3) interactions.

5.3.5. Redox properties

Cyclic voltammetry has been used to scrutinize the redox properties of **1**–**5**. The measurements were performed under nitrogen atmosphere at 298 K with ~10^{-3} M solutions of the corresponding complexes in dimethylformamide containing tetrabutylammonium perchlorate as the supporting electrolyte. The three electrode setup was comprised of a Pt-disk working electrode, a Pt-wire auxiliary electrode and an Ag/AgCl reference electrode. The ferrocenium/ferrocene (Fc^+/Fc) couple was observed at $E_{1/2}$ = 0.66 V under identical condition. The cyclic voltammograms are illustrated in Fig. 5.8. All of **1**–**5** show an irreversible reduction response with cathodic peak potentials (E_{pc}) in the range –0.73 to –0.88 V. The one electron nature of these responses

has been inferred by comparing the cathodic peak currents with that of the Fc^{+}/Fc couple as well as with other known one electron processes [1,15,26]. Such irreversible cathodic responses observed for complexes of *cis*-dioxomolybdenum(VI) with ligands having similar type of coordinating atoms have been reported to be due to molybdenum(VI) → molybdenum(V) reduction [1,11,12,15,17,30].

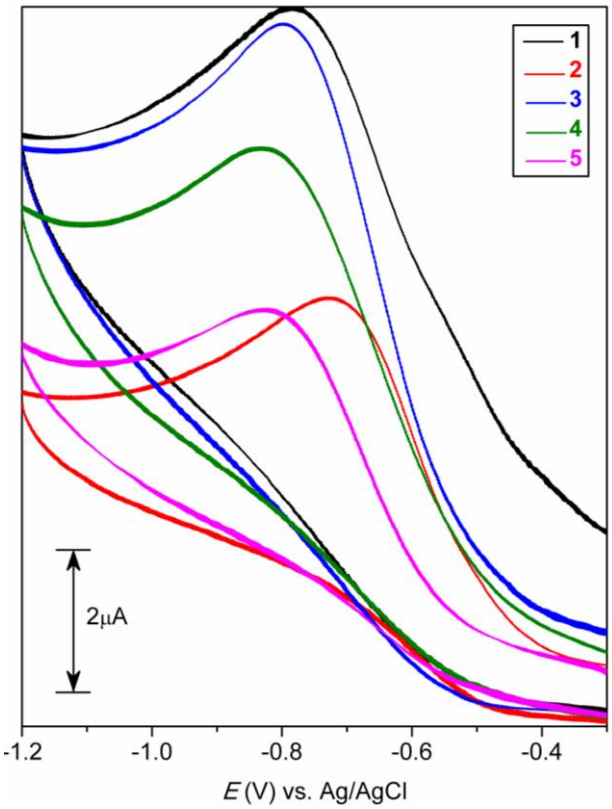

Fig. 5.8. Cyclic voltammograms (scan rate 100 mVs^{-1}) of *cis*-[$MoO_2(L^{1-5})$] (**1**–**5)** in $(CH_3)_2NC(O)H$.

5.3.6. Catalytic studies

Bromoperoxidase activities of **1**–**5** have been examined by oxidative bromination of a variety of olefinic compounds and salicylaldehyde in presence of H_2O_2, KBr and $HClO_4$. The product selectivity patterns are summarized in Scheme 5.1 and Table 5.4. Catalytic abilities of **1**–**5** in

benzoin and methyl(phenyl)sulfide oxidation reactions have been also investigated. The results are shown in Scheme 5.2 and Table 5.5.

5.3.6.1. Oxidative bromination.

Screening of solvents and oxidant (H_2O_2) and catalysts loading to optimize the reaction conditions at room temperature was done using **3** as catalyst and styrene as substrate. Reaction time was decided by considering maximum conversion of styrene. Different solvents such as methanol, ethanol, acetonitrile, dichloromethane and chloroform with water (in 1:1 ratio) as cosolvent were checked. The substrate conversion is low (~50%) in each of chloroform-water and dichloromethane-water mixtures, while it improves considerably (~70%) in acetonitrile-water mixture but remains incomplete. On the other hand, the conversion is essentially complete in both methanol-water and ethanol-water mixtures. Reaction of styrene, H_2O_2, KBr and $HClO_4$ in 1:1.5:2:2 mole ratio in presence of 0.1 mol% of the catalyst in methanol-water (1:1) was considered to be the best reaction condition. Only 10% of styrene was converted to the products in the control experiment without catalyst. The best reaction condition thus found except for the reaction time (determined separately for each substrate considering its maximum conversion) was used for the other olefinic substrates. The products obtained from various substrates using the optimized reaction conditions and **1**–**5** as catalysts are shown in Scheme 5.1 and the reaction times, conversion percentages and the product selectivities are summarized in Tables 5.4.

In the case of styrene, three products such as 1,2-diol, 2-bromo-1-ol and 1,2-dibromide were obtained as major products with very less amount of epoxide (≤ 6%). In our previous study on oxidative bromination of styrene using *cis*-dioxomolybdenum(VI) complexes with tetradentate but tripodal ligands as catalysts, with 2-bromo-1-ol the other two main products were 2-

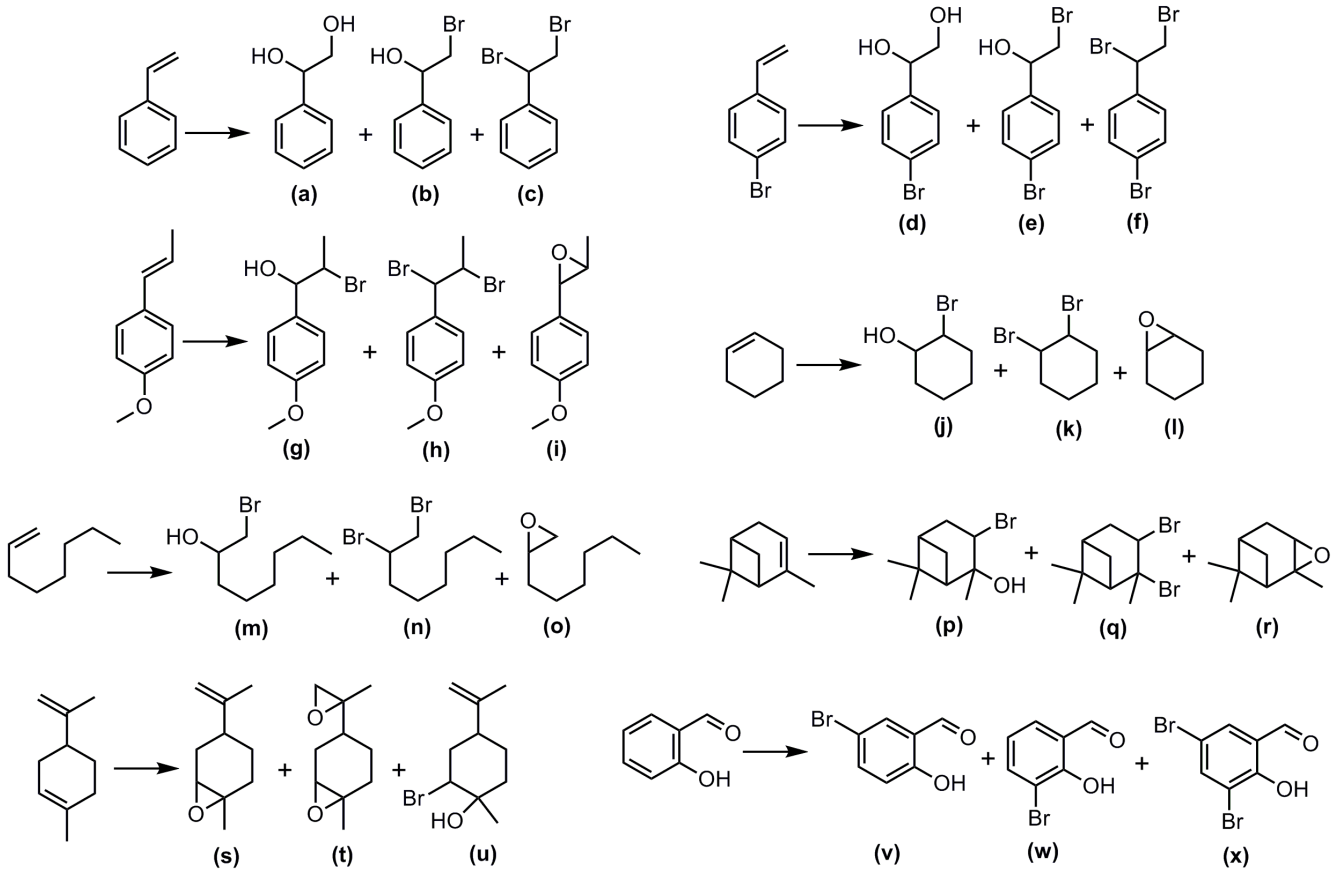

Scheme 5.1. *cis*-[$MoO_2(L^{1–5})$] (**1**–**5**) catalyzed oxidative bromination of various olefinic compounds and salicylaladehyde.

Table 5.4. Data for catalytic oxidative bromination.

Substrate and catalyst	Conversion (%)	Time (h)	TOF (h^{-1})	Product selectivity (%)		
Styrene				**(a)**	**(b)**	**(c)**
1	94	0.5	1880	37	40	18
2	98	0.5	1960	35	43	19
3	98	0.5	1960	32	41	21
4	94	0.5	1880	35	40	19
5	96	0.5	1920	36	42	18
4-Bromostyrene				**(d)**	**(e)**	**(f)**
1	96	0.5	1920	26	44	28
2	97	0.5	1940	26	48	18
3	98	0.5	1960	28	48	16
4	95	0.5	1960	35	45	15
5	96	0.5	1920	31	46	18
trans-Anethole				**(g)**	**(h)**	**(i)**
1	89	0.75	1187	52	32	15
2	92	0.75	1227	55	28	16
3	94	0.75	1253	56	28	16
4	88	0.75	1173	50	30	16
5	88	0.75	1173	51	30	16
Cyclohexene				**(j)**	**(k)**	**(l)**
1	95	0.66	1440	44	37	19
2	96	0.66	1455	43	37	20
3	98	0.66	1484	42	36	22
4	92	0.66	1393	44	35	21
5	93	0.66	1410	39	39	22
1-Octene				**(m)**	**(n)**	**(o)**
1	82	1	820	50	33	17
2	80	1	800	52	30	18
3	82	1	820	55	27	18
4	85	1	850	50	31	19
5	85	1	850	51	32	17
α-Pinene				**(p)**	**(q)**	**(r)**
1	72	2.5	288	40	33	25
2	75	2.5	300	42	30	27
3	78	2.5	312	42	26	30
4	73	2.5	292	40	35	23
5	75	2.5	300	39	36	22
Limonene				**(s)**	**(t)**	**(u)**
1	84	1.25	672	19	35	45
2	91	1.25	728	16	38	45

Table 5.4. Continued...

Substrate and catalyst	Conversion (%)	Time (h)	TOF (h^{-1})	Product selectivity (%)		
3	95	1.25	760	15	36	49
4	84	1.25	672	19	35	45
5	88	1.25	704	18	37	45
Salicylaldehyde				**(v)**	**(w)**	**(x)**
1	98	0.25	3920	71	13	16
2	98	0.25	3920	80	6	14
3	99	0.25	3960	90	8	2
4	96	0.25	3840	82	12	6
5	97	0.25	3880	83	5	12

bromo-1-one and epoxide instead of 1,2-diol and 1,2-dibromide [1]. Interestingly, studies on the same reaction catalyzed by *cis*-dioxomolybdenum(IV) complexes with tridentate ligands reported to produce the same three products as observed here but with different selectivities [27,29]. When 4-bromostyrene was used as substrate, the conversion percentages and the product selectivities were very close to that observed for styrene (Table 5.4). However, epoxides instead of 1,2-diols were obtained with 2-bromo-1-ols and 1,2-dibromides for substrates such as *trans*-anethole, cyclohexene, 1-octene and α-pinene (Scheme 5.1). In each case, 2-bromo-1-ol was produced more selectively than the dibromo derivative and the epoxide (Table 5.4). In the case of limonene, it is important to note that no dibromide was observed and with more selectively produced 2-bromo-1-ol both mono- and diepoxides were formed in significant amounts. Including the above mentioned olefinic compounds, the catalytic oxidative bromination of salicylaldehyde was also performed. In this reaction, although the products obtained were similar, but 5-bromosalicylaldehyde was formed with very high selectivity when compared with the previous observations[27–29] including our recent results [1]. Overall, catalytic efficiencies of **1**–**5** in all the above oxidative bromination reactions are comparable. Thus the variation of

substituents (*R*) on the ligand $(L^n)^{2-}$ has no effect on the bromoperoxidase activities of the present series of complexes.

5.3.6.2. Benzoin oxidation.

Complexes **1**–**5** were also used as catalysts in benzoin oxidation reaction in methanol. Optimized reaction condition was determined by varying the amounts of **3** as catalyst and H_2O_2 (30% w/w aqueous solution) as oxidant. It was found that maximum conversion of benzoin occurred in 1 h when it was reacted with H_2O_2 in 1:2 mole ratio in presence of 0.1 mol% of **3**. This same reaction condition was used for each of the remaining four complexes as catalyst. In all the cases, benzoic acid was obtained as the major product with benzil and α,α-dimethoxytoluene as the minor products (Scheme 5.2, Table 5.5). It may be noted that methyl benzoate was also produced but in very less amount (< 3%). The present product selectivity and yield patterns are very similar to those observed in our previous study [1]. However, methyl benzoate was reported to be produced in much larger amount with the other

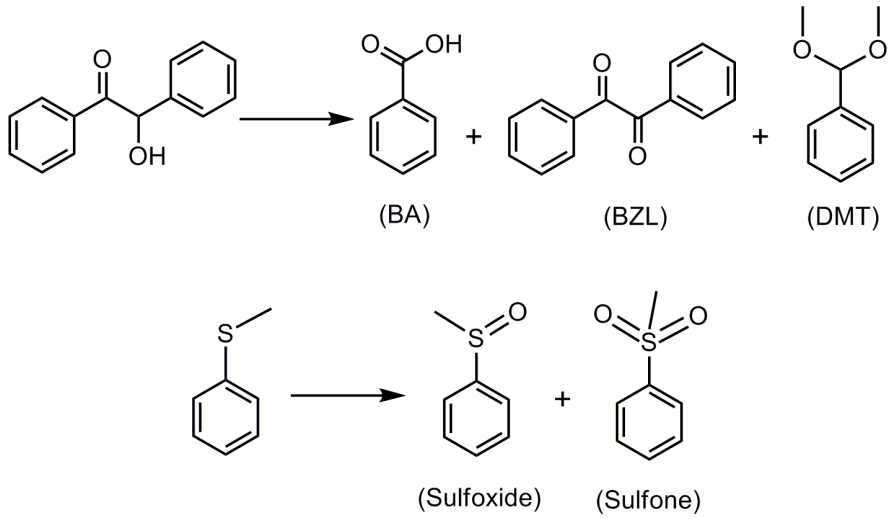

Scheme 5.2. *cis*-[$MoO_2(L^{1-5})$] (**1**–**5**) catalyzed oxidation of benzoin and methyl(phenyl)sulfide.

Table 5.5 Data for catalytic benzoin and methyl(phenyl)sulfide oxidation.

Reaction and catalyst	Conversion (%)	Time (h)	TOF (h^{-1})	Product selectivity (%)		
Benzoin oxidation				BA	BZL	DMT
1	96	1	960	46	33	18
2	97	1	970	48	31	19
3	98	1	980	53	28	18
4	94	1	940	46	31	21
5	95	1	950	49	30	18
Methyl(phenyl)sulfide oxidation				Sulfoxide		Sulfone
1	92	1	920	67		33
2	93	1	930	65		35
3	94	1	940	64		36
4	91	1	910	66		33
5	93	1	930	65		35

three products in benzoin oxidation reactions catalyzed by *cis*-dioxomolybdenum(IV) complexes with tridentate ligands [27,29]. In the control experiment without any catalyst, only eight percent of benzoin was converted to benzoic acid (major product), benzil (distant second major product) and α,α-dimethoxytoluene (very small amount) (Table 5.5). Regardless of the nature of the substituent (*R*) on $(L^n)^{2-}$, the catalytic performances of **1**–**5** in benzoin oxidation reaction remain comparable.

5.3.6.3. Oxidation of methyl(phenyl)sulfide.

The present series of complexes (**1**–**5**) was also tested for catalytic activity in oxidation of methyl(phenyl)sulfide with H_2O_2. The reaction condition was optimized by varying the amounts of **3** as catalyst and the oxidant H_2O_2 (30% w/w aqueous solution). A combination of methyl(phenyl)sulfide and H_2O_2 in 1:1.5 mole ratio in presence of 0.1 mol% of **3** was found to be the best for maximum conversion of the substrate to the products in 1 h. The catalytic activities of the remaining four complexes in methyl(phenyl)sulfide oxidation

were assessed using the above mentioned combination of substrate, oxidant and catalyst. In all the cases, two oxidized products namely the methyl(phenyl)sulfoxide and the methyl(phenyl)sulfone were formed in ~1.9:1 ratio (Scheme 5.2, Table 5.5). Twenty percent of the substrate was converted to the oxidized products under the optimized reaction condition without catalyst. There are few reports on sulfide oxidation using tridentate ligand supported *cis*-dioxomolybdenum(VI) complexes as catalysts [19,20,27]. When compared with present results, the catalytic activities and the product selectivities are similar in one case [30], while essentially 100% selectivity for the sulfoxide was reported in the other cases [19,20]. As observed in the oxidative bromination and benzoin oxidation, here also the catalytic activities of **1**–**5** are practically invariant with the change of substituents on their corresponding ligands.

5.4. Conclusions

A new series of complexes having the general molecular formula *cis*-[$MoO_2(L^n)$] (**1**–**5**) with unsymmetrical linear tetradentate 2-((2-(2-hydroxyethylamino)ethylamino)methyl)-4-*R*-phenols (H_2L^n) has been synthesized. Molecular structures of four out of five complexes have been determined by X-ray crystallography. In each structure, $(L^n)^{2-}$ coordinates to the *cis*-{MoO_2}$^{2+}$ unit through the phenolate-O, two secondary amine-N and the ethanolate-O atoms and completes a distorted octahedral N_2O_4 coordination geometry of the metal centre. Spectroscopic and redox characteristics are consistent with the same overall molecular structure for all five complexes. All the complexes are catalytically active in oxidative bromination of various olefinic compounds and salicylaldehyde and in benzoin and sulfide oxidation reactions. The product selectivities in each reaction are very similar for all five complexes. Thus the substituents at the

para position of the phenolate fragment of $(L^n)^{2-}$ have no significant effect on the catalytic abilities of **1**–**5**.

5.5. References

[1] S.K. Kurapati, S. Maloth, S. Pal, *Inorg Chim. Acta.*, 430, **2015**, 66–73.

[2] G.J.J. Chen, J.W. McDonald, W.E. Newton, *Inorg. Chem.*, 15, **1976**, 2612–2615.

[3] A. Neves, S.M.M. Romanowski, I. Vencato, A.S. Mangrich, *J. Chem. Soc., Dalton Trans.*, **1998**, 617–621.

[4] *SMART* version 5.630 and *SAINT−plus* version 6.45, *Bruker−Nonius Analytical X−ray Systems Inc*., Madison, WI, USA, **2003**.

[5] G.M. Sheldrick, *SADABS, Program for Area Detector Absorption Correction*, University of Göttingen, Göttingen, Germany, **1997**.

[6] *CrysAlisPro version 1.171.36.28, Agilent Technologies*, Yarnton, Oxfordshire, UK, **2013**.

[7] G.M. Sheldrick, *Acta Crystallogr., Sect. A*, 64, **2008**, 112–122.

[8] L.J. Farrugia, *J. Appl. Crystallogr.*, 45, **2012**, 849−854.

[9] A.L. Spek, *Platon, A Multipurpose Crystallographic Tool*, Utrecht University, Utrecht, The Netherlands, **2002**.

[10] C.F. Macrae, I.J. Bruno, J.A. Chisholm, P.R. Edgington, P. McCabe, E. Pidcock, L. Rodriguez-Monge, R. Taylor, J. van de Streek, P.A. Wood, *J. Appl. Crystallogr.*, 41, **2008**, 466−470.

[11] S. Gupta, S. Pal, A.K. Barik, S. Roy, A. Hazra, T.N. Mandal, R. J. Butcher, S. K. Kar, *Polyhedron*, 28, **2009**, 711–720.

[12] N.K. Ngan, K.M. Lo, C.S.R. Wong, *Polyhedron*, 30, **2011**, 2922–2932.

[13] S.K. Kurapati, U.Ugandhar, S. Maloth, S. Pal, *Polyhedron*, 42, **2012**, 161–167.

[14] S.K. Kurapati, *Acta Crystallogr. Sect. E*, 69, **2013**, m460–m461.

[15] S.K. Kurapati, S. Pal, *Dalton Trans.*, 44, **2015**, 2401–2408.

[16] C.J. Hinshaw, G. Peng, R. Singh, J.T. Spence, J.H. Enemark, M. Bruck, J. Kristofzski, S.L. Merbs, R.B. Ortega, P.A. Wexler, *Inorg. Chem.*, 28, **1989**, 4483–4491.

[17] X. Lei, N. Chelamalla, *Polyhedron*, 49, **2013**, **49**, 244–251.

[18] R. Mayilmurugan, P. Traar, J.A. Schachner, M. Volpe, N.C. Mösch-Zanetti, *Eur. J. Inorg. Chem.*, **2013**, 3664–3670.

[19] M. Bagherzadeh, M.M. Haghdoost, A. Ghanbarpour, M. Amini, H.R. Khavasi, E. Payab, A. Ellern, L.K. Woo, *Inorg. Chim. Acta*, 411, **2014**, 61–66.

[20] I. Sheikhshoaie, A. Rezaeifard, N. Monadi, S. Kaaf, *Polyhedron*, 28, **2009**, 733–738;

[21] F.R. Sensato, Q.B. Cass, B.R. Lopes, T.C. Lourenço, J. Zukerman-Schpector, E.R.T. Tiekink, E. Longo, J. Andrés, *Inorg. Chim. Acta*., 375, **2011**, 41–46.

[22] A. Lehtonen, R. Sillanpää, *Polyhedron*, 24, **2005**, 257–265.

[23] H. Yang, H. Wang, Chengjian Zhu, *J. Org. Chem.*, 72, **2007**, 10029–10034.

[24] C.J. Whiteoak, G.J.P. Britovsek, V.C. Gibson, A.J.P. White, *Dalton Trans.*, **2009**, 2337–2344.

[25] J.E. Ziegler, G. Du, P.E. Fanwick, M.M. Abu-Omar, *Inorg. Chem.*, 48, **2009**, 11290–11296.

[26] S. Pal, R.N. Mukherjee, M. Tomas, L.R. Falvello, A. Chakravorty, *Inorg. Chem.*, 25, **1986**, 200–207.

[27] M.R. Maurya, S. Dhaka, F. Avecilla, *Polyhedron*, 67, **2014**, 145–159.

[28] S. Pasayath, S.P. Dash, S. Roy, R. Dinda, S. Dhaka, M.R. Maurya, W. Kaminsky, Y.P. Patil, M. Nethaji, *Polyhedron*, 67, **2014**, 1–10.

[29] M.R. Maurya, N. Kumar, F.Avecilla, *J. Mol. Catal. A. Chem.*, 392, **2014**, 50–60.

[30] J.A Brito, B. Royo, M. Gomez, *Catal. Sci. Tech.*, 1, **2011**, 1109–1118.

Appindex

FTIR spectrum of *cis*-[$MoO_2(L^3)$] (**3**).

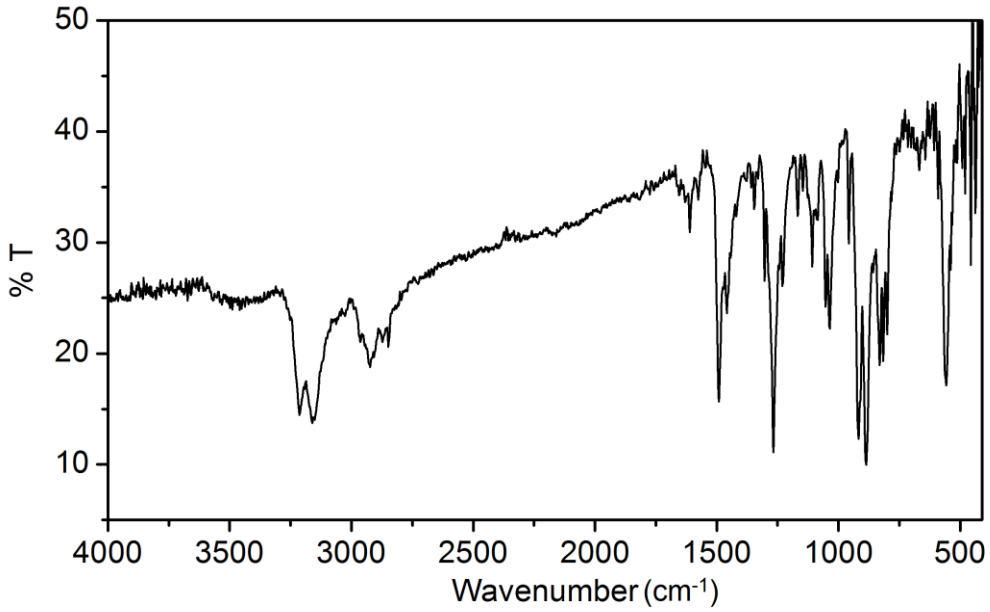

FTIR spectrum of *cis*-[$MoO_2(L^4)$] (**4**).

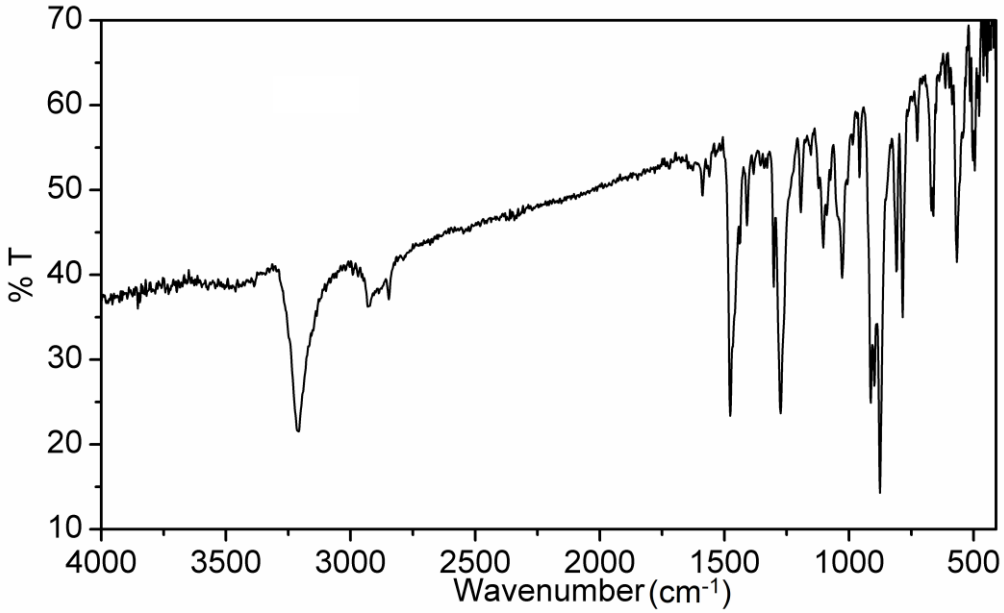

FTIR spectrum of *cis*-[$MoO_2(L^5)$] (**5**).

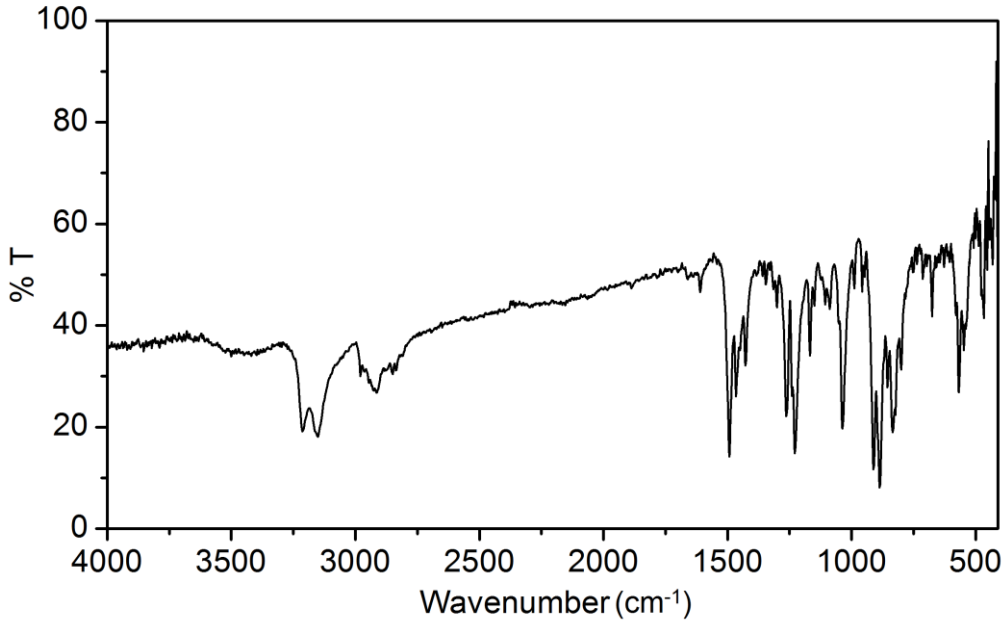

^{13}C-DEPT135 NMR Spectrum of *cis*-[$MoO_2(L^1)$] (**1**):

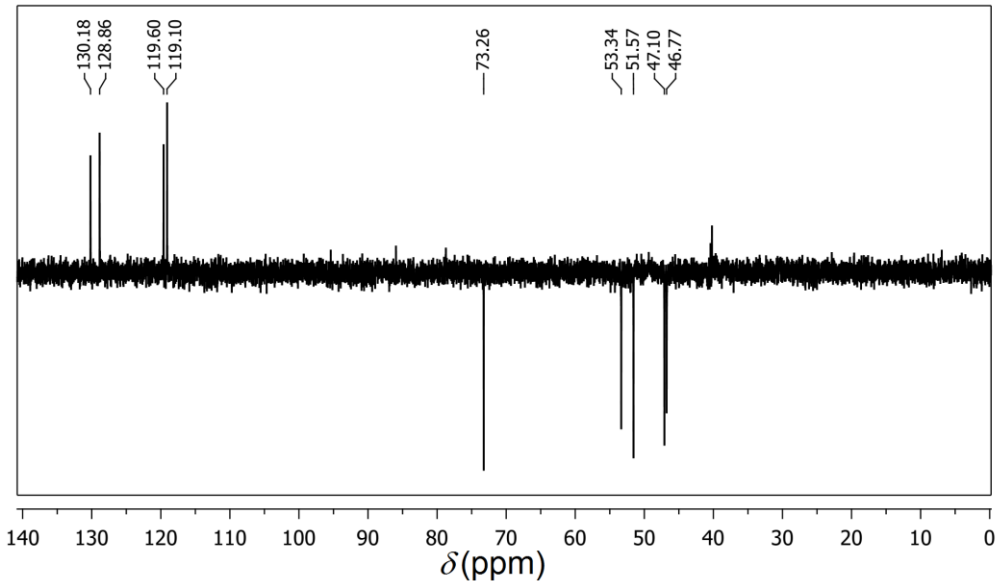

^{1}H-NMR Spectrum of *cis*-[$MoO_2(L^2)$] (**2**):

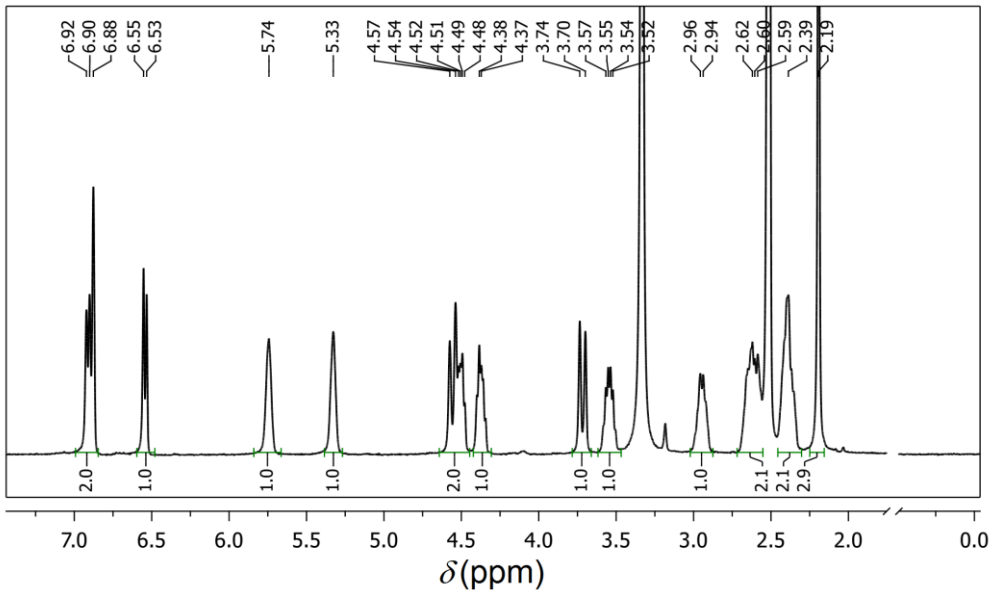

^{13}C- NMR Spectrum of *cis*-[$MoO_2(L^2)$] (**2**):

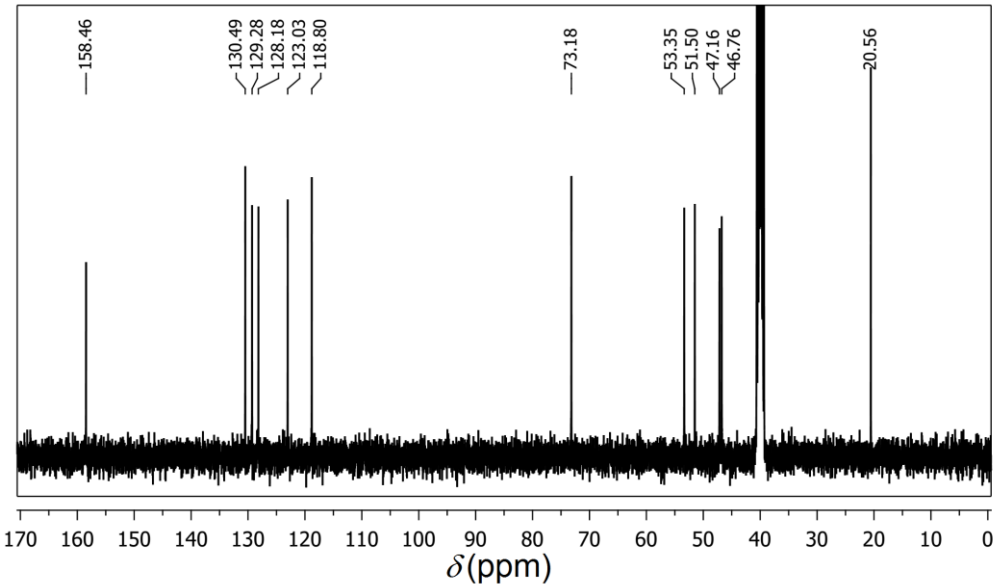

^{13}C-DEPT135 NMR Spectrum of *cis*-[$MoO_2(L^2)$] (**2**):

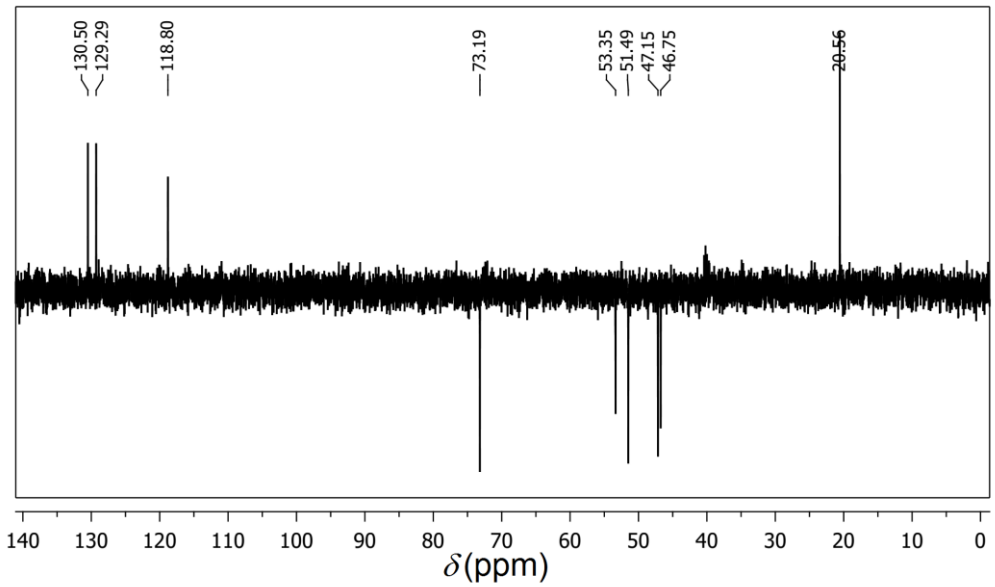

^{1}H-NMR Spectrum of *cis*-[$MoO_2(L^3)$] (**3**):

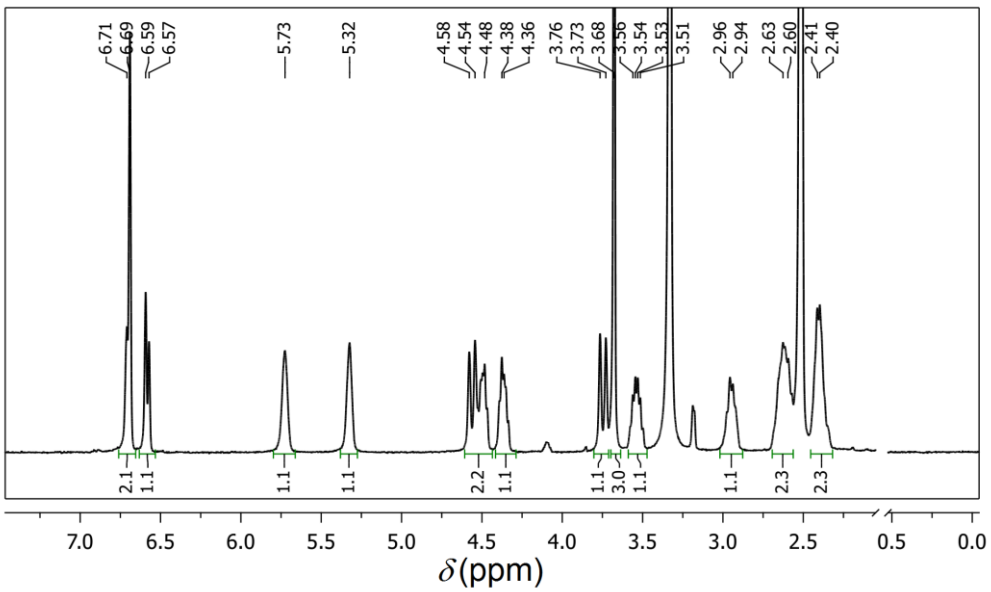

^{13}C- NMR Spectrum of *cis*-[$MoO_2(L^3)$] (**3**):

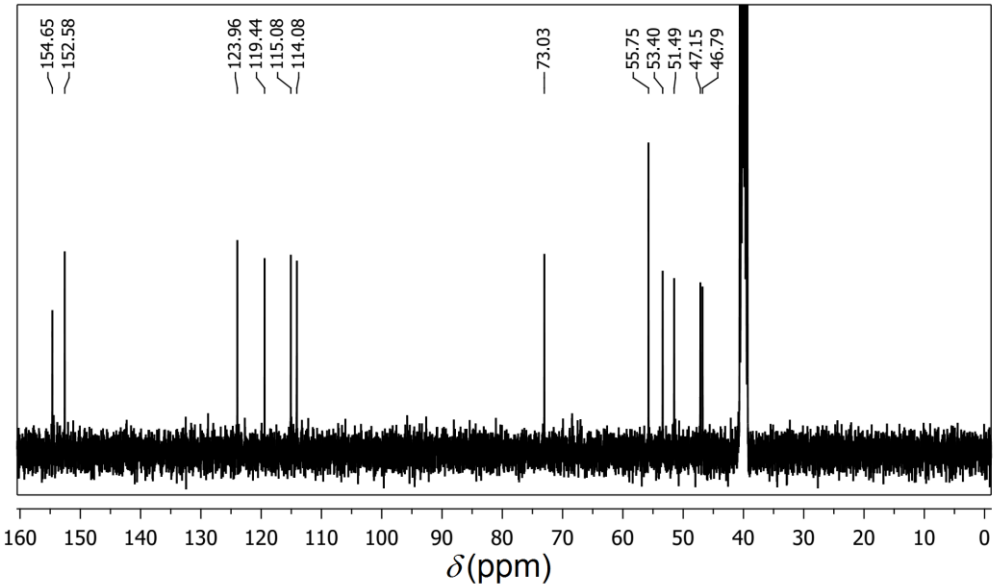

^{13}C-DEPT135 NMR Spectrum of *cis*-[$MoO_2(L^3)$] (**3**):

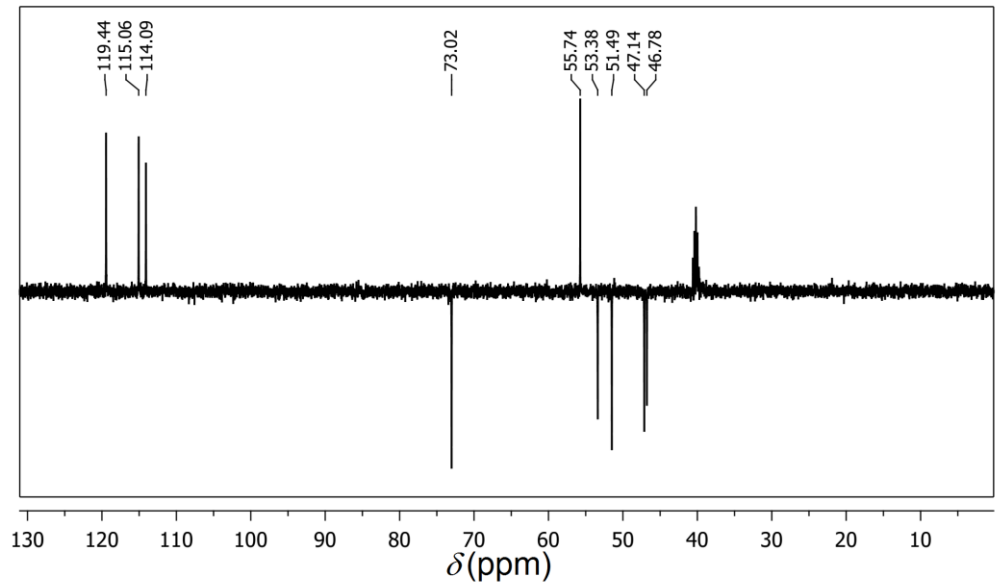

^{1}H-NMR Spectrum of *cis*-[$MoO_2(L^4)$] (**4**):

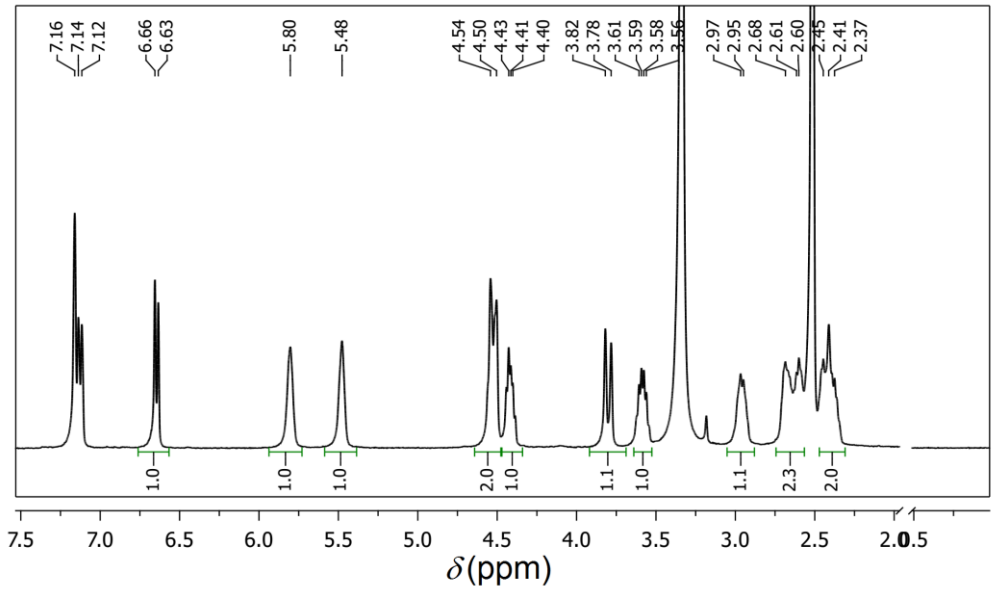

^{13}C-NMR Spectrum of *cis*-[$MoO_2(L^4)$] (**4**):

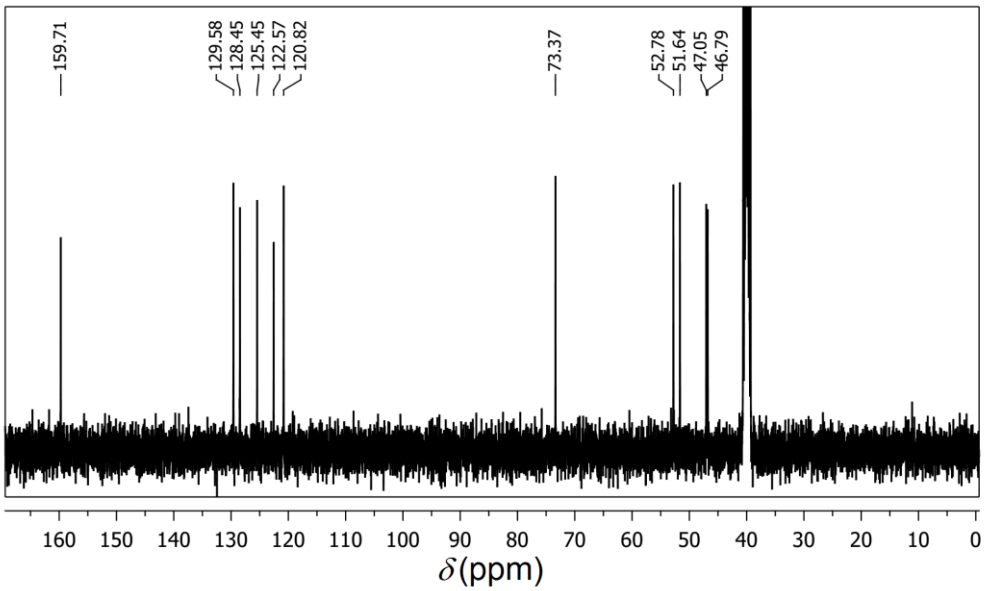

^{13}C-DEPT135 NMR Spectrum of *cis*-[$MoO_2(L^4)$] (**4**):

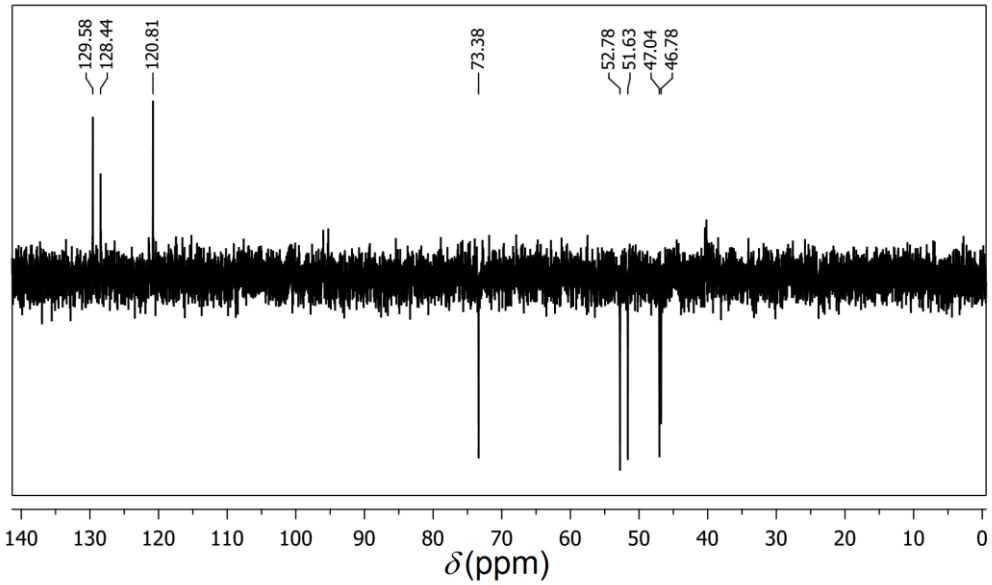

^{1}H-NMR Spectrum of *cis*-[$MoO_2(L^5)$] (**5**):

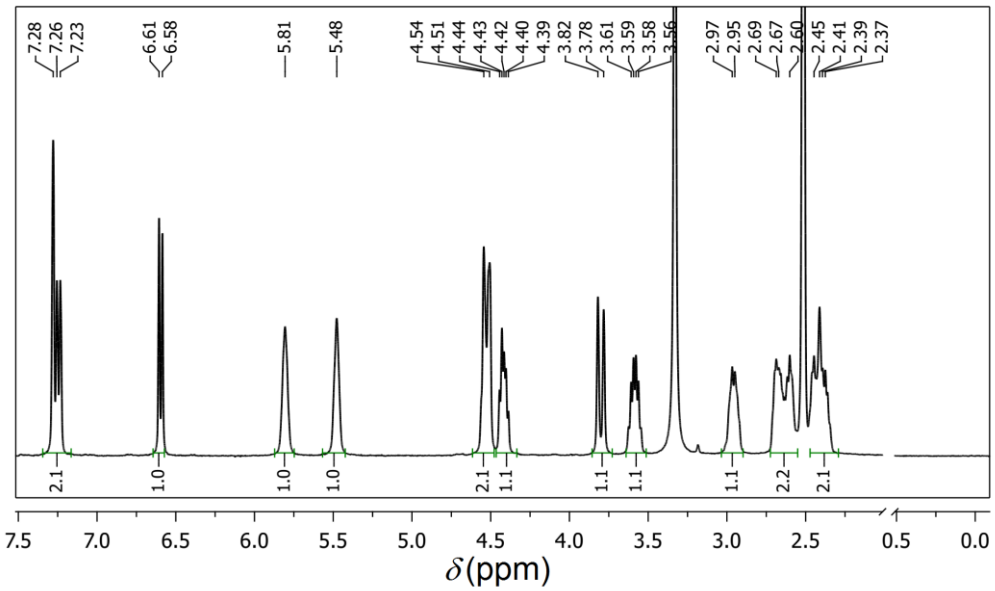

^{13}C-NMR Spectrum of *cis*-[$MoO_2(L^5)$] (**5**):

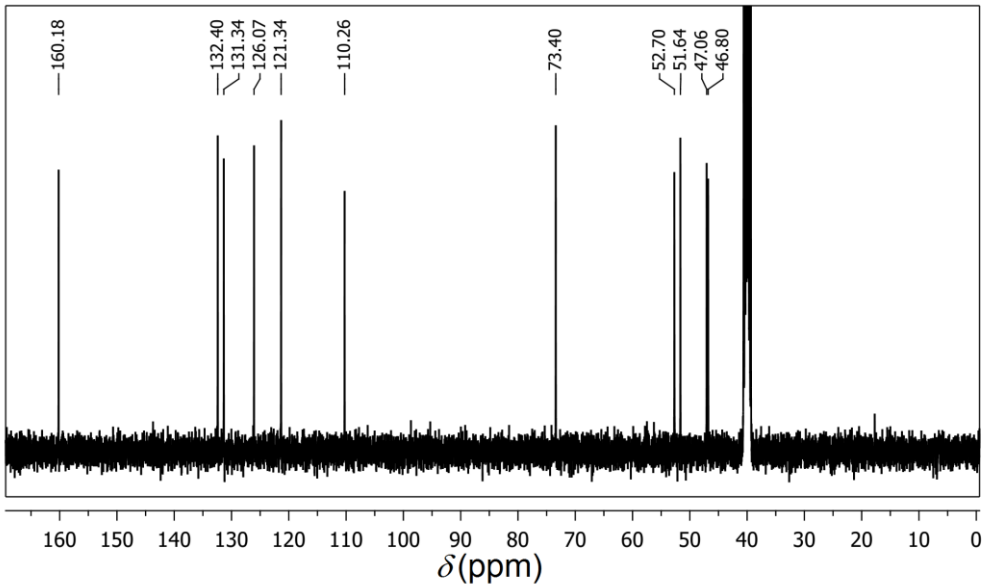

^{13}C-DEPT135 NMR Spectrum of *cis*-[$MoO_2(L^5)$] (**5**):

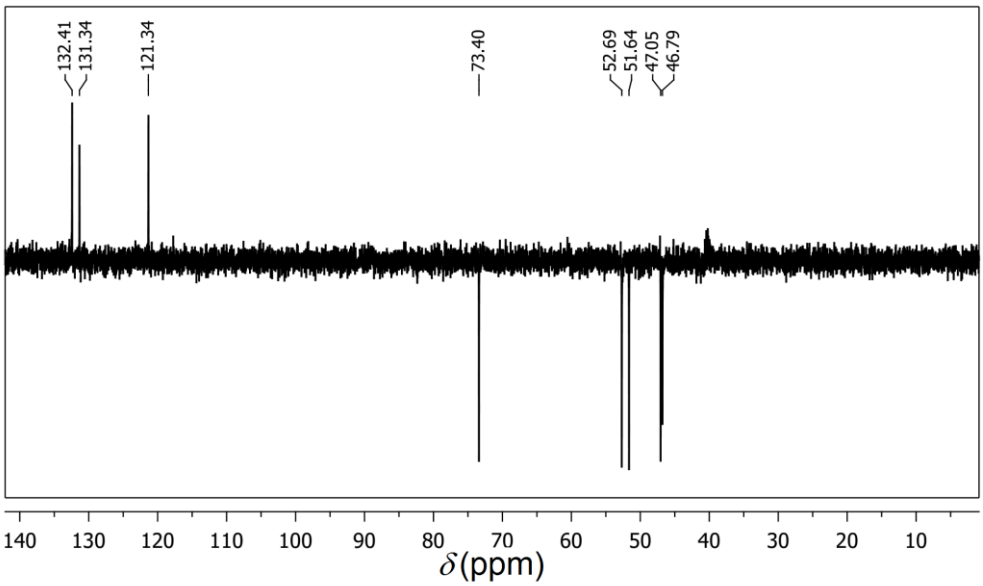

Atomic coordinates (x 10^4) and equivalent isotropic displacement parameters ($Å^2$ x 10^3). U(eq) is defined as one third of the trace of the orthogonalized Uij tensor.

Table A 5.1. For *cis*-[$MoO_2(L^1)$] (**1**)

	X	Y	Z	U (eq)
Mo(1)	2746(1)	6672(1)	-569(1)	27(1)
O(1)	4185(2)	7098(2)	164(1)	34(1)
O(2)	1424(1)	5184(2)	-1112(1)	35(1)
O(3)	3588(2)	7715(3)	-1295(1)	39(1)
O(4)	1620(2)	8307(2)	-233(1)	41(1)
N(1)	2194(2)	4604(3)	446(1)	33(1)
N(2)	3702(2)	3674(3)	-804(1)	35(1)
C(1)	4084(2)	7632(3)	901(1)	30(1)
C(2)	5051(2)	8906(3)	1172(1)	36(1)
C(3)	5051(3)	9499(3)	1917(2)	44(1)
C(4)	3108(3)	6956(3)	1389(1)	34(1)
C(5)	1962(2)	5677(4)	1152(1)	41(1)
C(6)	4090(3)	8819(4)	2403(1)	47(1)
C(7)	3149(2)	7568(4)	2139(1)	41(1)
C(8)	3218(3)	3089(4)	530(2)	40(1)
C(9)	3430(2)	2160(3)	-227(2)	42(1)
C(10)	3175(4)	3111(4)	-1551(2)	45(1)
C(11)	1682(3)	3469(4)	-1529(2)	46(1)

Table A 5.2. For *cis*-[$MoO_2(L^2)$] (**2**)

	X	Y	Z	U (eq)
Mo(1)	995(1)	7940(1)	1077(1)	29(1)
O(1)	202(5)	7325(3)	2518(3)	41(1)
O(2)	570(4)	8284(3)	-706(3)	36(1)
O(3)	2261(4)	6679(3)	708(4)	40(1)
O(4)	2675(4)	9539(3)	2012(4)	48(1)
N(1)	-1541(5)	9088(3)	1248(4)	33(1)
N(2)	-2034(5)	6286(3)	-473(4)	35(1)
C(1)	-1193(6)	7423(4)	3194(5)	34(1)
C(2)	-1675(7)	6390(4)	3781(5)	40(1)
C(3)	-3108(7)	6450(4)	4457(5)	39(1)
C(4)	-4122(6)	7477(4)	4561(5)	35(1)
C(5)	-3614(7)	8506(4)	3962(5)	36(1)
C(6)	-2174(7)	8503(4)	3296(5)	35(1)
C(7)	-1610(7)	9646(4)	2698(5)	40(1)
C(8)	-3490(6)	8288(4)	180(5)	40(1)
C(9)	-3774(6)	6704(4)	-139(5)	39(1)
C(10)	-2014(7)	6134(5)	-1910(6)	54(1)
C(11)	-228(11)	7080(6)	-1927(6)	81(2)
C(12)	-5706(7)	7533(5)	5287(5)	42(1)

Table A 5.3. For *cis*-[$MoO_2(L^3)$] (**3**)

	X	Y	Z	U (eq)
Mo(1)	956(1)	2794(1)	5950(1)	31(1)
O(1)	273(4)	2026(2)	7326(2)	41(1)
O(2)	392(4)	3351(2)	4239(2)	38(1)
O(3)	2250(3)	1570(2)	5588(3)	44(1)
O(4)	2666(4)	4297(2)	6916(2)	48(1)
O(5)	-5146(4)	1906(2)	10023(3)	52(1)
N(1)	-1590(4)	3938(2)	6120(3)	34(1)
N(2)	-2107(4)	1329(3)	4430(3)	37(1)
C(1)	-1049(5)	2066(3)	7994(3)	35(1)
C(2)	-1433(5)	987(3)	8579(3)	39(1)
C(3)	-2781(5)	973(3)	9261(3)	41(1)
C(4)	-3774(5)	2034(3)	9367(3)	38(1)
C(5)	-3397(5)	3119(3)	8800(3)	40(1)
C(6)	-2029(5)	3150(3)	8117(3)	37(1)
C(7)	-1603(6)	4355(3)	7539(4)	45(1)
C(8)	-3602(5)	3259(3)	5068(4)	45(1)
C(9)	-3860(5)	1700(3)	4732(4)	43(1)
C(10)	-2210(6)	1299(4)	3010(4)	56(1)
C(11)	-507(9)	2330(5)	3013(4)	92(2)
C(12)	-5942(6)	3060(4)	10367(4)	52(1)

Table A 5.4. For *cis*-[$MoO_2(L^4)$] (**4**)

	X	Y	Z	U (eq)
Mo(1)	4052(1)	7061(1)	3902(1)	27(1)
O(1)	4899(7)	7733(5)	2504(5)	41(1)
O(2)	4420(7)	6673(4)	5680(5)	36(1)
O(3)	2705(7)	8322(5)	4247(5)	40(1)
O(4)	2446(7)	5466(5)	2905(5)	48(1)
N(1)	6659(8)	5924(5)	3774(6)	33(1)
N(2)	7016(8)	8691(5)	5521(6)	32(1)
C(1)	6259(10)	7632(7)	1820(7)	33(2)
C(2)	6711(10)	8676(7)	1237(7)	35(2)
C(3)	8147(11)	8648(7)	560(7)	38(2)
C(4)	9151(10)	7566(7)	472(7)	34(2)
C(5)	8746(10)	6525(7)	1043(7)	35(2)
C(6)	7306(10)	6548(7)	1724(7)	33(2)
C(7)	6803(12)	5383(7)	2309(8)	43(2)
C(8)	8590(10)	6706(7)	4869(8)	39(2)
C(9)	8807(10)	8306(7)	5222(8)	40(2)
C(10)	6981(12)	8803(8)	6965(8)	50(2)
C(11)	5113(15)	7874(8)	6908(9)	68(3)
C(11)	5113(15)	7874(8)	6908(9)	68(3)

List of Publications

Thesis Work:

1. Dioxomolybdenum(VI) complexes with 2-((2-(pyridin-2-yl) hydrazono)-methyl)phenol and its derivatives
   Sathish Kumar Kurapati, Uppala Ugandhar, Swamy Maloth, Samudranil Pal*****
   Polyhedron, 42, **2012**, 161–167.
2. cis-$\{MoO_2\}^{2+}$ assisted Mannich-type addition of acetylacetonate methine to the azomethine of tridentate Schiff bases: racemic complexes with chiral transformed ligands
   Sathish Kumar Kurapati, Samudranil Pal*****
   Dalton Trans., 44, **2015**, 2401– 2408.
3. Complexes of cis-dioxomolybdenum(VI) with unsymmetrical tripodal NO3-donor ligands: Synthesis, characterization and catalytic applications
   Sathish Kumar Kurapati, Swamy Maloth, Samudranil Pal*****
   Inorg. Chim. Acta., 430, **2015**, 66–73.
4. cis-Dioxomolybdenum(VI) complexes with unsymmetrical linear tetradentate ligands: syntheses, structures and bromoperoxidase activities
   Sathish Kumar Kurapati, Samudranil Pal***** (to be communicated)

Other Work:

5. (Methanol-κO)-cis-dioxido{(4Z,N' E)-N' -[(Z)-4-oxido-4- phenylbut-3-en-2- ylidene]isonicotinohydrazidato}molybdenum(VI)
   Sathish Kumar Kurapati*
   Acta. Cryst., E69, **2013**, m460–m461.
6. Synthesis, structure, and properties of a pentanuclear cobalt(III) coordination cluster.
   Swamy Maloth, **Sathish Kumar Kurapati**, Samudranil Pal*****,
   J. Coord. Chem., 68, **2015**, 1402–1411.

7. New ω-ketovinyl phosphonates: inexpensive synthesis, isomerization studies and route for functionalized 1,3-butadienes.
   Gangaram Pallikonda, Swamy Maloth, **Satish Kumar Kurapati**, Khalid Zubair, Akhil Subhas Ghosal, Manab Chakravarty*****
   Tetrahedron Letters, **2015** (in press).
8. cis-$\{MoO_2\}^{2+}$ assisted ligand transformation via Mannich-type addition of tridentate NNO donar ligands to benzoyl acetone: Synthesis, Structures, Charecterization and catalysis
   Sathish Kumar Kurapati, Sabari Ghosh, Samudranil Pal***** (to be communicated)

Posters and Presentations

1. A Coper (II) Coordination Polymer with Succinate and Pyrazine: Interpenetrating Cubic Network

   Poster Presentation

   Modern Trends in Inorganic Chemistry-XV, December, 2011, School of Chemistry, University of Hyderabad.

2. MoO_2^{2+} Chemistry with pyridine based Schiff-bases: Expected meridional coordination and unexpected ligand transformation

   Poster Presentation

   Modern Trends in Inorganic Chemistry-XV, December, 2013, Department of Chemistry, Indian Institute of Technology Roorkee.

3. Complexes of *cis*–$\{MoO_2\}^{2+}$ with N–capped tripodal ligands: Synthesis, Characterization and Catalysis.

   Poster Presentation

   Recent Trends in Chemical Sciences, 1st Indo-Taiwan Symposium, November 2014, University of Hyderabad and Academica Sinica.

4. Complexes of *cis*-$\{MoO_2\}^{2+}$ with N-capped tripodal ligands and unsymmetrical diaminodiols: Synthesis, Characterization and Catalysis Oral and Poster presentation

   Chem Fest-2015, 12th Annual In-House Symposium, February, 2015, School of Chemistry, University of Hyderabad.